Advanced Laser Technologies

6 - 10 October 2014, Cassis, France

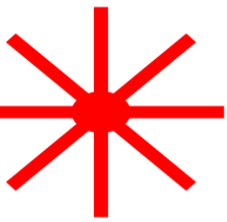

ALT'14 : International Conference on Advanced Laser Technologies 2014

Short description and history :

The annual International Conference on **Advanced Laser Technologies** (**ALT**) was established in 1992 by the Nobel Prize Laureate Alexander Prokhorov, member of the Russian Academy of Sciences and Director of the General Physics Institute.

There are two principal ideas of this international event. First of all, it brings together presentations on fundamental and engineering aspects of laser technologies along with their applications in various areas (materials processing, laser medicine, photonic devices, systems for process control, etc.). Thus the conference has become an important and well recognized Forum for both researchers and engineers. Second, Russian scientists, in particular from General Physics Institute (www.gpi.ru), play an prominent role in the organization of ALT meetings, and typically an essential part of the conference attendees represent former Soviet Union states. This fact together with the tradition that each year the ALT Conference takes place in a new country gives a unique mixture of specialists and thus a possibility of making new personal contacts and exchanging scientific and technological data and ideas between different scientific schools.

The total number of each conference attendees varies between 120 and 200, having a trend to increase year after year. The 4-5 days Program includes top-level plenary talks that outline the new trends or summarize extensive research results and are accompanied by invited, oral and poster presentations. Usually conferences proceed with one or two parallel sessions.

The key topics of each meeting are slightly varied. Depending on the current trends, the new topics appear while some traditional areas of R&D become less popular. At present ALT Conferences are focused on laser–matter interaction, ultra-fast phenomena, technological laser systems and diagnostics, biophotonics, photoacoustics, and THz technologies.

ALT Conferences took place in Russia, Germany, Greece, Romania, Czech Republic, France, Italy, Switzerland, United Kingdom, China, Hungary, Finland, Turkey, Netherlands, Bulgaria and Montenegro where in 2013 almost 200 people coming from 20 different countries attended.

Please you can see more details on the website: http://altconference.org/althistory.

Scientific program:

In 2014, ALT conference is held in Cassis (Provence, France) from 6th to 10th October. The topics are:

- ✓ Laser-matter interaction
- ✓ Biophotonics
- ✓ Laser systems and components
- ✓ Laser diagnostics and Spectroscopy
- ✓ Photoacoustics
- ✓ Micro- and Nano-Photonics
- ✓ Laser beam shaping
- ✓ THz laser source and Applications
- ✓ Ultra-intense lasers and Applications.

Each day is opened by a world-known plenary speaker providing an overview of on a particular topic of the Conference. It is completed by a large number of invited talks allowing us to gather in Cassis a panel of expert and leading scientists in each scientific topic of the Conference.

The list of plenary speakers of ALT 2014 is joined below.

Plenary Speakers:

"Interaction of ultra-short laser pulse with dielectrics: modification of optical and material properties before damage", *Pr. E. Gamaly, Australian National University, Canberra, Australia.*

"Development of the PETAL laser facility and its applications in physics", *Pr. D. Batani, University of Bordeaux 1, France.*

"Twists and more the complex shape of light", *Pr. M. Padgett, University of Glasgow, Scotland.*

"Shaped ultrafast laser pulses for micro/nanofabrication: from fundamentals to applications", *Pr. Lan Jiang, Beijing Inst. of Technology, China.*

"Semiconductor Beating Sources for tunable Continuous-Wave Terahertz Generation and its industrial application", *Pr. K. H. Park, THz Photonics Creative Research Center ETRI, South Korea.*

"Biophotonics – multimodal imaging for clinical applications", *J. Popp, Leibniz Institute of Photonic Technology, Jena, Germany*

Committees, ALT 2014

Aix-Marseille University and the Centre National de la Recherche Scientifique, France.

General Physics Institute of Russian Academy of Sciences, Russia.

Center of Laser Technology and Material Science, Russia.

International Laser Center of Moscow State University, Russia.

Conference Chairman

Ivan SHCHERBAKOV (RU)

Programm-Committee Chair

Vitaly KONOV (RU) Marc SENTIS (France)

Organizing Committee Co-Chairs

Vladimir PUSTOVOY (RU) Olivier UTEZA (France)

International Program Committee

Kerim ALLAHVERDIYEV (Azerbaijan)
Ekaterina BORISOVA (Bulgaria)
J.-L. COUTAZ (France)
Aladar CZITROVSKY (Hungary)
Boris DENKER (Russia)
Dan DUMITRAS (Romania)
Costas FOTAKIS (Greece)
Thomas GRAF (Germany)
Sergey GARNOV (Russia)
Fatih HUSEYINOGLU (Turkey)
Lan JIANG (China)
Frans HARREN (Netherlands)
Andrei KABASHIN(France)
Pavel KASHKAROV (Russia)
Laurent LARGER (France)
Yong Feng LU (USA)
Vladimir MAKAROV (Russia)
Andreas MANDELIS (USA)
Ion MIHAILESCU(Romania)
Ivan PELIVANOV (Russia)
Alexander PRIEZZHEV (Russia)
Bojan RADAK (Serbia)
Valerio ROMANO(Switzerland)
Philippe DELAPORTE (France)
Alexander SHKURINOV (Russia)
Vadim VEIKO (Russia)

International Organizing Committee

Ahmed AL-KATTAN (FR)
Patricia ALLONCLE (FR)
Pierre BLANDIN (FR)
Jean-Luc BELLEMAIN (FR)
Laurent CHARMASSON (FR)
Raphael CLADY (FR)
Gaelle COUSTILLIER (FR)
Thierry DJENIZIAN (FR)
David GROJO (FR)
Jörg HERMANN(FR)
Natalia KHAKAMOVA (RUS)
Max ROLLAND (FR)
Nicola SANNER (FR)
Thierry SARNET (FR)
Vadim TCHEREMISKINE (FR)
Tatiana VOLYAK(RU)

Organizers and Sponsors, ALT 2014

6-10 October 2014, Cassis, France

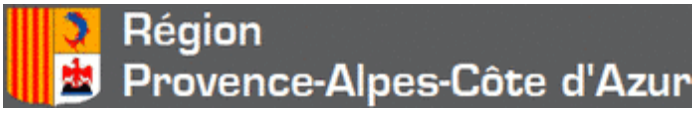

Conference time planner

Day 0 : Sunday, October 5

14:00 to 19:00 : Registration

18:30 - 20:00 Welcome cocktail reception at convention center of Cassis (Oustau Calendal)

Day 1 : Monday, October 6

ROOM 1	ROOM 2	ROOM 3
08:30 Opening remarks V. Konov and M. Sentis		
09:00 - *Plenary* **Interaction of ultra-short laser pulse with dielectrics: modification of optical and material properties before damage** E. Gamaly **P1**		

Laser-Matter Interaction I	Laser Systems and Materials I	Laser Diagnostics and Spectroscopy I
09:45 - *Invited*	**09:45** - *Invited*	**09:45** - *Invited*
Ultrashort pulse induced nanogratings inside glass – fundamentals and applications S. Nolte **P2**	**Broadband IR Hybrid Laser System Emitting Within 2.5 – 17.5 Micron** A. Ionin **P20**	**Carbon Nanotubes as Efficient Platform for Photonic Applications** A. Rozhin **P34**
10:10 - *Invited*	**10:10** - *Invited*	**10:10** - *Invited*
Laser processing of CFRP: Fundamental energy transport mechanisms R. Weber **P3**	**High-aperture-rod Nd:glass laser** E. Khazanov **P21**	**Nonlinear optics of silicon nanowire arrays: third-harmonic generation and coherent anti-stokes raman scattering** S. Zabotnov **P35**

10:35-11:00 Coffee Break

Laser-Matter Interaction II	Laser Systems and Materials II	Laser Diagnostics and Spectroscopy II
11:00 - *Invited*	**11:00** - *Invited*	**11:00** - *Invited*
Laser Nanomanufacturing B. Chichkov **P4**	**Ultrafast Thin-Disk Lasers with kW Average Output Power** T. Graf **P22**	**Optical Spectroscopy of Conductive Transparent Films of Single-Wall Carbon Nanotubes Filled with Acceptor Molecules** E. Obraztsova **P36**
11:25	**11:25** - *Invited*	**11:25**
Femtosecond-laser driven electron dynamics and resulting nanoscale surface instabilities A. Ionin **P5**	**Application of non-contact optical methods for study of aerosol deposition in human lungs** M. Veres **P23**	**Raman and Second-Harmonic Diagnostics of SiC-Based Nanostructures** L. Golovan **P37**

11:40	**11:50** - *Invited*	**11:40**
Formation of Micro- and Nanostructures on Solid Surfaces by ArF-laser Radiation S. Mikolutskiy **P6**	**Progress in Nd:YAG laser pumped mid-IR optical parametric oscillators based on non-oxide nonlinear crystals** V. Petrov **P24**	**On the optical centres in Bi/Ga(Al) co-doped silica glass** O. Laguta **P38**
11:55 - *Invited*		**11:55**
Electrofluidics fabricated by femtosecond laser direct writing J. Xu **P7**		**Talbot Interferometer for Measurement of Effect of Gradient Magnetic Field on Temperature and Temperature Profile of Gaseous Flame** S. Agarwal **P39**

12:20-14:00 Lunch at restaurant "Le grand Large"

Laser-Matter Interaction III	Laser Systems and Materials III	Laser Diagnostics and Spectroscopy III
14:00 - *Invited*	**14:00** - *Invited*	**14:00** - *Invited*
Femtosecond laser nanoablation of biodegradable polymer M. Terakawa **P8**	**Diamond components for lasers and photonics** V. Ralchenko **P25**	**Femtosecond laser diagnostics of plasmonic and magnetoplasmonic** A. Fedyanin **P40**
14:25 - *Invited*	**14:25** - *Invited*	**14:25** - *Invited*
Fundamentals of surface modification after irradiation of silicon with ultrashort laser pulses: from ripples to spikes G. Tsibidis **P9**	**Epitaxial fluoride layers for laser and amplifiers** P. Camy **P26**	**Harmonic nanoparticles for nonlinear imaging and photo-interaction** A. Rogov **P41**
14:50	**14:50**	**14:50**
Femtosecond Laser Tuning of Silicon Resonant Optical Devices Y. Tsui **P10**	**Modes of resonators with axially symmetric aberrational lens** V. Morozov **P27**	**Toxic influence of heavy metal ions on living organisms investigated by different laser optical methods** K.V. Fedorova **P42**

15:05	**15:05**	**15:05**
New High-Pressure Silicon Phases Formed in Fs-Laser Induced Confined Microexplosion A. Rode **P11**	**Comparison of Stored Energy in Disk and Composites Yb:YAG Active Element at Cryogenic and Ambient Temperature** O. Vadimova **P28**	**Development of a laser based laboratory light scattering instrument for light scattering studies on small particulate matter** A. Gogoi **P43**
15:20	**15:20**	**15:20**
Laser-induced synthesis of nanostructured carbon materials A. Kucherik **P12**	**Generation of new spatial and temporal coherent states using VECSEL technology** M. Seghilani **P29**	**LIBS-study of Graphite-Containing Composite Electrochemical Coatings** E. Surmenko **P44**
15:35	**15:35**	**15:35**
Guided Melting deformation: A novel Laser nanostructuring method P. Lorenz **P13**	**Laser operation of Tm:Ho:YbAG crystal pumped at 1678 nm** V. Mikhailov **P30**	**Determination of the elemental composition of optical glasses by laser-induced breakdown spectroscopy** C. Gerhard **P45**
15:50	**15:50**	**15:50**
Laser-Induced Cleavage of Graphene Structures and Synthesis of Nanostructured Layers on Surface of Carbon Materials D. Abramov **P14**		**Spectral analysis of protoplasmic streaming velocities in Ph ysarum Polycephalum obtained by laser Doppler spectroscopy** T. Avsievich **P46**

16:05-16:30 Coffee Break

Laser-Matter Interaction IV	Laser Systems and Materials IV
16:30 - *Invited*	**16:30** - *Invited*
Laser-induced nanocluster surface structures with controlled functional properties: demonstration by jump Coulomb conductivity in tunnelly coupling semiconductor islands S. Arakelian **P15**	**Mode-locking semiconductor disk lasers using single-walled carbon nanotube saturable absorbers** V. Pasiskevicius **P31**
16:55	**16:55** - *Invited*
Numerical Analysis of Promising Techniques of Nanoparticle Generation: Laser Ablation vs Spark Discharge at Atmospheric Pressure T. Itina **P16**	**High Performance Laser Combination Additive Manufacturing Technology and it's Applications** Jianhua Yao **P32**

17:10	17:20 - invited
A hybrid atomistic-continual simulation of ablation of metals under the action of powerful femtosecond laser pulses V. Fokin **P17**	**Spectral-Luminescence Investigations of Raman-active Strontium Molybdate Crystals Doped with Ho3+and Tm3+ions** L. Ivleva **P33**
17:25	
Crack-free fabrication of microchannels by femtosecond laser on a glass surface E. Bulushev **P18**	
17:40	
Numerical Investigation of Laser Interaction with Colloidal Nanoparticles T.Itina **P19**	

Day 2 : Tuesday, October 7

ROOM 1	ROOM 2	ROOM 3
08:30 - *Plenary* **Twists and more the complex shape of light** M. Padgett **P47**		
Laser-Matter Interaction V	**Laser Beam shaping I**	**Laser Systems and Materials V**
09:15 - *Invited*	**09:15** - *Invited*	**09:15** - *Invited*
Laser 3D printing for photonics, metamaterials and medicine A. Selimis **P48**	**Beam shaping for optical manipulation using conical refraction** D. McGloin **P60**	**Spectroscopic and laser properties of Cr2+ and Fe2+ ions in solid solutions based on ZnSe crystal** M. Doroshenko **P71**
09:40 - *Invited*	**09:40** - *Invited*	**09:40** - *Invited*
Lasers print and functionalize sensors Y. Zergioti **P49**	**Extreme nonlinear optics with intense shaped laser beams** P. Polynkin **P61**	**Purely Optical Orientational Phase Transitions in Nematic Liquid Crystals** V. Ochkin **P72**
10:05-10:30 Coffee Break		
Laser-Matter Interaction VI	**Laser Beam shaping II**	**Non linear Optics I**
10:30 - *Invited*	**10:30** - *Invited*	**10:30** - *Invited*
Laser Induced Forward Transfer printing of conductive materials for printed electronics E. Smits **P50**	**Hollow Bessel beam as an optical guide for a stream of microscopic particles** A. Rode **P62**	**Photonic Reservoir Computing** D. Brunner **P73**
10:55 - *Invited*	**10:55** - *Invited*	**10:55** - *Invited*
Laser nanocrystallization of metals I. Zavestovskaya **P51**	**Femtosecond laser ablation with high angle Bessel and Bessel Vortex beams** F. Courvoisier **P63**	**Resonant Radiation Physics in Collapsing Light Pulses** Th. Roger **P74**
11:20	**11:20**	**11:20**
Laser fabrication of microelectrodes on flexible substrates by subtractive and additive laser techniques D. Puerto **P52**	**Spatial transformation of optical beams using resonant diffraction structures** L. Doskolovich **P64**	**Nonlinear optical diagnostics of ferroelectric microstructures annealed by femtosecond laser** E. Mishina **P75**

11:35	**11:35**	**11:35**
Influence of the ps laser irradiation on the electrochemical and spectroscopic properties of graphene-chitosan composite film R. Trusovas **P53**	**Mechanism of micro-lens array formation by using four-beam interference lithography** E. Stankevicius **P65**	**Nonlinear evolution of polarization singularities in collinearly propagating light beams in isotropic gyrotropic medium** I. Perezhogin **P76**
11:50	**11:50**	**11:50**
Increasing the efficiency of selected laser processes by assisting atmospheric pressure plasmas C. Gerhard **P54**	**Ablation depth control of ITO thin film using a beam shaped femtosecond laser for mobile display** H.Y. Kim **P66**	**Adiabatic approx. approach to a system of nonlinear schrodinger eq. for elliptically polarized waves in an isotropic gyrotropic medium** V. Makarov **P77**

12:05-14:00 Lunch at restaurant "Le grand Large"

14:00 - *Plenary*
Shaped ultrafast laser pulse for micro/nanofabrication: from fundamentals to applications

Lan Jiang
P55

Laser-Matter Interaction VII	Photoacoustics
14:45 - *Invited*	**14:45** - *Invited*
Ion migration assisted femtosecond laser inscription of high performance active and passive waveguides for photonic devices J. Solis **P56**	**New applicative results in CO2 laser photoacoustic spectroscopy** D. Dumitras **P67**
15:10 - *Invited*	**15:10** - *Invited*
Picosecond-laser bulk modification, luminescence and Raman lasing in single-crystal diamond V. Romano **P57**	**Noninvasive detection of hematomas and patient monitoring with portable, medical grade laser optoacoustic systems** R. Esenaliev **P68**
15:35	**15:35**
Large-mode-area mid-infrared guiding in ultrafast generated waveguides in chalcogenide glasses R. Stoian **P58**	**Five Dimensional Optoacoustic Tomography Visualizes Fast Hemodynamic Changes in Whole Mouse Brain** D. Razansky **P69**
15:50:00 - Invited	**15:50**
Femtosecond laser micro-/nano- fabrication: new insights and its applications in optomechanics Y. Bellouard **P59**	**Breath biomarkers can help clinicians to assess the role of oxidative attack in young population with mental disorders** C. Popa-Achim **P70**

16:15-16:45 Coffee Break
16:45 - 18:15 Poster Session I, S1P1-S1P28

Day 3 : Wednesday, October 8

ROOM 1	ROOM 2	ROOM 3
08:30 - *Plenary* **Biophotonics – multimodal imaging for clinical applications** J. Popp **P78**		

Biophotonics I	Laser-Matter Interaction VIII
09:15 - *Invited*	**09:15** - *Invited*
Compact Diode Laser-based Systems for Biophotonics Application P. Andersen **P79**	**Recent progress in interfering femtosecond laser processing** Y. Nakata **P84**
09:40 - *Invited*	**09:40** - *Invited*
Laser-activated chromophores and nanoparticles in minimally-invasive diagnostics and therapies R. Pini **P80**	**Photonic crystal mirrors: a cornucopia of nanopatterned structures for the taming of light atthe wavelength scale** X. Letartre **P85**

10:05-10:30 Coffee Break

Biophotonics II	Non linear Optics II	THz sources and applications I
10:30 - *Invited*	**10:30** - *Invited*	**10:30** - *Invited*
Nanodiamond optical-spectroscopic properties and their optimization for development of theranostic applications E. Perevedentseva **P81**	**Exciton states of the optical electrons of dielectric nanoparticles in dielectric matrix** Yu. Kulchin **P86**	**Identifying hidden substances by THz remote sensing: realistic dream?** J-L. Coutaz **P90**
10:55 - *Invited*	**10:55** - *Invited*	**10:55** - *Invited*
Laser-stimulated Cavitation and Tissue Regeneration V. Bagratashvili **P82**	**All-optical polarization control in fibers for Telecom applications** J. Fatome **P87**	**Time-domain probe of THz nanostructure lasers** J. Darmo **P91**
11:20	**11:20**	**11:20**
Skin Fractional Ablation Using Multi-Micro-Beam Erbium Laser for Enhanced Particle Delivery E. Genina **P83**	**Laser-induced Damage in Second Harmonic Generation by Periodically Poled LiTaO3** O. Louchev **P89**	**Sub-gigawatt Terahertz Source Based on Optical Rectification and Its Non-thermal Impact on In-vivo Mouse Brain Neural Cell** Li-Guo Zhu **P92**

11:35	**11:35**	**11:35**
		Simultaneous generation of nonlinear optical harmonics and THz radiation in air: polarization discrimination of various nonlinear contributions M. Esaulkov **P93**
11:50	**11:50**	**11:50**
		Terahertz time-domain spectroscopy of diabetic rat blood plasma O. Cherkasova **P94**

12:05-14:00 Lunch at restaurant "Le grand Large"

14:00-16:00 Boat excursion in the famous National Park of Calanques

19:00 - 23:00 Conference dinner at restaurant "La Presqu'île"

Day 4 : Thursday, October 9

ROOM 1	ROOM 2	ROOM 3
08:30 - *Plenary* **The role of photonics in THz technology** K.H. Park **P95**		

Biophotonics III	Laser-Matter Interaction IX	THz sources and applications II
09:15 - *Invited*	**09:15** - *Invited*	**09:15** - *Invited*
Shaped light for imaging and manipulation J. Nylk **P96**	**Self-organization and nanostructuring in SiGe layers induced by pulse laser annealing** N. Sobolev **P109**	**Generation and Application of mJ-level Ultrashort Terahertz pulses** J. Hebling **P122**
09:40 - *Invited*	**09:40** - *Invited*	**09:40** - *Invited*
Non-invasive methods of imaging the human microcirculation M. Leahy **P97**	**Laser Ignition of Engines: Status, Current Problems, Solutions** E. Wintner **P110**	**Surface plasmon polariton studies in the terahertz range: A state of the art review** B. Knyazev **P123**

10:05-10:30 Coffee Break

Biophotonics IV	Laser-Matter Interaction X	THz sources and applications III
10:30 - *Invited*	**10:30** - *Invited*	**10:30** - *Invited*
Tissue imaging and therapeutic effects at laser-induced nanoparticle luminescence, heating, and ROS-generation V. Tuchin **P98**	**Color marking by laser oxidation** V. Veiko **P111**	**Nonlinear effects of strong THz fields** S. Tzortzakis **P124**
10:55 - *Invited*	**10:55**	**10:55** - *Invited*
Detection of metabolic tumor status, using genetically encoded sensors and optical imaging E. Zagaynova **P99**	**Nuclear-chemical processes under laser ablation of metals in aqueous mediums** S. Timashev **P112**	**Extreme nonlinear optics at THz frequencies** P. Jepsen **P125**
11:20	**11:10**	**11:20** - *Invited*
Dual Imaging System for Intraoperative Assessment of Positive Tumor Margins C. Matei **P100**	**Optimization of multispectral synchrotron photoluminescence at sub-microscale to image heterogeneity of historical metals** T. Séverin-Fabiani **P113**	**Interaction of Terahertz Radiation with Nanostructured Objects on a Surface** A. Shkurinov **P126**

11:35	**11:25**	**11:45**
Clinical experience in fluorescence diagnostics and photodynamic therapy control using laser imaging and laser spectroscopy technologies on photosensitized bio-tissues M. Loshchenov **P101**		**Interaction of strong THz fields with solids and liquids** A. Stepanov **P127**
11:50		
Method of combined optical spectroscopy in neurooncology: theoretical basis and clinical experience P.V. Grachev **P102**		

12:10-14:00 Lunch at restaurant "Le grand Large"

Biophotonics V	Ultra-High Intensity I	THz sources and applications IV
14:00 - *Invited*	**14:00** - *Invited*	**14:00** - *Invited*
Live dynamic imaging of developmental defects in mouse models with optical coherence tomography I. Larina **P103**	**Relativistic optics using engineered plasmas** P. Monot **P115**	**Wireless links in the THz range using UTC photodiodes** J.-F. Lampin **P128**
14:25 - *Invited*	**14:25** - *Invited*	**14:25** - *Invited*
Optical Biopsy for Initial Diagnosis of Cutaneous Tumours – Clinical Applications E. Borisova **P104**	**Multiterawatt hybrid (solid/gas) femtosecond systems of visible range** L. Mikheev **P116**	**Nanometer Plasma Field Effect Transistors for Detection of Terahertz Radiation** W. Knap **P129**
14:50	**14:50**	**14:50**
Laser modification of pore system in cartilage matrix – a novel approach for cartilage repair E. Sobol **P105**	**Optimization of the Vulcan 20 PW chirp compensated OPCPA front end** A. Wyatt **P117**	**Terahertz plasmons in active graphene: diffusion pumping concept** M. Morozov **P130**
15:05	**15:05**	**15:05** - *Invited*
Depth-Resolved Shear Wave Imaging in Tissues using Optical Coherence Elastography K. Larin **P106**	**Millijoule, femtosecond, near infrared, ultra-high contrast front end for a Petawatt-scale diode-pumped solid state laser** H. Liebetrau **P118**	**New applications for the intense and stable Coherent Synchrotron Radiation in the THz** P. Roy **P132**
15:20	**15:20**	**15:30**
Selective photoactivity of porphyrin- polymer complexes against Gram-negative and Gram-positive bacteria A. Solovieva **P107**	**Quasi-flat-top pulse generation in a powerful Nd:glass laser operating in the saturation regime** A. Kuzmin **P119**	

15:35	15:35	15:45
Characterization of fresh water centric diatom frustules (Stephanodiscus hantzschii sp.): a type of biogenic photonic crystals A. Gogoi **P108**	**High Bandwidth measurement and control of FM-AM modulation** S. Montant **P120**	
15:50	**15:50**	
	Improved Nonlinear Cross-Polarized Wave Generation in Crystal of 42m Point Group Symmetry M. Kuzmina **P121**	

16:05-16:30 Coffee Break

16:30 - 18:00 Poster Session II

Day 5 : Friday, October 10

ROOM 1	ROOM 2	ROOM 3
08:30 - *Plenary* **Development of the PETAL laser facility and its applications in physics** D. Batani **P133**		

Biophotonics VI	Ultra-High Intensity II	Laser-Matter Interaction XI
09:15 - *Invited*	**09:15** - *Invited*	**09:15** - *Invited*
Monitoring of PDT: What is the best for clinical practice N. Shakhova **P134**	**Ultrafast Laser Produced Non-equilibrium Warm Dense Matter** Y. Tsui **P139**	**Femtosecond laser filamentation: a tool from micro-nano surface structure fabrication to microwave energy guiding** J. Lin **P145**
09:40 - *Invited*	**09:40** - *Invited*	**09:40** - *Invited*
Impact of nanodiamonds on red blood cells studied by laser techniques A. Priezzhev **P135**	**Relativistic intensity sub-5-femtosecond laser pulses and their applications** L. Veisz **P140**	**Air lasing induced by tunnel ionization: from molecular physics investigation to remote sensing application** Jinping Yao **P146**

10:05-10:30 Coffee Break

Biophotonics VII	Ultra-High Intensity III	Laser-Matter Interaction XII
10:30 - *Invited*	**10:30** - *Invited*	**10:30** - *Invited*
Fluence compensated optoacoustic image reconstruction for quantitative imaging M. Frenz **P136**	**High field physics at ALLS: from electron acceleration to x-ray coherent imaging** J.-C. Kieffer **P141**	**Diamond deposition in open air using laser resonant vibrational excitation of precursor molecules** Y. Lu **P147**
10:55 - *Invited*	**10:55** - *Invited*	**10:55**
Optical elastography – Imaging tissue stiffness at high resolution D. Sampson **P137**	**Time-resolved XANES as an atomic-level diagnostic of non-equilibrium transition from solid to Warm Dense Matter** F. Dorchies **P142**	**Estimation of the wave process formed on the melt surface during laser cutting of steel** A. Dubrov **P148**

11:20	**11:20**	**11:10**
Laser assessment of human and rat blood microrheology alterations in Diabetes Mellitus A. Lugovtsov **P138**	**Femtosecond laser-induced damage of optical thin film materials, from the UV to the IR** L. Gallais **P143**	**Effect of high power CO2 and Yb:YAG laser radiation on the characteristics of TIG arc in atmospherical pressure argon and helium** S. Wu **P149**
11:35	**11:35**	**11:25**
	Laser-induced damage thresholds of high-reflective coatings for PW lasers A. Hervy **P144**	**High Fundamental Repetition Rate Fiber Laser Using a 45°-Tilted Fiber Grating** Z. Zhang **P150**

11:50 -12:15 Concluding remarks
V. Konov and M. Sentis

12:15-14:00 Lunch (on your own) and departure

Monday 6th October

ALT-2014

Transient optical properties of ultra-short laser affected dielectric and semiconductor

Eugene Gamaly

Laser Physics Centre, Research School of Physics and Engineering
The Australian National University, Canberra ACT 0200, Australia

eugene.gamaly@anu.edu.au

Interaction of intense fs-laser pulses with different media has broad areas of research and applications in micromachining of surfaces and in the direct fabrication of complicated 3D structures for photonics [1]. Ultra-short-laser induced micro-explosion confined in the bulk of a solid creates TPa range pressure allowing formation of novel materials [2]. These studies now are shifting to shorter time and space scales (respectively of the order of laser period and nanometer) [3] aiming for applications in photonics and photo-electronics.

In this talk I present the analysis of transient permittivity of laser-excited dielectric and semiconductor from the initial unperturbed state up to the ablation threshold. The competition between the electrons' oscillations in the laser field, collisions and ionization non-linearity results in unexpected minima and maxima in permittivity and reflection of swiftly excited dielectric on a few fs time scale. The impact ionization rate with these processes accounted for has a non-linear dependence on laser intensity. The comparative analysis of the transient permittivity of silica and silicon at 800 and 1300 nm reveals the differences in excitation of narrow and wide band gap dielectrics and distinguishing a metal-like state of the ionized dielectric from that in metals. The transient permittivity as function of local fluence can be directly mapped on the fluence distribution in time and space in real experiments. The effects of laser polarization on the ionization rates, electronic heat conduction and absorption are also discussed.

The exact definition of the ionization threshold through the transient permittivity indicates on the metallisation of dielectric and defines the proper experimental conditions for direct threshold observation.

Summing up, the fine-tuning of laser and material parameters may result in creation of unusual optical properties such a swift metallization of silicon useful for applications in photonics and photo-electronics. In conclusion unresolved problems and some experimental schemes are presented and discussed.

1. Eugene Gamaly, *Femtosecond Laser-Matter Interaction: Theory, Experiments and Applications,* (2011), Pan Stanford Publishing

2. A. Vailionis, E. G. Gamaly, V. Mizeikis, Wenge Yang, A. V. Rode & S. Juodkazis, Nature communications (2011) | DOI: 10.1038/ncomms1449 *"Evidence of super-dense aluminum synthesized by ultrafast micro-explosion"*

3. E. G. Gamaly and A. V. Rode, JOSA B, (2014) (in press) *Transient optical properties of dielectric and semi-conductor excited by the ultra-short laser pulse*,

Ultrashort pulse induced nanogratings inside glass – fundamentals and applications

S. Nolte[1], F. Zimmermann[1], S. Richter[1], A. Plech[2]

1- Institute of Applied Physics, Abbe Center of Photonics, Friedrich-Schiller-Universität Jena, Max-Wien-Platz 1,07734 Jena, Germany

2- Institute for Synchrotron Radiation, Karlsruhe Institute of Technology, PO box 3640, 76021 Karlsruhe, Germany

Main author email address: stefan.nolte@uni-jena.de

When intense femtosecond laser pulses are focused into a glass substrate, self-organized periodic nanostructures, so-called nanogratings, can be generated, which show strong form birefringence due to their anisotropic structure [1,2]. Emerging after several laser pulses [2,3] they are oriented perpendicular to the laser polarization (see Fig. 1(a)) and their properties depend on the processing parameters [4]. Potential applications include simple phase elements [4] to devices enabling the generation of optical vortices [5]. Nevertheless the self-organized formation process is not yet fully understood. One reason is that the actual structure of the nanogratings is difficult to explore. Due to the small feature size optical microscopy cannot be used and electron microscopic investigations require sample preparations leading to blurring and distortion of essential structure details.

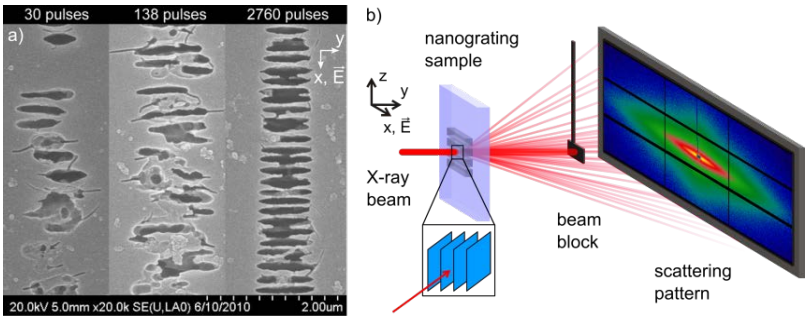

Figure 1 SEM micrograph of gratings after etching with hydrofluoric acid (a) and schematic of the SAXS measurement (b).

We employed small angle X-ray scattering (SAXS) as well as focused ion beam (FIB) milling and scanning electron microscopy (SEM) to determine the principal constituents of nanogratings in fused silica and borosilicate [6,7,8]. The results reveal that with ongoing illumination nanometric voids grow, join and organize in grating planes. While the nanograting period in fused silica is roughly determined by half of the inscribing laser wavelength, borosilicate shows a period five times smaller.

We gratefully acknowledge financial support from Deutsche Forschungsgemeinschaft DFG (priority program 1327). Furthermore, we thank the Swiss Light Source (cSAXS beamline at Paul Scherrer Institute, Villigen, CH) for the beamtime. Sören Richter acknowledges supported by the Hans L. Merkle Stiftung.

[1] Y. Shimotsuma, P.G. Kazansky, J. Qiu and K. Hirao, "Nanostructuring of transparent materials by ultrashort light pulses," Phys. Rev. Lett. 91, 247405 (2003).
[2] R. Taylor, C. Hnatovsky, and E. Simova, "Applications of femtosecond laser induced self-organized planar nanocracks inside fused silica glass," Laser & Photon. Rev. 2, 26–46 (2008).
[3] S. Richter, M. Heinrich, S. Döring, A. Tünnermann, and S. Nolte, "Formation of Femtosecond Laser-Induced Nanogratings at High Repetition Rates", Appl. Phys. A 104, 503-507 (2011).
[4] S. Richter, M. Heinrich, S. Döring, A. Tünnermann, S. Nolte, U. Peschel, "Nanogratings in fused silica: Formation, control, and applications," J. Laser Appl. 24(4), 4020081-4020088 (2012).
[5] M. Beresna, M. Gecevičius, P.G. Kazansky, and T. Gertus, "Radially polarized optical vortex converter created by femtosecond laser nanostructuring of glass", Appl. Phys. Lett. 98, 201101 (2011).
[6] S. Richter, A. Plech, M. Steinert, M. Heinrich, S. Döring, F. Zimmermann, U. Peschel, E.-B. Kley, A. Tünnermann, S. Nolte, "On the fundamental structure of femtosecond laser-induced nanogratings," Laser Photon. Rev. 6(6), 787-792 (2012).
[7] F. Zimmermann, A. Plech, S. Richter, S. Döring, A. Tünnermann, and S.Nolte, "Structural evolution of nanopores and cracks as fundamental constituents of ultrashort pulse-induced nanogratings," Appl. Phys. A 114, 75 (2014).
[8] F. Zimmermann, A. Plech, S. Richter, A. Tünnermann, and S.Nolte, "Ultrashort laser pulse induced nanogratings in borosilicate glass," Appl. Phys. Lett. 104, 211107 (2014).

Stuttgart, 10.3.2014

Laser processing of CFRP: Fundamental energy transport mechanisms

R. Weber[1], C. Freitag[1,2], M. Wiedenmann[1], V. Onuseit[1], T. Graf[1],
T.V. Kononenko[3,4], M.S. Komlenok[3,4], V.I. Konov[3,4]

[1]*Universität Stuttgart, Institut für Strahlwerkzeuge (IFSW), Pfaffenwaldring 43, 70569 Stuttgart, Germany*
[2]*GSaME Graduate School of Excellence advanced Manufacturing Engineering, Nobelstrasse 12, 70569 Stuttgart, Germany*
[3]*Natural Sciences Center, General Physics Institute, Vavilov str. 38, 119991 Moscow, Russia*
[4]*National Research Nuclear University „MEPhI“, Kashirskoye shosse 31, 115409 Moscow, Russia*

High quality laser structuring and cutting of Carbon Fibre Reinforced Plastics (CFRP) is very challenging. The main reason is the low damage threshold of the plastic matrix material. In the best case, the whole laser energy is just deposited in the processed area and used for ablation of both, the carbon fibres and the matrix material.
However, several energy transport mechanisms distribute a part of the incoming laser energy into the vicinity of the interaction region creating more or less severe damage to the matrix material. Important mechanisms are heat conduction, scattering of the laser light and the ablating hot vapor.
In the present talk, these fundamental energy transport mechanisms will be summarized and their contribution to the matrix damage will be discussed

LASER NANOMANUFACTURING

Boris N. Chichkov

Laser Zentrum Hannover e.V., Nanotechnology Department, Hollerithallee 8, 30419 Hannover, Germany

I will report on the development of laser-based nanomanufacturing technologies for applications in photonics and medicine. Fabrication of 3D nanostructured objects by two-photon polymerization (2PP) of photosensitive materials, generation of microstructures and nanoparticles by laser ablation, and direct laser printing of nanoparticle arrays will be discussed. Applications of these techniques for the realization of photonic and plasmonic components, sensors, biomedical implants, and tissue engineering constructs will be demonstrated.

Two examples of laser printed Si nanoparticles and living cells are shown below.

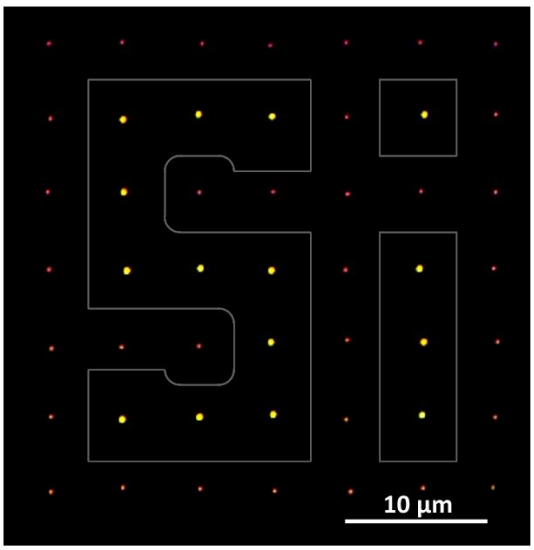

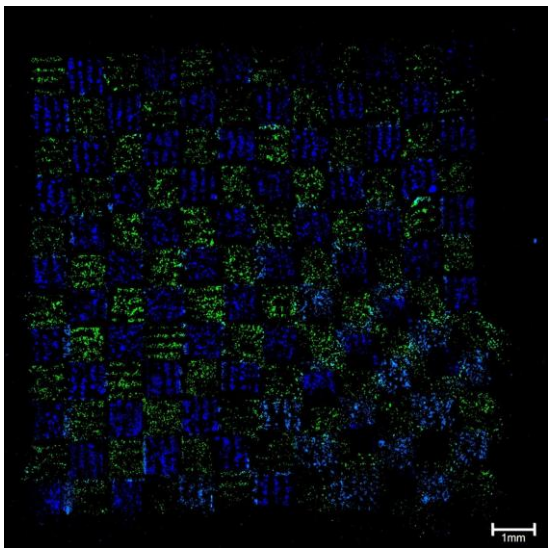

Femtosecond-laser driven electron dynamics and resulting nanoscale surface instabilities

A.A. Ionin,[1] V.I. Emel'yanov,[2] S.I. Kudryashov,[1] S.V. Makarov[1]

[1] *P.N. Lebedev Physical Institute of RAS, 119991 Moscow, Russia*
[2] *Physics Department, Moscow State University, 119899 Moscow, Russia*

Electronic dynamics induced by femtosecond laser pulses in metals was studied by diverse experimental methods to reveal the involved electron temperature-dependent emission, transport and electron-lattice coupling effects. On ablation timescales, different nano- and micro-scale surface relief instabilities – nanojets, nanocrowns, etc. – were driven by a single- or multiple ultrashort laser pulses and studied in details. The underlying instability mechanisms and related hydrodynamic models based on Kuramoto-Sivashinsky equation are discussed.

Formation of Micro- and Nanostructures on Solid Surfaces by ArF-laser Radiation

S. Mikolutskiy[1], V. Khomich[1], V. Shmakov[2], V. Yamshchikov[1]

1- Institute for Electrophysics and Electric Power RAS, 18, Dvortsovaya nab., 191186 St.-Petersburg, Russia
2- A.M. Prokhorov General Physics Institute RAS, 38, Vavilov st., 119991 Moscow, Russia

mikolserg@mail.ru

The paper describes the mechanisms of micro- and nanostructure formation on the surface of such industrial materials as titanium, germanium and zirconium dioxide under the action of ArF-laser radiation. In our work we use only one laser beam without masks and auxiliary tip of the atomic force microscope. This approach is called "direct" laser nanostructuring [1,2]. Such a method seems to be essentially simpler and more flexible as on the one hand using of small laser beam allows to achieve the highly local effect and on the other hand a computer-controlled beam scanning with a high pulse repetition rate allows to structure large enough surface areas.

In the paper we present experimental results for surface micro- and nanostructuring of industrial materials by ArF-laser with wavelength of 193 nm. Figure 1 shows 3D photographs of germanium and zirconium dioxide irradiated by ArF-laser. Images were made with atomic force microscope (AFM) in peripheral low-intensity region of the laser spot for germanium and in the center of laser spot for zirconium dioxide.

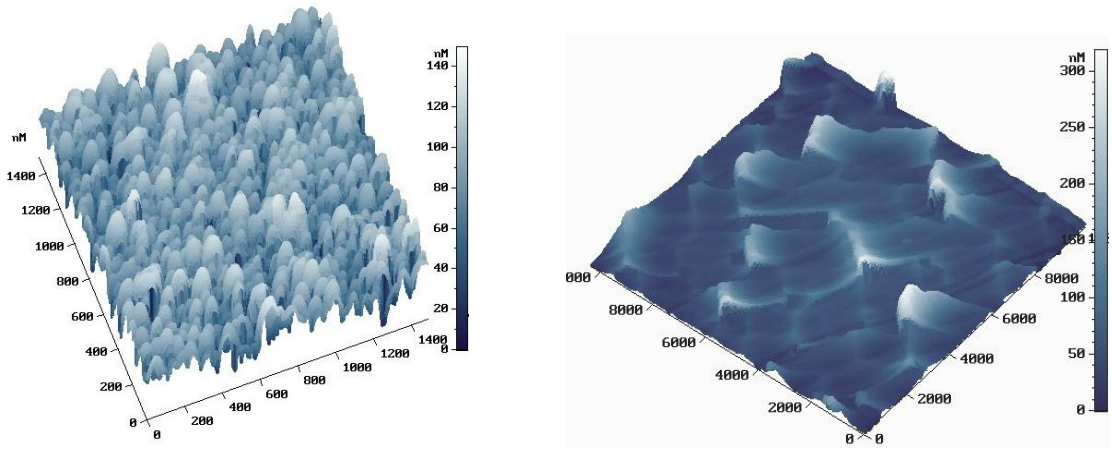

(a) (b)

Figure 1 3D photographs of material surface after irradiation by nanosecond ArF-laser with wavelength of 193 nm (a) germanium; (b)zirconium dioxide.

In this work we try to analyze the form of surface nanoreliefs and explain the mechanisms of micro- and nanostructure formation. So we propose theoretical model of nanostructure formation on solid surface melted by nanosecond laser pulses [3] for similar structures of titanium and germanium, and mechanism based on the nonlinear relaxation of temperature-induced stresses [4] for zirconium dioxide.

[1] K.E. Lapshin, A. Z. Obidin, V. N. Tokarev, V. Yu. Khomich, V. A. Shmakov, and V. A. Yamshchikov, Nanostructure Formation on the Surface of Silicium Nitride under the action of F_2-laser, Fiz. Khim. Obrab. Mater., vol. 1, pp. 43-48, (2008). [in Russian]
[2] V.N. Tokarev, V.Yu. Khomich, V.A. Shmakov, V.A. Yamshchikov, Formation of Nanostructures during Laser-Induced Melting of Solid Surfaces, Doklady Physics, vol. 53 (4), pp. 206-210, (2008).
[3] S.I. Mikolutskiy, V.Yu. Khomich, V.A. Shmakov, V.A. Yamshchikov, Formation and Growth of Nanostructures on the Surface of Solids Melted by Laser Pulses, Nanotechnologies in Russia, vol. 6 (12), pp. 733-738, (2011).
[4] D.V. Ganin, S.I. Mikolutkiy, V.N. Tokarev, V.Yu. Khomich, V.A. Shmakov, V.A. Yamshchikov, Formation of micron and submicron structures on a zirconium oxide surface exposed to nanosecond laser radiation, Quantum Electronics, vol. 44 (4), pp. 317-321, (2014).

Electrofluidics fabricated by femtosecond laser direct writing

Jian Xu, Katsumi Midorikawa, Koji Sugioka

RIKEN Center for Advanced Photonics, 2-1 Hirosawa, Wako, Saitama 351-0198, Japan

jxu@riken.jp; ksugioka@riken.jp

Focusing the femtosecond (fs) laser beam in glass materials with a proper pulse energy enables us to induce localized modification around the focal volume due to the highly confined nonlinear absorption. Translation of the sample with PC control performs the localized modification in three-dimensional (3D) manner. Such modification allows us to create various functionalities in glass such as optical functions and microfluidic functions. Furthermore, these functionalities can be easily integrated in a single glass chip to realize optofluidics, which are beneficial for many practical biochip applications [1]. Recently, we have developed a novel technique consisting of fs laser direct-write ablation followed by electroless metal plating, by which electrical functions can be integrated [2]. For fabrication of electrofluidics (microfluidics integrated with microelectric devices), 3D glass hollow structures with the smooth inner surface are first prepared by fs laser direct-write modification followed by annealing, successive chemical etching and additional annealing processes. Then by the laser direct writing using the same laser with larger pulse energy, the space-selective ablation on the internal walls of fabricated glass hollow structures is performed. With the help of successive electroless metal plating, the selective deposition of metal microstructures is realized on laser-abated areas in/on glass substrates. The mechanism for space-selective metallization is discussed in detail. To improve the qualities of direct-write ablation and consequent metal deposition, water-assisted ablation is proposed. The developed technique is applied to fabricate electrofluidics in which microheaters are integrated into the microfluidic channels to control the temperature of liquid samples for enhancement of chemical reactions. Additionally, another type of electrofluidics possessing metal microelectrodes with 3D flexible configurations in glass microchannels successfully demonstrates the electrical manipulation of biological samples such as electro-orientation and electro-taxis.

Reference:

[1] K. Sugioka and Y. Cheng, *Lab Chip* 12, 3576-3589 (2012).

[2] J. Xu, et al., *Lab Chip* 13, 4608-4616 (2013).

Femtosecond laser nanoablation of biodegradable polymer

M. Terakawa

Department of Electronics and Electrical Engineering, Keio University
3-14-1, Hiyoshi, Kohhoku-ku, Yokohama, Kanagawa, JAPAN 223-8522,

Author email address: terakawa@elec.keio.ac.jp

Femtosecond laser provides high-precision processing without heat-affected zone and thus playing an increasing role in biology and medicine as a method for precise ablation of biomaterials. We have been studying a laser processing of biodegradable polymers by enhanced optical near field and scattered far field excited by fs laser pulse. The nanoablation and fabricated precise structures open up emerging applications of femtosecond for biomedicine including drug delivery and tissue engineering.

Enhanced optical field can be generated in the vicinity of a nanostructure when femtosecond laser is irradiated. The combination of near-field optics and ultrafast optics can realize nanoablation of materials including biomaterials [1]. We have demonstrated simultaneous perforation of multiple cells by using femtosecond laser and biodegradable polymer spheres [2-4]. Nanoperforation of hollow polymer microcapsules was also demonstrated by the enhanced optical field generated at a spot on the shell of the microcapsule, which was excited by a femtosecond laser irradiation (Fig. 1(a)) [5]. By using such techniques, delivery and controlled release of drug molecules can be achieved.

The use of biodegradable polymers as a scaffold in tissue engineering has attracting increasing attention due to its high biocompatibility and mechanical strength. The interference of scattered far field and incident waves enables to fabricate ripple structure on a biodegradable polymer. We demonstrated ripple structure formation on poly-L-lactic acid (PLLA) film by using fs laser pulses. Figure 1 (b) shows the formation of laser-induced periodic surface structure (LIPSS) on the surface of PLLA. High-spatial frequency LIPSS (HSFL) was observed, which would contribute to scaffold fabrication in tissue engineering by controlling cell adhesive properties on the surface.

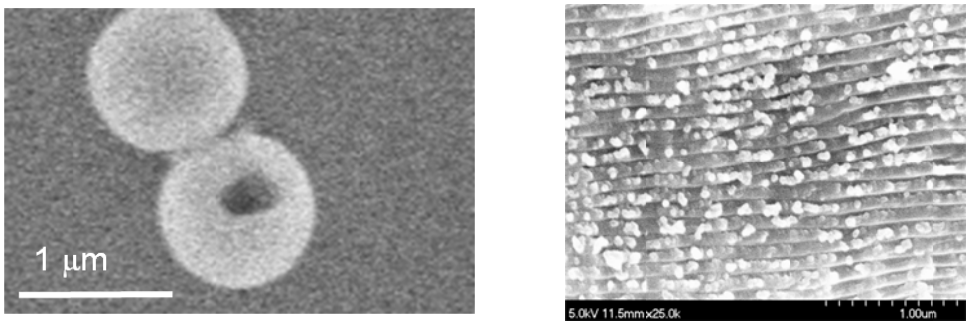

(a) (b)

Figure 1 (a) Nanoablation of a shell of microcapsule. Highly enhanced optical intensity was generated at a spot on the shell which in turn contribute to nanoperforation. Femtosecond laser pulses were weakly focused to spot size of 300 μm, enabling the simultaneous treatment of multiple microcapsules. (b) SEM image of ripple structure fabricated on PLLA surface by femtosecond laser irradiation. The incident wavelength, laser fluence, and number of pulses were 400 nm, 400 mJ/cm^2, and 5000.

[1] M. Terakawa, et al., Enhanced localized near field and scattered far field for surface nanophotonics applications, Progress in Quantum Electronics, vol. 36, pp. 194-271 (2012).
[2] M. Terakawa and Y. Tanaka, Dielectric microsphere mediated transfection using femtosecond laser, Opt. Lett., vol. 36, pp. 2877-2879 (2011).
[3] M. Terakawa, et al., In vitro perforation of human epithelial carcinoma cell with antibody-conjugated biodegradable microspheres illuminated by a single 80 fs near-infrared laser pulse, Int. J. Nanomed., vol. 7, pp. 2653-2660, (2012).
[4] T. Mitsuhashi and M. Terakawa, Evaluation of parameters influencing the molecular delivery by biodegradable microsphere-mediated perforation using femtosecond laser, J. Biomed. Opt., vol. 19, pp. 015003/1-7 (2014).
[5] M. Terakawa, et al., Near-infrared femtosecond laser-triggered nanoperforation of hollow microcapsules, Op. Exp., vol. 21, pp. 15604-12610, (2013).

Fundamentals of surface modification after irradiation of silicon with ultrashort laser pulses: from ripples to spikes

G. D. Tsibidis[1*], P. A. Loukakos[1], C. Fotakis[1,3], E. Stratakis[1,2]

1) Institute of Electronic Structure and Laser (IESL), Foundation for Research and Technology (FORTH), N. Plastira 100, Vassilika Vouton, 70013, Heraklion, Crete, Greece

2) Department of Materials Science and Technology, University of Crete, 710 03 Heraklion, Crete, Greece.

3) Physics Department, University of Crete, Heraklion 71409, Crete, Greece

** tsibidis@iesl.forth.gr, phone: 00302810391912, fax: 0030-2810391569*

The fundamentals of the physical mechanisms and simulation techniques are employed to conduct a thorough investigation of ultrashort pulsed laser induced surface modification due to conditions that result in a superheated melted liquid layer and material evaporation. The proposed theoretical model aims to address the laser-material interaction in conditions which lead to mass removal in combination with a hydrodynamics-based scenario of the crater creation and ripple formation following surface irradiation with single and multiple temporal separated pulses [1, 2]. The development of the periodic structures with an orientation perpendicular to the electric of the laser beam is based on a synergy of electron excitation and capillary wave solidification and the interference of the incident wave with a surface plasmon wave [3]. Details of the surface morphology attained are elaborated as a function of the imposed conditions and hydrodynamical principles and results are tested against experimental data. The theoretical framework aims to offer a thorough elucidation of laser-matter interaction fundamentals and facilitate production of well-defined micro/nanostructures with preferable optical properties.

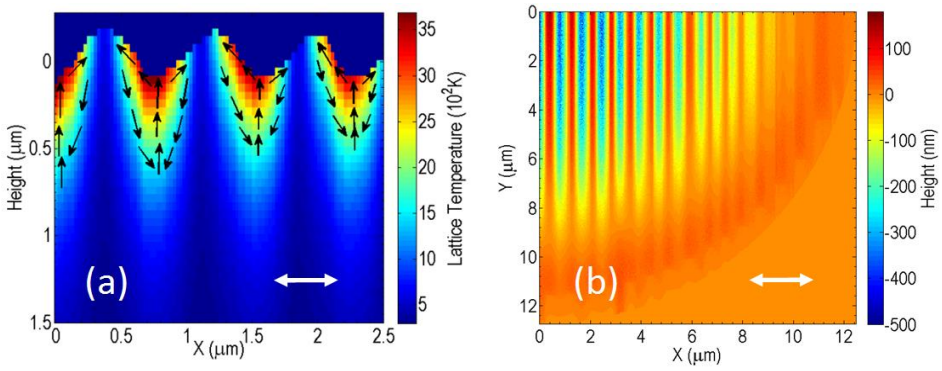

Figure 1. (a) Spatial distribution of lattice temperature at t=1ns for ten pulses. (Arrows indicate flow movement), (b) Ripple pattern for ten pulses, (fluence=0.6J/cm^2,pulse duration=430fs). (Double-ended arrow indicates the laser beam polarisation).

[1]. Barberoglou M, Tsibidis GD, Gray D, Magoulakis E, Fotakis C, Stratakis E, Loukakos PA: **The influence of ultra-fast temporal energy regulation on the morphology of Si surfaces through femtosecond double pulse laser irradiation.** *Applied Physics A: Materials Science and Processing* 2013, **113:**273–283.

[2]. Tsibidis GD, Stratakis E, Loukakos PA, Fotakis C: **Controlled ultrashort-pulse laser-induced ripple formation on semiconductors.** *Applied Physics A* 2014, **114:**57-68.

[3]. Tsibidis GD, Barberoglou M, Loukakos PA, Stratakis E, Fotakis C: **Dynamics of ripple formation on silicon surfaces by ultrashort laser pulses in subablation conditions.** *Physical Review B* 2012, **86:**115316.

Femtosecond Laser Tuning of Silicon Resonant Optical Devices

Y.Y. Tsui*, D. Bachman, Z. Chen, R. Fedosejevs and V. Van

Department of Electrical and Computer Engineering, University of Alberta, Edmonton, Alberta T6G 2V4, Canada

**tsui@ece.ualberta.ca*

Silicon is increasingly being embraced as a materials platform for integrated photonics due to its small footprint and relatively low-cost fabrication. However, phase sensitive integrated silicon photonics components cannot be fabricated across an entire wafer with enough precision to function properly without any post-fabrication tuning [1]. Tuning of silicon photonic components is usually achieved using local heaters placed near the device waveguide at the cost of extra power and fabrication complexity [1].

We have demonstrated femtosecond laser pulses can be used as a tool for post fabrication tuning of resonant optical devices including silicon on insulator (SOI) microring resonator [2, 3] and silicon DPSK demodulator.

The technique is able to tune the operational wavelength of the SOI resonators bi-directionally to a desired wavelength by varying the laser fluences by inducing amorphization or ablation [2, 3]. In order to approach and obtained desired resonant operational wavelength, step by step multiple shot tuning on a resonator is required. The growth of amorphous silicon under multiple shot laser excitation is studied by optical properties and Raman spectroscopy, and the ablation threshold on amorhous silcon is compared with that on a fresh crystalline silicon. The effect of this tuning technique on quality factor of the microring resonator devices is important for actual application and will be discussed.

We have also applied the technique for post-fabrication trimming of a silicon DPSK demodulator with a single femtosecond laser pulses. The trimming technique permanently converts a thin layer of the crystalline silicon waveguide to amorphous silicon, increasing the effective index of refraction of the waveguide which enables phase tuning. The technique is faster and simpler to implement than other demonstrated permanent trimming mechanisms [4] and may be applied to tune any phase sensitive silicon component.

[1] Krishnamoorthy et al., “Exploiting CMOS manufacturing to reduce the tuning requirements for resonant optical devices,” Opt. Express, 18, 23598 (2010).
[2] Bachman, et al., "Femtosecond laser tuning of silicon microring resonators", Opt. Lett. 36, 4695 (2011).
[3] Bachmen, et al., "Permanent fine tuning of silicon microring devices by femtosecond laser surface amorphization and ablation", Opt. Express 21, 11048 (2013).
[4] Canciamilla et al., “Photo-induced trimming of chalcogenide-assisted silicon waveguides,” Opt. Express, 20, 15807 (2012).

New High-Pressure Silicon Phases Formed in Fs-Laser Induced Confined Microexplosion

L. Rapp[1,2], B. Haberl[3], C. J. Pickard[4], J. E. Bradby[3], J. S. Williams[3], E. G. Gamaly[1], A. V. Rode[1]

[1]*Laser Physics Centre, Research School of Physics and Engineering, The Australian National University, Canberra ACT 0200 Australia*
[2]*Laboratoire LP3, Aix-Marseille Universite, FR-13288, France*
[3]*Electronic Materials Engineering, Research School of Physics and Engineering, The Australian National University, Canberra ACT 0200 Australia*
[4]*Department of Physics and Astronomy, University College London, London WC1E 6BT, UK*

avr111@physics.anu.edu.au

Intense ultrafast laser pulses tightly focused in the bulk well below the surface of transparent material interact with matter in the condition where the conservation of mass is fulfilled. Plasma produced by the laser pulses in confined geometry generates strong shock waves with the pressure at the shock wave front exceeding several times the Young modulus of solid material. Irreversible structural changes, often considered as damage, occur at an intensity level above the optical breakdown threshold. The essential distinctive feature of laser-driven microexplosion is that the modified material remains compressed and confined in a strongly localized region inside a bulk, and can be investigated later by Raman spectroscopy, electron beam, x-ray, and other structural diagnostics techniques. The extreme conditions produced in the ultrafast laser driven micro-explosion can serve as a novel microscopic laboratory for high-pressure studies above 10^{12} Pa (10 Mbar), well beyond the pressure levels achieved in diamond anvil cell.

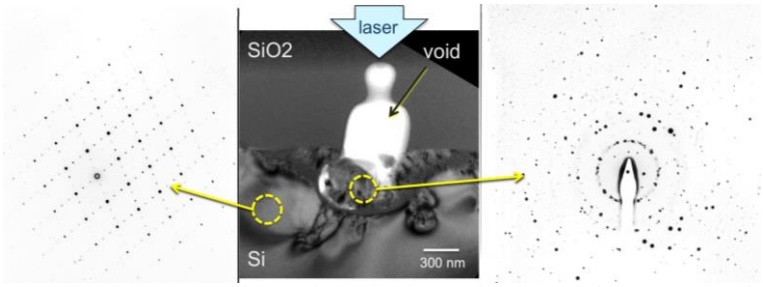

Figure 1. Transmission electron microscope image of a void formed by a single fs-laser pulse focused on Si-surface buried under a layer of SiO_2 (centre) and electron diffraction pattern from a pristine diamond-cubic silicon (left) and from a shock-wave affected area showing the presence of new tetragonal high-pressure phases of Si-BT8 and Si-S12 [3].

Here we expand the confined microexplosion method into the domain of non-transparent materials such as Silicon [1,2]. In this presentation we report the observation of two new pressure-induced tetragonal metastable polymorphs of Si formed via these highly non-equilibrium conditions of a confined microexplosion. Electron diffraction analysis of laser-modified Si clearly reveals the presence of crystal structures currently not assigned to any known phases of silicon. Silicon polymorphs, which are metastable in ambient conditions, under pressure demonstrate a wide range of characteristics, from semiconducting to metal, and even predicted to form superconducting phases, signifying their scientific and technological importance. In addition to some diffraction spots that we can not identify, three tetragonal phases are observed, two of which BT8 and ST12 have been predicted theoretically [4,5] but have previously never been observed experimentally, and one (Si-VIII) has only been observed in a single experimental study under very rapid unloading [6]. The formation of these tetragonal polymorphs, reliably repeatable in several microexplosion experiments, is evidence that Si has undergone pressure-induced transitions into the realm of the metallic high-pressure phases that are formed above 11 GPa [7]. The ability of ultrafast lasers to locally modify the electronic properties of silicon with sub-micron precision via non-equilibrium pressure/temperature processes with repetition rates up to and above 10^5 shots per second opens up novel opportunities for nanoelectronics through the incorporation of such nanostructures into semiconductor devices.

[1] E. G. Gamaly, L. Rapp, V. Roppo, S. Juodkazis and A. V. Rode, New J. Phys. **15**, 025018 (2013).
[2] L. Rapp, B. Haberl, J. E. Bradby, E. G. Gamaly, J. S. Williams, A. V. Rode, Appl. Phys. A **114**, 33-43 (2014).
[3] L. Rapp, B. Haberl, C. J. Pickard, J. E. Bradby, J. S. Williams, E. G. Gamaly, A. V. Rode, under preparation for publication.
[4] J.-T. Wang, C. Chen, H. Mizuseki, Y. Kawazoe, Phys. Rev. Lett. **110**, 165503 (2013).
[5]. B. D. Malone, J. D. Sau, M. L. Cohen, Phys. Rev. B **78**, 035210 (2008).
[6]. Y.-X. Zhao, F. Buehler, J. R. Sites, I. L. Spain, Sol. State Comm. **59**, 679-682 (1986).
[7]. J. C. Jamieson, Science **139**, 762-764 (1963).

Laser-inuced synthesis of nanostructured carbon materials

Arakelian S., Kutrovskaya S., Kucherik A., Nogtev D., Osipov A.

Department of Physics and Applied Mathematics, Stoletovs' Vladimir State University,

Gorky st. 87, Vladimir, 600000 Russia

Phone: +7(4922) 477796

Fax: +7(4922) 333369

E-mail: kucherik@vlsu.ru

Synthesis of new carbon materials by laser irradiation of carbon target is an actual branch of laser physics. Laser sources with different pulse duration allow to change the heating rate of carbon with realization of different transition scenarios such as solids-liquid-vapor.

The obtaining of different allotropic forms of carbon depends on the conditions (pulse duration, energy, repetition rate etc.) of laser action.

Last years, methods of laser irradiation on the carbon target in a liquid medium are actively developed. In this case the formation of a cavitation bubble, which can provide additional pressure on the target surface, the value of which can reach values of 10 GPa depends on laser irradiation conditions. Also, using laser setups with femtosecond pulse duration near the target surface, leads to a transition of the liquids into the "liquid plasma", which ensures both high temperature and high pressure in the area of influence.

Experiments of laser action on carbon target in the air and in water are presented in this paper.

For the realization of different regimes of laser surface modification of the target and the formation of micro- nanoparticles in a liquid the YAG: Nd laser with a pulse duration from 0.5 ms up to 20 ms (pulse energy up to 50J) and the Ti: Sp femtosecond laser with 50 fs pulse duration (pulse energy up to 0.01 J) were applied.

Melting processes were observed during the laser irradiation of samples in air by millisecond laser.

The dependence on the laser beam, pulse duration, focusing conditions leads to a formation of domains and centers of melting with dimensions which are defined by the conditions of the experiment

During the process of laser irradiation of the target in the water, the surface layer explosion of the target due to local boiling supercritical fluid, "cold" ablation, solid-phase modification of the sample surface were observed. During the colloidal droplets deposition the structures like carbon foam were observed.

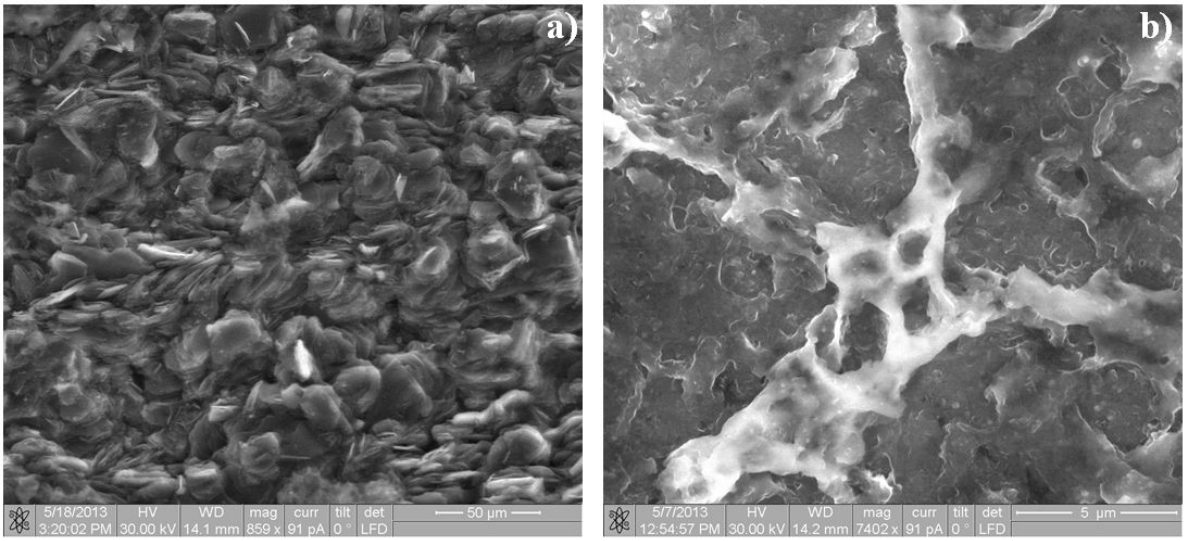

Figure 1 Laser modification of carbon after laser irradiation of pyrolytic graphite surface (a); deposition of colloidal system after irradiation of glassy carbon (b).

Guided Melting deformation: A novel Laser nanostructuring method

P. Lorenz[1], M. Klöppel[2], F. Frost, T. Smausz[3, 4], T. Csizmadia[3], M. Ehrhardt[1], K. Zimmer[1], B. Hopp[3]

1 Leibniz-Institut für Oberflächenmodifizierung e. V., Permoserstr. 15, D-04318 Leipzig, Germany
2 Institute of Scientific Computing, Department of Mathematics, TU Dresden, D-01062 Dresden, Germany
3 Department of Optics and Quantum Electronics, University of Szeged, H-6720 Szeged, Dóm tér 9, Hungary
4 MTA-SZTE Research Group on Photoacoustic Spectroscopy, University of Szeged, H-6720 Szeged, Dóm tér 9, Hungary

pierre.lorenz@iom-leipzig.de

The fast, well-defined and cost-effective production of nanostructures in dielectric surfaces is a big technological challenge. However, these structures have a widespread field of applications. Laser methods exhibit an outstanding potential for the effective production of nanostructures. In this study a novel laser method using a laser-induced molten metal layer deformation process for the surface nanostructuring of the dielectric substrates is depicted [1-3]. Low nanosecond laser fluence irradiation with $\Phi < 1$ J/cm² of a chromium-covered fused silica surface causes melting and deformation of the metal layer where the deformation behaviour is dependent on the surface tension of the liquid metal film and the laser irradiation-induced temperature gradient. Furthermore, the stepwise deformation of the metal layer leads to a modification of the fused silica surface. An irradiation with a homogeneous beam profile result in a well-defined a circular modification (see Fig. 1 (a) (h)) where the number of circles and the diameters are dependent on the laser parameters [2]. In this case, the deformation process is mainly defined by the surface tension. Furthermore, the deformation process can be guided by laser-induced temperature gradient using lateral modulated laser beam profiles (see Fig. 1 (a) (i) and (b)). The resultant structures were studied by scanning electron (SEM) and atomic force microscopy (AFM) and the time-dependence of the melting behaviour was studied by shadowgraph measurements.

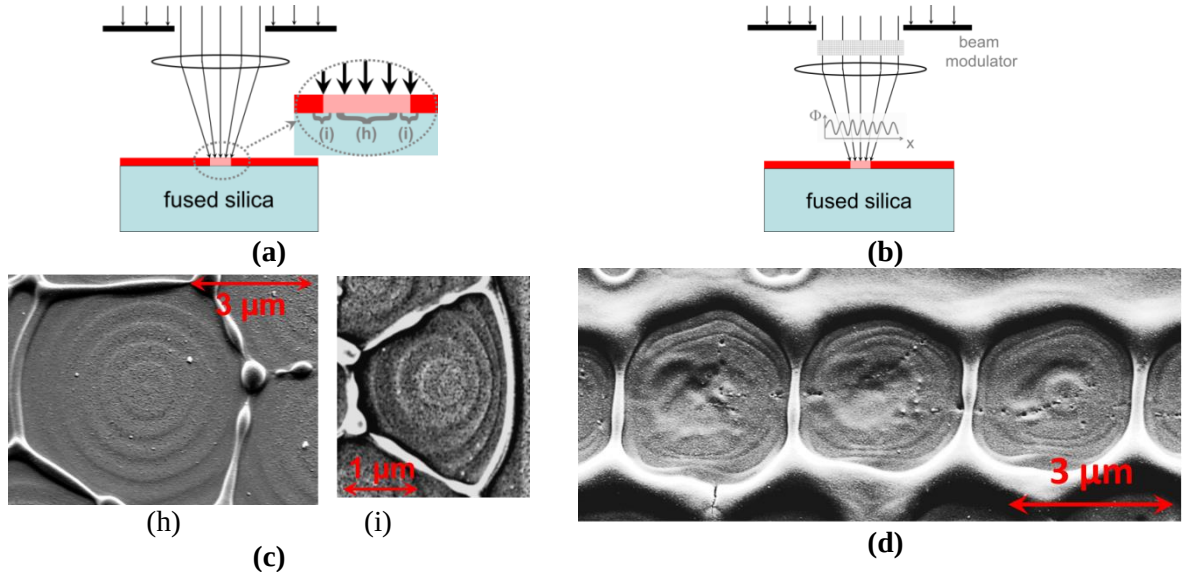

Figure 1 (a) and (b) Schematic illustration of the laser set-up for a top hat beam profile and a periodic modulated profile, respectively. SEM image of the laser-treated surface: image (c) at set-up (a) and image (d) at set-up (b).

[1] P. Lorenz, F. Frost, M. Ehrhardt, K. Zimmer, "Laser-induced fabrication of randomly distributed nanostructures in fused silica surfaces", Appl. Phys. A 111, 1025–1030, (2013)
[2] P. Lorenz, M. Klöppel, F. Frost, M. Ehrhardt, K. Zimmer, P. Li, "Laser-induced circular nanostructures in fused silica assisted by a self-assembling chromium layer", Appl. Surf. Sci. 280, 933–939, (2013)
[3] P. Lorenz, M Klöppel, F. Frost, M. Ehrhardt, P. Li, K. Zimmer, "Nanostructuring of fused silica surfaces induced by KrF excimer laser radiation: Experiment and theory", NSTI - Nanotech 1, 686–689, (2013)

Laser-Induced Cleavage of Graphene Structures and Synthesis of Nanostructured Layers on Surface of Carbon Materials

D. Abramov, S. Arakelian, D. Kochuev, S. Makov, V. Prokoshev, A. Tokareva, K. Khorkov

Vladimir State University, Gorki str., 87, 600000 Vladimir, Russia

awraam@mail.ru

Carbon is presented in modern nanomaterials the large variety of modifications. Various methods and technologies are developed to create them. Laser methods take up significant area in this diversity. Primarily laser treatment allows efficient structured the surface of carbon materials. This enables to form nanostructured carbon layers without compacting procedure. Furthermore, laser-induced splitting off the graphene layers could compete with micromechanical technology of the bundle of graphite [1], which is currently used by the majority of the experimental groups. Results of experimental studies in the field of laser synthesis of carbon nanostructures in these two directions are presented in this report.

Glassy carbon and highly oriented pyrographite (HOPG) were treated by radiation of femtosecond laser with Yb:KGW active medium in liquid nitrogen. Parameters of laser radiation: wavelength is 1029 nm, pulse duration is 300 fs, pulse energy is 0.15 mJ and pulse repetition frequency is 10 kHz. The laser beam was focused onto the sample surface to a spot with diameter 100 μm and moved along the samples surface with the speed 10 mm/s.

Laser-induced cleavage of graphite for producing graphene structures was realized under irradiation both a glassy carbon and HOPG. The difference in the structure of glassy carbon and HOPG leads to the difference in the shape of obtained structures (Figure 1). In the first case, the graphene was obtained in the form of crumpled sheets with characteristic sizes of the structures from 1 to 2 μm and sheet thickness about 20 nm (thickness of structure fold is about 40 nm). In the second case, the sheets with relatively large area of the flat surface are cleaved. Characteristic sizes of the sheets are order 10 μm and sheet thickness is about 14 nm. Geometric characteristics of the obtained graphene structures are comparable with the parameters of the objects which are most often described in the scientific publications (see review [2]). The experimental results also demonstrated the possibility of forming a nanostructured layer as an array of nanopeaks with a diameter from 30 to 100 nm on the surface of carbon materials.

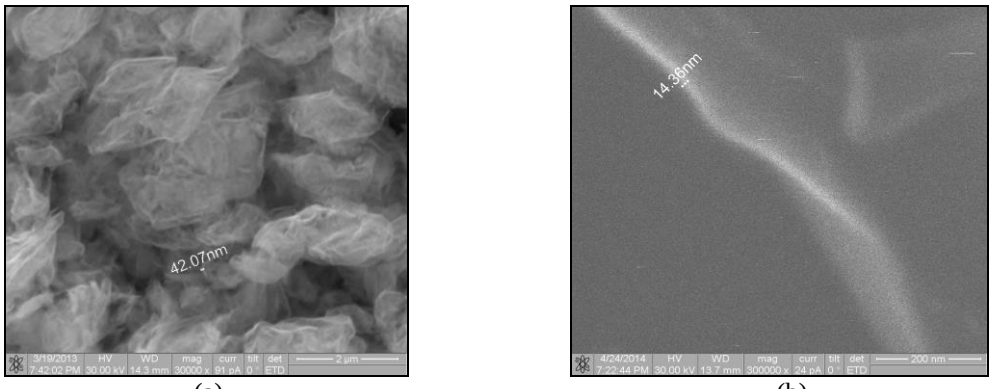

(a) (b)

Figure 1 Graphene structures, which were obtained after laser irradiation of carbon materials. (a) Results of laser-induced cleavage of a glassy carbon. (b) Results of laser-induced cleavage of a HOPG.

This study was performed as part of the state task VlSU № 2014/13 to perform state works in the field of scientific activity and also supported under grant of the President of the Russian Federation for state support of the leading scientific schools of the RF № NSh-89.2014.2 and grant of the Russian Foundation for Basic Research № 14-02-97508.

[1] K. Novoselov et al., Two-dimensional atomic crystals, PNAS, vol. 102, pp. 10451-10453, (2005).
[2] A. Eletskii et al., Graphene: fabrication methods and thermophysical properties, Phys. Usp., vol. 54, pp. 227-258, (2011).

Laser-induced nanocluster surface structures with controlled functional properties: demonstration by jump Coulomb conductivity in tunnelly coupling semiconductor islands

A.Antipov, S.Arakelian, S.Kutrovskaya, A.Kucherik, V.Prokoshev

Department of Physics and Applied Mathematics, Stoletovs Vladimir State University; Gorky str. 87, Vladimir,600000 Russia; Phone /Fax:+7(4922)333369

E-mail: arak@vlsu.ru

1. The paper represents the results of laser synthesis of semiconductor nanoparticles of PbTe by methods of both laser modification of thin films and laser evaporation of substance in liquid to produce the colloidal systems. Under a cw-laser radiation the nanoparticles become quantum dots. By drop deposition technique it has been obtained the structures with various morphology which depends on the substrate temperature. The optical and electro-physical properties of the structures can be controlled, and are very important to construct the devices of optoelectronics and photonics on new physical principles.

2. The cw-laser ablation experiments (λ=1.06 μ, laser intensity – up to 10^6 W/cm^2) with colloidal systems to induce the surface semiconductor nanostructure on substrate have been carry out to study electrical transport properties under quantum tunneling effect.

Comparison of sizes R_0 of the particles being obtained (see Table) with the value of exciton Bohr radius a_B shows that the strict condition $R_0 \leq a_B$ = 50-100 nm is true. The above comparison enables to say that the conditions of dimensional quantization are satisfied for PbTe nanoparticles. On the other hand, when the nanoparticles drop on the solid surface they are accumulated in clusters of bigger size (see Fig. 1a). So, we can study the macroscopic quantum phenomena development in dependence on R_0.

3. The main conclusion of our study is that the island conductivity is dominant for the case. An electroresistance can dramatically decrease due to spontaneous selected multichannel/parallel electron transportation trajectories (Fig. 2).

Two conditions are the vital items for that: the cluster size $a<l$, where l is the inelastic length, and distance a between two neighboring clusters less the de Broglie wavelength λ_{dB}. So, the tunneling quantum effect takes place.

For such nanostructures we demonstrated the superconductivity tendency (Fig. 1b) to increase the electrical conductivity (in several times for our case) at room temperature in comparison with homogenous sample. The fact can be explained in analogy with correlated particles/coupling pairs from two sides of the border for double electric layer/two barriers due to quantum hole being under a coherent tunnel effect.

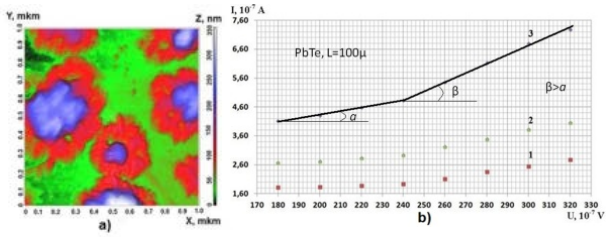

Figure 1 (a) AFM-image of deposited PbTe-clusters and (b) the Volt-Amper experimental data view in the frames of the tunneling mechanism conductivity for PbTe deposited layers under average cluster size l and average distance between clusters (a), correspondly: (1) 120 nm and 20 nm; (2) 210 nm and 8 nm; (3) 120 nm and 8 nm. The electroresistance dependence R=U/I=ctg(α,β) (less R more aβ) means more tunneling impact in the case (3).

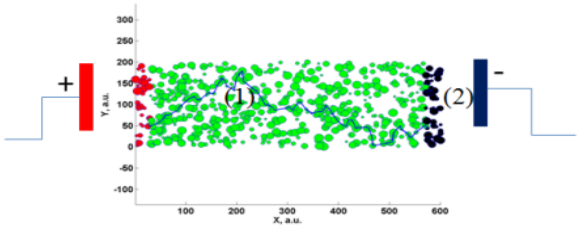

Figure 2 Spontaneous conductivity channels for semicoductor grain layer: modeling for both (1) a single electron transportation trajectory and (2) a summarize electro conductivity for different trajectories over cross-section.

Numerical Analysis of Promising Techniques of Nanoparticle Generation: Laser Ablation vs Spark Discharge at Atmospheric Pressure

A. Voloshko and T.E. Itina

Hubert Curien Lab., UMR 5516 CNRS/Lyon University, 18 rue du Prof. Benoit Lauras, 42000, Saint-Etienne, France

tatiana.itina@univ-st-etienne.fr

Laser ablation (LA) and spark discharge (SD) techniques are commonly used for nanoparticle formation. On one hand, the main advantage of the LA method is the high ablation rate and in the possibilities of changing laser parameters and background conditions. On the other hand, the major advantage of the SD technique is in the possibility of using several facilities in parallel to increase the yield of nanoparticles [1]. To optimize these processes, we consider different stages involved and analyze the resulting plasma and nanoparticle (NP) parameters. Thus, laser ablation includes [2]

(i) laser-induced material heating and laser plume formation;
(ii) plasma plume formation and its expansion in a background gas;
(iii) particle ejection, formation by expansion-driven nucleation and growth during diffusion.

Then, spark discharge is numerically analyzed. The model consists of several parts as follows

(i) streamer formation and its propagation at atmospheric pressure;
(ii) gas breakdown, plasma column formation and its expansion;
(i) electrode heating, evaporation and erosion;
(ii) particle formation by collisional growth.

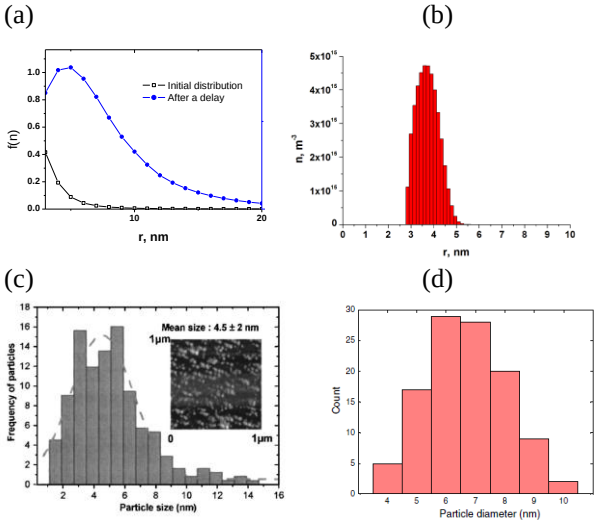

Figure 1 (a) Calculated NP size distribution for laser ablation in inert gas. (b) Calculated NP size distribution formed by spark discharge in inert gas (Ar) at atmospheric pressure. (c) Experimental size distribution obtained for steel in air [3]. (d) Typical size distribution obtained in spark experiments [4]

Based on the performed calculations, we analyze nanoparticle parameters, such as mean size and mean density. The performed analysis shows how the experimental conditions are connected with the resulted nanoparticle characteristics in agreement with previous experiments [3,4].

Support from the European Union Seventh Framework Program (FP7/2007-2013) under grant agreement n° 280765 (BUONAPART-E) is gratefully acknowledged.

[1] T.E. Itina and A. Voloshko, Nanoparticle formation by laser ablation in air and by spark discharges at atmospheric pressure, Appl. Phys. A. vol. 113, n°3, pp. 473-478,(2013) .
[2] T.E. Itina, M.E. Povarnitsyn, A. Voloshko, Laser-based synthesis of nanoparticles: role of laser parameters and background conditions, SPIE Proc. Vol. 8969, Synthesis on Photonics of Nanoscale Materials XI, 896905 (2014)
[3] A. Pereira, P. Delaporte, M. Sentis, W. Marine, A. L. Thomann, C. Boulmer-Leborgne, J. Appl. Phys. Vol. 98, pp. 064902 (2005).
[4] N. S. Tabrizi, Q. Xu, N. M. van der Pers, A. Schmidt-Ott, J. Nanopart. Res. Vol. 12, pp. 247-259 (2010).

A HYBRID ATOMISTIC-CONTINUAL SIMULATION OF ABLATION OF METALS UNDER THE ACTION OF POWERFUL FEMTOSECOND LASER PULSES

V.B. Fokin[1], P.R. Levashov[1,2], M.E. Povarnitsyn[1], K.V. Khishchenko[1,2]

1 - Joint Institute for High Temperatures RAS, Izhorskaya 13 Bldg 2, Moscow 125412, Russia

2 - Moscow Institute of Physics and Technology, Institutsky 9, Dolgoprudny 141707, Russia

Vladimir.Fokin@phystech.edu

A numerical simulation of process of interaction of femtosecond powerful laser pulses with metals is performed using a combined model, which was developed to describe effects of laser-matter interaction correctly. We use the approach [1] with modifications, which provide more precise consideration of laser energy absorption (by solving the Helmholtz equation with a given complex dielectric function), electron-phonon coupling, and electronic heat transfer in our model [2]. The Thomas–Fermi model is used to calculate the electronic heat capacity, the inter-ions interaction is described using inter-particle EAM-potential.

This combined model is useful for theoretical investigation of the dynamics of laser ablation, melting, evaporation, ionization, nucleation, shock and rarefaction wave propagation, as well as nanoparticles formation. In the present work, we perform simulation of laser ablation of aluminum by 100 fs pulses with fluence up to 20 J/cm^2 and find out the ablation crater depth as a function of laser fluence. Besides, we investigate regimes of nanoparticle formation and their size distribution. Results of modeling are in good agreement with experimental data.

[1] Ivanov D.S., Zhigilei L.V. Combined atomistic-continuum modeling of short-pulse laser melting and disintegration of metal films // Phys. Rev. B. V. 68. P. 064114, (2003)

[2] Povarnitsyn M.E., et al. // Appl. Surf. Sci. V. 258. P. 9480, (2012)

Crack-free fabrication of microchannels by femtosecond laser on a glass surface

V. Bessmeltsev, E. Bulushev, A. Dostovalov

Institute of Automation and Electrometry SB RAS, Novosibirsk, Russia
e.d.bulushev@gmail.com

Laser 3D micromachining of glass and other dielectrics without chipping and cracking is challenging due to the high brittleness and low thermal conductivity of materials. Applying ultra-short pulses with high peak intensities is a promising solution. At optimal processing modes high quality microchannels can be formed with submicron resolution, minimal heat-affected zone (HAZ), negligible damage and destruction of material. Effects of thermal gradients and stresses on glass are well studied in the case of processing using CO_2 laser and controlled fracture technique (e.g. [1, 2]), but formation of micro cracks and cleavages during melting, evaporation and ablation of substance is still not well established. In this paper we show the possibility of fabrication of microchannels with the desired spatial characteristics on surface of borosilicate BK-7 glass by a femtosecond laser. Much attention is given to the definition of laser radiation and micromachining modes at which the substrate is less damaged.

For fabrication of microchannels on a glass surface the experimental setup based on Pharos 6W laser (λ = 1026 nm, pulse duration 232 fs) and Aerotech actuators was used. A set of test objects were formed in a single-pass operation (part is depicted in Fig. 1) at pulse frequency 1 kHz, pulse energies changed in 300 nJ increment in the range of 500-1400 nJ, scanning speed was in the range of 0.1-3 mm\sec; size of workpiece – 32×32×8 mm^3; spot size – 3.7 μm. Test objects were measured by the confocal laser scanning microscope Carl Zeiss LSM 700, and height maps were reconstructed. We developed an image processing algorithm for automated inspection of height maps, which provides the detection of boundaries of channels based on the adaptive statistical criterion. For each channel characteristics were extracted: width, roughness of boundaries (R_a), maximum depth (D_m) and volume of removed material; the material removal rate was calculated (MRR).

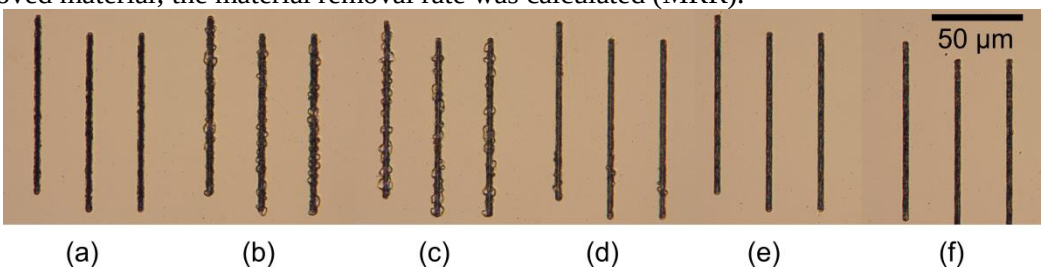

Figure 1 Test objects at glass: 500 nJ, (a)-(f) - 0.1-0.6 mm\sec, Leica DM IRB 40x.

As a result statistical models were obtained that show the dependence of characteristics of channels from pulse energy and scanning speed. Models may be applied to find optimal laser processing modes to fabricate channels with the required width in the range of 2-7 μm and depth in the range of 0.5-3 μm. In case of not optimal processing modes roughness of boundaries reached 1 μm, which corresponds well to size of cleavages. It was found that cleavages and cracks are formed at middle scanning speed, e.g. for 500 nJ at 0.2-0.4 mm\sec (Fig. 1). Moreover, interestingly, processing of glass with little chipping and cracking is achievable at low scanning speeds (0.1 mm\sec at 500 nJ), but the productivity is relatively low (~1000 μm^3\sec). We aim to verify the developed statistical models, perform multi-objective optimization of characteristics and explain the observed effects using mathematical modeling.

[1] S. Nisar, M. A. Sheikh, L. Li, and S. Safdar, The effect of material thickness, laser power and cutting speed on cut path deviation in high-power diode laser chip-free cutting of glass, Opt. Laser Technol., vol. 42, no. 6, pp. 1022–1031, (2010).
[2] J. Jiao and X. Wang, A numerical simulation of machining glass by dual CO_2-laser beams, Opt. Laser Technol., vol. 40, no. 2, pp. 297–301, (2008).

Numerical Investigation of Laser Interaction with Colloidal Nanoparticles

L. Delfour[1] and T.E. Itina[1]

1- Hubert Curien Laboratory, UMR CNRS 5516/Lyon University, Bât F, 18 rue du Prof. Benoît Lauras, Bat. B, Saint-Etienne, 42000, France

Main author email address: laure.delfour@univ-st-etienne.fr

Colloidal nanoparticles have found numerous applications in different fields and in particular in medicine [1]. Lasers are commonly used to produce these nanoparticles, but can be also considered as powerful tools of size and shape tailoring through laser-induced fragmentation. In this area, many promising experiments have already demonstrated tremendous laser capacities [2,3]. In addition, laser interactions with nanoparticles in a confined environment are considered to have possible applications for energy production. The corresponding experiments are underway in several groups too.

To better control over the laser-induced fragmentation, it is important to better understand the mechanisms involved in nanoparticle heating and fragmentation in the presence of a liquid. For this, numerical modeling is performed based on a combination of different approaches. First, we use the discrete dipole approximation method to calculate absorption of nanoparticle ensemble. Then, we apply two-temperature model to study particle heating, together with the third equation for the environment. Then, electron emission is calculated to verify electrostatic stability of nanoparticles couples. Finally, we use molecular dynamics simulations to examine nanoparticle melting, evaporation and thermo-mechanical fragmentation. The calculation results are analysed as a function of mean particle size [see, for instance, Figure 1] and of laser parameters.

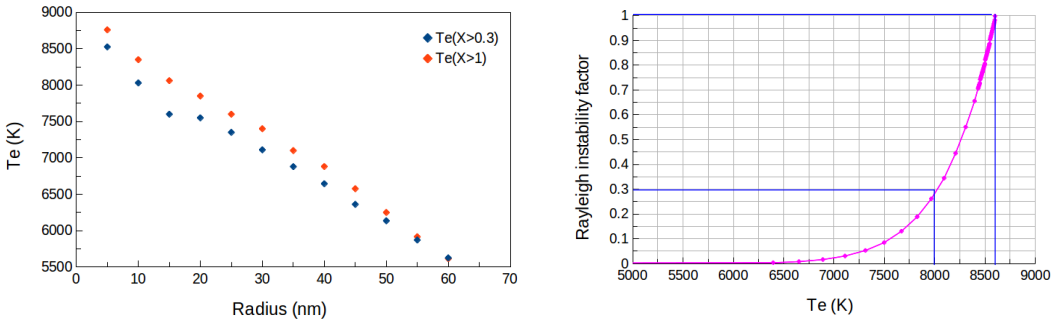

(a) (b)

Figure 1 Calculation results for gold nanoparticles in water (a) - maximum electron temperature as a function of size for a given laser fluence,
(b) Rayleigh instability factor as a function of electron temperature for 30 nm gold particles, showing $T_{e\text{-}fr}$~8000K and $T_{e\text{-}multi}$=8600 K in agreement with [2]. Here laser fluence 12.3 mJ/cm^2 and 150 fs laser pulse at 400 nm

The performed analysis allows us to predict optimum laser parameters for nanoparticle size manipulation, but also to recommend nanoparticle sizes and density for the enhanced absorption, which is particularly interesting for the development of novel energy sources.

[1] R. R. Letfullin, Ch. Joenathan, T. F George and V. P Zharov Laser-induced explosion of gold nanoparticles: potential role for nanophotothermolysis of cancer, Nanomedecine, vol. 1, No. 4, pp 473-480 (2006)

[2] S. Hashimoto, D.Werner and T. Uwada : Studies on the Interaction of Pulsed Lasers with Plasmonic Gold Nanoparticles toward Light Manipulation, Heat Management, and Nanofabrication, Journal of Photochemistry and Photobiology C: Photochemistry Reviews, vol.13, No.1, pp.28-54, (2012).

[3] P. Blandin et al., Femtosecond laser fragmentation from water-dispersed microcolloids : toward fast controllable growth of ultrapure Si-based nanomaterials for biological applications', J. Mater. Chem. B. vol. 1, pp 2489-2495, (2013)

Broadband IR Hybrid Laser System Emitting Within 2.5 – 16.5 Micron

Andrey Ionin, Igor Kinyaevsky, Yu.Klimachev and Andrey Kotkov

P.N Lebedev Physical Institute of Russian Academy of Sciences , 53Leninskii pr. 119991Moscow, Russia

aion@sci.lebedev.ru

A broadband IR hybrid laser system emitting within 2.5 – 16.5 micron is discussed. The system consists of two IR electric discharge molecular lasers emitting high-power nanosecond and/or microsecond pulses. Radiation of these lasers is mixed in various nonlinear crystals producing sum and difference frequency conversion into above mentioned IR spectral range.

High-aperture-rod Nd:glass laser

Andrey Shaykin, Alexander Soloviev, Andrey Fokin, Alexey Kuzmin, Ilya Shaykin, Efim Khazanov)

Institute of Applied Physics of the Russian Academy of Science

khazanov@appl.sci-nnov.ru

Laser pulse energy at the output of petawatt lasers is determined by pulse energy of the Nd:glass laser used for pumping terminal parametric amplifiers or Ti:sapphire amplifiers. The main factor impeding pump pulse energy enhancement is damage threshold of Nd:glass amplifiers. One of the ways to solve this problem is to increase the amplifier aperture. As compared to rod amplifiers, Nd:glass disk amplifiers deteriorate beam quality and need systems of much larger size. The currently used rod amplifiers have a diameter up to 100 mm, which limits the output pulse energy to several hundred Joule at a pulse duration of 1 ns. In this work we present results of investigation of the Nd:glass amplifier with a diameter of 150 mm developed by our team.

The laser amplifier consists of a cylindrically shaped active element with beveled ends fixed in a laser head and provides optical pumping of the active element, its cooling, as well as angular and coordinate alignment. Pumping is done by 16 gas-discharge lamps arranged near the lateral surface and along the axis of the element (fig. 1). The amplifier is connected to two power supply units (8 lamps in each) with the voltage up to 13 kV. The power supply units are described in detail in [1]. The lamps are surrounded by mirror reflectors of original design that ensures high efficiency and, at the same time, small pump inhomogeneity.

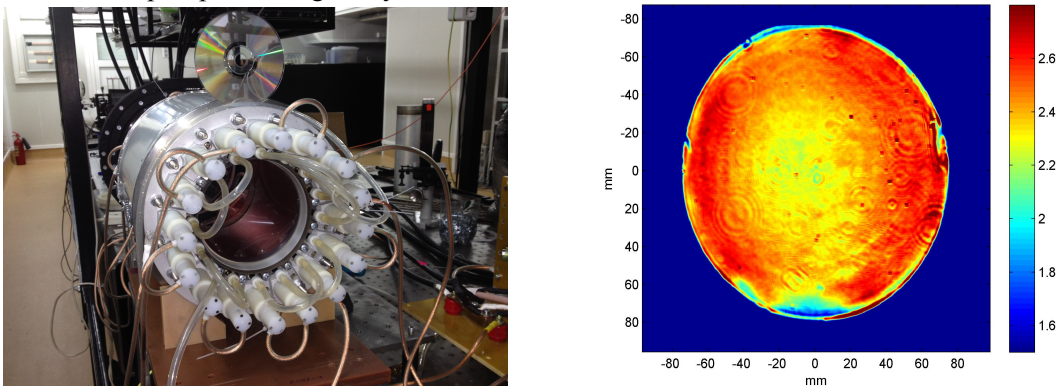

Figure 1 General view of the amplifier (left) and weak signal gain distribution at 12.5 kV voltage in pump lamps (right).

The active element is cooled by a water stream flowing along the lateral surface of the cylinder. This provides not only cooling needed for increasing pulse repetition rate, but also increased gain as a result of suppression of whispering gallery modes.

We measured the transverse distribution of weak signal gain as a function of the energy stored in the capacitors of the power supply units. The results are presented in fig. 1 (right). The observed radial inhomogeneity is caused by absorption of lamp radiation in the course of propagation through the active medium, and the polar angle inhomogeneity is due to the arrangement of individual pump lamps. The topology with depression in the center is typical for large laser elements with side pumping. We believe that the obtained inhomogeneity is not too large to restrict usage of the amplifier as an output cascade.

We have fabricated and studied a unique rod Nd:glass amplifier with a diameter of 150 mm. The measured weak signal gain was 2.3 on the average over the aperture and the stored energy was 380 J. Repetition rate was 1 shot per 10 minutes. The use of such amplifiers will enable a significant increase of the pulse energy of pulsed rod Nd:glass lasers.

[1] A.K. Potemkin, K.A. Zhurin, A.V. Kirsanov, E.A. Kopelovich, M.V. Kuznetsov, A.A. Kuz'min, F.A. Flat, E.A. Khazanov, A.A. Shaikin, Efficient wide-aperture neodymium glass rod amplifiers, Quantum Electronics 41 (2011) 487-491.

Ultrafast Thin-Disk Lasers with kW Average Output Power

J.-P. Negel[1], A. Loescher[1], A. Voss[1], D. Bauer[2], D. Sutter[2], A. Killi[2], M. Abdou Ahmed[1], T. Graf[1]

1- Institut für Strahlwerkzeuge (IFSW), University of Stuttgart, Pfaffenwaldring 43, 70569 Stuttgart, Germany
2- TRUMPF Laser GmbH, Aichhalder Straße 39, 78713 Schramberg, Germany

graf@ifsw.uni-stuttgart.de

Based on the concept of a multipass thin-disk laser amplifier, which was originally developed by the IFSW as a high-energy pump for spectroscopic investigations of the lamb-shift in muonic hydrogen [1, 2, 3], we now report on an Yb:YAG system delivering sub-8 ps pulses with an average power exceeding 1 kW at a wavelength of 1030 nm. The amplifier with 40 double passes of the beam (see Figure 1) through one thin-disk laser crystal was pumped by up to 2.7 kW into the zero-phonon line [4] and seeded by pulses with a duration of 6.5 ps. At a repetition rate of 800 kHz and an average seed power of 80 W the amplifier produced an output power of 1.1 kW (with 2.3 kW of pumping) which corresponds to 1.4 mJ of energy per pulse [5]. At a repetition rate of 300 kHz and a seed power of 115 W the average output power was 1.4 kW (with 2.7 kW of pumping), corresponding to 4.7 mJ of pulse energy. The optical efficiency of the amplifier was 48 % and the beam quality factor was better than M^2=1.4. This output was frequency doubled to a wavelength of 515 nm using an LBO crystal and resulted in a second-harmonic power of 820 W with 2.7 mJ of pulse energy, corresponding to a conversion efficiency of 70%.

Figure 1. Mirror array of multi-pass amplifier to geometrically fold the beam path 40 times on the amplifying thin-disk crystal.

[1] A. Antognini, K. Schuhmann, F. D. Amaro, F. Biraben, A. Dax, A. Giesen, T. Graf, T. W. Hänsch, P. Indelicato, L. Julien, C.-Y. Kao, P. E. Knowles, F. Kottmann, E. Le Bigot, Y.-W. Liu, L. Ludhova, N. Moschüring, F. Mulhauser, T. Nebel, F. Nez, P. Rabinowitz, C. Schwob, D. Taqqu, and R. Pohl, "Thin-Disk Yb:YAG Oscillator-Amplifier Laser, ASE, and Effective Yb:YAG Lifetime" IEEE J. Quantum Electron. 45, 993 (2009)

[2] R. Pohl, A. Antognini, F. Nez, F. D. Amaro, F. Biraben, J. M. R. Cardoso, D. S. Covita, A. Dax, S. Dhawan, L. M. P. Fernandes, A. Giesen, T. Graf, T. W. Hänsch, P. Indelicato, L. Julien, C.-Y. Kao, P. Knowles, E.-O. Le Bigot, Y.-W. Liu, J. A. M. Lopes, L. Ludhova, C. M. B. Monteiro, F. Mulhauser, T. Nebel, P. Rabinowitz, J. M. F. dos Santos, L. A. Schaller, K. Schuhmann, C. Schwob, D. Taqqu, J. F. C. A. Veloso, and F. Kottmann, "The size of the proton", Nature Letter 466, 213-216 (8. July 2010)

[3] A. Antognini, F. Nez, K. Schuhmann, F. D. Amaro, F. Biraben, J. M. R. Cardoso, D. S. Covita, A. Dax, S. Dhawan, M. Diepold, L. M. P. Fernandes, A. Giesen, A. L. Gouvea, T. Graf, T. W. Hänsch, P. Indelicato, L. Julien, C. Y. Kao, P. Knowles, F. Kottmann, E. O. Le Bigot, Y. W. Liu, J. A. M. Lopes, L. Ludhova, C. M. B. Monteiro, F. Mulhauser, T. Nebel, P. Rabinowitz, J. M. F. dos Santos, L. A. Schaller, C. Schwob, D. Taqqu, J. F. C. A. Veloso, J. Vogelsang, and R. Pohl, "Proton Structure from the Measurement of 2S-2P Transition Frequencies of Muonic Hydrogen", Science 339, 417 (2013)

[4] B. Weichelt, A. Voss, M. Abdou Ahmed, and T. Graf, "Enhanced performance of thin-disk lasers by pumping into the zero-phonon line", Optics Letters 37 (15), 3045-3047 (August 2012).

[5] J.-P. Negel, A. Voss, M. Abdou Ahmed, D. Bauer, D. Sutter, A. Killi, and T. Graf, "1.1 kW of average output power from a thin-disk multipass amplifier for ultrashort laser pulses", Optics Letters 38 (24), 5442-5445 (15. December 2013)

APPLICATION OF NON-CONTACT OPTICAL METHODS FOR STUDY OF AEROSOL DEPOSITION IN HUMAN LUNGS

Aladár Czitrovszky, Attila Nagy, Attila Kerekes, Szilvia Kugler

Wigner Research Centre for Physics, Institute for Solid State Physics and Optics
H-1121 Budapest, Konkoly Thege Miklós st. 29-33.

czitrovszky.aladar@wigner.mta.hu

The study of aerosol deposition in human lungs is important not only for investigation of the toxicity of different artificial/factitial aerosols having sometimes rather high concentration (e.g. in mining- and iron-industry, mill-dust, etc.), but also for measurement of aerosol drug deposition within human lungs, where their deposition should be allocated on the appropriate region. In the presentation we will describe our *in vitro* experimental study of aerosol delivery and deposition in various generations of transparent hollow realistic human lung models, using a special miniature laser Doppler velocimeter (developed by previously), Raman spectroscopy, video-microscopy and light scattering. The spray of a number of aerosol drugs having different size-, velocity-distribution and concentration where inhaled and delivered into the lung models using a PC controlled pulmonary waveform generator (breathing simulator) with programmable air velocity profiles. The spatial air flow velocity profiles were measured mainly at bifurcations, where the deposition have local maximum. The concentration of deposited aerosols where measured by Raman spectroscopy. Prior the measurements the system was calibrated for different drugs. The mapping of 3D topology of the drug deposition in different lung generations were determined. Using these results different aerosol drugs could be optimized.

Acknowledgement

The authors are acknowledging the support of the KTIA_AIK_12-1-2012-0019 project .

References

[1] A. Kerekes, A. Nagy, A. Czitrovszky, Experimental air flow and deposition studies with hollow bronchial airway models, Journal of Aerosol Medicine and Pulmonary Drug Delivery 22(2)., pp.175-176., (2009)
[2] A. Kerekes, A. Nagy, A. Czitrovszky, Theoretical and experimental investigation of aerosol deposition in realistic human airway model, European Aerosol Conference EAC2012, Sept. 2-7. Granada, Spain, A-WG06S1P30, P253, 1094. (2012) http://www.eac2012.com/EAC2012Book/3.html
[3] Salma I, Balásházy I, Winkler-Heil R, Hofmann W, Záray Gy; Effect of particle mass size distribution on the deposition of aerosols in the human respiratory system; J AEROSOL SCI; 33: 119-132; (2002)
[4] Balásházy I, Hofmann W, Heistracher T; Local particle deposition patterns may play a key role in the development of lung cancer J APPL PHYSIOL 94, 1719-1725 (2003).

Progress in Nd:YAG laser pumped mid-IR optical parametric oscillators based on non-oxide nonlinear crystals

Valentin Petrov[1]

[1]Max-Born-Institute for Nonlinear Optics and Ultrafast Spectroscopy, Max-Born-Str 2A, D-12489 Berlin, Germany,
e-mail: petrov@mbi-berlin.de

The mid-IR spectral range extends from 3 to 15 µm, representing a very wide „gap", where gas lasers emitting at discrete lines are well-known but solid-state lasers (SSLs) are scarce. Indeed, the upper limit of practical SSLs, such as Er^{3+} or Cr^{2+}, extends up to about 3 µm [1]. Other transitions at longer wavelengths exist but temperature quenching of the mid-IR fluorescence (e.g. Fe^{2+}) or the lack of suitable pump sources represent basic limitations. Low-phonon non-oxide host materials have to be used above ~3 µm [1] and in many cases operation at low temperature and/or using pulsed pumping is required. The recent progress in tunable transition-metal mid-IR lasers is impressive [2], nevertheless, at present the main approach to cover the mid-IR spectral range relying on all-SSL technology is still down-conversion employing nonlinear crystals (NLCs).

The fundamental nonlinear process for down-conversion of the frequency of SSLs which operate in the near-IR is difference-frequency generation (DFG). It can be used on all time scales but two input wavelengths are required and the parametric gain is too low for efficient conversion. The parametric gain is much higher in optical parametric amplifiers (OPAs) where high intensity ultrashort (ps or fs) pump pulses are employed, however, higher order nonlinear and dispersive effects limit the energy conversion efficiency and the achievable average power when low-repetition-rate amplified systems are used for pumping. Synchronously-pumped optical parametric oscillators (OPOs) operating at ~100 MHz may have very high conversion efficiency but they require mode-locked pump sources which again poses a limit on the achievable average output power. Thus, nanosecond (ns) OPOs provide optimum conditions for the generation of high energies and average powers in the mid-IR above 3 µm which are important for numerous applications [3].

OPOs emitting their idler wave in the mid-IR can be pumped by SSLs operating in the 1-3 µm range but NLCs which are transparent in the mid-IR normally exhibit smaller band-gap which sets a lower limit to the pump wavelength in order to avoid two-photon absorption (TPA). This lower limit is at present ~1-µm, a spectral region where the most advanced Nd^{3+}- (and more recently Yb^{3+}-) based laser systems operate.

This talk reviews the progress achieved with ns mid-IR OPOs based on non-oxide NLCs which are pumped at 1.064 µm by the most widely spread and mature Nd:YAG laser based systems (Q-switched oscillators and amplifiers). Note that continuous-wave (cw) operation of such OPOs has not been demonstrated, yet. An alternative approach is to pump such materials near 2 µm (Tm^{3+}- and Ho^{3+}-lasers or near-IR OPO based on oxide NLCs) [3]. Although impressive results have been obtained with such OPOs as well, the laser pump sources are by far not so mature and commercially available or the whole set-up is much more complex when cascaded OPOs are employed starting again from wavelengths near 1 µm [3].

[1] A. A. Kaminskii, "Laser crystals and ceramics: recent advances," Laser & Photon. Rev., vol. 1, pp. 93-177 (2007).
[2] S. Mirov, V. Fedorov, I. Moskalev, M. Mirov, and D. Martyshkin, "Frontiers of mid-infrared lasers based on transition metal doped II–VI semiconductors," J. Lum., vol. 133, pp. 268-275 (2013).
[3] V. Petrov, "Parametric down-conversion devices: The coverage of the mid-infrared spectral range by solid-state laser sources," Opt. Mater., vol. 34, pp. 536-554 (2012).

Diamond components for lasers and photonics

Victor Ralchenko
A.M. Prokhorov General Physics Institute RAS, 38 Vavilov str. 119991 Moscow, Russia, ralchenko@nsc.gpi.ru

The progress in growth of diamond by chemical vapor deposition (CVD) makes this material more accessible for practical purposes, including laser and photonic applications. Diamond possesses exceptional optical and thermal properties, in particular, transparency in broadest spectral range, from λ=225 nm to THz, and further to radio frequencies, and extremely high thermal conductivity ~2000 W/mK @ R.T. Chemical inertness, high hardness (57-100 GPa) and fracture strength of 300-600 MPa add even more value to diamond. Here some recent results on optical applications of polycrystalline and single crystal CVD diamonds produced by a microwave plasma assisted CVD process using CH_4-H_2 gas mixtures will be reported.

Large size diamond windows serve to handle with high power laser beams. As an example, a water-cooled polycrystalline CVD diamond window (1 inch diameter, 1.3 mm thickness) being exposed to a cw terbium fiber laser irradiation withstands 10 kW incident power (11.7 MW/cm^2 power density) [1]. Optical absorption data for diamond in IR and millimeter waves will be given. Radiation-hard UV and X-ray diamond detectors based on diamond, including multipixel devices for imaging, are realized owing to high charge carrier mobility in diamond [2].

The principle of molding technique to grow shaped diamond using the diamond deposition on a patterned template is illustrated by fabrication of (i) 3D diamond photonic crystal with Bragg reflection peak in the visible, (ii) periodic antireflective surface structures designed for ~10 μm wavelengths, (iii) diamond pillars with color centers (Si-vacancy) a bright photoluminescence source. Finally, attention will be paid to achievements in the field of diamond Raman lasers (DRL). Diamond is excellent choice for DRL due to large Raman shift of 1332 cm^{-1}, high gain (>12.5 cm/GW for the 1st Stokes at 1240 nm) and low thermo-optics coefficient. Efficient operation of a pulsed single crystal diamond Raman laser at power of 14.5 W at 1240 nm and 1485 nm has been recently reported [3]. The problem of distortions and deformation of a conventional Raman crystal caused by its nonuniform heating is greatly reduced for DRL that allows a high power laser performance.

References

1. V.E. Rogalin, E.E. Ashkinazi, A.F. Popovich, V.G. Ralchenko, V.I. Konov, S.M. Aranchii, M.V. Ruzin, S.A. Uspenskii, Resistance of diamond optics to high-power fiber laser radiation. Russian Microelectronics, 41, 464-468 (2012).
2. M Girolami, P. Allegrini, G. Conte, S. Salvatori, D. M. Trucchi, A. Bolshakov, V. Ralchenko, V. Konov, Diamond detectors for UV and X-ray source imaging, IEEE Electron Device Lett. 33, 224-226 (2012).
3. A. McKay, H. Liu, O. Kitzler, R.P. Mildren, An efficient 14.5 W diamond Raman laser at high pulse repetition rate with first (1240 nm) and second (1485 nm) Stokes output. Laser Phys. Lett. 10, 105801 (2013).

EPITAXIAL FLUORIDE LAYERS FOR LASER AND AMPLIFIERS

W. Bolaños, G. Brasse, J.L. Doualan, A. Braud, R. Moncorgé and P. Camy

Centre de recherche sur les Ions, les Matériaux et la Photonique (CIMAP) UMR 6252

CNRS-CEA-ENSICAEN, Université de Caen, 6 blvd Maréchal Juin, 14050 Caen, France

patrice.camy@ensicaen.fr

The development of miniaturized optoelectronic devices is a technologic challenge of the current decade to improve the performance and the compacity of photonic devices. Integrated optics allows to implement various functionalities on a same substrate such as lasers sources for labs on chips devices. Among the different interesting materials for laser media, fluoride crystals are recognized as good host materials for rare earth ions because of their low phonon energies (< 450 cm^{-1}) that reduces the non-radiative transitions between adjacent energy levels and of their negative thermo-optic coefficients that compensates for thermal lensing effects when operating at high power levels.

Fluorides crystals can be grown by using standard Bridgman or Czochralski methods, but also in the form of thick crystalline layers by using the Liquid Phase Epitaxy (LPE) technic. In this form, efficient and compact waveguide and high power thin-disk lasers can be realized. There are only few reports on the fabrication of fluoride waveguides [1,3], but the LPE technique has been proven to be a suitable way for the fabrication of rare earth doped waveguide lasers since it is possible to obtain high quality, lattice matched, single crystalline layers (see fig. 1) with very low scattering losses..

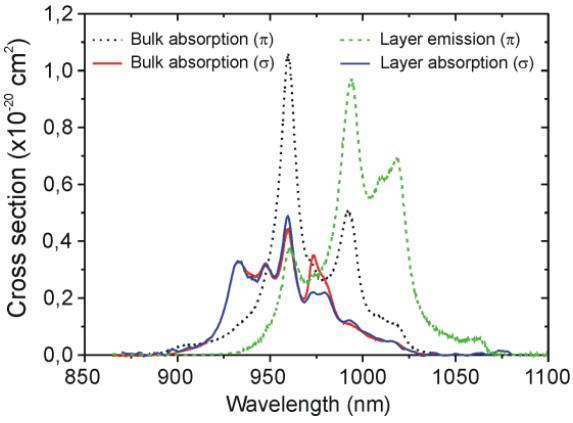

Fig 1.Emission and absorption spectra of an Yb :$LiYF_4$ layer compared to the bulk crystal

In this talk, we will report the recent advances in this field with the recent improvements obtained in the visible range (red orange and green laser emissions) with Pr:LiYF4 epitaxial layers and the first results concerning Yb:LiYF4 planar waveguide amplifiers.

References:

1. L. Douysset-Bloch, B. Ferrand, M. Couchaud, L. Fulbert, M. F. Joubert, G. Chadeyron and B. Jacquier, "Growth by liquid phqse epitaxy and characterization of Nd:$YLiF_4$ layers" J. Alloy & Comp. 275-277, 67 (1998)

2. W. Bolanos, F. Starecki, A. Benayad, G. Brasse, V. Menard, JL. Doualan, A. Braud, R. Moncorgé, P. camy, "Tm:LiYF4 planar waveguide laser at 1.9 µm", Opt. Lett. 37 4032-4034 (2012)

3. F. Starecki, W. Bolanos, A. Braud, JL. Doualan, G. Brasse, A. Benayad, V. Nazabal, B. Xu, R. Moncorgé, P. camy, "Red and orange Pr3+:LiYF4 planar waveguide laser" Opt. Lett. 38 455-457 (2013)

Modes of resonators with axially symmetric aberrational lens

V.B. Morozov, A.N. Olenin, D.V. Yakovlev

International Laser Centre and Physics Faculty of M.V.Lomonosov Moscow State University, Moscow 119992, Russia

morozov@phys.msu.ru

In this paper we propose simple and visual approach for analysis of mode composition and beam quality evaluation at longitudinal pumping accompanied by axially symmetric aberrational thermal lens. This applies, in particular, to diode end-pumping which is widely used in laser systems due to compactness, reliability and provides efficient amplification of lowest cavity mode and excellent output beam spatial quality. Focused longitudinal pump beam usually produces essentially inhomogeneous intensity distribution in radial direction inside active medium. This results in aberrational component of thermal lens formation and in essentially inhomogeneous amplification profile even at low pump powers. With pump power increase, growing up aberrations leads to laser beam quality degrading and falling down of output power. In some cases, it is suitable to consider aberrations as a mechanism of additional diffraction losses for lowest Gaussian mode of resonator without aberrations [1,2]. It allows defining stable laser operation condition [2]. Such approach thought contains definite internal contradiction since mode of resonator with aberrational lens principally is not Gaussian. Universal way of aberrations accounting and finding resonator modes is Fox-Li method [3]. However, it does not provide visual presentation of resonator mode composition and its dependence on aberrational lens parameters.

We present here an approach for finding modes of resonator with aberrational thermal lens in axially symmetric case on the basis of field decomposition into Laguerre-Gaussian beams. Aberrational thermal lens works as a phase screen redistributing energy between different order components. Field roundtrip through resonator is described by action of a linear operator on vector with coordinates equal to decomposition coefficients. Each operator eigenvector defines some resonator mode and consists of decomposition coefficients set, which depends on specific form of aberrational lens, and each eigenvalue defines roundtrip losses and phase shifts for corresponding mode. Width of “embedded” Laguerre-Gaussian beams may be found on the basis of mode field distribution [4]. Coefficients set of “embedded” beams gives visual presentation of mode structure and clearly characterizes space quality of laser output. Results for typical resonator with aberrational thermally induced power depending lens will be presented.

Radially inhomogeneous amplification in steady-state may be incorporated into roundtrip operator that makes it possible to find field distribution in this case. Profiled amplification influence on mode structure of resonator with aberrational lens is analyzed.

Performance of pulsed end-diode-pumped laser will be examined on the basis of proposed approach. Using pulsed pump regime usually implies energy accumulation during the pump pulse and subsequent fast amplification of pico- or nanosecond radiation pulse. Round trip amplification in this case usually is much higher than in cw lasers. Therefore relation between transversal sizes of pumped region in active medium and of laser mode affects not only pump power transfer efficiency, but the laser mode profile too. On the basis of modeling results, we propose optimization criterion for efficient generation of high-quality beam in end-diode-pumped picosecond laser with aberrational thermal lens.

[1] J.Bourderionnet, A.Brignon, J.-P.Huignard, R. Frey, Influence of aberrations on fundamental mode of high power rod solid-state lasers, Opt. Commun., **204**, 299-310 (2002);

[2] V.B. Morozov, A.N. Olenin, V.G. Tunkin, D.V. Yakovlev, Operation conditions for a picosecond laser with an aberration thermal lens under longitudinal pulsed diode pumping, Quant. Electron., **41**, 508-514 (2011);

[3] A.G. Fox, T. Li, Resonant modes in a maser interferometer, Bell Syst. Tech. J., **40**, 453-488 (1961);

[4] A. Siegman, “How to (Maybe) Measure Laser Beam Quality,” in DPSS (Diode Pumped Solid State) Lasers: Applications and Issues p. MQ1 (OSA, 1998).

Comparison of Stored Energy in Disk and Composites Yb:YAG Active Element at Cryogenic and Ambient Temperature

I. Kuznetsov[1], I. Mukhin[1], O. Palashov[1], O. Vadimova[1]
(List of authors in 11 point, centred and bold: the presenting author underlined)

1- Institute of Applied Physics of Russian Academy of Science,46 Ul'yanov street, 603950, Nizhny Novgorod, Russia

musfex@mail.ru

Yb:YAG disk lasers are one of the most perspective design of laser systems with high peak and averaged power simultaneously due to effective heat removal, weak self-focusing and good thermooptical characteristics [1, 2]. However, amplified spontaneous emission (ASE) which limits stored energy becomes significant in disk active element due to high transversal gain [3]. The investigation of ASE impact on stored energy in different active element (AE) configuration at cryogenic and ambient temperature was carried out.

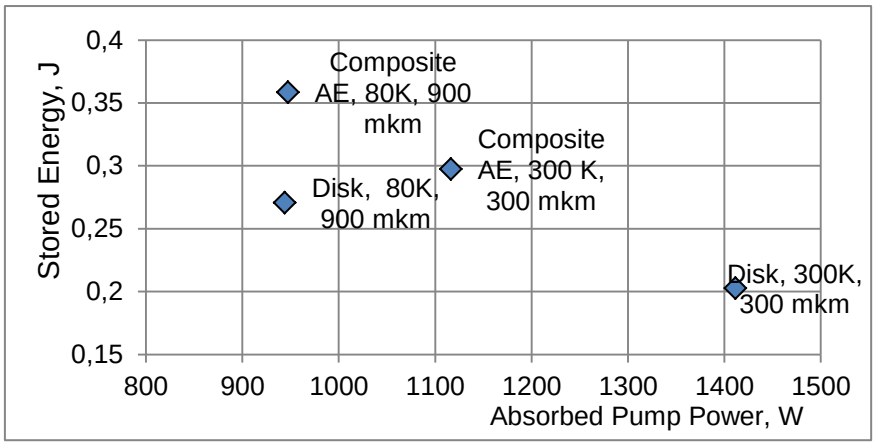

Figure 1 The highest stored energy for disk and composite active element at cryogenic and ambient temperature.

Two geometries of the disk AE were considered. The first one is the thin disk made from active medium, the second one is the same disk with undoped cup – a layer of YAG which is in optic contact with Yb:YAG[4]. The cup allows decreasing negative effect of ASE by preventing its return in the pump area. Besides, undoped layer reduce thermal loading of the active element.

Energy stored calculation was performed with taking into account ASE which is calculated in case of non-uniform populations distribution without any approximations [5]. Cryogenic and ambient temperature regimes were considered. Active ion Yb^{3+} demonstrates quasi-three level operations at ambient temperature, but in the cryogenic temperature the lower laser laver is depopulated. Besides, laser and thermooptical properties of Yb:YAG are better at the liquid nitrogen temperature but ASE enhances due to increasing of emission cross-section.

Calculations of stored energy were carried out for several thickness of the AE. The results are represented on the Fig. 1. The usage of undoped cup leads to increasing of AE stored energy at both temperatures. In case of liquid nitrogen temperature, thicker composite AE allows storage more energy at the same absorbed pump power than thinner does. The disk with undoped cup at cryogenic temperatures demonstrates the highest efficiency equals 40% while thin disk at room temperature has efficiency below 15%.

[1] Brown D.C., The promise of cryogenic solid-state lasers, IEEE Journal of Selected Topics In Quantum Electronics, vol. 11, 587 (2005).
[2] Perevezentsev E.A., Mukhin I.B., Palashov O.V., Khazanov E.A., Amplification of laser radiation in disk Yb:YAG crystals cooled down to the liquid nitrogen temperature, Quantum Electronics, vol. 39, 9 pp. 807-813 (2009).
[3] J. Speiser, Thin Disk Laser – Energy Scaling, ISSN 1054-660X, Laser Physics , vol. 19, No. 2, pp 274-280. (2009)
[4] D. Kouznetsov, J.-F. Bisson, Role of undoped cap in the scaling of thin-disk lasers, J. Opt. Soc. Am. B, vol. 25, No. 3, pp. 238-345 (2008)
[5] O.L. Vadimova, I.B. Mukhin, I.I. Kuznetsov, O.V. Palashov, E.A. Perevezentsev, E.A. Khazanov, Calculation of the gain coefficient in cryogenically cooled Yb :YAG disks at high heat generation rates, Quantum Electronics, vol. 43 (3), pp. 201 – 206 (2013)

Generation of new spatial and temporal coherent states using VECSEL technology: VORTEX, high order Laguerre-Gauss mode, continuum source

***Mohamed Seghir Seghilani*[1], *Mohamed Sellahi*[1], *Mikhael Myara*[1], *Isabelle Sagnes*[2], *Gregoire Beaudoin*[2], *Philippe Lalanne*[3], *and Arnaud Garnache* [1]**

1- IES - CNRS UMR5214, Université Montpellier II, France,
2- LPN-CNRS - UPR20, Marcoussis, France
3- LP2N - IOGS-Bordeaux, Talence, France;

Main author email address: arnaud.garnache@ies.univ-montp2.fr

Since years, the Vertical-External-Cavity-Surface-Emitting-Laser [1] concept is pointed out as a technology of choice for beyond-state-of-the-art laser light sources, demonstrating wavelength flexibility, high power, high spatial, temporal and polarization coherence, CW or ultra short pulsed operation, compactness and functionalities. The targeted coherent state is typically the common gaussian TEM00, single frequency, linearly polarized light state. In this work, we take advantage of the VeCSEL III-V technology for the generation of non-conventional coherent states, thanks to the insertion of intracavity functions. These new kinds of coherent light states target many applications including optical tweezers, telecommunications, fundamental physics, sensors...

A first part of this work aims at demonstrating new spatial domain coherent state. For this purpose, we developed a semiconductor flat photonics technology for transverse phase and intensity control, as well as spectral and polarization control, inside the cavity. The intensity control is obtained thanks to sub-wavelength metallic masks deposited on the surface of the semiconductor gain structure. For phase-amplitude and polarization control, we developed an ultra low-loss photonic-crystal bragg mirror technology. All this technological development allow generation of highly coherent single frequency high order Laguerre-Gauss mode (degenerated or non generated, including VORTEX beam exhibiting Orbital Angular Momentum), preserving the full coherence properties (diffraction limited low divergence beam, highly polarized E-field, very low noise) of usual TEM00 VeCSEL source. It also paves the way for the generation of other coherent states (Bessel beams, light with spin orbital momentum...) or new functionalities (wavelength filtering, chirality...).

In a second part, we explore new time domain coherent state, i.e. continuum source operating in cw : owing to a high gain semiconductor structure design and the insertion of intracavity acousto-optics frequency shifter, we demonstrated the first Frequecy-Shifted-Feedback VeCSEL, with a spectrally broadband modeless coherent state, as wide as 300 GHz, exibiting a large coherence length of ~4km.

[1] A. Laurain, M. Myara, G. Beaudoin, I. Sagnes, and A. Garnache. Multiwatt–power highly–coherent compact single–frequency tunable vertical–external–cavity–surface–emitting–semiconductor–laser. Optics Express, 18(14):14627–14636,2010.

Laser operation of Tm:Ho:YbAG crystal pumped at 1678 nm.

V. A. Mikhailov, Yu. D. Zavartsev, A. I. Zagumennyi, Yu. L. Kalachev, S. A. Kutovoi, I. A. Shcherbakov
A.M. Prokhorov General Physics Institute, RAS, 38 Vavilov str., 119991 Moscow, Russia
mihailov@kapella.gpi.ru

The laser crystal Tm:Ho:YbAG (Tm^{3+}:Ho^{3+}:$Yb_3Al_5O_{12}$) was suggested as the active element for lasing in 2 um spectral range. The laser properties of this crystal can be comparable with properties of one of the best Tm:Ho:YAG laser crystal, were all Y^{3+} ions are replaced with Yb^{3+} ions [1].The Tm:Ho:YbAG crystals were grown by the Czochralski method from an iridium crucible. The concentration of Tm^3+ and Ho^{3+} ions in the active elements was 6,4% and 0,8%, respectively. Active elements was cut out along [100] axis in form of cube with an edge length of 3 mm without antireflection coatings. Active element was cooled by a contact with copper heat sink.Tm:Ho:YbAG crystal was pumped by a Raman shifted Erbium fiber laser at 1678 nm ($^3H_6$-$^3F_4$ transition). Absorption of pumping in laser crystal was ~ 48%. Hemispherical laser cavity was formed by a high reflection flat mirror and 50 mm radius of curvature of output coupler with ~97% reflectivity.

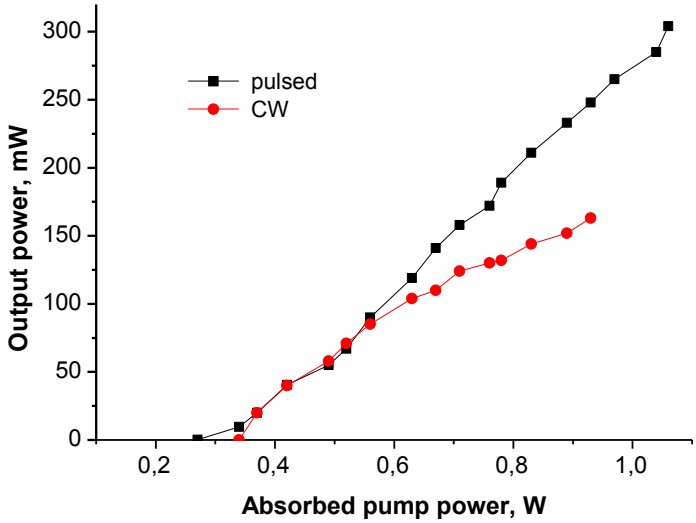

Fig.1. Tm:Ho:YbAG laser output power as a function of absorbed pump power.

Lasing at a wavelength ~ 2,1 um was realized in pulsed and CW regimes at crystal temperature 16 C^0. Threshold of Tm:Ho:YbAG crystal lasing was reached at comparatively lower absorbed pump power ~ 250 mW at CW and pulsed regimes of operation (duty cycle 1:20). The pulsed output laser power was increased almost linearly up to 307 mW at increasing of pump power up to ~ 1,1 W. The slope and total laser efficiencies were ~ 41% and 28%, respectively. CW laser efficiency was reduced at pumping higher 600 mW. The highest total laser efficiency 18% was reached at pump power 930 mW. This reduction of laser efficiency can be explained by more intensive heating of pumping channel in Tm:Ho:YbAG crystal at CW pumping. Absorption, luminescence, lasing spectra and temperature dependence of laser efficiency were investigated.

Acknowledgements
This work was supported by the Russian government in the frame of Program of RAS № III.8.

References:
1. D. Fagundes-Peters, N. Martynyuk, K. Lunstedt, V. Peters, K. Petermann, G.Huber, S. Basun, V. Laguta, A. Hofstaetter, “High quantum efficiency YbAG-crystals,” Journal of Luminescence, vol. 125, pp. 238-247, 2007.

MODE-LOCKING SEMICONDUCTOR DISK LASERS USING SINGLE-WALLED CARBON NANOTUBE SATURABLE ABSORBERS

K. Seger[1], N. Meiser[1], S. Y. Choi[2], B. H. Jung[2], D.-I. Yeom[2], F. Rotermund[2], O. Okhotnikov[3], F. Laurell[1], and V. Pasiskevicius[1]

[1]*Royal Institute of Technology, Roslagstullsbacken 21, 106 91 Stockholm, Sweden*

[2]*Ajou University, 443-749 Suwon, South Korea*

[3]*Optoelectronics Research Centre, Tampere University of Technology, Tampere, Finland*

vp@laserphysics.kth.se

Optically pumped semiconductor disc lasers (OPSDL) employ probably the most versatile gain media, whereas the emission wavelength, electric field structure and dispersion can be engineered by taking advantage of well-established and high precision techniques in semiconductor epitaxy, bandgap engineering and density of states engineering in quantum confined structures. Owing to the emission geometry, perpendicular to the wafer plane, the OPSDL can be power-scaled and retain single-transversal mode operation at high powers [1,2] thanks to low thermal lensing in the beneficial disk geometry which facilitates one-dimensional heat removal. Robust fundamental transversal mode operation is crucial for stable mode-locked operation. On the other hand OPSDLs are characterized by relatively small roundtrip gain of few percent at most, which, in turn, mandates careful choice of passive mode-locking intracavity elements. In general for mode-locking OPSDL one needs nonlinear intensity modulators with low saturation fluence, low nonsaturable loss and low modulation depth as well as fast relaxation of the saturated absorption. Semiconductor structures seem to be obvious choice. Indeed, semiconductor quantum-well (QW) and quantum-dot (QD) saturable absorber mirrors (SAMs) have been successfully used for mode-locking these lasers [3]. In recent years saturable absorbers based on semiconducting single-wall carbon nanotubes (SWCNT) have been demonstrated as a viable technology for mode-locking solid state lasers [4]. Along with graphene, SWCNT-based intensity modulators seemingly offer more universal and flexible technology for achieving pulsed laser operation over wide spectral ranges. These elements do have fast recovery times of the order of one picosecond and low saturation fluence suitable for OPSDL mode-locking. Advances in fabrication technology now allow manufacturing of SWCNT absorbers with nonsaturable single-pass losses below 0.5% making the mode-locking of OPSDLs feasible [5]. In this presentation we will overview recent advances in mode-locked OPSDL using SWCNT and graphene and will put these technologies in the context of more established mode-locking techniques using semiconductor QW and QD-SAMs.

References:

1. J. Chilla, S. Butterworth, A. Zeitschel, J. Charles, A. Caprara, M. Reed, and L. Spinelli, "High power optically pumped semiconductor lasers," Proc. SPIE, **5332**, 143-150 (2004).
2. C. Tropper, H. D. Foreman, A. Garnache, K. G. Wilcox, and S. H. Hoogland, "Vertical-external-cavity semiconductor lasers," J. Phys. D **37**, R75-R85 (2004).
3. U. Keller and A. Tropper, "Passively modelocked surface-emitting semiconductor lasers," Phys. Rep., **429**, 67-120 (2006).
4. F. Rotermund, W. B. Cho, S. Y. Choi, I. H. Baek, J. H. Yim, S. Lee, A. Schmidt, G. Steinmeyer, U. Griebner, D.-I. Yeom, K. Kim, and V. Petrov, "Mode-locking of solid-state lasers by single-walled carbon-nanotube based saturable absorbers," Quantum Electron. 42, 663-670 (2012).
5. K. Seger, N. Meiser, S. Y. Choi, B. H. Jung, D.-I. Yeom, F. Rotermund, O. Okhotnikov, F. Laurell, and V. Pasiskevicius "Carbon nanotube mode-locked optically-pumped semiconductor disk laser," Optics Express, 21, 17806-17813 (2013).

High Performance Laser Combination Additive Manufacturing Technology and it's Applications

Jianhua Yao

Research Center of Laser Processing Technology and Engineering, Zhejiang University of Technology,Hangzhou,310014,China

Main author email address: laser@zjut.edu.cn

In recent years, laser additive manufacturing technologies have accelerated the development of a new generation of manufacturing technology which is characterized by high quality, high efficiency, energy saving and materials saving. Especially, the sustainable remanufacturing technology has received great attention around the world. The author reviews the technical characteristics of laser combination additive manufacturing and remanufacturing technology, points out that laser combination manufacturing technology aims at structural optimization manufacturing of parts with the layer materials being gradient and composite, and eventually realizing materials combination, method combination and function combination. Laser combination manufacturing technology has advantages of low cost, good economy and high availability, thus more suitable for the current situation. The laser combination additive remanufacturing technology focusing on the repair of failure parts has played a pivotal role in the civilian industry due to its innovative design concept and unique effect. This report emphasizes the key technology of laser combination additive manufacturing and remanufacturing, presents typical application cases and research progress according to the author's many years research and practice in this field, analyzes the application prospect, development potential and the main problems associated with these technologies, and finally provides some preliminary thoughts on how to effectively develop the laser combination additive manufacturing and remanufacturing technology.

Spectral-Luminescence Investigations of Raman-active Strontium Molybdate Crystals Doped with $Ho^{3+}$and Tm^{3+}ions

P.G. Zverev, L.I. Ivleva, M.E.Doroshenko, E.E. Dunaeva, A.V. Nekhoroshikh

A.M. Prokhorov General Physics Institute, Russian Academy of Sciences
119991 Moscow, Vavilov str., 38, Bld. D
e-mail: ivleva@lst.gpi.ru

One of the modern tendencies of laser physics is the development of new materials which combine the properties of active and non-linear medium. We consider scheelite type $SrMoO_4$ crystal as the matrix with high Raman gain coefficient which can simultaneously work as laser-active element under doping with RE elements. The task is the development of compact lasers capable for intracavity Raman scattering. The present work is devoted to the development of the technology of new crystals synthesis for 2-5 μm mid IR lasers. For this purpose the concentration series of $SrMoO_4$ crystals doped with Ho^{3+} and co-doped with Ho^{3+}+Tm^{3+} ions were grown and investigated.
The Czochralski method with specially growth and weight control PC program was used to obtain optically homogeneous $SrMoO_4$ crystals doped with RE elements. The crystals were grown perpendicular to tetragonal C-axis ([100] crystallographic direction) that provided maximal Raman scattering cross section for SRS elements. Stoichiometric $SrMoO_4$ as a charge was prepared by solid state synthesis. To increase the effective segregation coefficient of the RE in the matrix and to obtain excessive charge compensation the dopants were added into the melt in the form of $RENbO_4$. Bulk growth velocity strongly decreased with dopant concentration increase and was not more than 0.5 cm^3/h for co-doped crystals. Typical dimensions of the crystals were 18x16x60mm. Dynamic holographic method was used to control optical homogeneity of as-grown crystals. Crystallization conditions were optimized to reproducible synthesis of high optical quality crystals.
Investigations of Tm^{3+} and Ho^{3+} absorption spectra have shown that thulium ions have suitable absorption bands for commercial 790 nm diode lasers pumping while holmium ions for spectroscopic measurements can be excited by pulsed GaN blue 450 nm laser diode. As follows from fluorescence measurements spectra of Tm^{3+} and Ho^{3+} ions in $SrMoO_4$ crystal well cover broad spectral range from 1650 nm to 2100 nm suitable for mid IR lasing. Intensive fluorescence of Ho^{3+} ions in Tm^{3+}, Ho^{3+} co-doped crystal under 790 nm excitation (see Fig.1) demonstrate effective energy transfer from thulium to holmium for concentrations 1 wt.% for both ions. As follows from Fig.1 measured in similar conditions under unpolarized diode laser excitation Re^{3+} doping ions fluorescence is different for Z-cut and C-cut $SrMoO_4$ crystals. The lifetime measurements are presented in Fig.2 and demonstrate rather long Ho^{3+} lifetime of about 5 ms well suitable for long pulse diode pumping. The Tm^{3+} ions lifetime is quite short (about 1 ms) and is most probably quenched due to Tm^{3+}-Ho^{3+} ions interaction. Results on Tm^{3+}-Ho^{3+} ions energy transfer mechanism and efficiency as well as results on laser experiments under laser diode pumping will be presented.

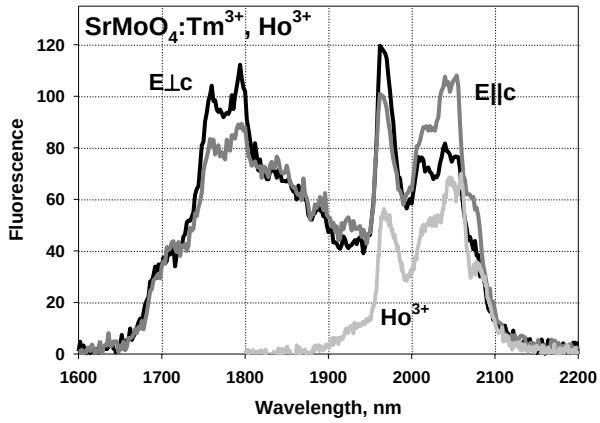

Fig.1 Fluorescence spectra of Ho^{3+} and Tm^{3+}, Ho^{3+} doped $SrMoO_4$ crystal

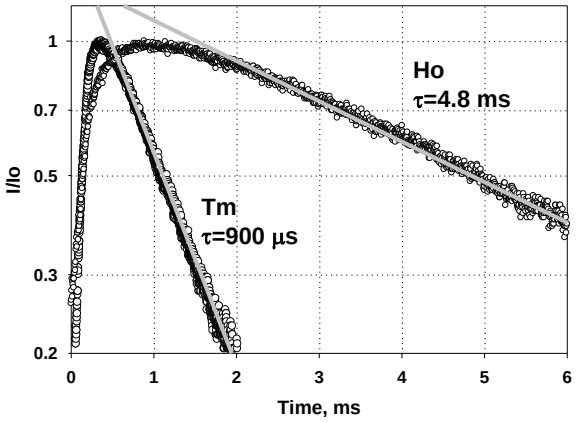

Fig.2 Decay curves of Tm^{3+} and Ho^{3+} ions in Tm^{3+}, Ho^{3+} co-doped $SrMoO_4$ crystal under 790 nm excitation.

Carbon Nanotubes as Efficient Platform for Photonic Applications

A.G. Rozhin

Nanotechnology Research Group & Aston Institute of Photonics Technologies, Aston University, Aston Triangle, Birmingham, B47ET, The United Kingdom

E-mail: a.rozhin@aston.ac.uk

Over the past decade, the optical properties of Single Wall Carbon NanoTubes (SWNTs) have attracted significant attention due to great promise for application in various photonic devices including bio-medical and environmental sensors, ultra-short pulse lasers and optical switches [1]. The optical absorption, photoluminescence (PL) and Raman spectroscopy are powerful tools for assignment for SWNTs of different chirality, energy transfer in SWNTs bundles [2] and in molecular complexes with SWNTs [3]. Additionally, SWNTs possess ultrafast optical nonlinearity due to saturation of exciton transitions in semiconducting SWNTs.

In my report, I will review the wet chemistry methodology for fabrication of SWNTs materials with a strong PL and saturable absorption properties and will reveal the importance of SWNTs bundle engineering for both applications [1]. Then, I will demonstrate a possibility of PL enhancement by non-covalent functionalization of SWNTs with polymers and organic dyes [3]. I will show the ultrafast nonlinear optical properties of materials determined by Z-scan and pump-probe techniques [4,5]. Finally, I will demonstrate advanced fibre lasers with liquid and polymer SWNTs saturable absorbers generating sub picosecond pulses [6,7].

Acknowledgements: The work was supported by NATO SPS project (NUKR.SFPP 984189) and by TeLaSens (Project # 269271) FP7 Marie Currie International Research Staff Exchange Scheme.

[1] T. Hasan, Z. Sun, F. Wang, F. Bonaccorso, P. H. Tan, A. G. Rozhin, A. C. Ferrari "Nanotube–Polymer Composites for Ultrafast Photonics", Adv. Materials 21, 3874 (2009).
[2] P.H. Tan, A. G. Rozhin, T. Hasan, P. Hu, V. Scardaci, W.I. Milne, A.C. Ferrari, "Photoluminescence Spectroscopy of Carbon Nanotube Bundles: Evidence for Exciton Energy Transfer", Phys. Rev. Lett., 99, 137402 (2007)..
[3] M.P. Shandura, Yu.P. Kovtun, V.P. Yakubovskyi, Yu.P. Piryatinski, P.M. Lutsyk2, R.J. Perminov, R.N. Arif, A.B. Verbitsky, A. Rozhin "Dioxaborine Dyes as Fluorescent Probes for Amines and Carbon Nanotubes", Sensor Letters, (2014) in press.
[4] A. G. Rozhin, Y. Sakakibara, H. Kataura, S. Matsuzaki, K. Ishida, Y. Achiba, M. Tokumoto, " Anisotropic saturable absorption of single wall carbon nanotubes aligned in polyvinyl alcohol", Chem. Phys. Lett., 405, 288 (2005).
[5] A. Gambetta, G. Galzerano, A. G. Rozhin, A.C. Ferrari, R. Ramponi, P. Laporta, M. Marangoni, "Sub-100 fs pump-probe spectroscopy of Single Wall Carbon Nanotubes with a 100 MHz Er-fiber laser system", Optics Express, 16, 11727 (2008).
[6] C. Mou, A.G. Rozhin, R. Arif, K. Zhou, S. Turitsyn "Polarization insensitive in-fiber mode-locker based on Carbon Nanotube with N-methyl-2-Pryrrolidone solvent filled fiber microchamber", Appl. Phys. Lett. 100, 101110 (2012).
[7] S.V. Sergeyev, C. Mou, E.G Turitsyna, A. Rozhin, S.K. Turitsyn, K. Blow "Spiral attractor created by vector solitons", Light: Science & Applications3, e131; doi:10.1038/lsa.2014.12 (2014.

NONLINEAR OPTICS OF SILICON NANOWIRE ARRAYS: THIRD-HARMONIC GENERATION AND COHERENT ANTI-STOKES RAMAN SCATTERING

S.V. Zabotnov[1], M.M. Kholodov[1], P.K. Kashkarov[1], V.V. Yakovlev[2], and L.A. Golovan[1]
[1]*M.V. Lomonosov Moscow State University, 1/2 Leninskie Gory, Moscow, 119991 Russia*
[2]*Texas A&M University, College Station, TX 77843-3120 USA*
e-mail: zabotnov@physics.msu.ru

Nowadays arrays of silicon nanowires (SiNWs) attract more and more interest of researchers due to large potential of their applications in photonics, electronics, and sensing [1]. Often such arrays formed via the metal-assisted chemical etching (MACE) technique [2] and consist of crystalline silicon (c-Si) wires of 20-200 nm in diameter and of 1-200 μm in length. In this report interrelations between structural and optical properties of SiNWs and their influence on the efficiency of such processes as third-harmonic (TH) generation and coherent anti-Stokes Raman scatering (CARS) are discussed.

Fabrication of the mentioned structures on c-Si substrates of different doping and crystallographic surface orientation leads to variation of diameter and order of SiNWs. As a result we have an opportunity to change optical and nonlinear optical properties of the SiNW arrays in a wide range. Particularly, the orientation dependencies of the TH signal demonstrate such difference. Also these dependencies differ from ones for c-Si sufficiently. The increase of TH signal up to by an order of magnitude was registered in a number of cases. Such enhancement is caused by the light localization effects.

The polarization dependence measurements of the CARS signal carried out in the cases when the laser radiation propagates along the SiNWs and perpendicular to them gave the following. As a whole the CARS signal in SiNW arrays is weaker than one in c-Si owing to extinction in the effective scattering medium. The polarization dependences as well as the signal magnitude strongly depends on the SiNW orientation. Particularly, the more effective CARS signal for the SiNWs oriented perpendicular to the incident wave in comparison with the parallel geometry was registered. It is explained by more effective pumping by the electromagnetic field which is parallel to the SiNWs and does not subjected to depolarization weakening.

So we have demonstrated that TH efficiency in SiNW arrays strongly depends on SiNW size and order and can an order-of-magnitude exceed the TH efficiency in c-Si. Both orientation dependences and magnitude of the TH and CARS signal strongly depends on the SiNW orientation.

References:

1. P. Yang, R. Yan, and M. Fardy, “Semiconductor nanowire: Whats Next?”, Nano Lett., Vol. 10, 1529-1536 (2010).
2. V.A. Sivakov, G. Bronstrup, B. Pecz, et al., “Realization of vertical and zigzag single crystalline silicon nanowire architectures”, J. Phys. Chem. C, Vol. 114, 3798-3803 (2010).

Optical Spectroscopy of Conductive Transparent Films of Single-Wall Carbon Nanotubes Filled with Acceptor Molecules

E.D. Obraztsova*[1], A.A. Tonkikh[1], V.I. Tsebro[2], E.A. Obraztsova[1], P.V. Fedotov[1], A.A. Dolgopolov[2], A.G. Nasibulin[3], E.I. Kauppinen[3], H. Kataura[4], K. Suenaga[4], A.L. Chuvilin[5]

[1] *A.M. Prokhorov General Physics Institute, RAS, 38 Vavilov street, 119991 Moscow, Russia*
[2] *Lebedev Physical Institute, RAS, Moscow, Russia*
[3] *Department of Applied Physics, Aalto University, Espoo, Finland*
[4] *Nanosystem Research Institute, AIST, Tsukuba, Japan*
[5] *Electron Microscopy Laboratory, CIC nanoGUNE Consolider, San Sebastian, Spain*
elobr@kapella.gpi.ru

Materials with a high optical transparency and a low electrical resistance are needed for formation of conductive electrodes for optoelectronics and solar cells. Today the most popular material used for this purpose is indium tin oxide (ITO). Its main disadvantages are a fragility and an insensibility in UV spectral range.

In this work we propose and investigate a new material - thin (with thickness less than 100 nm) films of single-wall carbon nanotubes (SWNTs) filled with different acceptor molecules (iodine, CuCl) - being able to replace ITO. The optical spectroscopy (Raman scattering and UV-vis-NIR optical absorption) plays a key role in characterization of such films.

We have realized a gas-phase filling of aerosol-grown SWNTs and have revealed (by a high resolution transmission electron microscopy) the formation inside nanotubes of one-dimensional crystasls or molecule chains (depending on the tube diameter). The size- dependent

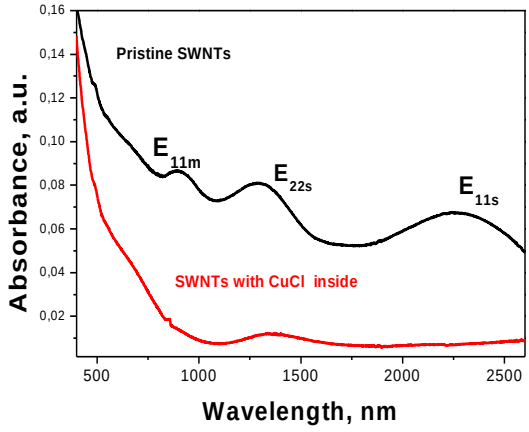

Fig.1. *UV-vis-NIR optical absorption spectra for film of SWNTs before (black) and after (red) filling with CuCl .*

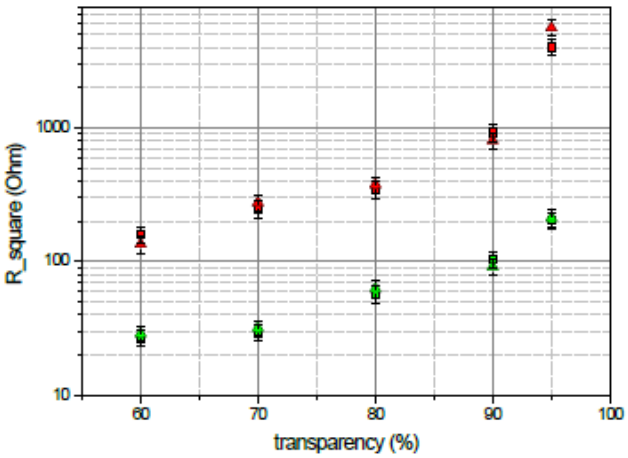

Fig.2. *A comparison of electrical resistance per square and transparency for SWNT films before (red) and after (green) gas-phase filling with CuCl.*

additional signal from the filler has appeared also in Raman spectra. The most remarkable changes after SWNT filling were observed in UV-vis-NIR optical absorption spectra. The bands, corresponding to E_{11} and even E_{22} electronic transitions,were suppressed. This can be interpreted as a result of a Fermi level shift into a valence band and a complete metallization of the material. To confirm this suggestion we have measured the electrical resistance of filled SWNT films and registered a big drop of electrical resistance (of one order of magnitude). A set of measurements of 2 parameters "optical transparency- electrical resistance" has demonstrated their comparability with those of ITO films.

The work was supported by RFBR grants 13-02-01354, 14-02-31818, 14-02-31829, RAS research programs and MK-6201.2014.2.

Raman and Second-Harmonic Diagnostics of SiC-Based Nanostructures

L.A. Golovan[1], A.A. Sokolov[1], V.Yu. Timoshenko[1], A.V. Semenov[2], V.M. Puzikov[2], V. Lysenko[3]

1- Faculty of Physics, M.V. Lomonosov Moscow State University, 119991, Moscow, Russia
2- Institute for Single Crystals NAS of Ukraine, 61001, Kharkov, Ukraine
3- INSA de Lyon, INL, UMR-5270, 69621, Villeurbanne, France
golovan@physics.msu.ru

Silicon carbide (SiC) nanostructures attract more and more attention of the researchers due to their unique optical and electronic properties. Crystalline SiC is a wide bandgap semiconductor (2.4 to 3.3 eV depending on polytype), which possesses high temperature and radiation stability. Additionally, crystalline SiC is characterized by high quadratic and cubic nonlinear-optical responses [1,2]. In this paper we report on applications of a method of the second-harmonic (SH) generation to detect formation of SiC nanocrystals grown on different substrates by means of direct-beam ion deposition technique [3]. Porous SiC (por-SiC) film formed by electrochemical etching of polycrystalline 3C-SiC (poly-SiC) wafer was investigated for comparison. The obtained results were compared with the Raman scattering data measured for the same samples.

Quasi-cw Cr-forsterite laser (1250 μm, 80 fs, 80 MHz, 2 nJ) and cw Nd:YAG (532 nm) laser were employed to excite the SH and the Raman scattering signals, correspondingly. Por-SiC film exhibits three-order-of-magnitude enhanced SH efficiency in comparison with poly-SiC. The spikes in the SH spectrum in por-SiC indicate light localization effects (Fig. 1a); autocorrelation function measurement evidences a significant rise of the photon lifetime in por-SiC film (up to 300 fs). For SiC films formed by direct-beam ion deposition technique the SH signals were found. The efficiency of the SH generation depends on amount of the formed SiC nanocrystals and their polytype (samples with 27R-SiC demonstrated more intensive SH than ones with 3C-SiC). The SH intensity was in good correlation with Raman signal intensity measured at 797 cm^{-1}(TO phonons in SiC). Due to the quadratic dependence on the excitation intensity, the SH generation seems to be more sensitive technique for the diagnostics of SiC nanocrystals on any substrate.

This work was supported by the Russian Foundation for Basic Research (grant no. 13-02-90424) and the State Fund for Fundamental Research (grant no. F53.2/096).

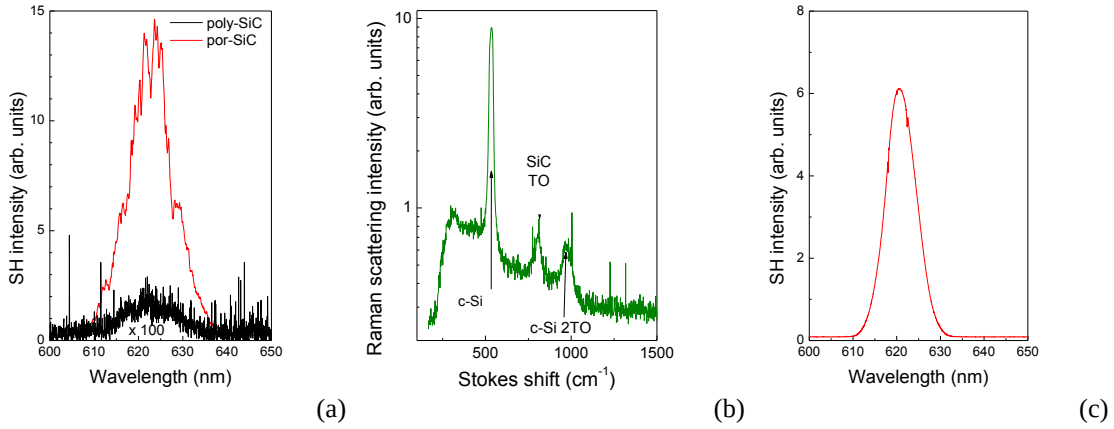

Figure 1. (a) The SH spectra for polycrystalline 3C-SiC(black line) and porous SiC (red line). Raman (b) and SH (c) spectra of SiC film formed by means of direct-beam ion deposition technique on crystalline silicon substrate.

[1] S.O. Konorov, et al., Diffuse optical harmonic generation in SiC nanopowder films: hunting scattered photons, Appl. Phys. B., vol. **78,** pp. 73-77 (2004).
[2] A.A. Borshch, et al., Nonlinear refraction in nanocrystalline silicon carbide films, JETP Letters, vol. **88**, pp. 386-388, (2008).
[3] A. V. Semenov, et al., Nanocrystalline SiC films prepared by direct deposition of carbon and silicon ions, Thin Solid Films, vol. **516**, pp. 2899–2904, (2008)

ON THE OPTICAL CENTRES IN Bi/Ga(Al) CO-DOPED SILICA GLASS

O. Laguta[1], H. El Hamzaoui[2], V. B. Arion[3], M. Bouazaoui[2] and I. Razdobreev[1]

[1]*CERLA/PHLAM, UMR CNRS 8523, University Lille-1, 59655 Villeneuve d'Ascq, France*

[2]*IRCICA - UMR8523/FR3024 CNRS, Parc de la Haute Borne, 50 av. Halley, 59658 Villeneuve d'Ascq, France*

[3]*Institute of Inorganic Chemistry, University of Vienna, Waehringer Str., A-1090 Vienna, Austria*

Igor.Razdobreev@univ-lille1.fr

Bi-doped silica glasses have attracted much attention due to promising applications in the field of fibre lasers and amplifiers [1]. Unfortunately, since the first demonstration of the near infrared photoluminescence (NIR PL) in Al/Bi co-doped silica glass [2], its nature remains unclear. Recently, we have demonstrated that the novel Bi/Ga co-doped silica glass exhibits analogous luminescent properties [3]. To explain the observed features we have also proposed the model of the complex centre, which consists of Bi^+ ion interacting with the defect, the latter bing responsible for the amplification and lasing in the optical fibres.

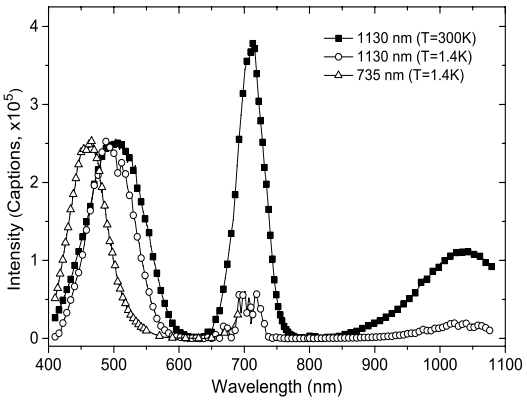

Fig 1. Excitation spectra in Bi/Ga co-doped silica glass.

In the present talk we report the results of the experiments on PL in magnetic field, and the temperature dependent excitation spectra (Fig. 1). The latter clearly indicate that (i) NIR PL bands at 1130 and 735 nm belong to different centres; (ii) there exists the temperature dependent energy transfer between these centres. We discuss the possible energy structure of the complex centre.

Acknowledgements: This work was supported by the "Agence Nationale de la Recherche" through the contract ANR "BOATS" 12BS04-0019-01.

References:

1. I. Bufetov and E. Dianov, "Bi-doped fiber lasers", Laser Phys. Lett. 6, 487-504 (2009).
2. Y. Fujimoto and M. Nakatsuka, "Infrared luminescence from Bismuth-doped silica glass", Jpn. J. Appl. Phys. 40, L279 - L281 (2001).
3. I. Razdobreev, H. El Hamzaoui, V. B. Arion and M. Bouazaoui, "Photoluminescence in Ga/Bi co-doped silica glass", Opt. Express 22, 5659-5674 (2014).

Talbot Interferometer for Measurement of Effect of Gradient Magnetic Field on Temperature and Temperature Profile of Gaseous Flame

Shilpi Agarwal, Manoj Kumar and Chandra Shakher

Instrument Design Development Centre, Indian Institute of Technology Delhi, Hauz Khas, New Delhi – 110016, India

sipi.agarwal@gmail.com, cshakher@iddc.iitd.ac.in

The influence of magnetic fields on gaseous flames has been investigated and is of great practical importance. Several authors [1-3] provide theoretical and experimental evidence that combustion temperature is increased and controlled with the use of suitable magnetic field. They have used thermocouple for the measurement of temperature, which do not provide full field temperature data and is likely to disturb the flow field. Circular grating Talbot interferometer has been used to visualize [4] and measure the temperature and its profile in gaseous flames [5-6]. Circular grating are easy to align and no prior information is needed regarding temperature profile. In this paper circular grating Talbot interferometer is used to study the temperature and temperature profile of butane torch burner flame in premixed, partially premixed with 50% air and diffusion condition under the influence of gradient magnetic field.

The experimental results show that the presence of gradient magnetic field has significantly increased the temperature of diffusion flame while a less effect on temperature is observed for partially premixed and premixed flame of butane torch burner. The magnetic behaviour of the flame depended on the oxygen concentration, which is paramagnetic in nature and attracted by a magnetic field, in contrast, butane gas escaped from the high intensity magnetic field. The effect of magnetic field is explained by the difference between the force acting on fuel gas and surrounding air.

[1] T. Aoki, Radical emissions and butane diffusion flames exposed to upward-decreasing magnetic fields, Japanese Journal of Applied Physics, 28, pp. 776-785, (1989).
[2] S. Ueno, Quenching of Flames by Magnetic Fields, Journal of Applied Physics, 65, pp. 1243-1245, (1989).
[3] N. I. Wakayama, Behavior of gas flow under gradient magnetic fields, Journal of Applied Physics, 69, pp. 2734-2736, (1990).
[4] A. W. Lohmann and D. E. Silva, A Talbot interferometer with circular gratings, Optics Communications, 4, pp. 326-328, (1972).
[5] C. Shakher and A. J. P. Daniel, Talbot interferometer with circular gratings for the measurement of temperature in axisymmetric gaseous flames, Applied Optics, 33, pp. 6068-6072 (1994).
[6] C. Shakher, A. J. P. Daniel, and S. K. Angra, Measurement of temperature profile of atomic absorption spectrophotometer burner (pre-mixed laminar flow slot burner) using Talbot interferometer, Optical Engineering, 33, pp. 2663-2669, (1994).

Femtosecond Laser Diagnostics of Plasmonic and Magnetoplasmonic Nanostructures

M.R. Shcherbakov, P.P. Vabishchevich, A.Yu. Frolov, T.V. Dolgova, and A.A. Fedyanin
Faculty of Physics, Lomonosov Moscow State University, Moscow 119991, Russia
fedyanin@nanolab.phys.msu.ru

Surface plasmon-polaritons (SPPs) are quasi-planar electromagnetic waves coupled to free-electron plasma, which can be excited at the boundary between metal and dielectric. These waves are believed to be the candidate for everyday-use information units as opposed to diffraction- limited photons and bandwidth-limited electrons. However, for plasmon-based technologies to be realized, efficient techniques for active manipulation of SPP signals are required. Considerable effort was afforded to actively control plamonic devices by external DC electric field, AC electromagnetic field, and DC magnetic field. The latter works describe how CW light beams interacting with a magnetic plasmonic medium are affected by magnetization. On the other hand, one of the most prominent opportunities of using SPP nanostructures is to shape femtosecond laser pulses. The mean lifetime of SPPs in nanostructures varies from several femtoseconds to several hundreds of femtoseconds. A femtosecond laser pulse interacting with such a short-living excitation gets coherently modified as indicated in many preceding works. Temporal shaping of femtosecond laser pulses by plasmonic nanostructures was observed both for the intensity and polarization state. However, the active control of the laser pulse shaping effect with plasmonic nanostructures has not been demonstrated yet.

In this work, we will discussed experimental demonstration of the mag-netic field-controlled shaping of femtosecond laser pulses reflected from a one-dimensional magnetoplasmonic crystal, which is a nickel diffraction grating supporting the SPP excitation via the +/-1st diffraction orders. External magnetization of the magnetoplasmonic crystal induces temporal modulation of 200 fs laser pulses when the SPP resonance is tuned across the spectral range of the femtosecond pulse being used. The switching of the pulse shape is attributed to modification of the surface magnetoplasmon dispersion law under magnetization applied in the Voigt configuration with respect to the SPP wavevector. We also use time-delayed optical anisotropy of resonantly excited surface plasmon polaritons to realize an ultrafast control over the state of polarization inside a single subpicosecond telecom laser pulse reflected from a plasmonic crystal of subwavelength thickness. Time-dependent nonzero depolarization has been found which indicates the sub-130-femtosecond polarization change inside the pulse. Experimental data are supported by an analytic model that predicts the fivefold enhancement of polarization conversion efficiency, which makes plasmonic crystals a promising compact media for ultrafast polarization control at room temperature.

HARMONIC NANOPARTICLES FOR NONLINEAR IMAGING AND PHOTO-INTERACTION

Andrii Rogov and Luigi Bonacina

GAP-Biophotonics, University of Geneva, 22 chemin de Pinchat, CH-1211 Geneva 4, Switzerland

luigi.bonacina@unige.ch

Nanoparticles are being increasingly applied as contrast agents for various imaging techniques (optical microscopy, MRI, PET, X-ray, computed tomography, and so on) or as treatment agents exploiting their preferential accumulation in targeted structures for drug delivery or their response to external stimuli (magnetothermal therapy, laser activation). Concerning the optical properties addressed, fluorescence/luminescence is by far the most exploited observable at present, followed by plasmonic response in metal NPs. One very recent development, yet little-known and strongly related to the evolution of ultrafast laser technology, is the use of so-called harmonic nanoparticles (HNPs). The latter designate a family of inorganic nanometric crystals (size < 100 nm) of different materials (KNbO3, BiFeO3, LiNbO3, KTP, …) sharing the characteristic of noncentrosymmetric structure. This property determines their large nonlinear optical efficiency, and, in fact, in the last years they have been mostly investigated as localized sources for second harmonic generation. After introducing this approach and comparing it with respect to other nanoparticles-based labelling strategies (quantum dots, up-conversion NPs), I will highlight some recent applications in the field of (multi-photon) imaging and optical detection of biological samples together with NPs-mediated photo-interaction with cellular DNA.

Acknowledgments:

European FP7 project “NAMDIATREAM” (http://www.namdiatream.eu), Swiss NCCR “MUST” (http://www.nccr-must.ch) .

References

1. L. Bonacina, “Nonlinear Nanomedecine: Harmonic Nanoparticles toward Targeted Diagnosis and Therapy” Mol. Pharmaceutics, **10**, (3) 783-792 (2013)

2. T. Magouroux et al., “High-Speed Tracking of Murine Cardiac Stem Cells by Harmonic Nanodoublers”, SMALL, **8** (17), 2752-2756 (2012)

3. D. Staedler et al., “Harmonic Nanocrystals for Biolabeling: A Survey of Optical Properties and Biocompatibility”, ACS Nano, **6** (3), 2542–2549 (2012)

Toxic influence of heavy metal ions on living organisms investigated by different laser optical methods

Petrova G.P., Sergeeva I.A, Fedorova K.V.

Physics Department
of Lomonosov Moscow State University, Moscow, Russia

E-mail: petrova@phys.msu.ru

Toxicity influence of heavy metal ions with large ionic radii (like Pb^{2+} (1,2 Å), Rb^{+} (1,47 Å), Cs^{+}(1,65 Å), Eu^{3+} (1,33 Å), Gd^{3+} (0,98 Å) and etc.) on living organisms are discussed on the base of the physical mechanisms of metal ions interaction with charged macromolecules – proteins and enzymes. The behavior of some proteins (like protein of serum blood and fibrillar protein like collagen) and some enzymes - pepsin, collagenase, lysozyme, creatine kinase in water solutions in the presence of different toxic metals ions at the very low concentrations of the salts were investigated by the used some optical methods - Laser light scattering (photon correlation spectroscopy) , fluorescence spectroscopy and polarized fluorescence. Interaction of the proteins and enzymes in solutions containing heavy metal ions results in the formation of large (nano size) clusters. These processes can to disturb metabolic processes in the organism (celles, membranes, plasma blood). The nanoparticle formation molecular mechanism is considered in terms of dipole-dipole and charge-charge interaction of the macromolecules in its water shells.

[1] Petrova G.P. “Physical Mechanisms of “Poisoning” the Living Organism by Heavy Metals” in the book ENVIRONMENTAL MONITORING, Ed.by E.O.Ekundayo, INTHECH open , 2011.

Development of a laser based laboratory light scattering instrument for light scattering studies on small particulate matter

A. Gogoi[1] and G. A. Ahmed[2]

1- Department of Physics, Jagannath Barooah College, Jorhat 785001, Assam, India
2- Department of Physics, Tezpur University, Tezpur 784028, Assam, India

Main author email address: ankurgogoi@gmail.com

The light scattering patterns of small particulate matter contains characteristic information about their physical and optical properties. These particles are normally found as aerosols, suspended particles in solutions (hydrosols) or as embedded particles, especially nanoparticles in optically transparent media. The intensity of light scattered by a particle (or ensemble of particles) is a function of the angle between the incident and scattered radiation. This angular dependence is also a function of size, shape, optical properties of particles (refractive index, permittivity, absorption), particle orientation, incident wavelength, polarization of the incident wave, density, structure of aggregates (fluffy, fractal, dense, etc.), and quality of particle surfaces (roughness, buffing, etc.) [1 – 3]. It is very important to study the angular scattering dependency of small particulate matter as such results contain information by which the particle may often be classified or even identified and helps for better understanding of radiation transfer through a medium containing the scatterer [2].

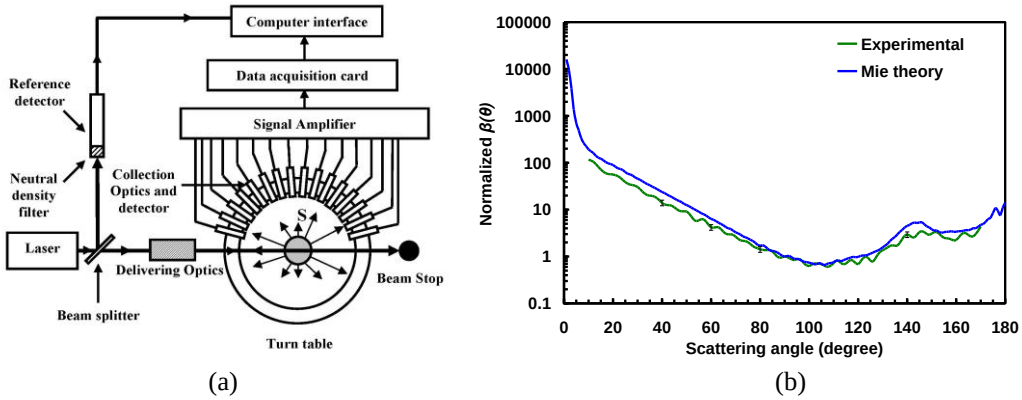

(a) (b)

Figure 1 (a) Schematic diagram of the light scattering setup. (b) Measured volume scattering function (VSF) of water droplets (solid green line) at 543.5 nm incident laser wavelength. The result was compared with Mie calculations (solid blue line).

In this contribution the design and fabrication of a miniaturized detector array incorporated laser based light scattering instrument and its application in measuring the scattering properties of different types of small particulate matter (for example graphite flakes, soot particles, ice analogue crystals etc.) are presented. The instrument can measure scattered light signals from 10° to 170° in steps of 1° and can be operated at three different incident laser wavelengths (543.5 nm, 594.5 nm and 632.8 nm). The accuracy and the reliability of the setup were verified by conducting light scattering measurements on spherical water droplets and comparing the results with theoretical Mie calculations. The particles were sprayed into the laser beam by using a particle sprayer. The experimental results were compared with theoretically generated Mie and T-matrix plots for scattering particles of equivalent size to yield more fruitful conclusions. Significant variations of the scattering behavior of the samples were observed for the three different incident laser wavelengths.

[1] M. I. Mishchenko, J. W. Hovenier and L. D. Travis (editors), Light Scattering by Nonspherical Particles: Theory, Measurements, and Applications (Academic, San Diego, California), (2000).
[2] P. H. Kaye, Spatial light-scattering analysis as a means of characterizing and classifying non spherical particles, Meas. Sci. Technol., vol. 9, pp. 141–149, (1998).
[3] A. Gogoi, A. K. Buragohain, A. Choudhury and G. A. Ahmed, Laboratory measurements of light scattering by tropical fresh water diatoms, J. Quant. Spectrosc. Radiat. Transfer, vol. 110, pp. 1566–1578, (2009).

LIBS-study of Graphite-Containing Composite Electrochemical Coatings

E. Surmenko[1], T. Sokolova[1], D. Bessonov[1], T. Shevchenko[2], E. Vasilenko[2]

1- Saratov State Technical University named after Yu.A. Gagarin, 77 Polytechnicheskaya st., 410054, Saratov, Russia

2- Engels Technological Institute, 17 Svobody sq., 413100, Engels, Saratov region, Russia

surmenko@yandex.ru

Anti-abrasion and corrosion-resistant electrochemical coatings are widely used in technics for increase resistance and durability of metal products. The protective ability of such coatings can be increased by implantation into a metal matrix nonmetallic disperse inclusions, i.e., by electrodeposition of composite electrochemical coating (CEC). As a disperse material in coatings, graphite and its derivatives are of interest. Methods of obtaining, deposition and modifying of graphite-containing CEC affect the final chemical composition of a surface.

The penetration of coating substance into the substrate and the estimation of electrodeposition quality were characterized by means of laser induced breakdown spectroscopy (LIBS). Two main types of CEC – «zinc-graphite» and «nickel-chrome-graphite» - deposited on steel substrates in different modes were studied with the aid of scanning sampling. This way the layer-by-layer investigation are available. Every scanning sampling was carried out three or four times from the same sampling path. Nine types of samples obtained in different modes were studied with the same equipment and parameters.

The experimental set-up LDMA was used. The source of spectra excitation is a Q-switched Nd:YAG laser (λ=1.06 μm). A pulse repetition rate is 25 Hz. The power density in a monopulse mode 10^{10}-10^{12} W/cm$^{2.}$ The limit of element detection is 10^{-10} g; the relative limit of detection is 0.001 %. The registration of spectra is implemented by diffraction spectrograph and CCD camera.

«Nickel-chrome-graphite» coatings were studied with four laser shots from the same path, depth of a laser crater is approximately 15, 23, 30, 35 μm. It was found out that besides main components Ni, Cr and C, alien impurities Al and Cu enter the composition of graphite nitrate. Since the coating itself has a small thickness, it appeared to be more appropriate to consider the composition of the material as steel and Ni, Cr, Al, Cu, C as additives. Although graphite bisulfate was cleaner than graphite nitrate, LIBS study showed that the distribution of carbon structures is more homogeneous in graphite nitrate coatings.

«Zinc-graphite» coatings were studied with three laser shots from the same path, depth of a laser crater is approximately 35, 44, 50 μm. It was found out that the element composition of the obtained CEC includes Zn, Fe, Al, C. The number of components depends on the electrolysis current density during the anodic polarization and the ratio t_k/t_a, where t_k and t_a – duration of cathodic and anodic polarization correspondingly.

Acknowledgements: The work was partly supported by Russian Scientific Fund (appl. 14-12-00395); equipment of VCCU “Laser & Optical Technologies”.

Determination of the elemental composition of optical glasses by laser-induced breakdown spectroscopy

C. Gerhard[1], J. Hermann[2], L. Mercadier[2], L. Loewenthal[1], E. Axente[3], C. R. Luculescu[3], T. Sarnet[2], M. Sentis[2], W. Viöl[1]

[1]Laboratory of Laser and Plasma Technologies, University of Applied Sciences and Arts, Von-Ossietzky-Straße 99, 37085 Göttingen, Germany
[2]LP3, CNRS - Aix Marseille University, 163 Av. de Luminy, 13288 Marseille, France
[3]Laser-Surface-Plasma Interactions Laboratory, Lasers Department, National Institute for Lasers, Plasma and Radiation Physics, Măgurele, Romania

gerhard@hawk-hhg.de

Optical glasses are complex materials with strong variations of minor and major element concentrations, making their analytical investigations particularly difficult. In this contribution we present a calibration-free laser-induced breakdown spectroscopy (LIBS) method for quantitative elemental analysis of such optical glasses with a measurement precision of approx. 10%. We recorded plasma emission spectra during ultraviolet nanosecond laser ablation of barite crown and heavy flint glass samples. These spectra were subsequently compared to the particular theoretical spectral radiance, calculated for plasmas in local thermodynamic equilibrium. We determined the relative elemental fractions as well as the plasma properties by an iterative calculation algorithm, successively computing the best agreement between both measured and computed spectra [1].
For validation, we performed comparative experiments on fused silica of high purity. Further, we compared the measured oxygen fractions to the theoretical stoichiometry expected from the glass composing oxides. Based on the measured elemental compositions, the mass fractions of glass forming oxides were deduced additionally and compared to reference values reported in literature. As shown in figure 1, the measured and calculated composition of the investigated glasses features a sufficient agreement with the reference values.

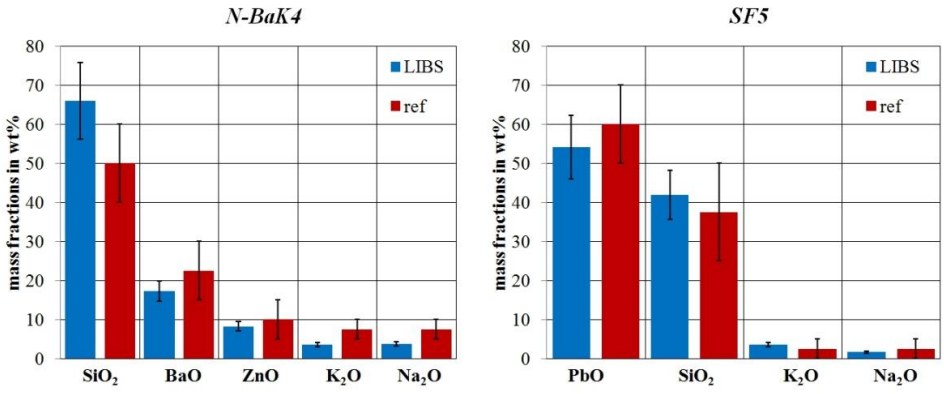

Figure 1 Mass fractions of glass forming oxides in wt% for barite crown glass N-BaK4 (left) and heavy flint glass SF5 (right), deduced from the elemental compositions measured by LIBS, and typical reference (ref) values of the investigated glass families as reported in [2]

The results confirm the suitability of the presented LIBS method, based on accurate plasma modeling, for quantitative elemental analysis of optical glasses and complex materials in general (avoiding thus the need of standard samples). Here, good accuracy is obtained for short delays between the laser pulse and the detector gate, when the electron density is larger than 10^{17} cm^{-3}. Based on comparative measurements using both X-ray photoelectron spectroscopy and energy-dispersive X-ray spectroscopy it can be stated that LIBS analytical performance is comparable or even better than that obtained with such standard techniques.

[1] E. Axente, J. Hermann, G. Socol, L. Mercadier, S. Beldjilali, M. Cirisan, C. R. Luculescu, C. Ristoscu, I. N. Mihailescu, V. Craciun, Accurate analysis of indium-zinc oxide thin films via laser-induced breakdown spectroscopy based on plasma modeling, Journal of Analytical Atomic Spectrometry 29, 553-564, (2014).
[2] W. Vogel, K. Gerth, W. Heindorf, Zur Entwicklung der optischen Gläser, Jenaer Rundschau 1, 75-76, (1965).

Spectral analysis of protoplasmic streaming velocities in *Physarum Polycephalum* obtained by laser Doppler spectroscopy

S. Proskurin[1], T. Avsievich[2]

1, 2- Tambov State Nechnical University, 106 Sovetskaya St, Tambov, 392000, Russia
email: tavsievich@tamb.ru

Amoeboid motility is a typical example of self-oscillating waves, which are inherent for a wide class of cells from single-celled amoeboid to cancer cells in multicellular organisms [1]. In the present study the time-dependent velocity spectra of self-oscillating motility of the isolated plasmodium strand of plasmodium *P. Polycephalum* upon exposure to inhibitors of cellular respiration: potassium cyanide (KCN) and salicylhydroxamic acid (SHAM) was analyzed.

Cytoplasmic streaming velocity registration was carried out using a sign-sensitive laser Doppler microscope [2]. Carved out strand of plasmodium was treated by KCN and SHAM (5 and 7 μM respectively) which leads to a cessation the movement of protoplasm. Further strand was placed in buffer, and resumed locomotion activity through 10 min was recorded. Measurements are presented in Fig . 1A.

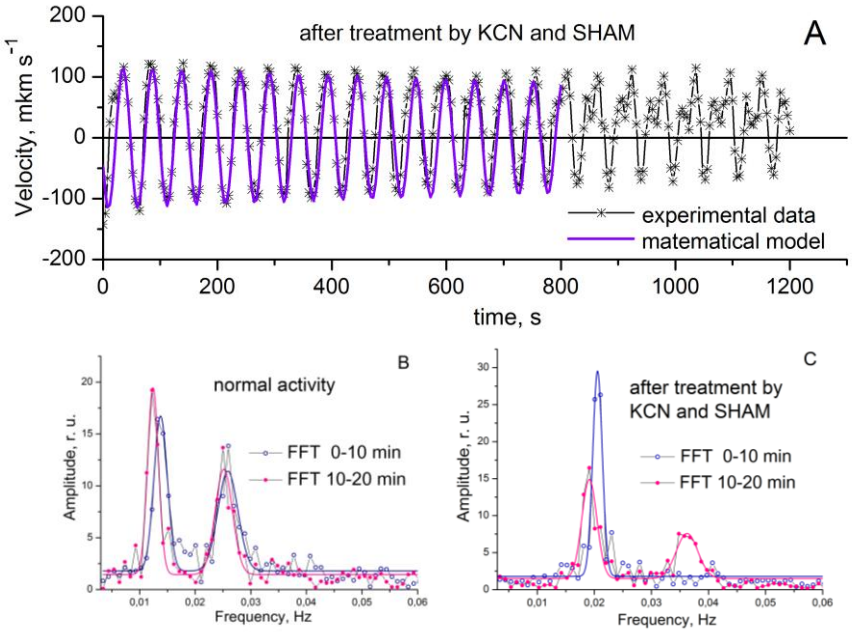

Figure 1. A – time time dependence of protoplasmic streaming in plasmodium strand after removing the inhibitors of respiration; B - frequency spectra of the time time dependence of protoplasmic streaming from 0 (blue) and after (pink) 600 seconds B - in buffer, C – after treatment by KCN and SHAM (solid lines - Gaussian approximation of frequencies peaks).

Spectral analysis of the time time dependence of protoplasmic streaming (length 600 s) from 0 and 600 s allows to distinguish two distinct harmonic signals, which in the original signal are not tracked (Fig. 1B, C). Oscillation frequencies of the protoplasm in the buffer were ω_1=0.013±0.0004 и ω_2=0.0254±0.0001. At first 10 min after treatment by KCN and SHAM just one source of oscillations with frequency ω_1 = 0.0198 ± 0.0004 Hz is present, in the next 10 minutes noted the appearance of a second frequency peak with ω_2 = 0.0388 ± 0.0013 Hz. On the 12 minute, the system returns to the normal state with two harmonic components. Despite the frequencies are differs in first and second signals, the ratio ω_2/ω_1=1.96±2% in each of them remains constant.

The mathematical model (solid purple line, Fig. 1A) of the signal was constructed using the found frequencies values. Significant correlation between mathematical model and experimental data are shown (R^2= 0.843).

[1] Y. Romanovsky, V. Teplov, V. Mitrofanov. Synchronization of mechanochemical auto-oscillations within the Physarum polycephalum plasmodium by periodical external actions. Biofizika, vol. 50, pp. 704-12, (2005).
[2] S. Proskurin, Doppler spectroscopy alternating unsteady flow in living objects, PhD dissertation, Moscow State University, (1993).

Tuesday 7th October

Twists and more: the complex shape of light

Miles Padgett

School of Physics and Astronomy, The University of Glasgow, Glasgow, Scotland UK.

E-mail: miles.padgett@glasgow.ac.uk

For much of the last Century it was recognized that the spin angular momentum of $\hbar$ per photon is insufficient to account for the conservation of angular momentum associated with high-order atomic transitions. The concept of non-spin angular momentum of light was hence understood, albeit as a rare phenomenon. This understanding changed in 1992 when Allen *et al*. [1] detailed how laser beams could be produced such that all their photons were in the same, non-zero, orbital angular momentum (OAM) state. In that work the laser beams were exemplified as Laguerre-Gaussian (LG) modes, that are examples of beams possessing helical phasefronts described by $\exp(i\ell\vartheta)$ and carrying an OAM corresponding to $\ell\hbar$ per photon. However, these LG modes are just one particular basis set and without any recognition of their momentum properties, methods to create laser beams with helical phasefronts had been previously reported. For example, it is possible to modify a laser cavity such that LG modes are produced directly [2], or a diffraction grating containing a fork dislocation on the beam axis creates a beam with helical phase-fronts in the first diffraction order [3]. This last approach is now commonly implemented using programmable spatial light modulators, pixelated liquid crystal devices with which any diffractive optical element can be created. Many groups world-wide have subsequently used OAM beams and the technology associated with their study in a various applications [4].

Classically, OAM is described by 19th century electromagnetism and in the quantum regime OAM is but one example of a spatial state. However, since 1992, OAM and other spatial modes have attracted interest in their use in applications ranging from optical manipulation [5] to imaging [6] and communications [7]. In addition to applications, the analysis of problems in terms of OAM has highlighted new effects ranging from rotational Doppler shifts [8] to angular uncertainty relationships [9]. Most generally, OAM has illustrated that with respect to the optical behavior of a light beam, the phase-structure of the beam is of equal importance as the intensity. Hopefully OAM will continue to inform and contribute to modern optics over coming years too.

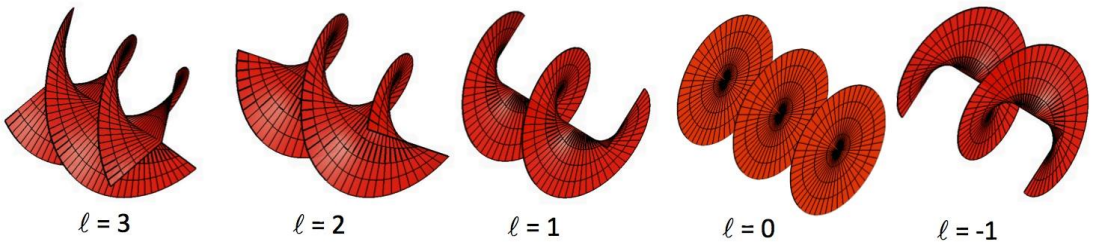

Figure 1. When laser beams have helical phasefronts their energy and momentum twist around the beam axis and the beam carries an orbital angular momentum of $\ell\hbar$ per photon.

[1] L. Allen, M.W. Beijersbergen, R.J.C. Spreeuw, J.P. Woerdman, Orbital angular-momentum of light and the transformation of Laguerre-Gaussian laser modes, Phys Rev A. 45 (1992) 8185–8189.
[2] C. Tamm, Frequency locking of 2 transverse optical modes of a laser, Phys Rev A. 38 (1988) 5960–5963.
[3] V.Y. Bazhenov, M.V. Vasnetsov, M.S. Soskin, Laser-beams with screw dislocations in their wave-fronts, Jetp Lett. 52 (1990) 429–431.
[4] A.M. Yao, M.J. Padgett, Orbital angular momentum: origins, behavior and applications, Adv. Opt. Photon. 3 (2011) 161.
[5] M. Padgett, R. Bowman, Tweezers with a twist, Nat Photonics. 5 (2011) 343–348.
[6] C. Maurer, A. Jesacher, S. Bernet, M. Ritsch-Marte, What spatial light modulators can do for optical microscopy, Laser & Photon Rev. 5 (2010) 81–101.
[7] A.E. Willner, J. Wang, H. Huang, A Different Angle on Light Communications, Science. 337 (2012) 655–656..
[8] M.P.J. Lavery, F. Speirits, S.M. Barnett, M.J. Padgett, Detection of a Spinning Object Using Light's Orbital Angular Momentum, Science. 341 (2013) 537–540.
[9] S. Franke-Arnold, S.M. Barnett, E. Yao, J. Leach, J. Courtial, M. Padgett, Uncertainty principle for angular position and angular momentum, New J Phys. 6 (2004) 103.

"Laser 3D printing for photonics, metamaterials and medicine"

Maria Farsari

IESL-FORTH, N. Plastira 100, 70013, Heraklion, Crete, Greece.

*mfarsari@iesl.forth.gr

Direct Laser Writing (DLW) is a technique that allows the fabrication of three-dimensional structures with sub-100 nm resolution. It is based on multi-photon absorption; when the beam of an ultra-fast laser is tightly focused into the volume of a transparent, photosensitive material, polymerization can be initiated by non-linear absorption within the focal volume. By moving the laser focus three-dimensionally through the material, 3D structures can be fabricated. The technique has been implemented with a variety of materials and several components and devices have been fabricated such as photonic crystals (Fig. 1a), biomedical devices (Fig. 1b), and microscopic models (Fig. 1c).

The unique capability of DLW lies in that it allows the fabrication of computer-designed, fully functional 3D devices. Here, we summarize the principles of microfabrication, and present our recent work in materials processing and functionalization of 3D structures. Finally, we discuss the future applications and prospects for the technology.

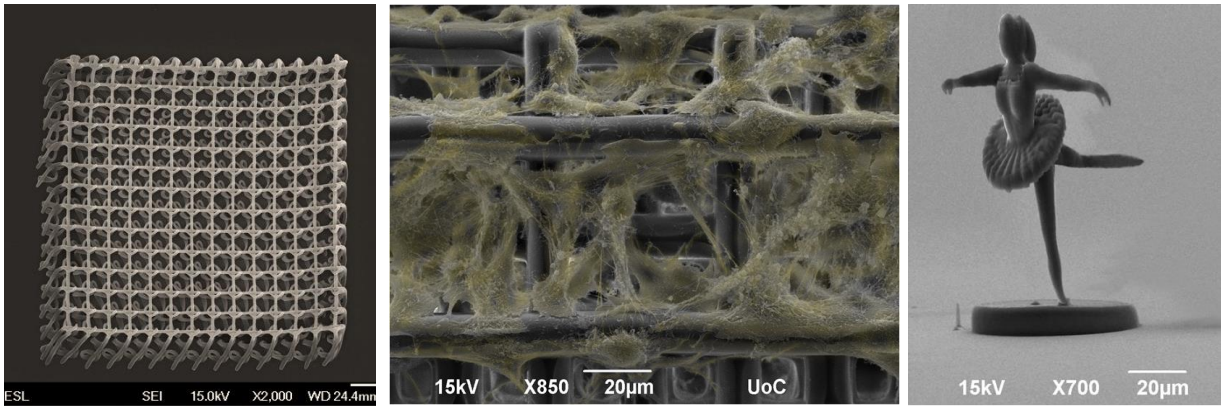

Fig. 1: (a) A spiral photonic crystal. (b) Scaffold for cell growth (c) A micro-dancer

Lasers print and functionalise biosensors

Ioanna Zergioti

National Technical University of Athens, Physics Department, Iroon Polytechneiou 9, 15780 Zografou, Athens, Greece

Laser Induced Forward Transfer (LIFT) enables the direct printing in high spatial resolution of biomaterials on sensors substrates. It is also used as an advanced functionalisation process of the sensors surface without the need for intermediate layers. The LIFT technique is applied for the fabrication of several types of biosensors with high spatial resolution in a direct approach. Examples to be presented include photosynthetic, enzymatic biosensor, and DNAzyme biosensors. The laser printing experiments are performed with a nanosecond or picosecond laser beam in a high image projection optical system operating at 266 nm, 355 nm, 532 nm, or 1064 nm.
The mechanism of the laser process has been investigated by a laser pump-probe experiment so as to observe the real time process and to measure the speed of the ejected bioliquid jet. The direct functionalisation process is accomplished due to the high printing velocity of the liquid biomaterial and the high impact pressure on the sensor substrate. Several examples for the functionalization of biosensor by laser means will be presented.

Laser Induced Forward Transfer printing of conductive materials for printed electronics

Edsger Smits[1], Merijn Giesbers[1], Rajesh Mandamparambil[1], Jeroen van den Brand[1]

1- Holst Centre / TNO, High Tech Campus 31, 5656AE, Eindhoven, The Netherlands.

Edsger.smits@tno.nl

Direct printing of conductive tracks is an attractive proposition for printed electronics. The conventional methods of patterned printing includes ink jetting and screen printing. The disadvantages of both printing techniques includes their high dependencies on viscosities, lower resolution, limited aspect ratios. In the case of inkjet printing although customization is possible, it is limited to low viscous materials leading to low aspect ratios and as a consequence lower conductivities. Meanwhile screen printing can give higher aspect ratios but the expense of customization. Laser printing offers the advantage of attaining higher resolutions, speed, and aspect ratio in a free form patterned deposition with the ability to handle wide range of materials.

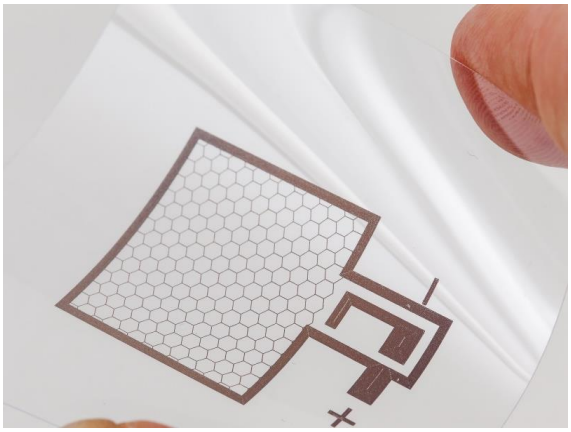

Figure 1. Laser printed silver paste based current spreading bus bar structures for OLED applications.

In this presentation we will discusses the potential use of lasers to print high resolution conductive tracks using silver pastes with feature sizes ranging from 30µm to 100 µm. The height of the conductive tracks deposited ranges between 1µm to 15 µm enabling the process to achieve high aspect ratio structures. A solid state based laser capable of high frequencies is guided using a galvo scanner on to a donor substrate. The donor material is propelled by the vaporization of the material at the substrate-material interface. An acceptor material such as a flexible polymer foil is placed at a separation from the donor substrate on which the transfer occurs. To achieve various deposit sizes the spot size of the laser beam is varied by choosing appropriate projection lenses for the experiments. Continuous tracks are patterned deposited on the donor substrate and are sintered at elevated temperatures to achieve up low bulk resistivity. The paper will in part discuss the ejection phenomena of the paste from the donor substrate using our high speed visualization setup. We will review how the appropriate laser process and donor system can yield satisfying direct printing of the pastes.

Laser nanocrystallization of metals

I. Zavestovskaya[1,2]

1-P.N. Lebedev Physical Institute of RAS, Leninsky pr.53, Moscow, 119991, Russia
2- National research Nuclear University MEPhI (Moscow Engineering Physics Institute), Rashirskoe sh.31, Moscow, 115409, Russia

INZavestovskaya@mephi.ru; zavest@sci.lebedev.ru

Laser micro- and nanostructuring of materials is important in many scientific, technological and medical applications [1-3]. Nanostructures resulting from laser material processing have unique properties and cannot be produced by other, nonlaser techniques.

In optimizing laser nanostructuring conditions, an important point is to optimize the size of the resulting structures. The minimum possible size of the structures (tens of nanometers) produced by direct laser ablation of the surface is possible in two cases: 1) intense laser ablation due to cluster redeposition in and outside the ablation crater and 2) ultrashort laser pulses which ensure very rapid heating, melting and solidification of metal surfaces.

Laser structuring without ablation is possible when the pulse energy density is slightly below the ablation threshold but exceeds the melting threshold. Use is typically made of short and ultrashort (nano-, pico- and femtosecond) laser pulses with near-threshold intensities, which cause local metal melting with no significant ablation.

In recent years, controlled direct surface nanostructuring with laser pulses under such conditions has been the subject of intense research. Attempts were made to systematically study laser nanostructuring mechanisms and optimize processing conditions (intensity, duration, number and repetition rate of laser pulses) with consideration for the thermodynamic characteristics, mechanical properties and surface quality of the target material [4,5].

This Paper reviews the results of experimental and theoretical studies of micro- and nanomodification processes induced on the surface of metals and other materials by short and ultrashort laser pulses. Particular attention is paid to the possibility of direct laser nanostructuring through melting of the material (with or without ablation), followed by ultra-rapid solidification of the molten surface.

The focus of attention have been the results on studying the kinetics of ultra-rapid solidification of the molten surface, and determination of the conditions which ensure forming of surface nano-scale structures.

An analytical solution to the rate equation for the crystallite size distribution after ultrarapid cooling has been found. The average number of atoms per crystallite and the size of crystalline grains resulting from pulsed laser irradiation of metal surfaces have been evaluated.

Determination of the volume fraction of crystallised phase allows one to find the critical cooling rate at which crystallization is impossible and the structure amorphises, i.e. to establish a kinetic amophisation criterion.

The model for laser modification of porous metallic films called as “the instant collapse of the pores” was considered [6].

The presented data can be used to optimize direct laser micro- and nanostructuring conditions and to ensure process control and reproducibility.

[1] I.N. Zavestovskaya, “Laser assisted metal surface micro- and nanostructurization”, Laser and Particle Beams,, vol. 28,p. 437 (2010).
[2] I.N. Zavestovskaya. «Laser nanostructurization of metal surfaces», Quantum Electronics, vol.40 (11), pp. 942-954 (2010).
[3] A. Y. Vorobyev, C. Guo, «Colorizing metals with femtosecond laser pulses», Appl.Phys.Lett. 92, 041914-3 (2008).
[4]A. Kanavin, N. Kozlovskaya, O. Krokhin, I. Zavestovskaya, “Laser nanostructurization of the metal and alloy surfaces”. American Institute of Physics Conf. Proc., vol. 1278, pp. 111-120, (2010).
[5] V.Bezotosny, I. Zavestovskaya, A. Kanavin, N. Kozlovskaya, O. Krokhin, V. Oleshenko, Yu. Popov, E.Cheshev. Trudy II Simpoziuma po kogerentnomu opticheskomu izlucheniyu poluprovodnikovyh soedinenii I struktur (Proc. II Symp. On Coherent Optical Radiation from Semiconductor Materials and Structures), (RIIS FIAN, Moscow, 2010), p.165 (in Russian).
[6] M.S. Zolotykh, I.N. Zavestovskaya, A.P. Kanavin, in Trudy III Simpoziuma po kogerentnomu opticheskomu izlucheniyu poluprovodnikovyh soedinenii I struktur (Proc. III Symp. On Coherent Optical Radiation from Semiconductor Materials and Structures), (RIIS FIAN, Moscow, 2011), p. 221 (in Russian).

Laser fabrication of microelectrodes on flexible substrates by subtractive and additive laser techniques

D. Puerto[1], G. Coustillier[1], M. Sentis[1], A.P. Alloncle[1], Ph. Delaporte[1], D. Karnakis[2], M. Makrygianni[3], M. Chatzipetrou[2], A. Kyritsis[3], C. Chatzimanolis Moustakas[3], and I. Zergioti[3]

1- Aix-Marseille University, CNRS, LP3 laboratory, Luminy Campus, C.917, 13288 Marseille cedex 9, France
2- Oxford Lasers Ltd., Unit 8, Moorbrook Park, Didcot, OX11 7HP, United Kingdom
3- National Technical University of Athens, 9, Heroon Polytechneiou, Athens, 15780, Greece

Laser processes represent a key technology in the next decade for manufacturing flexible organic electronics. In the frame of the LaserMicroFab European project [1], we investigate two major laser applications; thin film patterning and laser printing. Different approaches are investigated to optimize these laser processes and to integrate the solutions in laser manufacturing tools [2]. The challenge for thin film patterning of organic stacks is to reach sub-micrometer resolution together with the preservation of the quality and functional properties of the remaining unpatterned layers. The main difficulty of the printing process (Laser-Induced Forward Transfer-LIFT) is to combine high velocity with high resolution printing [3] in order to fulfill the requirements of industrial manufacturing.
In this study, we used these subtractive and additive laser techniques to realise electrodes on flexible substrate (PET). Some samples are realised by laser scribing of a uniform metallic layer deposited on PET, and others are obtained by LIFT printing silver nanoparticle inks followed by curing and sintering steps (Figure 1).

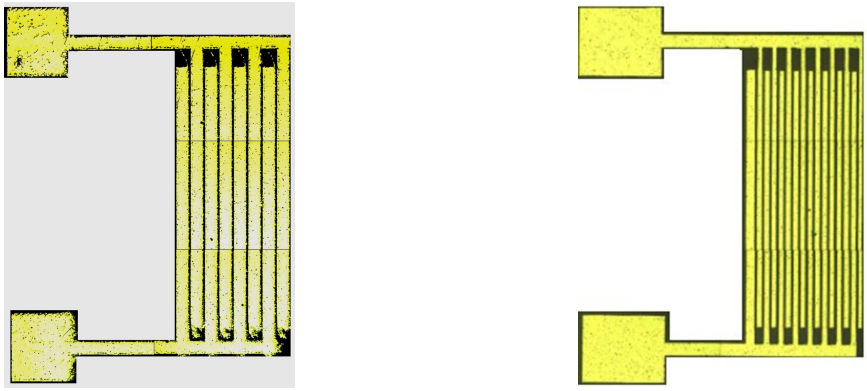

(a) (b)

Figure 1. Microelectrodes fabricated by (a) laser printed from silver nanoparticle inks on PET flexible substrates and (b) laser ablation of a thin layer of silver deposited by evaporation methods in PET.

The sensor is composed of a sensitive material deposited on the microelectrodes on PET substrates by mans of laser transfer. Different sensing materials based on PVA/CNT composites and Nafion/CNT composites, have been studied for the fabrication of humidity sensors. By incorporating CNT into non-conductive polymer matrices, the newly formed conductive polymer composites can be used as the sensing materials in sensors. The fabrication of microsensors demands accurate deposition and/or patterning of polymer/CNT composite layers with micrometric size. Finally, the sensors were electrically characterized by measuring the conductivity of the sensing layer as a function of the humidity of the surrounding environment.
After some optimisation steps mainly focused on beam shaping, ink viscosity, and usual laser process parameters, the morphological and electrical properties of the electrodes realised by laser printing and laser ablation are characterized. The sensor performances are measured and correlated to the electrodes characteristics, and compared with those of sensors realised with other processes.

[1] http://lasermicrofab.ntua.gr/
[2] http://www.oxfordlasers.com
[3] L. Rapp, E. Biver, A. P. Alloncle, Ph. Delaporte., 'High-Speed Laser Printing of Silver Nanoparticles Ink', J. of Laser Micro/NanoEnginnering (2014)

Influence of the picosecond laser irradiation on the electrochemical and spectroscopic properties of graphene-chitosan composite film

R. Trusovas[1], A. Radzevič[2], R. Celiešiūtė[2], R. Pauliukaite[2]. G. Račiukaitis[1]

1- Department of Laser Technologies, Center for Physical Sciences and Technology, Savanoriu Ave. 231, LT-02300, Vilnius, Lithuania
2- Department of Nanoengineering, Center for Physical Sciences and Technology, Savanoriu Ave. 231, LT-02300, Vilnius, Lithuania

romualdas.trusovas@ar.fi.lt

Graphene is one atom thick two-dimensional crystal, consisted from carbon atoms, joined into a honeycomb lattice. Graphene has unique physical properties, such as high carrier mobility, high thermal conductivity and quantum hall effect at room temperature, high optical transparence at visible range. These properties made graphene very attractive material to various applications. Use of graphene in electrochemical applications is a complicated task due to the requirements of a stable layer on an electrode surface. Lasers are yet not widely applied for graphene activation [1, 2].
In this work, activation of the chitosan-modified graphene on indium-tin-oxide (ITO) electrodes was performed with picosecond laser irradiation. Experimental setup consisted from picosecond laser (Atlanic, 10 ps, 100 kHz, Ekspla), beam expanding optics and galvanometric scanner. Graphene-chitosan composites were casted on ITO electrodes on a glass substrate. The thickness of the film was ~1 μm. During laser treatment experiments, the average laser power and pulse overlap were varied.
The composite electrodes were characterized with Raman spectroscopy, cyclic voltammetry (CV), electrochemical impedance spectroscopy (EIS) and SEM (Figure 1).

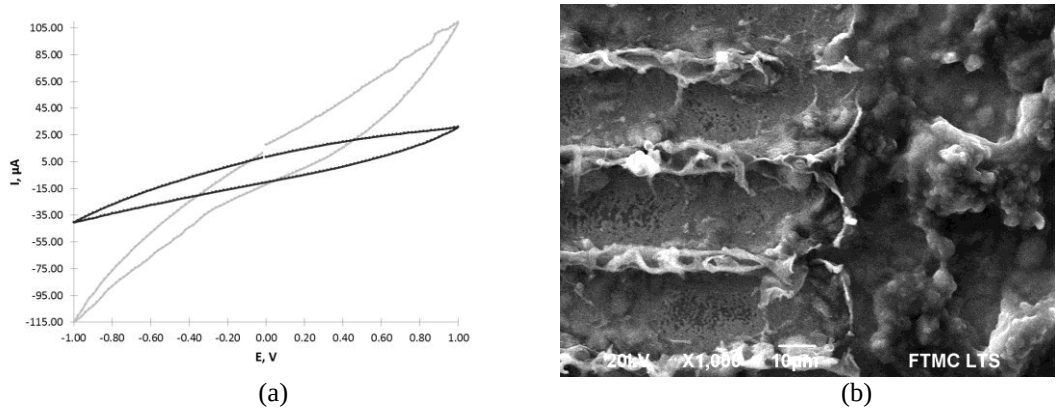

(a) (b)

Figure 1 (a) CV measured in 0.1 mol/l KCl solution. Black curve – untreated graphene-chitosan film , gray – graphene-chitosan film after laser treatment (b) SEM image of boundary of laser treated (left) and untreated (right) graphene-chitosan film. Laser treatment parameters: average laser power – 200 mW, pulse repetition rate – 100 kHz, scanning speed – 300 mm/s.

The laser treatment improved electrochemical properties of the electrodes made of the modified chitosan-graphene-film due to creation of edge defects and formation of nanocrystalline structures from graphene flakes and increase of surface area.

This research is funded by the European Social Fund under the Global Grant measure, Project No. VP1-3.1-ŠMM-07-K-01-124

[1] R. Trusovas, K. Ratautas, G. Račiukaitis, J. Barkauskas, I. Stankevičienė, G. Niaura, R. Mažeikienė, Reduction of the graphite oxide to graphene with laser irradiation, Carbon, 52, 574-582 (2013).
[2] R. Celiešiūtė, R. Trusovas, G. Niaura, V. Švedas, G. Račiukaitis, Ž. Ruželė, R. Pauliukaite, Influence of the laser irradiation on the electrochemical and spectroscopic peculiarities of graphene-chitosan composite film, Electrochimica Acta, 132, 265-276 (2014).

Increasing the efficiency of selected laser processes by assisting atmospheric pressure plasmas

C. Gerhard, S. Wieneke, W. Viöl

University of Applied Sciences and Arts, Laboratory of Laser and Plasma Technologies, Von-Ossietzky-Straße 99, 37085 Göttingen, Germany

gerhard@hawk-hhg.de

In this contribution, the potential of assisting atmospheric pressure plasmas (APP) for increasing the efficiency of laser material processing methods is presented. APP were introduced to laser ablation, laser annealing and laser cleaning. In the first case, two different novel approaches, sequential and simultaneous APP-assisted laser ablation were applied. For the sequential method the chemical composition of the particular sample is modified by a chemically reactive APP prior to ablation [1], giving rise to significantly altered laser-matter interactions. As an example, this method allows reducing the required ablation threshold energy for laser machining of fused silica by a factor of 4.6 whereas the surface roughness of the ablated area is notably decreased (factor 2.3) [2]. Further, a higher contour accuracy and the mitigation of debris can be realised [3]. For simultaneous APP-assisted ablation the laser beam is guided coaxially to an argon plasma beam. The laser-matter interaction is thus subject to a further component, i.e. an additional plasma-physical energy contribution to the ablation process. This allows a considerable increase in the ablation rate of optical glasses [4], metals [5] and ceramics [6] as shown representatively in figure 1(left).

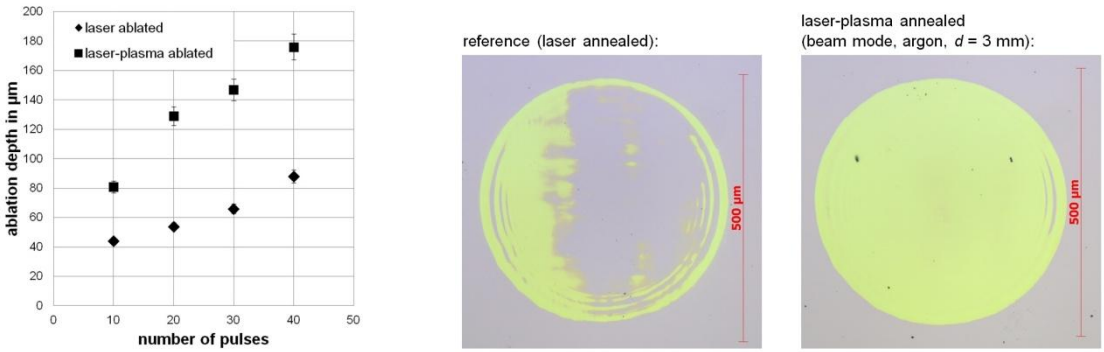

Figure 1 Comparison of the ablation depth of barite crown glass for laser and APP-assisted laser ablation (left) and comparison of the area of crystalline silicon for laser and APP-assisted laser annealed silicon coatings (right)

This setup for simultaneous APP-assisted laser processing was also applied for annealing of amorphous silicon coatings. In comparison to pure laser annealing, the area of crystalline silicon could be increased by a factor of approx. 2 [7] as also visualised in figure 1 (right). Further, the additional use of air APP was shown to be suitable for increasing the laser cleaning efficiency of contaminated and corroded surfaces [8]. A detailed presentation of these effects and the particularly underlying plasma-laser-matter interactions are the subject of the present contribution.

[1] C. Gerhard, D. Tasche, S. Brückner, S. Wieneke, W. Viöl, Near-surface modification of optical properties of fused silica by low-temperature hydrogenous atmospheric pressure plasma, Optics Letters 37, 566-568, (2012).
[2] S. Brückner, J. Hoffmeister, J. Ihlemann, C. Gerhard, S. Wieneke, W. Viöl, Hybrid laser-plasma micro-structuring of fused silica based on surface reduction by a low-temperature atmospheric pressure plasma, Journal of Laser Micro/Nanoengineering 7, 73-76, (2012).
[3] C. Gerhard, J. Heine, S. Brückner, S. Wieneke W. Viöl, A hybrid laser-plasma ablation method for improved nanosecond laser machining of heavy flint glass, Lasers in Engineering 24, 391-403, (2013).
[4] C. Gerhard, S. Roux, S. Brückner, S. Wieneke, W. Viöl, Low-temperature atmospheric pressure argon plasma treatment and hybrid laser-plasma ablation of barite crown and heavy flint glass, Applied Optics 51, 3847-3852, (2012).
[5] C. Gerhard, S. Roux, S. Brückner, S. Wieneke, W. Viöl, Atmospheric pressure argon plasma-assisted enhancement of laser ablation of aluminum, Applied Physics A 108, 107-112, (2012).
[6] C. Gerhard, S. Roux, F. Peters, S. Brückner, S. Wieneke, W. Viöl, Hybrid laser ablation of Al_2O_3 applying simultaneous argon plasma treatment at atmospheric pressure, Journal of Ceramic Science and Technology 4, 19-24, (2013).
[7] A. Gredner, C. Gerhard, S. Wieneke, K. Schmidt, W. Viöl, Increase in generation of poly-crystalline silicon by atmospheric pressure plasma-assisted excimer laser annealing, Journal of Materials Science and Engineering B 3, 346-351, (2013).
[8] N. Mainusch, C. Pflugfelder, J. Ihlemann, W. Viöl, Plasma jet coupled with Nd:YAG laser: new approach to surface cleaning, Plasma Processes and Polymers 4, S33-S38, (2007).

Shaped ultrafast laser pulse for micro/nanofabrication: from fundamentals to applications

Lan Jiang[1], Xiaowei Li[1], Xin Li[1], YongFeng Lu[2]

1- Laser Micro/Nano Fabrication Laboratory, School of Mechanical Engineering, Beijing Institute of Technology, Beijing 100081, People's Republic of China
2- Department of Electrical Engineering, University of Nebraska-Lincoln, Lincoln, NE 68588-0511, USA

jianglan@bit.edu.cn

The duration of a femtosecond laser pulse is much shorter than the electron-lattice relaxation time (10^{-10}~10^{-12}s). Therefore, laser energy absorption is completed before the lattice changes. Laser-material interactions, including phase change and material removal, are actually determined by laser-electron interactions. Hence, femtosecond laser fabrication must be improved by controlling electrons dynamics, such as electron density, temperature, and excited state distribution. Further, femtosecond pulse duration and its subpulse delays can be shorter than electron relaxation times (10^{-13}-10^{-15} s). During femtosecond laser irradiation, the electron-electron nonequilibrium state greatly increases the capability of electrons dynamics control (EDC). We propose to control localized transient electrons dynamics by temporally/spatially shaping femtosecond pulse energy distribution. Then the subsequent processes can be controlled by adjusting laser-electron interactions.

A multiscale model is developed, which consists of the *ab initio* calculations for electrons dynamics, revised molecular dynamics simulation for phase change, plasma model for ionization processes, and improved two-temperature model for energy transport. Our simulation shows that it is feasible to control electron dynamics to adjust localized transient material properties, phase changes, and micro/nanostructures [1,2].

Based on our theoretical predictions, the proposed fabrication methods are validated experimentally. We propose to: i) control the localized transient electron density to induce resonance absorption, by which microchannel processing efficiency is increased by 56 times and the maximum aspect ratio is extended by 3 times [3]; ii) adjust the phase change mechanism by changing photon-electron interactions, which reduces the recast layer thickness by 60% [4]; iii) adjust electron generation on fabricated material surface, by which the periods, orientations and structures of the surface ripples can be effectively adjusted [5-9]; and iv) control electron density and its distribution, which obtains controllable micro/nano hierarchical structures on material surfaces and enhancement factors up to 2.2×10^8 of surface-enhanced Raman scattering [10].

Our proposed methods are used to fabricate some key structures and novel fiber sensors [11,12]. Microholes with a diameter of 19 μm and an aspect ratio of 103:1 are drilled by adjusting electron density in plasma with temporally-shaped ultrafast pulse trains. Using spatially-shaped ultrafast pulses, we optimize electron density distribution in plasma in the focus point, and then to manipulate plasma expansion and filamentation, which drills microholes with a diameter of 4 μm and an aspect ratio of 150:1.

[1] C. Wang, L. Jiang, F. Wang, X. Li, Y.P. Yuan, and Y.F. Lu, Journal of Physics: Condensed Matter, vol. 24, pp. 275801, (2012).
[2] Y.P. Yuan, L. Jiang, X. Li, C. Wang, and Y.F. Lu, Journal of Applied Physics, vol. 112, pp. 3327-3331, (2012).
[3] L. Jiang, P.J. Liu, X.L. Yan, N. Leng, C.C. Xu, H. Xiao, and Y.F. Lu, Optics Letters, vol. 37, pp. 2781-2783, (2012).
[4] N. Leng, L. Jiang, X. Li, C. Xu, P.J. Liu, and Y.F. Lu, Applied Physics A, vol. 109, pp. 679-684, (2012).
[5] X.S. Shi, L. Jiang, X. Li, S.M. Wang, Y.P. Yuan, and Y.F. Lu, Optics Letters, vol. 38, pp. 3743-3746, (2013).
[6] L. Jiang, X.S. Shi, X. Li, Y.P. Yuan, C. Wang, and Y.F. Lu, Optics Express, vol. 20, pp. 21505-21511, (2012).
[7] W.N. Han, L. Jiang, X. Li, P.J. Liu, L. Xu, and Y.F. Lu, Optics Express, vol. 21, pp. 15505-15513, (2013).
[8] L. Jiang, W.N. Han, X. Li, Q. Wang, F. Meng, and Y.F. Lu, Optics Letters, vol. 39, pp. 3114-3117, (2014).
[9] X. Li, C. Li, L. Jiang, X.S. Shi, N. Zhang, and Y.F. Lu, Optics Letters, vol. 39, pp. 2382-2385, (2014).
[10] N. Zhang, X. Li, L. Jiang, X. Shi, C. Li, and Y.F. Lu, Optics Letters, vol. 38, pp. 3558-3561, (2013).
[11] L. Jiang, J.P. Yang, S.M. Wang, B.Y. Li, and M.M. Wang, Optics Letters, vol. 36, pp. 3753-3755, (2011).
[12] L. Jiang, L.J. Zhao, S.M. Wang, and J.P. Yang, Optics Express, vol. 19, pp. 17591-17598, (2011).

Ion migration assisted femtosecond laser inscription of high performance active and passive waveguides for photonic devices

J. Solis, T. T. Fernandez, J. del Hoyo and J.Siegel

Laser Processing Group, Instituto de Optica, CSIC, Serrano 121, 28006-Madrid, Spain 2

j.solis@io.cfmac.csic.es

Refractive index changes upon femtosecond (fs) laser writing are related to a variety of mechanisms that include changes of the glass density, point defects, photochemical changes of the network, changes of polarizability, or,in the case o crystalline materials, laser induced damage. However, with just a few exceptions, the refractive index contrast achievable (Δn) is below ~10^{-2}. The feasibility of inducing controlled migration of ions by fs-laser irradiation would thus open up new prospects for fabricating efficient integrated optical devices inside glasses.

Indeed, although element redistribution has been observed upon fs-laser irradiation in a variety glasses (mostly silica-based) [1,2], evidence of local compositional changes leading to light guiding in the written structures has not been provided. Only recently [3,4], it has been shown that changes of the glass composition induced by fs-laser irradiation lead to production of extremely efficient active/passive waveguides in phosphate glasses with Al_2O_3, K_2O and La_2O_3 glass modifiers. The refractive index changes are due to the cross migration of La and K ions leading to values in the $\Delta n \sim 1.5 \times 10^{-2}$. A similar mechanism has also recently shown to assist guiding in a tellurite glass where cross migration of Te and Na ions generates refractive index changes of $\Delta n \sim 3.5 \times 10^{-3}$.

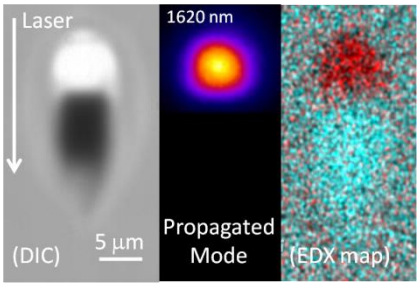

Fig.1. (left) Differential interference contrast microscopy image of waveguide written with an Yb-fibre, fs-amplifier at 1030 nm, 500 kHz rep. rate, 0.68 NA writing optics, slit width of 1.4 mm, 60 μm/s can speed, 100 μm writing depth and and 670 nJ pulses. The writing de, using a, along with the propagated mode profile at 1620 nm. The EDX map shows the spatial distribution of La (red) and K (red) in the laser-modified region.

In the presentation we will review our results regarding the use of ion migration for the production of guiding structures in functional glasses with special emphasis in the control that can be exerted over their characteristics (size, refractive index change and local composition). For such purpose, we will describe different results regarding local morphological, compositional, luminescent and structural properties of the laser-written structures by a variety of characterization techniques including optical microscopy, micro-photoluminescence, micro-Raman, X-rays micro-analysis and near field refractometry. Recent results regarding the use in situ plasma emission imaging during the writing process will also be presented in order to discuss the origin of the ion cross-migration phenomenon.

[1] M. Sakakura, T. Kurita, M. Shimizu, K. Yoshimura, Y. Shimotsuma, N. Fukuda, K. Hirao, and K. Miura, "Shape control of elemental distributions inside a glass by simultaneous femtosecond laser irradiation at multiple spots," Opt. Lett. **38**, 4939 (2013).

[2] F. Luo, J. Song, X. Hu, H. Sun, G. Lin, H. Pan, Y. Cheng, L. Liu, J. Qiu, Q. Zhao, and others, "Femtosecond laser-induced inverted microstructures inside glasses by tuning refractive index of objective's immersion liquid," Opt. Lett. **36**, 2125–2127 (2011).

[3] J. Hoyo, V. Berdejo, T. Toney Fernandez, a Ferrer, a Ruiz, J. a Valles, M. a Rebolledo, I. Ortega-Feliu, and J. Solis, "Femtosecond laser written 16.5 mm long glass-waveguide amplifier and laser with 5.2 dB cm −1 internal gain at 1534 nm," Laser Phys. Lett. **10**, 105802 (2013).

[4] T. Toney Fernandez, P. Haro-González, B. Sotillo, M. Hernandez, D. Jaque, P. Fernandez, C. Domingo, J. Siegel, and J. Solis, "Ion migration assisted inscription of high refractive index contrast waveguides by femtosecond laser pulses in phosphate glass," Opt. Lett. **38**, 5248 (2013).

[5] T. T. Fernandez, M. Hernandez, B. Sotillo, S. M. Eaton, G. Jose, R. Osellame, a. Jha, P. Fernandez, and J. Solis, "Role of ion migrations in ultrafast laser written tellurite glass waveguides," Opt. Express **22**, 15298 (2014).

Picosecond-laser bulk modification, luminescence and Raman lasing in single-crystal diamond

V.Romano[1], B. Neuenschwander[1], S.M. Pimenov[2]

1-Bern University of Applied Sciences, Institute for Applied Laser, Photonics and Surface Engineering ALPS, , Pestalozzistrasse 20, CH-3400 Burgdorf; Switzerland
2-Natural Sciences Center, Prokhorov General Physics Institute, 38, Vavilov Street, Moscow 119991, Russia

Valerio.romano@bfh.ch

Bulk modification and micro-structuring of diamonds using ultra-short laser pulses is of great interest due to its potential in photonic applications, radiation detectors and diamond gem marking. We report on bulk micro-structuring and stimulated Raman scattering (SRS) in type IIa single crystal diamond with multi pulse irradiation by picosecond-laser pulses at the wavelength 532nm (10ps and 44ps). On-line video imaging and spectroscopic measurements during laser irradiation and structure growth in the bulk diamond from the backside of the crystal were also performed. We discuss the influence of the crystal orientation ({100} and {110}) relative to the laser beam onto (i) the optical breakdown threshold, (ii) the character of the structural modifications and (iii) generation of SRS during irradiation.

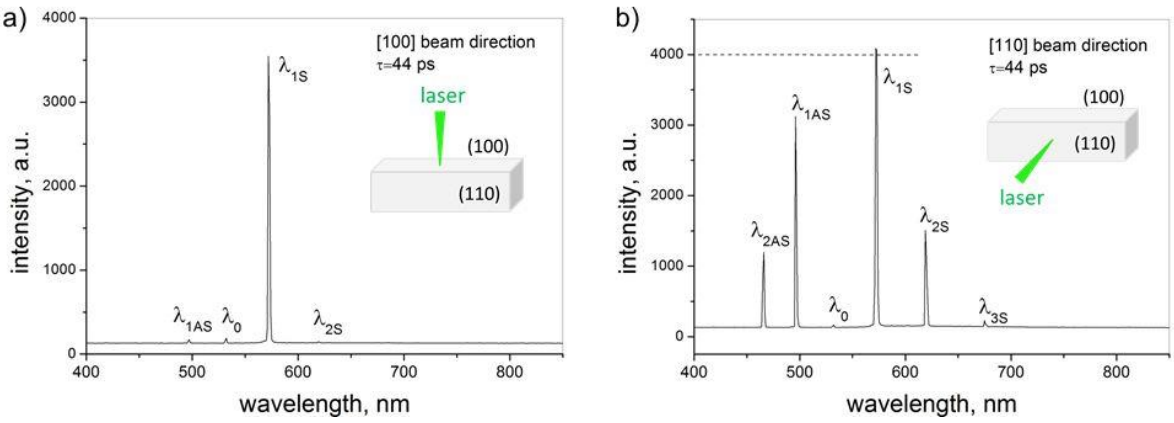

Measured PL spectra during 44-ps-laser irradiation of diamond at the [100] beam direction (a) and the [110] beam direction (b). The spectrum for the [100] beam direction was recorded with ε = 2.6μJ / f = 50kHz / P = 130mW (before bulk damage at ε_{th} = 2.8μJ) and focus position 0.5mm beyond the sample. For the [110] direction the parameter were ε = 4.5μJ / f = 50kHz / P = 225mW (before bulk damage at ε_{th} = 5μJ).

We show that the formation of bulk microstructures dramatically influences the behavior of the SRS and that the structure growth and the laser-induced breakdown in the bulk are governed by the dielectric breakdown mechanism.

We will further present the conditions for efficient SRS lasing depending on the different pulse durations. Based on the Stokes-to-anti-Stokes intensity ratio in the recorded SRS spectra we will finally propose a method of local temperature measurements in the bulk of diamond to determine the "pre-breakdown" temperature.

Large-mode-area mid-infrared guiding in ultrafast laser generated waveguides in chalcogenide glasses

C. D'Amico[1], G. Cheng[1,2], C. Mauclair[1], J. Troles[3], L. Calvez[3], V. Nazabal[3], C. Caillaud[3], G. Martin[4], B. Arezki[4], E. LeCoarer[4], P. Kern[4], and R. Stoian[1]

1- Laboratoire Hubert Curien, UMR 5516 CNRS, Université de Lyon, Université Jean Monnet, 42000 St. Etienne, France
2- State Key Laboratory of Transient Optics and Photonics, Xi'an Institute of Optics and Precision Mechanics, CAS, 710119 Xi'an Shaanxi, China
3- Chemical Sciences Institute of Rennes, UMR 6226 CNRS, University of Rennes I, 35042 Rennes, France
4- Institut de Planetologie et d'Astrophysique de Grenoble, UMR 5274 CNRS, Université Joseph Fourier, 38041 Grenoble, France

razvan.stoian@univ-st-etienne.fr

Current demands in astrophotonics impose advancing optical functions in infrared spectral domains within embedded refractive index designs. We demonstrate concepts for large-mode-area guiding involving ultrafast laser photowritten waveguides in bulk Sulfur-based chalcogenide glasses. If positive index contrasts are weak in As_2S_3, Ge doping increases the matrix rigidity and allows for high contrast (10^{-3}) positive refractive index changes. Guiding with variable mode diameter and large-mode-area light transport is demonstrated up to 10 μm spectral domain using transverse slit-shaped and evanescently-coupled multicore traces. Laser structuring of localized index-change domains permits as well direct access to the evanescent field. Various linear and nonlinear optical functions are discussed.

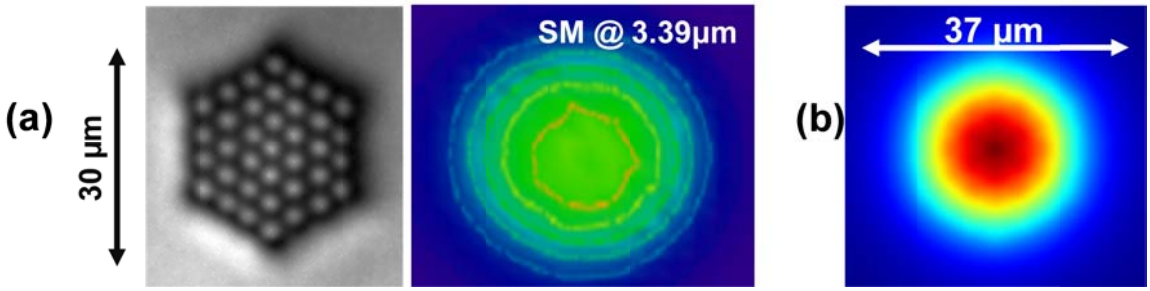

Figure 1 Single mode guiding at 3.39 μm in multicore bundles (a) and calculated mode (b).

[1] C. D'Amico, G. Cheng, C. Mauclair, J. Troles, L. Calvez, V. Nazabal, C. Caillaud, G. Martin, B. Arezki, E. LeCoarer, P. Kern, and R. Stoian, Large-mode-area infrared guiding in ultrafast laser written waveguides in Sulfur-based chalcogenide glasses, Opt. Express 22, 13091-13101 (2014).

Femtosecond laser micro-/nano- fabrication: new insights and its applications in optomechanics

Yves Bellouard

Mechanical Engineering Dpt, Eindhoven University of Technology, The Netherlands.

Email: yves@bellouard.eu

Non-ablative femtosecond laser pulses applied on various dielectrics induce mainly two types of modifications: homogeneous modifications and self-organized nanogratings [1,2]. The switching between different material modification types is controlled by the laser exposure parameters. In fused silica in particular, a localized net volume expansion is associated with the occurrence of self-organized nanogratings [3]. For shorter pulses (< 200 fs) and low-energy – corresponding to the regime of homogeneous modifications, densification is observed [5]. The laser pulse duration can therefore be used to introduce either tensile and compressive stress, which intensity and direction can be fine-tuned by controlling the pulse energy [3] and the laser polarization [4].

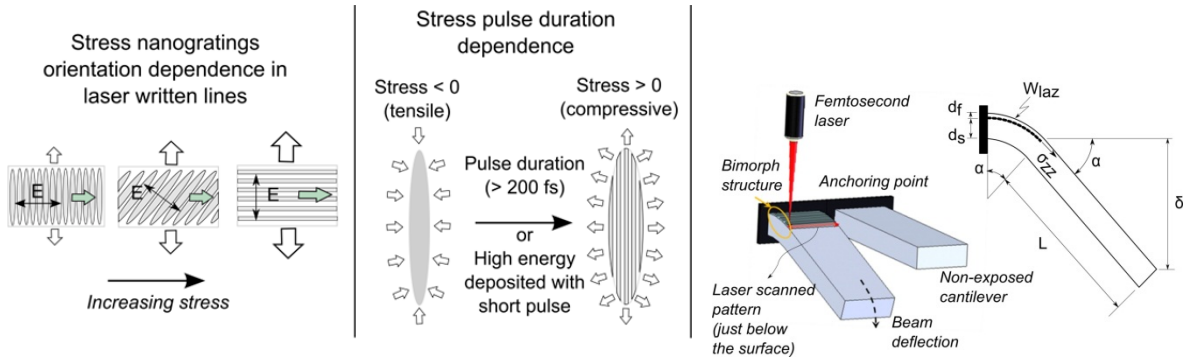

Figure 1. Left: Illustration of the effect of nanogratings orientation in laser-written line on stress intensity [4]. The maximum intensity is found for nanogratings perpendicular to the writing direction. Middle: stress-state inversion by switching between the continuous modification regime to the regime where nanogratings forms [3,5]. Right: mechanical method based on micro-machined cantilever for measuring quantitatively volume expansion resulting from laser exposure in the non-ablative regime [3].

Here, we will discuss these laser modifications from the view point of stress-states induced in the material and show evidences of stress-state inversion. In particular, we will discuss the role of the stress induced in the material for promoting and enhancing selective etching effects.

Finally, we will show how these controlled stress-states can be used for novel applications in optomechanics but also, as a possible route for generating high-pressure phases in silica.

[1] K. M. Davis, K. Miura, N. Sugimoto, and K. Hirao, "Writing waveguides in glass with a femtosecond laser," Opt. Lett. 21, 1729–1731 (1996).
[2] Y. Shimotsuma, P. G. Kazansky, J. Qiu, and K. Hirao, "Self-Organized Nanogratings in Glass Irradiated by Ultrashort Light Pulses," Phys. Rev. Lett. 91, 247405 (2003).
[3] A. Champion and Y. Bellouard, "Direct volume variation measurements in fused silica specimens exposed to femtosecond laser," Opt. Mater. Express 2, 789–798 (2012).
[4] A. Champion, M. Beresna, P. Kazansky, and Y. Bellouard, "Stress distribution around femtosecond laser affected zones: effect of nanogratings orientation," Opt. Express 21, 24942–24951 (2013).
[5] Y. Bellouard, T. Colomb, C. Depeursinge, M. Dugan, A. A. Said, and P. Bado, "Nanoindentation and birefringence measurements on fused silica specimen exposed to low-energy femtosecond pulses," Opt. Express 14, 8360–8366 (2006).

"Conical Refraction for Optical Manipulation and other studies in biophysics and bioaerosols"

Dr David McGloin
Associate Dean - Research
School of Engineering, Physics and Maths
University of Dundee
Nethergate
Dundee DD1 4HN
d.mcgloin@dundee.ac.uk

Pleanary

In this talk I will discuss a form of optical beam shaping based on the transmission of light through a biaxial crystal - conical refraction - and discuss how such beams can be used in optical manipulation experiments. In particular CR beams are shown to act as optical tweezers only in the lower Raman spot and as optical levitation devices away from this point. I will discuss the applications of such a beam. In addition I will highlight some of our recent work studying cellular adhesion using optical tweezers, new studies of biofuel evaporation dynamics and methods of making optical traps using very low cost optics such as home made PDMS lenses.

Extreme nonlinear optics with intense shaped laser beams

Pavel Polynkin[1]

1- College of Optical Sciences, The University of Arizona, 1630 E. University Blvd., Tucson, AZ 85721, USA

Email: ppolynkin@optics.arizona.edu

I discuss recent experiments on the propagation dynamics of ultraintense femtosecond laser pulses with shaped beam profiles. Various beam shapes that have been investigated include Bessel, Airy and vortex beams. Self-focusing of these beam types in air results in the production of dilute plasma channels and channel arrays with peculiar properties. Plasma channels produced through filamentation of intense Airy beams in air are curved. Filamentation of intense optical vortices results in the production of bottle-like distributions of plasma channels that may be useful for extended guidance of microwave radiation. I will further discuss an approach for length extension of a femtosecond laser filament through the application of an axillary conical "dress" beam.

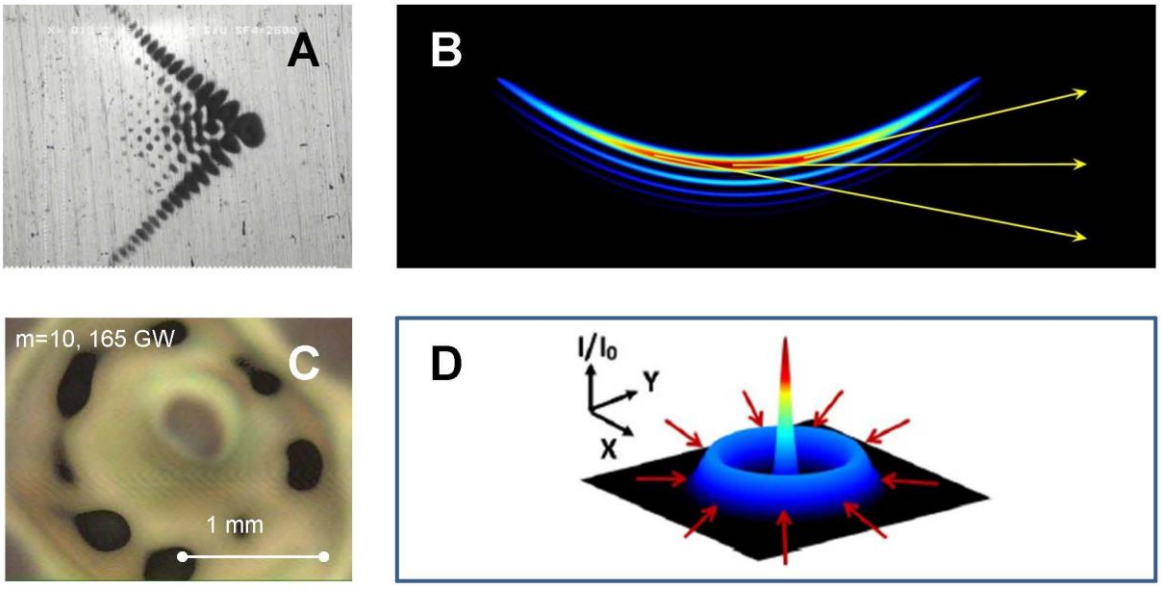

Figure 1 Burn pattern produced by an intense femtosecond Airy beam on aluminum foil. The intense feature in the corner of the beam intensity patterns propagates along a curved trajectory (A). Curved path of an Airy beam. The broadband conical emissions generated at different points along the beam's trajectory propagate along angularly resolved paths, which allows for probing the entire beam trajectory in a single laser shot. (B). Ring-shaped pattern of plasma filaments produced through self-focusing collapse of an intense optical vortex beam in air (C). Intensity pattern of a "dressed" optical beam used to maximize the length of a plasma channel in air at a given fixed total energy of the laser pulse (D).

This work was supported by the United States Air Force Office of Scientific Research (US AFOSR) through grants FA9550-12-1-0143, FA9550-12-1-0482 and FA9550-10-1-0561 and by the United States Defense Threat Reduction Agency (DTRA through grant HDTRA 1-14-1-0009.

[1] P. Polynkin, M. Kolesik, J. Moloney, G. Siviloglou, D. Christodoulides, Curved plasma channel generation using ultraintense Airy beams, Science, vol. 324, pp.229-232 (2009).
[2] P. Polynkin, M. Kolesik, J. Moloney, Filamentation of femtosecond laser Airy beams in water, Phys. Rev. Lett., vol. 103, p. 123902 (2009).
[3] P. Polynkin, C. Ament, J. Moloney, Self-focusing of ultraintense femtosecond optical vortices in air, Phys. Rev. Lett., vol. 111, p. 023901 (2013).
[4] M. Scheller, M. Mills, M. Miri, W. Cheng, J. Moloney, M. Kolesik, P. Polynkin, D. Christodoulides, Externally refueled optical filaments, Nat. Photonics, vol. 8, pp. 297-301 (2014).

Mapping laser-induced thermal forces acting on particles in air in a diverging hollow-core vortex beam

Niko Eckerskorn,[1] Richard Bowman,[2,3] Richard A. Kirian,[4] Jochen Küpper,[4] Henry N. Chapman,[4] Miles J. Padgett,[2] Andrei V. Rode[1]

[1]*Laser Physics Centre, RSPE, The Australian National University, Canberra ACT 0200 Australia*
[2]*Department of Physics and Astronomy, University of Glasgow, Glasgow G12 8QQ, UK.*
[3]*Queens' College, Cambridge Nanophotonics Centre, Cavendish Laboratory, University of Cambridge, CB3 0HE, UK*
[4]*Center for Free-Electron Laser Science, DESY, Notkestrasse 85, 22607 Hamburg, Germany*

avr111@physics.anu.edu.au

Optical trapping of light absorbing particles in gas environment has shown to be governed by optically induced thermal or photophoretic forces [1-3]. The applied photophoretic force propels a particle when an incident light beam nonuniformly heats the surface of the particle [3-5]. Optical guiding of absorbing particles by photophoretic force over large distances in open air was recently realised by an optical pipeline [4,5]. It was performed using a vortex beam, a donut-like intensity structure with a high-intensity ring of light that surrounds a dark core. Optical vortices create a ring-shaped transverse intensity distribution, while the particles are trapped at the intensity minima. Photophoretic force depends on the particle size relative to the mean-free path of gas molecules, absorption of laser light, and thermal conductivity. In the presented levitation experiments the thermal force is two to three orders of magnitude larger than the radiation–pressure force, rendering opaque particles impervious to conventional optical traps.

Here we present the results on quantitative evaluation of the photophoretic force and trapping stiffness by levitating graphite particles and carbon-coated glass shells of calibrated sizes in a vertically directed diverging hollow-core vortex beam. The axial equilibrium position of a suspended particle with known mass in the diverging beam with known intensity distribution immediately provides the axial force acting on the particle. Changing the beam power changes the intensity on the particle surface, which in turn force the particle to find a new equilibrium position. In the transverse plane. The trap's stiffness was measured using well-established position tracking with a fast CCD [6]. By repeating such experiments with different particle sizes and at different pressure we calibrate the force acting on the particle in the beam. The measurements were conducted at various air pressures from 0.1-1.5 bar and compared with the light pressure forces evaluated for the known intensity illuminating the particle.

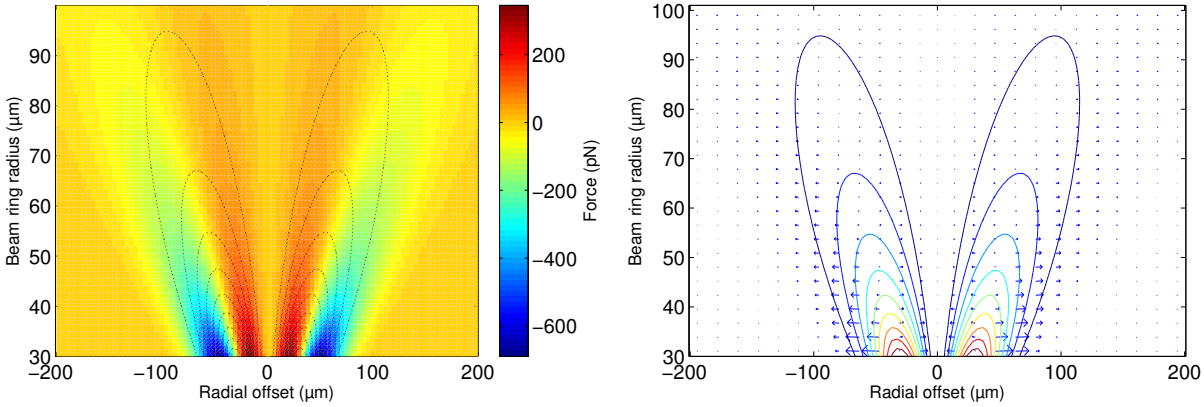

Figure 1. Measured force acting on a spherical carbon coated glass shell or graphite sphere (r=1µm), situated in linearly polarized first order vortex beam (LG01) carrying 1 W, under atmospheric pressure. The left panel shows the magnitude of the vectorial force (red – towards the axis, blue – away from axis) as displayed in the right panel. The contour overlays indicate the intensity distribution.

The forces recovered from our experiments range around ~10^{-10} N per Watt of total power in the beam, at atmospheric pressures, see Fig. 1, with force increasing near linearly with decrease of pressure. The maximum intensity encountered by the particle is ~30 kW/cm^2, given a maximum particle radius to vortex 'ring' radius of 1/30. Intensities of this order of magnitude are suitable for handling biological samples without damage. The results provide grounds to link the position and size of a spherical particle in an arbitrary intensity distribution to the value of photophoretic and light pressure forces under various gas pressures.

[1] E. J. Davis, G. Schweiger, *The Airborne Microparticle* (Springer, Berlin, 2002).
[2] D. McGloin, *et.al.*, *Optical manipulation of airborne particles*, Faraday Discussions **137**, 335-350 (2008).
[3] V. G. Shvedov, et al., *Optical guiding of absorbing nanoclusters in air*, Opt. Ex. **17**, 5743- 5757 (2009).
[4] V. G. Shvedov, et al, *Giant optical manipulation*, Phys. Rev. Lett. **105**, 118103 (2010).
[5] N. Eckerskorn, et al., *Hollow Bessel-like beam as an optical guide for a stream of particles*, Opt. Ex. **21**, 30492-30499 (2013).
[6] R. W. Bowman M. J. Padgett, *"Optical trapping and binding,* J. Opt. **76**, 026401 (2013).

3D imaging of femtosecond Bessel vortex filaments in glass

F. Courvoisier[1], C. Xie[1], V. Jukna[2,3], I. Ouadghiri[1], R. Giust[1], L. Furfaro[1], M. Jacquot[1], L. Froehly[1], R. Stoian[3], T. Itina[3], J. M. Dudley[1], A. Couairon[2]

1- Département d'Optique P. M. Duffieux, Institut FEMTO-ST, UMR 6174 CNRS Université de Franche-Comté, F-25030 Besançon cedex, France
2- Centre de Physique Théorique, CNRS, Ecole Polytechnique, F-91128 Palaiseau, France
3- Laboratoire Hubert Curien, UMR CNRS 5516, Université de Lyon, Université Jean Monnet, F-42000 Saint-Etienne, France

francois.courvoisier@femto-st.fr

Glass processing is an important technological problem since this class of material generates an increasing number of applications (solar calls, flat panel displays, microfluidics, optofluidics). But deep processing is a technological challenge. In this context, the ability of femtosecond laser pulses to deposit energy deep in the bulk of transparent material is an important benefit.

At high intensities, femtosecond pulses in glass undergo Kerr self-focusing and interact with laser-generated free-electron plasma. Gaussian beams usually undergo strong spatio-temporal distorsions during propagation in dielectrics. We recently demonstrated that stationary Bessel filaments overcome the limitations of Gaussian beams for uniform energy deposition and high aspect ratio drilling of nanochannels [1]. Further investigations of the filamentation regime require thorough comparisons between experiments and simulations.

We have developed a novel 3D beam imaging technique in solid dielectrics by progressive scanning, allowing for direct and quantitative comparison between numerical and experimental beam fluence distributions in glass.
We report on the domain of existence of stationary femtosecond Bessel vortices in dielectrics and the emergence of unstabilities from studies both in near and far field [2,3]. 3D imaging of the nonlinear propagation of Bessel beams provide a valuable new tool for the investigation of plasmas and plasma-light interaction.

[1] M. Bhuyan et al, High aspect ratio nanochannel machining using single shot femtosecond Bessel beams, Applied Physics Letters, 97, 081102 (2010)
[2] C. Xie et al, submitted (2014)
[3] V. Jukna et al, submitted (2014)

Spatial transformation of optical beams using resonant diffraction structures

L. Doskolovich, V. Soifer

Image Processing Systems Institute of the Russian Academy of Sciences,
151 Molodogvardeiskaya st., Samara 443001, Russia
Technical Cybernetics Department, Samara State Aerospace University,
151 Molodogvardeiskaya st., Samara 443001, Russia

Leonid@smr.ru

Spatiotemporal optical beam transformations are of great interest for a wide variety of applications, including ultrafast all-optical data processing and optical computing. For differentiation and integration of temporal optical signals, various types of Bragg gratings [1, 2] and resonant diffraction gratings [3, 4] have been proposed. In a recently published paper we have demonstrated for the first time that a phase-shifted Bragg grating (PSBG) is able to perform spatial differentiation of 2D optical beams in reflection regime [5] (see Fig.1). In this way, the PSBG structure can be considered as an ultra-compact analogue of a classic 4*f* Fourier-transform correlator consisting of a pair of lenses with a spatial filter in the Fourier plane. However, the article [5] does not consider the general class of spatial beam transformations which can be realized with a PSBG.

In the present work, we derive a first-order differential equation describing the general form of the optical 2D beam spatial transformation implemented by a PSBG. In particular, we demonstrate that under certain conditions the above differential equation describes the spatial differentiation of the incident 2D beam in reflection regime and the spatial integration in transmission regime. The proposed approach is generalized to the case of resonant diffraction gratings having more complex form of the reflection or transmission coefficient and thus extending the class of possible spatial transformations. In particular, dielectric resonant diffraction gratings can be used to perform spatial differentiation in transmission regime. Numerical simulations based on the rigorous coupled-wave analysis demonstrate high-quality spatial differentiation and spatial integration in reflection and transmission regimes.

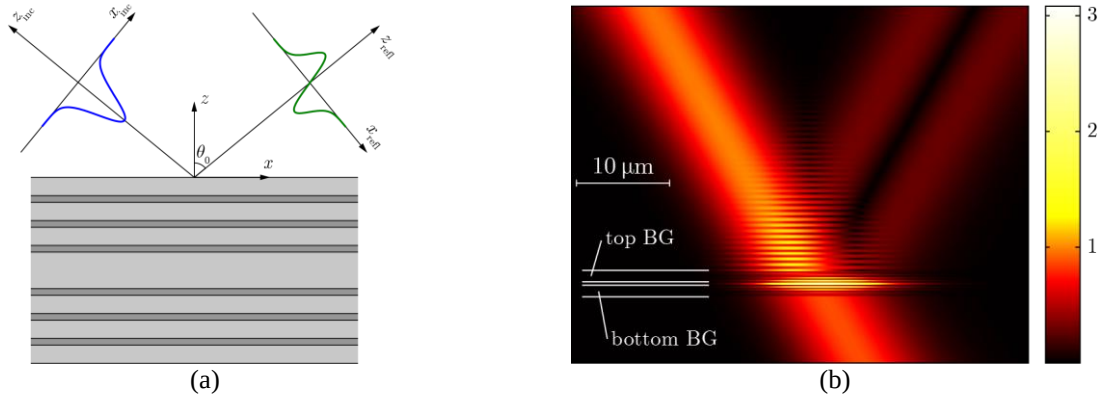

(a) (b)

Figure 1 (a) Geometry of the beam diffraction by a PSBG. (b) The electromagnetic field (the amplitude of the *y*-component of the electric field) generated upon diffraction of a Gaussian beam on PSBG differentiating in reflection.

This work was supported by RSF grant 14-19-00796, and RFBR grants 12-07-00495, 13-07-00464.

[1] L.M. Rivas, S. Boudreau, Y. Park, R. Slavík, S. LaRochelle, A. Carballar, J. Azaña, Experimental demonstration of ultrafast all-fiber high-order photonic temporal differentiators, Opt. Lett., 34, 1792–1794 (2009).
[2] N.Q. Ngo, Design of an optical temporal integrator based on a phase-shifted fiber Bragg grating in transmission, Opt. Lett., 32, 3020–3022 (2007).
[3] D.A. Bykov, L.L. Doskolovich, V.A. Soifer, Temporal differentiation of optical signals using resonant gratings, Opt. Lett., 36, 3509–3511 (2011).
[4] D.A. Bykov, L.L. Doskolovich, V.A. Soifer, Single-resonance diffraction gratings for time-domain pulse transformations: integration of optical signals," J. Opt. Soc. Am. A, 29, 1734–1740 (2012).
[5] L.L. Doskolovich, D.A. Bykov, E.A. Bezus, V.A. Soifer, Spatial differentiation of optical beams using phase-shifted Bragg grating, Opt. Lett., 39, 1278–1281 (2014).

Mechanism of micro-lens array formation by using four-beam interference lithography

E. Stankevicius, M. Gedvilas, M. Garliauskas, G. Raciukaitis
Center for Physical Sciences and Technology (CPST), Savanoriu av. 231, LT-02300 Vilnius, Lithuania

e-mail: estankevicius@ar.fi.lt

Photo-polymerization processes induced by ultra-short pulsed lasers [1-3] have drawn a lot of attention in the past few years due to its precision and flexibility. The higher process efficiency can be achieved by the parallel processing technique using interference of several laser beams [4-7]. Depends on the interfering beams parameters (phase, angle between beams, number of beams, used wavelengths, etc) [6] different types of micro-structures are possible to form. Micro-structures fabricated by four-beam interference lithography have shape of the micro-pillar array [8]. The shape of fabricated micro-pillars strongly depends on the laser irradiation dose [6]. Top of the micro-pillars in a single-photon excitation case have a spherical shape, acting as micro-lenses (Fig. 1).

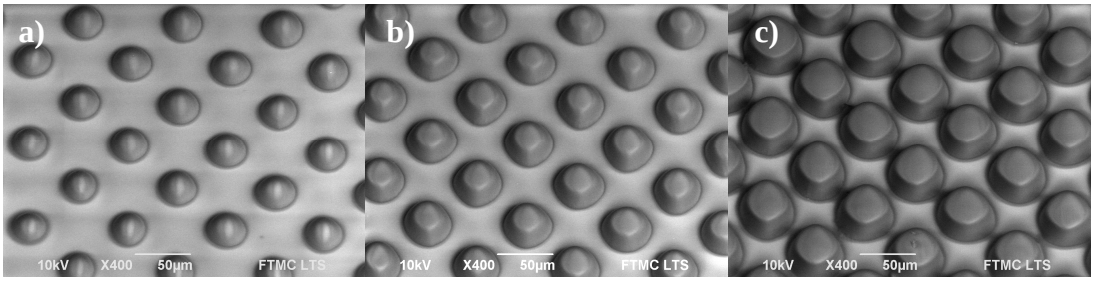

Fig. 1 Micro-lenses fabricated by interference lithography by using the same exposure time (30 s) and different laser average power: a) ~ 470 mW, b) ~ 630 mW and c) ~ 930 mW. The distance between micro-lenses is ~ 60 µm. Laser processing parameters are: wavelength - 515 nm, repetition rate - 100 kHz. SEM images of the structures are tilted by 34 deg.

Here, we will introduce rapid and flexible micro-lens array fabrication method by using four-beam interference lithography and a single-photon excitation technique. Also we will analyze the influence of the laser processing parameters (the average laser power and the irradiation time) to the shape of these micro-lenses and propose a model which explicitly treats the close relationship between the laser intensity, the irradiation time, period of intensity distribution and the diameter of the fabricated micro-lens. The proposed model is in good agreement with the experimental results and explains the mechanism of micro-lens formation.

[1] S. Maruo, O. Nakamura and S. Kawata, *"Three-dimensional microfabrication with two-photon-absorbed photopolymerization"*, Opt. Lett. **22**, 132-134, 1997.

[2] J. Serbin, A. Egbert, A. Ostendorf, B. N. Chichkov, R. Houbertz, G. Domann, J. Schulz, C. Cronauer, L. Fröhlich and M. Popall, *"Femtosecond laser-induced two-photon polymerization of inorganic organic hybrid materials for applications in photonics"*, Opt. Lett. **28**, 301-303, 2003.

[3] R. Guo, S. Xiao, X. Zhai, J. Li, A. Xia and W. Huang, *"Micro lens fabrication by means of femtosecond two photon photopolymerization"*, Opt. Express **14**, 810-816, 2006.

[4] M. Campbell, D. N. Sharp, M. T. Harrison, R. G. Denning and A. J. Turberfield, *"Fabrication of photonic crystals for the visible spectrum by holographic lithography"*, Nature **404**, 53-56, 2000.

[5] T. Kondo, S. Matsuo, S. Juodkazis and H. Misawa, *"Femtosecond laser interference technique with diffractive beam splitter for fabrication of three-dimensional photonic crystals"*, Appl. Phys. Lett. **79**, 725-727, 2001.

[6] E. Stankevicius, M. Gedvilas, B. Voisiat, M. Malinauskas and G. Raciukaitis, *"Fabrication of periodic micro-structures by holographic lithography"*, Lith. J. Phys. **53**, 227-237, 2013.

[7] H. Misawa, T. Kondo, S. Juodkazis, V. Mizeikis and S. Matsuo, *"Holographic lithography of periodic two- and three-dimensional microstructures in photoresist SU-8"*, Opt. Express **14**, 7943-7953, 2006.

[8] E. Stankevicius, M. Malinauskas, M. Gedvilas, B. Voisiat and G. Raciukaitis, *"Fabrication of periodic micro-structures by multi-photon polymerization using the femtosecond laser and four-beam interference"*, Mat. Sci. (Medžiagotyra) **17**, 244-248, 2011.

Ablation depth control of ITO thin film using a beam shaped femtosecond laser for mobile display

H. Y. Kim[1,2], J. W. Yoon[1,2], W. S. Choi[1,2], S. H. Cho[1,2]

1- Nano Machining Laboratory, KIMM (Korea Institute of Machinery and Material)
171 Jang-dong, Yuseong-gu, Daejeon, 305-343, Korea
2- Department of Nano-Mechatronics, UST (University of Science and Technology)
176 Gajung-dong, Yuseong-gu, Daejeon, 305-343, Korea

hykim@kimm.re.kr

Indium tin oxide (ITO) is an important transparent conducting oxide (TCO). ITO films have been widely used as transparent electrodes in optoelectronic devices such as organic light-emitting devices (OLEDs) because of their high electrical conductivity and high transmission in the visible wavelength. Finding ways to control ITO micromachining depth is important role in the fabrication and assembly of display field[1-3]. This study presented the depth control of ITO patterns on glass substrate using a femtosecond laser and slit. In the proposed approach, a Gaussian beam was transformed into a quasi-flat top beam by slit. In addition, pattern of square type shaped by slit were fabricated on the surfaces of ITO films using femtosecond laser pulse irradiation, under 1030nm, single pulse. Using femtosecond laser and slit, we selectively controlled forming depth and removed the ITO thin films with thickness 150nm on glass substrates. In particular, we observed when the 6 pulse number at 2.8TW/cm2. Furthermore, the morphologies and fabricated depth were characterized using a optical microscope, atomic force microscope (AFM), and energy dispersive X-ray spectroscopy (EDS).

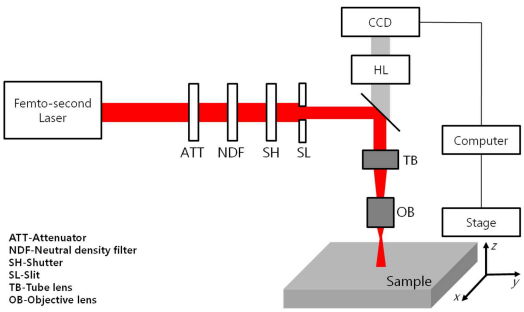

Figure 1 Schematic diagram of femtosecond laser system with slit.

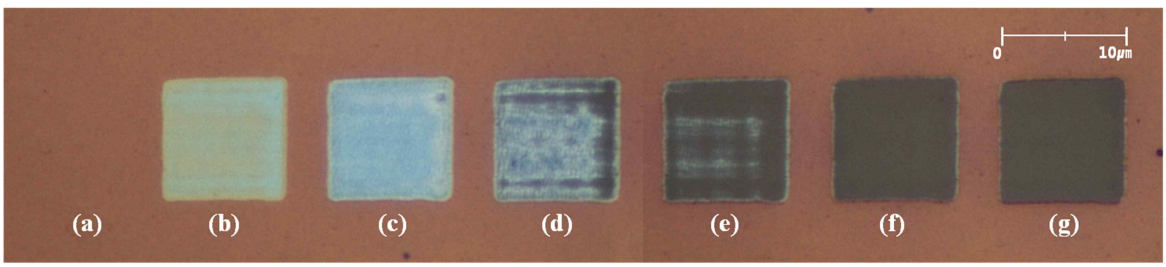

Figure 2 Optical microscopic views of morphology on ablated ITO film by NIR femtosecond laser irradiation with each different pulse shots: 0 shot (a), 1 shot (b), 2 shots (c), 3 shots (d), 4 shots (e), 5 shots (f), 6 shots (g).

[1] M. Hoheisel, A. Mitwalsky, C. Mrotzek, Microstructure and etching properties of sputtered indium-tin-oxide, Phys. Stat. Soli., vol. 123, pp. 461-472, (1991).
[2] M. Morikawa and M. Fujita, Crystallization and electrical property changes on the annealing of amorphous indium-oxide and indium-tin-oxide thin films, Thin Solid Films., vol. 359, pp. 61-67, (2000).
[3] M.F. Chen, W.T. Hsiao, Y.S. Ho, S.F. Tseng, Y.P. Chen, Laser patterning with beam shaping on indium tin oxide thin films of glass/plastic substrate, Thin Solid Films, vol. 518, pp. 1072-1078, (2009).

NEW APPLICATIVE RESULTS IN CO_2 LASER PHOTOACOUSTIC SPECTROSCOPY

D.C. Dumitras, S. Banita, M. Bercu, A.M. Bratu, I. Ivascu, C. Matei, M. Patachia, C. Popa

Department of Lasers, National Institute for Laser, Plasma and Radiation Physics, P.O. Box MG-36, 077125 Bucharest-Magurele, ROMANIA

✉ *E-mail: dan.dumitras@inflpr.ro*

Using a very sensitive instrument based on CO_2 laser photoacoustic spectroscopy [1, 2], several applications developed in our laboratory offered very interesting new results. They are systematised in 7 directions which are shortly described below.

1) New precise values of **absorption coefficients** were measured for molecular gases at the wavelengths of the CO_2 laser, namely **methanol, ethanol and carbon dioxide**. A high accuracy was assured by: a) using a frequency stabilized laser (1 MHz laser linewidth), so the absorption coefficients are measured only at the top of the laser line; b) using certified gas mixtures; c) avoiding saturation and the influence of foreign gases; and d) averaging over several independent measurements at each line to improve the overall accuracy of the results.

2) Measurements of **ammonia and ethylene in exhaled breath at patients with renal failure** indicated that a non-invasive ammonia test can be applied for selecting the optimum hemodialysis session duration and could also serve as a broad noninvasive screen for incipient kidney disease. The increasing ethylene concentration that occurs immediately after hemodialysis treatment is proving the higher rate of oxidative stress due to dialysis.

3) Using the exhaled ethylene as a biomarker, we monitored the evolution of the oxidative attack before, immediately after and at 15 minutes from the **radiotherapy**. The breath air samples from patients subjected to radiation treatment with a high dose fraction, demonstrated that patients treated by external radiotherapy suffer a slight increase in the generation of oxidants; however, in accordance with the clinical practice, this increase is sufficient to assess the body response to the treatment: the smaller the increase, the higher the radio-resistivity developed by the patient.

4) Studying the **surgical smoke** produced by CO_2 laser vaporization of different biological tissues, we measured the concentration of 9 gases: carbon dioxide, methanol, water vapors, acetonitrile, acrolein, ammonia, benzene, ethylene and toluene. We found that the average measured concentrations for three gases (acetonitrile, acrolein and benzene) are many times higher than the limits accepted by established organizations.

5) A new study was aimed to determine if **electronic cigarettes** (E) are less dangerous than **traditional cigarettes** (T). Analysing the behaviour of the ethylene biomarker at active smokers, a decrease of about 35% was obtained by switching from T to E cigarettes, and a corresponding increase of about 50% by replacing E with T cigarettes. Based on our results, we concluded that E-cigarettes are at the first glance safer than T-cigarettes.

6) Another experiment was aimed to investigate the oxidative stress for women practicing Kangoo Jumps (KJ) **aerobics**. Because it is not possible to directly measure free radicals in the body, we approach that by measuring the exhaled ethylene as by-product resulting from free radical reactions. Comparing the levels before and after the exercise program, we detected a lower concentration after the aerobics session, proving once again the health benefits of sports.

7) Valuable information was further obtained in **plant physiology**, especially on the behavior of fruits and vegetables in aerobic and anaerobic conditions. Measuring the plant hormone ethylene released by strawberries, raspberries, cherries, bananas, apricots, tomatoes, mushrooms, and zucchinis, we identified a very useful and easy applicable criterion to discriminate between organic and nonorganic samples (a much lower emission of ethylene from organic fruits and vegetables).

We conclude that a CO_2 laser photoacoustic spectroscopy based instrument can be successfully used in many life sciences fields.

[1] D.C. Dumitras et al., "CO2 Laser – Optimisation and Application" (Intech, Croatia), Chapter 1-2, (2012)
[2] A.M. Bratu et al., U.P.B. Sci. Bull., Series A 75, 139- 146 (2013)

NONINVASIVE DETECTION OF HEMATOMAS AND PATIENT MONITORING WITH PORTABLE, MEDICAL GRADE LASER OPTOACOUSTIC SYSTEMS

Rinat O. Esenaliev

Laboratory for Optical Sensing and Monitoring,
Center for Biomedical Engineering,
Department of Neuroscience and Cell Biology,
Department of Anesthesiology
University of Texas Medical Branch,
301 University Blvd., Galveston, Texas 77555-1156, USA

riesenal@utmb.edu

Our group has pioneered a number of biomedical applications of noninvasive optoacoustic imaging, sensing, and monitoring. The optoacoustic technique is a novel diagnostic modality with high optical contrast and ultrasound spatial resolution resulted from time-resolved detection of thermoelastic waves generated in tissues by short optical pulses. Noninvasive detection and characterization of intracranial hematomas and monitoring of physiologic variables including oxygenation in specific blood vessels are important applications of this technique. We built a number of tunable solid-state and laser diode-based optoacoustic systems in the 700-1064 nm spectral range. In this work we report our results on development and pre-clinical and clinical tests of portable, medical grade optoacoustic systems that are based on optical parametric oscillators or on pulsed laser diodes generating nanosecond pulses for stress-confined condition which is necessary for high resolution and contrast. Ultra-sensitive, wide-band probes were developed and built for detecting optoacoustic waves from hematomas and specific blood vessels such as the radial artery, superior sagittal sinus, and central and peripheral veins. The studies were performed in small and large animals and in clinical studies in patients with traumatic brain injury, healthy volunteers, anemic patients, and neonatal patients. The optoacoustic systems can rapidly detect and characterize hematomas and provide real-time, continuous monitoring of clinically important blood parameters. Further refinement and tests of the optoacoustic systems will noninvasively provide valuable diagnostic information for patients with traumatic brain injury and circulatory shock, anemic, surgical, critically ill, and anemic patients.

The authors acknowledge support of these studies by the NIH (Grants # U54EB007954, R01EB00763, R01NS044345, R41HL103095, R43HD075551, and R41HD076568), John Sealy Memorial Endowment Fund for Biomedical Research, Moody Center for Traumatic Brain Injury Research, 2 DOD grants, UTMB Business Acceleration Program, and Texas Emerging Technology Fund. Drs. Esenaliev and Prough are co-owners of Noninvasix, Inc., a UTMB-based startup that has licensed the rights to optoacoustic monitoring, sensing, and imaging technology.

Five Dimensional Optoacoustic Tomography Visualizes Fast Hemodynamic Changes in Whole Mouse Brain

S. Gottschalk[1], T. Fehm[1,2], X. L. Deán-Ben[1], D. Razansky[1,2]

[1]*Institute for Biological and Medical Imaging (IBMI), Helmholtz Center Munich, Neuherberg, Germany*
[2]*Faculty of Medicine, Technical University of Munich, Germany*
Correspondence to dr@tum.de

Currently available methods for functional neuroimaging, such as fMRI, optical and optoacoustic microscopies, cannot adequately assess changes in multiple hemodynamic parameters in the entire brain and in real-time. Here, we demonstrate imaging of fast cerebral hemodynamic changes in deep mouse brain by using a fully noninvasive acquisition of five-dimenional [1] (i.e. real-time volumetric multispectral) optoacoustic data from animals subjected to oxygenation stress.
Mice under isoflurane anesthesia were subjected to hyperoxic (100% O_2) and normoxic (20% O_2) conditions in an alternating order. Associated changes in cerebral hemodynamics were measured volumetrically with an optoacoustic tomography system employing a spherical array probe [2]. For multispectral signal acquisition, eight wavelengths in the near-infrared range were used to analyze HbO- and Hb-distributions by unmixing to a linear combination of their known absorption spectra.
The spatial resolution of the system allows efficient visualization of the three-dimensional (3D) anatomy of major cerebral veins and their oxygenation profiles in real-time. We analyzed SO_2-changes following hyperoxia/normoxia in specific volumes of interest (VOI) in the superior sagittal sinus and in the deep in the brain located longitudinal hippocampal vein (Fig. 1).

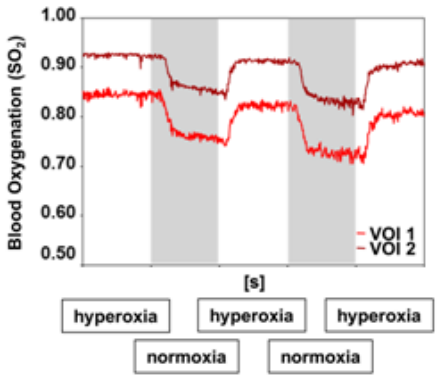

Figure 1. SO_2-changes following hyperoxia/normoxia can be readily analyzed in specific volumes of interest (VOI) in the superior sagittal sinus (VOI 1) and in the deep in the brain located longitudinal hippocampal vein (VOI 2).

For visualization purposes a threshold-based segmentation was used, thus, mainly the major cerebral veins are visible. Nevertheless, an analysis of SO_2 in areas that only partially consist of cerebral vasculature is also possible, albeit with significantly lower sensitivity when compared to the analysis within major vasculature.
In conclusion, the presented volumetric multispectral acquisition enables simultaneous label-free assessment of cerebral hemodynamic parameters in real-time. The results indicate that the proposed methodology could serve as a powerful complementary, and potentially superior, method for functional neuroimaging studies in rodents.

Acknowledgements: The research leading to these results has received funding from the European Union under grant agreement *ERC-2010-StG-260991*.

[1] X. L. Deán-Ben and D. Razansky. Adding fifth dimension to optoacoustic imaging: Volumetric time-resolved spectrally enriched tomography. *Light: Science & Applications*, Vol. 3, p. e137 (2014).
[2] X. L. Deán-Ben and D. Razansky. Portable spherical array probe for volumetric real-time optoacoustic imaging at centimetre-scale depths. *Optics Express,* Vol. 21, pp. 28062-28071 (2013).

Breath biomarkers can help clinicians to assess the role of oxidative attack in young population with mental disorders

C. Popa (Achim)[1,2], M. Petrus[1], C. Matei[1], S. Banita[1], A. M. Bratu[1], D. C. Dumitras[1]

[1] Department of Lasers, National Institute for Laser, Plasma, and Radiation Physics, 409 Atomistilor St., PO Box MG-36, 077125 Bucharest, Romania
[2] Physics Department, Faculty of Applied Sciences, University "Politehnica" of Bucharest, 313 Splaiul Independentei, Bucharest - 060042, ROMANIA
cristina.achim@inflpr.ro

Ongoing research is investigating the evaluation of oxidative stress in children with mental disorders. The quest for non-invasive and real-time monitoring tools is a characteristic of the modern medicine. The technique that is developed in this research complies with this requirement, ensuring the advantages of health state assessment by monitoring the evolution of gaseous biomarkers in human body. We chose to characterize by breath air the assessment of ethylene in mental disorders, but the techniques can be easily extended to other pathological issues.

Furthermore, we concentrate our goals to a new emerging frontier: the immune dysfunctions in mental illness. The impacts of environmental and food allergies, asthma, seizures, unexplained skin rashes, and persistent intestinal yeast infections are some of the few common signs of immune dysfunction. In the past 40 years of research [1-5], in this category of articles, 90% of them are examining immune deregulations and different mental disorders like Autism, Schizophrenia, and Depression, while 100% are referring to the oxidative attack. So, this is a very important issue in patients with different mental disorders (mainly Autism and Schizophrenia) [5-9].

Exhaled breath was investigated using a CO_2 laser photoacoustic system (LPAS), a well known method in the field of trace gas detection, used in our study for quantitative determination of biomarkers [9-12].

There have been multiple studies demonstrating an increase in inflammation markers and oxidative stress in patients with mental disorders [1-9].

These studies can demonstrate that laser photoacoustic spectroscopy is a sensitive, non-invasive and real time method to accurately investigate exhaled breath of children with mental illness for the detection of important biomarkers.

[1]. P. Ashwood, S. Wills, J. V. de Water, Journal of Leukocyte Biology 80: 1-15 (2006).
[2]. W. R. McGinnis, Alternative Therapies 10 (6): 22-37 (2004).
[3]. A. Chauhan, V. Chauhan, Pathophysiology 13: 171-181 (2006).
[4]. M. Phillips, G. A. Erickson, M. Sabas, J. P. Smith, J. Greenberg, J. Clin. Pathol 48: 466-469 (1995).
[5]. M. Shirasu, K. Touhara, J. Biochem 150 (3): 257-266 (2011).
[6]. B. K. Y. Bitanihirwe, T-U W. Woo, Neurosci Biobehav Rev. 35(3): 878-893, (2011).
[7]. M. Caldeira, A. S. Barros, M. J. Bileo, A. Parada, J. S. Camara, S.M. Rocha, J. of Cromatography A, 1218: 3771-3780 (2011).
[8]. M. Caldeira, R. Perestrelo, A. S. Barros, M. J. Bileo, A. Morete, J. S. Camara, S.M. Rocha, J. of Cromatography A, 1254: 87-97 (2012).
[9]. J. Saarela, Gas-Phase Photoacoustic Spectroscopy, Thesis for the degree of Doctor of Science in Technology at Tampere University of Technology, Julkaisu 998, Publication 998, (2011).
[10]. D.C. Dumitras, S. Banita, A.M. Bratu, R. Cernat, D.C.A. Dutu, C. Matei, M. Patachia, M. Petrus, C. Popa, Infrared Physics & Technology Journal 53 (5): 308-314 (2010)
[11]. C. Popa, A. M. Bratu, C. Matei, R. Cernat, A. Popescu, and D.C. Dumitras, Laser Physics 21(7): 1336-1342 (2011)
[12]. C. Popa, Ş. Băniţă, A. M. Bratu, M. Paţachia, C. Matei, and D. C. Dumitraş, "The level of ethylene biormarker in renal failure of elderly patients analyzed by photoacoustic spectroscopy", Laser Physics, Vol. 23, No. 12, doi:10.1088/1054-660X/23/12/125701, Article ID 125701 (2013)

Spectroscopic and laser properties of Cr^{2+} and Fe^{2+} ions in solid solutions based on ZnSe crystal.

M.E. Doroshenko[1], H. Jelinkova[2], M. Jelinek[2], M. Nemec[2], Yu.A. Zagoruiko[3], N.O. Kovalenko[3], A.S. Gerasimenko[3], V.M. Puzikov[3]

1- General Physics Institute RAS, Moscow, Russia
2- Czech Technical University, Prague, Czech Republic
3- Institute for Single Crystals NAN, Kharkov, Ukraine
email:dorosh@lst.gpi.ru

A set of $Zn_{1-x}Mg_xSe$ crystals with different Mg content x doped with divalent chromium and iron was synthesized using Bridgman technique and spectroscopic and laser properties in broad temperature range were investigated.

The room temperature fluorescence spectra of Cr^{2+} and Fe^{2+} ions measured in different $Zn_{1-x}Mg_xSe$ solid solutions were approximated by a pair of Gaussian curves as shown in Fig.1 and the corresponding Gaussian curves maximums were plotted versus Mg content (x). As follows from Figs. 2 and 3 increase in Mg content (x) results in close to linear shift of fluorescence maximums to longer wavelengths compared to ZnSe crystal as $\lambda_{max}=\lambda_{max}(ZnSe)+500x$ for chromium and twice stronger $\sim 1000x$ for iron. This shift results from changes in $Zn_{1-x}Mg_xSe$ solid solution elementary cell size with x followed by crystal field strength increase and corresponding increase of electronic transitions probability. Together with radiative lifetime decrease in $Zn_{1-x}Mg_xSe$ solid solution nonradiative quenching is increased with x as follows from Fig.4. The same tendency was also observed for Fe^{2+} ions with much stronger lifetime temperature dependence.

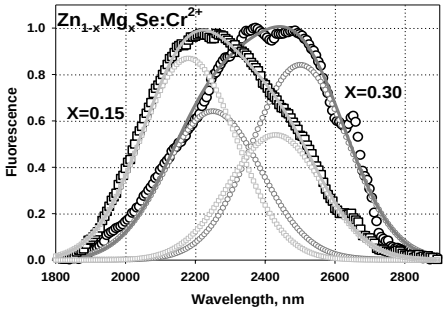

Fig.1 Fluorescence spectra of Cr^{2+} ions in $Zn_{1-x}Mg_xSe$ crystal for different Mg content (x) with decomposition into two Gaussian lines.

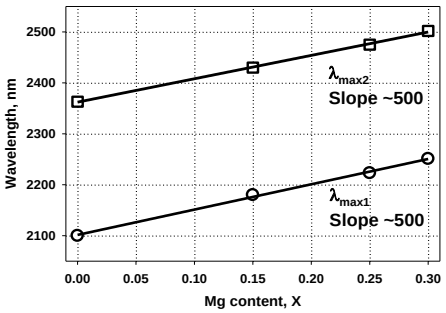

Fig.2 Position of two Gaussian lines maximums of Cr^{2+} ions in $Zn_{1-x}Mg_xSe$ crystal for different Mg content (x)

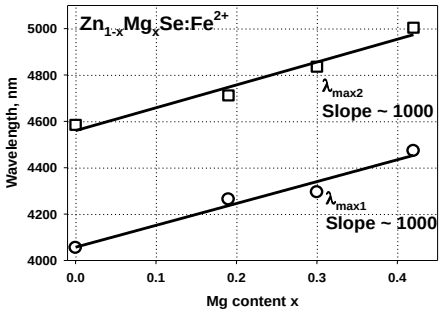

Fig.3 Position of two Gaussian lines maximums of Fe^{2+} ions in $Zn_{1-x}Mg_xSe$ crystal for different Mg content (x)

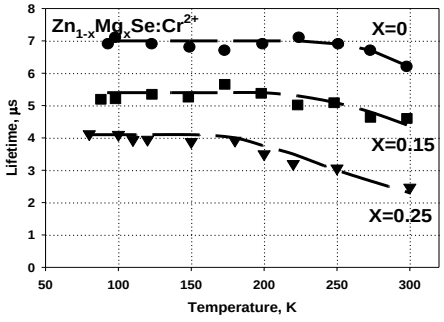

Fig,4 Temperature dependence of Cr^{2+} ions lifetime in $Zn_{1-x}Mg_xSe$ crystal for different Mg content (x)

The investigations of fluorescence properties in broad range of temperatures have shown that Cr^{2+} ions demonstrate very weak dependence of fluorescence spectrum shape with temperature decrease up to 77K. Unlike chromium ions Fe^{2+} demonstrates much stronger changes of fluorescence and laser properties with temperature decrease. Though for $Zn_{1-x}Mg_xSe$ solid solutions these changes are less drastic compared to ZnSe crystal. This allows to obtain lasing up to 4800 nm at 80K for $Zn_{1-x}Mg_xSe$ (x~0.4). Laser properties of Cr^{2+} and Fe^{2+} ions in $Zn_{1-x}Mg_xSe$ solid solutions under optical pumping at different temperatures will be also discussed.

Purely Optical Orientational Phase Transitions in Nematic Liquid Crystals

I.A. Budagovsky[1], V.N. Ochkin[1], S.A. Shvetsov[1,2], M.P. Smayev[1], A.S. Zolot'ko[1]

[1]P. N. Lebedev Physical Institute, Russian Academy of Sciences, Leninsky pr. 53, 119991 Moscow, Russia
[2]Institute of Physics and Technology (State University), Institutskii per. 9, 141700 Dolgoprudnyi, Moscow region, Russia

e-mail: ochkin@lebedev.ru

Various external fields (ac electric, ac magnetic, and light ones) can induce in nematic liquid crystals (NLCs) orientational phase transitions (Freedericksz transitions), at which the NLC director is distorted above a certain threshold. The ac-field-induced transitions (with the only exception of the ac electric field parallel to the NLC layer [1]) and the light-induced transitions in transparent (undoped) NLCs are of the second order.

We address the problem of the possibility of the first-order orientational transitions in NLC doped with dyes. In such NLCs, the director rotation occurs not due to the light action on the induced dipoles (as in the transparent NLCs) but owing to changing intermolecular forces upon dye excitation. When a dye has different isomeric forms, their concentrations are affected by the angle between the light field **E** and the NLC director **n** [2]. This leads to a new feedback channel between the director rotation and optical torque (for some dyes it can even change the sign of the optical torque). An additional attractive feature stimulating the study of the light-induced transitions in dye-doped NLCs is the possibility of significant reduction of the transition thresholds. The light-induced orientational phase transitions in planar NLC doped with various high-molar-mass azobenzene compounds (polymers and dendrimers) have been studied in [3-6].

Fig.1 demonstrates the phase diagram for optically induced transition. The transitions were observed using aberrational self-action of a light beam (e-wave); they featured a wide hysteresis loop (the optical bistability, i.e. memory). It was found that the additional external electric field transforms the first-order transition to the second-order one. Similar transformation was also observed at the light polarization rotation. In an illuminated NLC, the ac-electric-field-induced first-order transition was also found.

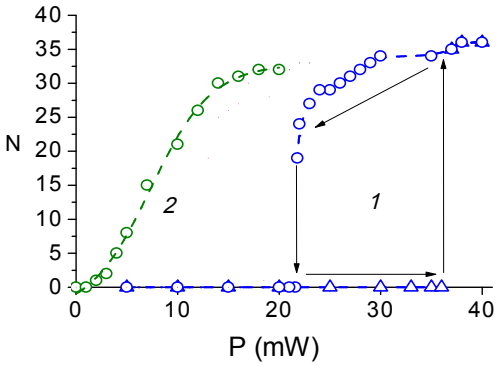

Figure 1. The dependence of the number N of the self-defocusing rings on the power P of the light beam incident on NLC doped with dendrimers for different ac voltages: U = (*1*) 0, (*2*) 0.7 V. In dependence *1*, triangles and circles show increasing and decreasing P.

The observed NLC behavior in the light and ac fields is discussed in the framework of the Landau theory. Instead of conventional free energy for equilibrium matter, our consideration is based on a certain phenomenological potential. When using this modification, the Landau theory was shown to describe satisfactory the regularities of the optically induced orientational transitions in dye-doped NLCs.

The study was supported by the Russian Foundation for Basic Research, project no. 14-02-00791, the grant of the President of the RF no. MK-970.2013.2, and the Russian Scientific Foundation.

[1] B.J. Frisken and P. Palffy-Muhoray, Electric-field-induced twist and bend Freedericksz transitions in nematic liquid crystals, Phys. Rev. A, Vol. 39, 1513-1518 (1989).
[2] I. Janossy and L. Szabados, Optical reorientation of nematic liquid crystals in the presence of photoisomerization, Phys. Rev. E, Vol. 58, 4598-4604 (1998).
[3] E.A. Babayan, I.A. Budagovsky, S.A. Shvetsov, et al., Light- and electric-field-induced first-order orientation transitions in a dendrimer-doped nematic liquid crystals, Phys. Rev. E, vol. 82, 061705 (2010).
[4] I.A. Budagovsky, A.S. Zolot'ko, V.N. Ochkin, et al., Orientational optical nonlinearity of nematic liquid crystals induced by high-molecular-mass azo-containing compounds, Polymer Science, Ser. A, Vol. 53, 655-665 (2011).
[5] I.A. Budagovsky, D.S. Pavlov, S.A. Shvetsov, et al., Light Interaction with NLCs Doped with Comb-Shaped Azopolymers with Different Degrees of Polymerization, Mol. Cryst. Liq. Cryst., Vol. 561, 89–96 (2012).
[6] A.S. Zolotko, M.P. Smaev, S.A. Shvetsov, et al., Light-induced first-order orientational transitions in a nematic liquid crystal in the presence of an ordinary wave, Quantum Electron., Vol. 42, 327–331 (2012).

Photonic Reservoir Computing

D. Brunner[1], I. Fischer[1]

1- Institute for Cross-Disciplinary Physics and Complex Systems (IFISC),

University of the Balearic Islands, 07122 Palma de Mallorca, Spain

dbrunner@ifisc.uib-csic.es

During the last decade, the novel information processing scheme of Reservoir Computing (RC) [1,2] was introduced. What makes RC unique within neuro-inspired information processing concepts is its suitability for hardware implementation in analog and photonic systems. Using delayed-feedback systems, the concept was initially demonstrated in electronic hardware [3]. An all-optical realization was demonstrated using a delay-coupled semiconductor laser at telecommunication wavelengths [4]. Nowadays, experimental and numerical implementations have been evaluated for multiple hardware systems. What all implementations have in common is an outstanding performance in solving complex and abstract computational tasks, e.g. patter recognition and chaotic timeseries prediction.

As most machine learning concepts, RC is based on the computational power of complex nonlinear networks. Inside such a network, information experiences a dimensionality expansion, enabling computation simply via a linear superposition of network states (see Figure 1 (a)). After the highly successful realizations using delay embedded nonlinear networks, the scheme now moves to other photonic network realizations. I will report on the latest advances made in the implementation of RC in spatially extended networks of semiconductor lasers. We realize a novel coupling methodology, utilizing a diffractive optical element in order to image neighbouring lasers on top of each other (see Figure 1 (b) and (c)).

Exclusively using the intrinsic nonlinearity of the semiconductor laser, our approach demonstrates a rout towards simplistic, yet highly powerful implementations of machine learning in photonic hardware. When successful, such systems have the potential of all-optical, standalone information processing with massive parallelism at 10s of GHz processing bandwidths.

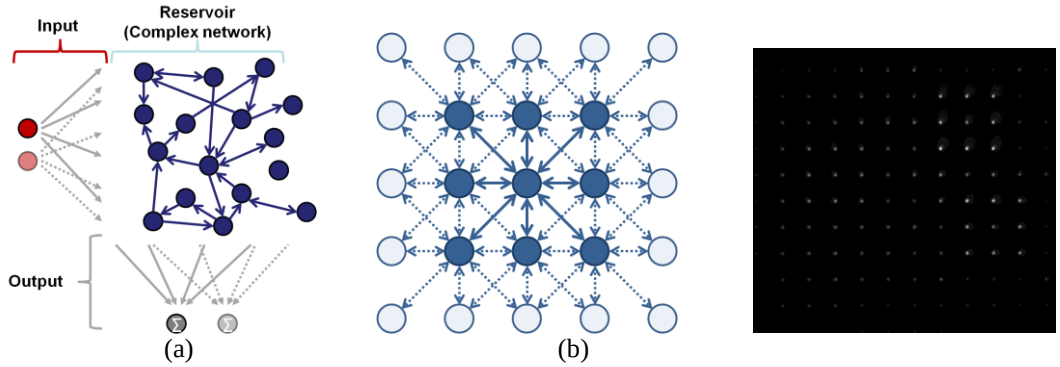

Figure 1 (a) Schematic illustration of RC, showing data injection into the recurrent nonlinear network (Reservoir) and the linear readout. (b) The connectivity structure created in our laser network. (c) Optical emission of an array of VCSELS under aligned coupling conditions.

[1] H. Jaeger, H. Haas, "Harnessing nonlinearity predicting chaotic systems and saving energy in wireless communication," Science, vol. 5667, pp.78–80, 2004.

[2] W. Maass, T. Natschl¨ager, H. Markram, "Real-time computing without stable states: a new framework for neural computation based on perturbations," Neural computation, vol.11, pp.2531–2560, 2002.

[3] L. Appeltant, M. C. Soriano, G. Van Der Sande, *et al.*, "Information processing using a single dynamical node as complex system," Nature communications, vol.2,.468, 2011.

[4] D. Brunner, M. C. Soriano, C. R. Mirasso, I. Fischer, "Parallel photonic information processing at gigabyte per second data rates using transient states," Nature communications, vol.4, 1364, 2013.

Resonant Radiation Physics in Collapsing Light Pulses

D. Faccio[1], T. Roger[1], F. Biancalana[1], M. Petev[1], M. Clerici[1,2], R. Morandotti[2], F. Legare[2], D. Majus[3], G. Tamosauskas[3], A. Dubietis[3], A. Couairon[4], P. Panagiotopoulos[5], M. Kolesik[5], G. Genty[6]

1-School of Engineering and Physical Sciences, SUPA, Heriot-Watt University, Edinburgh EH14 4AS, UK
2-INRS-EMT, 1650 Blvd. Lionel-Boulet, Varennes, Qubec J3X 1S2, Canada
3-Department of Quantum Electronics, Vilnius University, Sauletekio Ave. 9, LT-10222 Vilnius, Lithuania
4-Centre de Physique Theorique CNRS, Ecole Polytechnique, F-91128 Palaiseau, France
5-College of Optical Sciences, University of Arizona, Tucson AZ 85721, USA
6-Tampere University of Technology, Institute of Physics, Optics Laboratory, FIN-33101 Tampere, Finland

Resonant Radiation (RR) was originally discovered as a form of optical fibre soliton instability due to the presence of high order dispersion terms: it is a non-solitonic (therefore also referred to as "dispersive") emission that will typically lie in the opposite group velocity dispersion (GVD) regime of the pump pulse. Recent work in the field has highlighted that RR may appear in a very wide range of operating parameters and with some unexpected features.

In particular we will overview recent results highlighting the presence of RR in bulk media pumped with intense laser pulses. For powers higher than the critical threshold for self-focusing, the pulse will start to collapse and finally form a light filament. The formation dynamics of the filament are characterised by strong spatiotemporal coupling and shock front formation, the combination of which lead to RR. Depending on the specific input regime that can be controlled by the experimenter, we observe different forms of RR:

- RR driven by shock front formation with both the pump and RR in the normal GVD regime [1]
- Soliton-like RR from 3D light bullets, dominated by spatiotemporal coupling that leads to extreme rogue-like events in the statistics of the RR energy
- A novel form of RR that finds its origin in the negative frequency (i.e. complex conjugate) spectral content of the pump pulse [2]
- RR stimulated by an intense pump through cross-phase modulation onto a weaker probe pulse, even when the pump and probe have dramatically different wavelengths, e.g. 800 nm for the pump and 30 microns for the THz probe pulse [3]. RR is observed at 440 nm, thus spanning more than six octaves in the spectrum and leading to novel opportunities for THz radiation detection.

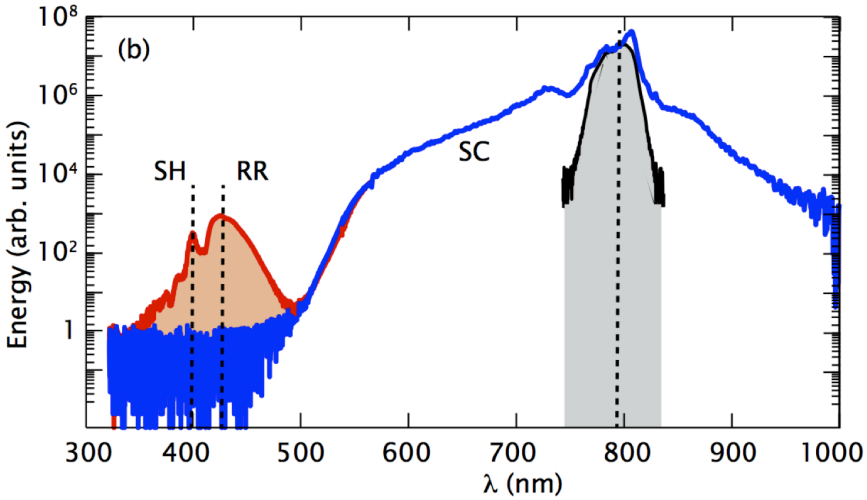

Fig.1 Experimentally measured RR emitted from a THz pulse, stimulated by an intense 800 nm pulse. The nonlinear medium is a 0.5 mm thick sample of diamond. The RR peak is the feature located at 440 nm . The shaded grey region is in the input pump spectrum and SC indicates the supercontinuum generated by the 800 nm pump pulse. SH indicates the THz-field-induced-second-harmonic (TFISH) signal.

[1] T. Roger et al., Phys. Rev. A **88**, 05180 (2013)
[2] E. Rubino, et al., Phys. Rev. Lett., **108**, 253901 (2012)
[3] M. Clerici et al., arXiv:1403.6026v1 (2014)

Nonlinear optical diagnostics of ferroelectric microstructures annealed by femtosecond laser

E. Mishina, S. Lavrov, A. Elshin, N. Firsova

Moscow State Technical University of Radioengineering, Electronics and Automation (MSTU-MIREA), Vernadsky ave. 78, 119454 Moscow, Russia

mishina_elena57@mail.ru

Femtosecond lasers are widely used for material treatment such as laser cutting (including laser surgery) and drilling, micro- and nano-structuring. Main advantages of femtosecond laser use are based on details of laser-matter interaction which provides the lower energy impact accompained by high pulse power density, the reduction of thermal damage, the elimination of laser-plume interaction. In this paper we report about developing a method of femtosecond laser annealing of precursor ferroelectric film to perovskite microstructures accompained by in-situ SHG monitoring of annealing process and ex-situ SHG microscopy of annealed areas.

Quazi-amorphous $PbZrTiO_2$ (PZT) film which was deposited by RF magnetron sputtering on a platinized silicon substrate was annealed by femtosecond laser pulses at the wavelength which falls into transparency band of PZT. Power was absorbed by platinum layer and the growing of perovskite phase started near it. Annealing was performed using femtosecond titanium-sapphire laser with pulse duration of 100 fs, wavelength of 800 nm, and repetition rate of 100 MHz. Beam was focused on the sample by confocal microscope.

In-situ method of diagnostics was used during the process of crystallization. This method is based on second harmonic generation (SHG) by noncentrosymmetric perovskite. SHG intensity was measured as function of time during annealing. After the process was finished, annealed areas were studied by confocal microscopy : SHG images were compared with conventional linear ones.

Annealing process is very critical to laser power rather than exposition: laser power density change by 5 % cancels perovskite formation independent on exposition time. Two shapes of annealed area were obtained in SHG images: “low” power density provides a circle shape of ferroelectric areas with 2 μm diameter, and “high” power gives ring-type areas with no ferroelectric properties in the center (Figure 1). Conventional linear images are circles in both cases.

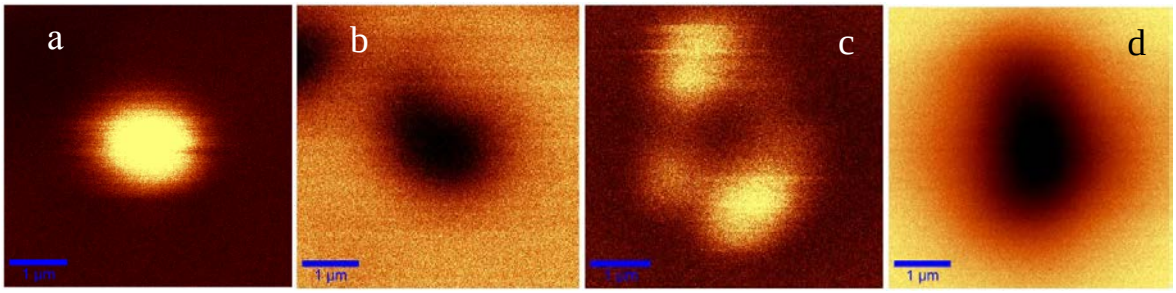

Figure 1. SHG (a, c) and linear (b, d) confocal images of annealed area. Pulse power density for annealing 1,5 MW/cm^2 (a, b) and 2,2 MW/cm^2 (c, d), annealing time 10 s. For imaging pulse power density is 200 kW/cm^2 (SHG, a and c) and <1 kW/cm^2 (linear, b and d)

Temperature distribution was estimated using COMSOL Multiphysics software with finite element method and its consent with experimental data was shown.

Since linear images give structureless circles for all annealing power densities, obvious advantage of SHG microscopy over linear one is demonstrated in this way. Another advantage was shown in our previous paper [1]: piezo force microscopy demonstrates coincidence of SHG bright areas with switchable ferroelectric areas.

[1] N.Yu. Firsova, E.D. Mishina, A.S. Sigov, S.V. Senkevich, I.P. Pronin, A. Kholkin, I. Bdikin, Yu.I. Yuzyuk, Femtosecond Infrared Laser Annealing of PZT Films on a Metal Substrate, Ferroelectrics, vol. 433, №1, 164-169 (2012).

Nonlinear evolution of polarization singularities in collinearly propagating light beams in isotropic gyrotropic medium.

K.S. Grigoriev[1], V.A. Makarov[1,2], I.A. Perezhogin[2]

1-Physics Faculty of M.V. Lomonosov Moscow State University
2- International Laser Center of M.V. Lomonosov Moscow State University

i.a.perezz@gmail.com

C-points (points of circular polarization) are phase singularities of the circularly polarized (CP) components of the electromagnetic radiation [1]. Their trajectories in propagating paraxial light beams are known as C-lines. The features accompanying the formation of polarization singularities in nonlinear optical processes and their subsequent evolution are almost unknown up to day.

In our work we have numerically modeled and studied the interaction of C-points in collinearly propagating beams in isotropic gyrotropic medium with spatial dispersion (nonlocality) of cubic optical response. We assume the beams each having the following structure: the right-hand circularly polarized (RHCP) component has Gaussian profile, while the left-hand circularly (LHCP) polarized one has Laguerre-Gaussian profile. So, each of two beams has RHCP C-point in its center. In the course of propagation (both linear and nonlinear) the C-points undergo creation and annihilation processes. In the linear medium two Gaussian beams (RHCP) merge in the center forming an intensity maximum there (“central maximum”), while the Laguerre-Gaussian beams (LHCP) lose their cylindrical symmetry, and form intensity maxima (“spots”) at their “rings” (“lateral maxima”).

In a nonlinear medium the features of the interaction of the polarization singularities are similar to those in linear medium. They are determined by the initial distance between the C-points, phase shift between the beams and the nonlinear susceptibilities of the medium. If the CP components undergo mutual focusing, then the events of pairwise creation and annihilation of C-points take place at smaller distances traversed in a medium with the growth of the intensity and/or nonlinear susceptibilities, compared to the case of linear interaction. The lateral maxima will be attracted by the two Gaussian intensity maxima, and there will appear not three, but only two intense peaks in the transversal section of the propagating light. Otherwise, (in case of mutual defocusing, which depends on the medium parameters) all the characteristic events happen faster (at closer distances) with the increase of the intensity than in linear medium, and the intensity maxima with opposite handedness of the polarization rotation defocus each other and tend to occupy different (not overlapping) areas in the transversal plane of the propagating field. The presence of the spatial dispersion causes faster pairwise creation of the C-points with corresponding handedness (Fig. 1; positive values of spatial dispersion parameter favor the formation of RHCP C-points, and vice versa).

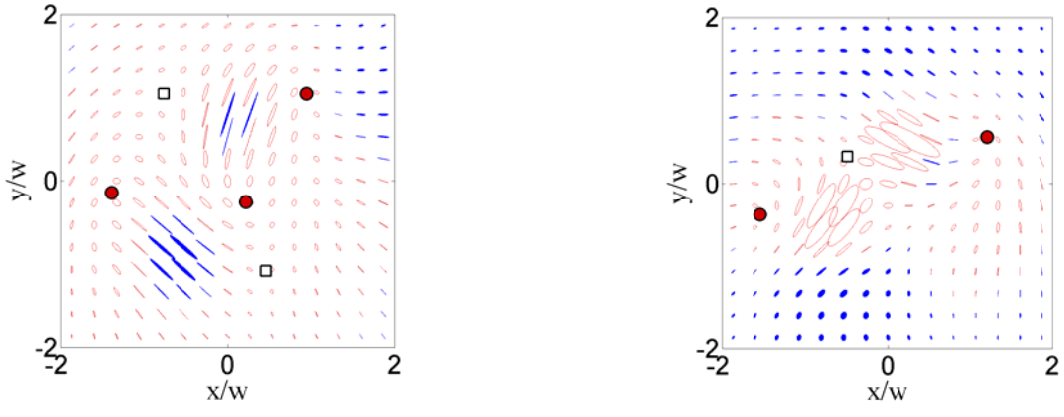

(a) (b)

Figure 1. The transversal polarization distribution at the distance of two diffraction lengths in the medium in case of equal topological charges of the singularities in the incident beams. The medium parameters correspond to the case of mutual focusing of RHCP and LHCP components. The spatial dispersion of nonlinearity favors the self-focusing of a) RHCP component; b) LHCP component.

[1] J.F. Nye Proc. R. Soc., **389**, 279 (1983).

ADIABATIC APPROXIMATION APPROACH TO A SYSTEM OF NONLINEAR SCHRODINGER EQUATIONS FOR ELLIPTICALLY POLARIZED WAVES IN AN ISOTROPIC GYROTROPIC MEDIUM

V.A. Makarov, V.M. Petnikova, V.V. Shuvalov

Faculty of Physics and International Laser Center of M.V. Lomonosov Moscow State University

Leninskie Gori, 1, str. 62, Moscow, 119991, Russia

vamakarov@phys.msu.ru

Propagation of plane elliptically polarized light wave through an isotropic medium with second-order frequency dispersion and spatial dispersion of cubic nonlinearity of Kerr-type is described by nonintegrable system of two coupled nonlinear Schrödinger equations. There are available a number of particular analytical solutions of this system. One of them corresponds to elliptically polarized cnoidal waves, which arise under the conditions of formation of the waveguides of the same type for each of the circularly polarized components of the light field. Some years ago, we obtained [1] the approximate solutions of this system of nonlinear equations, which keep all characteristics of medium under study and describe the propagation of chirped elliptically polarized periodic waves as well as aperiodic ones. The conditions for the implementation of propagation regimes and their relation to the initial conditions have been also determined.

Now we report about analytical results of the adiabatic approximation approach (the frequencies of the two excited normal modes of electromagnetic field are significantly different) to description of coherent nonlinear evolution of two orthogonally polarized light field components with phases linearly increasing with propagation through a nonlinear gyrotropic medium. We found the conditions of applicability of the adiabatic approximation and the analytical expressions for propagated elliptically polarized light field components.

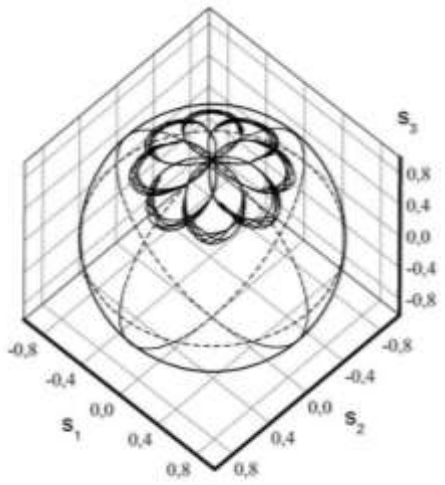

The represented figure illustrates the evolution character of the polarization state of electric field for the obtained solutions in adiabatic approximation. It shows the trajectory of the end of the normalized Stokes vector on the Poincare sphere then the observation plane moves with constant velocity. One can see an aperiodic evolution of the light field polarization state slightly reminding "palarization chaos". The obtained solutions are similar to the well-known [2] "soliton – multisoliton complex" pairs which are generalized to the case of interaction of two cnoidal waves with significantly different periods of oscillations.

References

1. V.A. Makarov, V.M. Petnikova, V.V. Shuvalov. Chirped elliptically polarized waves in an isotropic gyrotropic nonlinear medium: approximate solution to the propagation problem. Laser Physics Letters, vol. 10, 075404 (2013).

2. A.A. Sukhorukov, A. Ankiewicz, N.N. Akhmediev. Multisoliton complexes in a sea of radiation modes". Opt. Comm. vol. 195, 283 (2001).

Wednesday
8th October

Biophotonics – multimodal imaging for clinical applications

J. Popp[1,2]

1- Institute of Physical Chemistry and Abbe Center of Photonics, Friedrich-Schiller-University Jena, Helmholtzweg 4, 07743 Jena, Germany

2- Leibniz-Institute of Photonic Technology Jena (IPHT), Albert-Einstein-Str.9, 07745 Jena, Germany
Juergen.popp@ipht-jena.de

Optical imaging technologies such as Raman imaging have proven to be a valuable tool in medical diagnostics. Within the last years a rapid increase of applications of Raman spectroscopy in particular to address biomedical questions has been observed. New concepts of cancer diagnostics towards a rapid identification of sepsis pathogens were among the most important questions answered by innovative Raman approaches. Raman spectroscopy probes molecular vibrations within cells and tissues. Spectral contributions are assigned to proteins, lipids, nucleic acids and carbohydrates. As cancer and other pathologic anomalies are accompanied by changes in the biochemical composition and structure of biomolecules, the Raman spectrum provides a sensitive and specific fingerprint of the type and state of the specimen. Advantages of the technique for biomedical problems include that (i) it is label-free, (ii) non-destructive and (iii) rapid. Combination of the spectral and the lateral information gives a powerful imaging technique. The hyperspectral data sets need to be analysed and classified by multivariate chemometric algorithms.
The contribution will first summarize the principles of data acquisition and then give an overview of Raman imaging for an early disease diagnosis like e.g. cancer.[1] Besides these ex-vivo Raman studies on excised tissue first steps towards in-vivo Raman spectroscopy will be introduced. By doing so novel Raman fiber probes for an intravascular monitoring of the artheriosclerotic plaque in living rabbits will be presented.[2] The low Raman scattering cross section often results in long acquisition times which can be reduced by utilizing non-linear Raman approaches like CARS (coherent anti-Stokes Raman scattering). In order to further improve the diagnostic result CARS microscopy can be easily extended by the two other non-linear contrast phenomena second harmonic generation (SHG) and two-photon fluorescence (TPF). While CARS microscopy is focusing on fast image generation using specific Raman marker bands, e.g., CH_2 at 2850 cm^{-1}, SHG and TPF highlight additional structural features by displaying collagen structures (SHG) and the spatial distribution of autofluorophores like e.g. NAD(P)H, flavines and elastin. We will present the development of a compact CARS/SHG/TPF multimodal nonlinear microscope in combination with novel fiber laser sources for use in clinics.[3] The diagnostics potential of this microscope as compared to conventional histopathological images has been demonstrated for the examples of atherosclerosis and cancer.[4]
Overall the presented examples show the great potential of Raman imaging to complement histopathology in diagnosis and disease recognition.

Acknowledgments
Funding of our research from the BMBF (German Research Ministry), DFG, EU, EFRE, FCI and state of Thuringia (TMBWK and TMWAT) is highly acknowledged.

[1] N. Bergner, A. Medyukhina, K. D. Geiger, M. Kirsch, G. Schackert, C. Krafft, J. Popp, Hyperspectral unmixing of Raman micro-images for assessment of morphological and chemical parameters in non-dried brain tumor specimens, Anal. Bioanal. Chem. 405, 8719-8728 (2013).
[2] C. Matthäus, S. Dochow, G. Bergner, A. Lattermann, B. F. Romeike, E. T. Marple, C. Krafft, B. Dietzek, B. R. Brehm, J. Popp, In Vivo Characterization of Atherosclerotic Plaque Depositions by Raman-Probe Spectroscopy and in Vitro Coherent Anti-Stokes Raman Scattering Microscopic Imaging on a Rabbit Model, Anal. Chem. 84, 7845-7851 (2012).
[3] T. Meyer, M. Baumgartl, T. Gottschall, T. Pascher, A. Wuttig, C. Matthaeus, B. F. M. Romeike, B. R. Brehm, J. Limpert, A. Tuennermann, O. Guntinas-Lichius, B. Dietzek, M. Schmitt, J. Popp, A compact microscope setup for multimodal nonlinear imaging in clinics and its application to disease diagnostics, Analyst, 138, 4048-4057 (2013).
[4] T. Meyer, M. Chemnitz, M. Baumgartl, T. Gottschall, T. Pascher, C. Matthaus, B. F. M. Romeike, B. R. Brehm, J. Limpert, A. Tuennermann, M. Schmitt, B. Dietzek, J. Popp, Expanding Multimodal Microscopy by High Spectral Resolution Coherent Anti-Stokes Raman Scattering Imaging for Clinical Disease Diagnostics, Anal. Chem. 85, 6703−6715 (2013).

Compact Diode Laser-based Systems for Biophotonics Application

P. E. Andersen,[1,*] O. B. Jensen,[1] A. Müller,[2] B. Sumpf,[2] A. K. Hansen,[1] P. M. Petersen,[1] Peter M. Skovgaard,[3] A. Unterhuber,[4] and W. Drexler[4]

*1 - Technical University of Denmark, Roskilde, Denmark, * peta@fotonik.dtu.dk*
2 - Ferdinand-Braun-Institut, Leibniz-Institut für Höchstfrequenztechnik, Berlin, Germany
3 - Norlase ApS, Roskilde, Denmark
4 - Medical University of Vienna, Vienna, Austria

Diode lasers are by far the most efficient lasers currently available [1]. With the ever-continuing improvement in diode laser technology, this type of laser has become increasingly attractive for a wide range of biomedical applications. Compared to the characteristics of competing laser systems, diode lasers simultaneously offer tunability, high-power emission and compact size at fairly low cost. Therefore, diode-based lasers are increasingly preferred in important applications [2], such as photocoagulation, optical coherence tomography, diffuse optical imaging, fluorescence lifetime imaging, and terahertz imaging.

Diode lasers have proven to be versatile light sources for pumping Ti:Sappphire lasers offering advantages over current solid-state lasers in terms of compactness, noise characteristics, and no need for water cooling [3,4]. Whilst direct green laser diodes at several Watts of output power are not available, nonlinear frequency conversion of high brightness diode lasers has recently resulted in visible light power levels in the watts range enabling an increasing number of applications within biophotonics.

This talk review provides an overview of the developments within nonlinear frequency converted high power laser diodes in the blue-green spectral range. Single-pass nonlinear frequency doubling is presented as a non-sophisticated method to achieve watt-level output powers. Furthermore, potential routes to higher power and increased conversion efficiency are discussed. In particular, so-called cascaded frequency-doubling will be discussed as a means of power scaling, involving one laser and several nonlinear crystals. By beam combining, sum-frequency generation can be achieved, thus combining several lasers in one crystal to obtain higher power [5,6]. Application examples within pumping of mode-locked Ti:sapphire lasers and implementation of such lasers in optical coherence tomography are presented showing the application potential of these lasers [4].

[1] B. Sumpf, K.-H. Hasler, P. Adamiec, F. Bugge, F. Dittmar, Jö. Fricke, H. Wenzel, M. Zorn, G. Erbert, and G. Tränkle, "High-Brightness Quantum Well Tapered Lasers," IEEE. J. Sel. Topics. in. Quantum. Electron. **15**(3), 1009-1020 (2009)
[2] A. Müller, S. Marschall, O. B. Jensen, J. Fricke, H. Wenzel, B. Sumpf, and P. E. Andersen, "Diode laser based light sources for biomedical applications," Laser & Photonics Review **7**(5), 605-627 (2013).
[3] A. Müller, O. B. Jensen, A. Unterhuber, T. Le, A. Stingl, K.-H. Hasler, B. Sumpf, G. Erbert, P. E. Andersen, and P. M. Petersen, "Frequency-doubled DBR-tapered diode laser for direct pumping of Ti:sapphire lasers generating sub-20 fs pulses," Opt. Express **19**, 12156-12163 (2011).
[4] A. Unterhuber, B. Považay, A. Müller, O. B. Jensen, M. Duelk, T. Le, P. M. Petersen, C. Velez, M. Esmaeelpour, P. E. Andersen, and W. Drexler, "Simultaneous dual wavelength eye-tracked ultrahigh resolution retinal and choroidal optical coherence tomography," Opt. Lett. **38**, 4312-4315 (2013)
[5] A. Müller, D. Vijayakumar, O. B. Jensen, K.-H. Hasler, B. Sumpf, G. Erbert, P. E. Andersen, and P. M. Petersen, "16 W output power by high-efficient spectral beam combining of DBR-tapered diode lasers," Opt. Express **19**, 1228-1235 (2011)
[6] A. Müller, O. B. Jensen, K.-H. Hasler, B. Sumpf, G. Erbert, P. E. Andersen, and P. M. Petersen, "Efficient concept for generation of diffraction-limited green light by sum-frequency generation of spectrally combined tapered diode lasers," Opt. Lett. **37**, 3753-3755 (2012)

Laser-activated chromophores and nanoparticles in minimally-invasive diagnostics and therapies

R. Pini[1], F. Ratto[1], F. Rossi[1], P. Matteini[1], F. Tatini[1], S. Centi[2], F. Fusi[1,2]

1- Institute of Applied Physics, National Research Council of Italy, Florence, Italy
2- Department of Experimental Biomedical and Clinical Science, University of Florence, Italy

Main author email address:r.pini@ifac.cnr.it

We review our experimental, preclinical and clinical activities on the exploitation of a light stimulation produced by a laser source to "activate" suitable photothermal enhancers like organic chromphores and plasmonic nanoparticles for applications in bonding and repair of biotissues, and in cancer diagnostics and therapy.

Laser-assisted tissue repair or laser welding has been proposed to close chronic accidental and surgical wounds. Typically, laser light is delivered 1) to a wound site to be repaired, which has been stained with an exogenous optical absorber or 2) to a photoresponsive medical dressing (e.g. patches, stents, etc) placed in intimate contact with the tissue to be repaired, in order to produce a photothermal effect. An exemplary application, already in the clinical phase, is corneal laser welding, which is obtained by staining the cut edges of a stromal tissue with the photosensitizer Indocyanine green (ICG) and by irradiating them with a near-infrared laser light to produce collagen denaturation and reorganization of the noncollagenous components, which can ultimately sustain wound closure and tissue fusion. For applications in micro-vascular surgery aiming at the repair of arterial wounds we have recently engineered a hybrid bioadhesive consisting in a chitosan film doped with ICG or gold nanorods (GNRs) that can be activated by NIR laser light. These films (0.8 cm diameter, 40 μm thickness) are insoluble, flexible, resistant and stable in a physiological environment. Upon laser irradiation a well-localized photothermal effect can thus take place to induce adhesion of the film with the arterial wall. The excellent biocompatibility and biodegradability of chitosan, as well as the effectiveness of the patches to close arterial wounds, has been tested in vivo in preclinical studies.

Moreover, the combination of pulsed and CW near-infrared laser light with plasmonic particles such as gold nanorods is gaining relevance for the photoacoustic imaging and photothermal ablation of cancer. Selective targeting of malignant cells with these contrast agents may rely on complementary biochemical and biological strategies, including the use of specific probes or the exploitation of cellular vehicles. Here we moved from a platform of PEGylated gold nanorods with plasmonic bands around 800 nm, good biological profiles, stability and efficiency of photoacoustic and photothermal conversion as well as potential to passively accumulate into solid tumors by their enhanced permeability and retention. In order to enhance this potential, we implemented different approaches for active delivery by functionalization with (i) antibodies against cancer antigen 125 (CA125), which is a common biomarker for ovarian lesions; (ii) inhibitors of carbonic anhydrases 9 and 12 (CAIX and CAXII), which are expressed by hypoxic cells such as those found in solid tumors; and (iii) by introducing macrophages as a versatile model of cellular vehicles that would phagocytose the particles and home to inflammatory lesions. In vitro studies on cell cultures on those different approaches will be presented and discussed.

Nanodiamond optical-spectroscopic properties and their optimization for development of theranostic applications.

E. Perevedentseva[1,2], A. Karmenyan[3], Y.C. Lin[1], K.T. Wu[1], Ashek-I-Ahmed[1], N.N. Melnik[2], C.L. Cheng[1]

1- National Dong Hwa University, 1 Sec. 2 Da Hsueh Rd, Shoufeng, Hualien 974 Taiwan
2- P.N. Lebedev Physics Institute, 53 Leninskii pr-t, Moscow 199911 Russia
3- Biophotonics and Molecular Imaging Research Center, National Yang Ming University, 155 Sec.2 Linong Str, Taipei, 112 Taiwan

elena@mail.ndhu.edu.tw, clcheng@mail.ndhu.edu.tw

Nanodiamond-based systems are developed and realized for bio-imaging as an alternative to fluorescent dyes and quantum dots due to nanodiamond (ND) photoluminescence (fluorescence) properties. The main origins of the ND's fluorescence are color centers - defects and admixtures embedded in the diamond lattice. They reveal well-detectable, stable luminescence in different ranges of spectra, which can be excited with various excitations. At that the ND fluorescence strongly depends on ND structure and, as one can see from current studies, on surface properties. That allows the fluorescence properties modification for further development of ND theranostics applications, as imaging and delivery tracing, bio-sensing, photothermal treatment, etc. First of all, there are methods developed to increase the ND fluorescence [1], to improve their use both for fluorescent imaging and for fluorescence lifetime imaging (FLIM). Importantly, fluorescent ND (FND) emits the fluorescence with lifetime longer than lifetimes of dyes for the biological samples staining or of cellular autofluorescence sources, allowing separation of FND emission from the fluorescence background [2]. We also consider the methods of control the ND fluorescence properties by ND's treatment with temperature and surface termination [3], noble metal coating [4], macromolecules attachment [5].
To understand the influence of color center state and environment as well as role of the nanoparticles surface structure and chemistry the fluorescence spectra of differently treated nanodiamonds and ND conjugated with various macromolecules (proteins, amino acids, etc.) have been analyzed together with life-time measurements data. We have demonstrated that nitrogen-vacancy (NV^-, NV^0) centers fluorescence properties can be modified by the surface oxidation and hydrogenation of ND. The fluorescence lifetimes measurements reveal also dependence on surface interactions with adsorbed or chemically attached molecules (proteins, amino acids, etc.). The possible mechanisms of interactions between color centers, surface and environment are discussed involving electron/energy transfer [5]. New possibilities for nanodiamond use for bio-sensing and bio-imaging are supposed.

[1] Y.-R. Chang, H.-Y. Lee, K. Chen, C.-C. Chang, D.-S. Tsai, C.-C. Fu, T.-S. Lim, Y.-K. Tzeng, C.-Y. Fang, C.-C. Han, H.-C. Chang, W. Fann, Mass production and dynamic imaging of fluorescent nanodiamonds, Nature Nanotechnology 3, 284 - 288 (2008)
[2] Y. Kuo, T.-Y. Hsu, Y.-C. Wu, H.-C. Chang, Fluorescent nanodiamond as a probe for the intercellular transport of proteins in vivo, Biomaterials 34 8352-8360 (2013)
[3] J. Mona, E. Perevedentseva, A. Karmenyan, H.-M. Liou, T.-Y. Kang, C.-L. Cheng, Tailoring of structure, surface, and luminescence properties of nanodiamonds using rapid oxidative treatment, J. Appl. Phys. 113, 114907 (2013)
[4] A.V. Karmenyan, E. Perevedentseva, M. Veres, C.-L. Cheng, Simultaneous PL and SERS observation of ND at laser deposition on noble metals, Plasmonics 8, 325–333 (2012)
[5] E. Perevedentseva, N. Melnik, C.-Y. Tsai, Y.-C. Lin, M. Kazaryan, C.-L. Cheng, Effect of surface adsorbed proteins on the photoluminescence of nanodiamond, J. Appl. Phys. 109, 034704 (2011)

Laser-stimulated Cavitation and Tissue Regeneration

V. Bagratashvili
Institute of Laser and Information Technologies RAS, Russia

bagrat@laser.ru

Modern laser medical technologies widely employ the delivery of laser radiation to the irradiated tissues via optical fibers. Optical fibers easily penetrate through needles and endoscopic channels, and lasers can be used for puncture and endoscopic operations. Several laser medical technologies (laser engineering of cartilages, puncture multichannel laser decompression of disc, laser intervention upon osteochondrosis, surgical treatment of chronic osteomyelitis, endovenous laser ablation) are based on the effective cavitation processes in water-saturated bio-tissues. These cavitation processes trigger cellular response and regenerative effects through the mechanisms of mechano-biology.

We study the effects of cavitation hydrodynamics stimulated by medium power (1–5 W) laser radiation in the vicinity of the heated end surface of the optical fiber in water. We perform the measurements in bulk liquid and in the glass capillary that simulates the laser channel. A developed threshold character of the dynamics of liquid is demonstrated. At a relatively low laser power (about 1 W), we observe the slow formation of air–vapor bubbles with sizes of hundreds of microns on the end surface of the optical fiber. The bubbles can be attached to the end surface during the irradiation session.

When the laser power increases, we observe the effective processes cavitation hydrodynamics related to the explosive boiling in the vicinity of the hot end surface. The resulting bubbles with sizes ranging from a few microns to several tens of microns provide the motion of liquid. The estimations yield a velocity of up to 100 mm/s for the bubbles in the vicinity of the end surface. The generation of bubbles in the capillary leads to the circulating liquid flows with periods ranging from 0.2 to 1 s. Note that the circulation intensity increases with the laser power. For the laser radiation with a wavelength of 0.97 μm, we observe such effects only for the blackened end surface of silica fiber, which serves as a point heat source. At a laser power of less than 3 W, stable bubble microjets, which consist of the bubbles whose sizes range from several to ten microns, can be generated in the vicinity of the blackened end surface.

Specific features of acoustic vibrations generated at the hot blackened end face of an optical fiber (the so-called hot tip) delivering medium power CW laser radiation in contact with water or a water-saturated biotissue are studied. Generated upon such a contact is a wideband acoustic signal whose characteristics largely depend on the object exposed and treatment scheme. Placing the hot tip in an acoustic resonator is demonstrated to cause distinct amplitude modulation of the acoustic noise. The formation of laser canals in an intervertebral cartilage or the intramedullary cavity of a bovine thighbone gives rise to the emission of a quasiperiodic train of pulses associated with the explosive growth and collapse of steam-gas bubbles in the hot-tip-to-biotissue contact region. The resultant pressure pulses 20±12 MPa in amplitude cause damage to the adjacent tissue and facilitate the production of a laser canal at a rate of some 0.4 to 5 mm/s. During the course of laser treatment the biotissue gradually gets saturated with steam-gas bubbles, which results in the development of low-frequency pressure oscillations in the range 0.1–10 Hz and gradual pressure rise to around 200 kPa and makes for reduction of the natural frequencies of the resonance modes of the biotissue.

The effects of laser-stimulated cavitation on the proliferation of human and rabbit multipotent mesenchymal stromal cells (MMSC) were studied in vitro. It is shown, that laser-stimulated cavitation stimulates the increase of proliferation activity of "suppressed" human MMSC up to 80%.

Possible mechanisms of the effect of effect of laser-stimulated cavitation on biotissue regeneration are discussed.

Skin Fractional Ablation Using Multi-Micro-Beam Erbium Laser for Enhanced Particle Delivery

E.A. Genina[1], A.N. Bashkatov[1], L.E. Dolotov[1], I.V. Yaroslavsky[2], G.B. Altshuler[2], V.V. Tuchin[1,3,4]

[1]Institute of Optics and Biophotonics, Saratov State University, 83, Astrakhanskaya str., Saratov, 410012, Russia
[2]Cynosure Inc, 15 Network Dr, Burlington, Massachusetts 01803, USA
[3]Institute of Precise Mechanics and Control of RAS, 24, Rabochaya Str., Saratov 410028, Russia
[4]University of Oulu, P.O. Box 4500, Oulu FIN-90014, Finland

e-mail of corresponding author: eagenina@yandex.ru

There are many studies demonstrating importance of the transcutaneous drug delivery and ability to create a long-term reservoir in the dermis for topically applied compounds [1-3]. The main advantages of transcutaneous administration of preparations are: 1) minimal invasiveness or even noninvasiveness; 2) improved drug pharmacokinetics; and 3) targeted drug delivery [1].
Fractional laser microablation (FLMA) is one of the relatively safe and minimally invasive methods used to administer micro- and nanoparticles into the skin at sufficiently large depth in comparison with surface ablation and mechanical treatments because of the low area of skin damage and, therefore, reduced risk of infection [1, 4, 5].
We are presenting the results of delivery of TiO_2 nanoparticles, ZrO microparticles, and Al_2O_3 microparticles into skin. Fractional laser microablation of skin was provided by a system based on a pulsed Er:YAG laser with the following parameters: the wavelength 2940 nm, the pulse energy 2.0 J, the pulse duration 10 ms. The laser emission beam was split into 169 micro-beams using an array of micro-lenslets. 169 vertical micro-channels were created in the skin in the area with the dimensions of 6×6 mm^2. The suspensions of TiO_2, ZrO, and Al_2O_3 powder in polyethylene glycol with the particle size about 100 nm, 5 μm, and 27 μm, respectively, were used. For delivery of the particles the following modes were used: massage, shockwave pulses and shockwave pulses through sapphire plate. The concentration of the particles in the suspensions was 0.5 g/mL. *In vivo* human skin was investigated. For quantitative analysis of ablated and treated skin sites optical coherence tomography (OCT) was used.

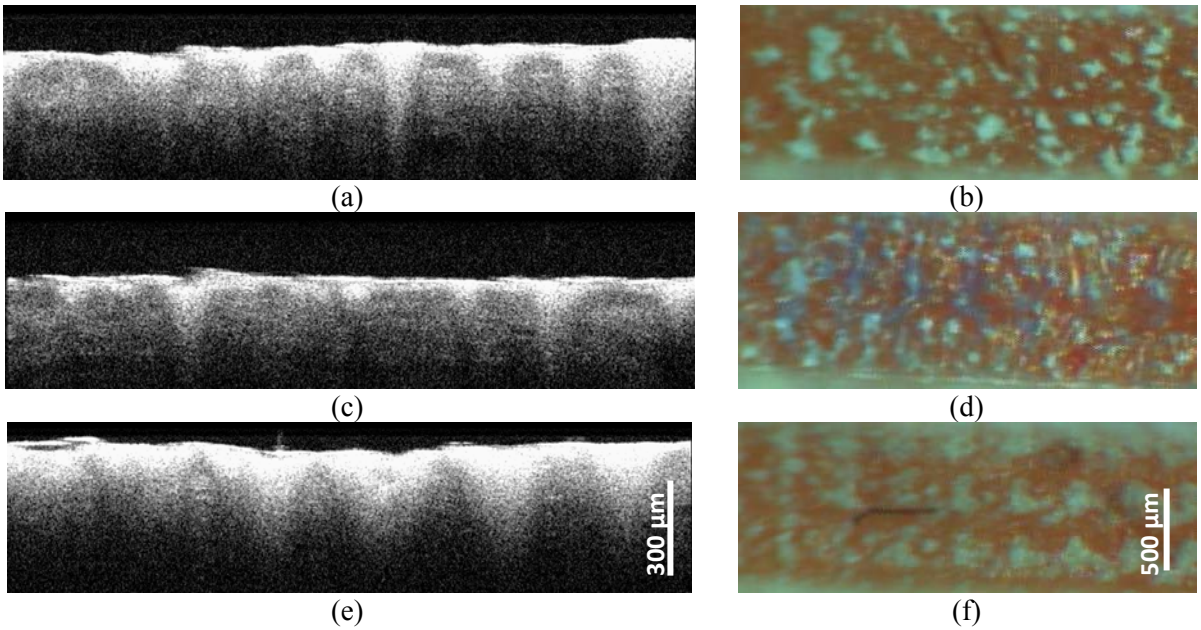

(a) (b) (c) (d) (e) (f)

Figure 1 Series of OCT images (a), (c), and (e) and microphotorgraphs (b), (d), and (f) of the human skin areas *in vivo* after fractional laser micro-ablation (six pulses) and ZrO suspension application: (a) and (b) images correspond to the site after 5-min massage; (c) and (d) images correspond to the site after 5-min massage and 6 pulses of shockwaves; and (e) and (f) images correspond to the site after 3 pulses of shockwaves through sapphire plate.

Figure 1 shows result of fractional laser microporation of human skin in vivo with different modes of ZrO microparticle delivery.

This study shows that the use of fractional laser microablation with Er:YAG laser allows for efficient administering TiO_2 nanoparticles (< 100 nm), ZrO microparticles (~5 μm) and Al_2O_3 microparticles (~27 μm) into the dermis. Particles can be delivered to the different depths in dependence on delivery mode. The microscopic channels, created in the tissue by ablation, allowed for particle penetration up to 230 μm deep into the dermis. Multi-micro-beam laser microporation has a significant potential as a rapid, complications-free transcutaneous delivery technique.

The work was carried out under the partial support by Russian Scientific Foundation (grant No. 14-15-00186); Russian Federation Governmental No. 11.G.34.31.0030 designed to support scientific research projects implemented under the supervision of leading scientists at Russian institutions of higher education; and project № 1.4.09; and FiDiPro, TEKES Program (40111/11), Finland.

[1] G. Cevc, and U. Vierl, Nanotechnology and the transdermal route. A state of the art review and critical appraisal, J. Control. Release, vol. 141, pp. 277-299 (2010).

[2] J. Lademann, H. Richter, A. Teichmann, N. Otberg, U. Blume-Peytavi, J. Luengo, B. Weiss, U. F. Schaefer, C. M. Lehr, R. Wepf, and W. Sterry, Nanoparticles—an efficient carrier for drug delivery into the hair follicles, Eur. J. Pharm. Biopharm., vol. 66, pp. 159–164 (2007).

[3] S. Khandavilli and R. Panchagnula, Nanoemulsions as versatile formulations for paclitaxel delivery: peroral and dermal delivery studies in rats, J. Invest. Dermatol., vol. 127, pp. 154-162 (2007).

[4] B.D. Zelickson, S.E. Walgrave, M.Y.H. Al-Arashi, G.B. Altshuler, I.V. Yaroslavsky, J.J. Childs, R.H. Cohen, A.V. Erofeev, E.F. Depina, M.Z. Smirnov, D.A. Kist, and D.R. Tabatadze, Semi-automated method of analysis of horizontal histological sections of skin for objective evaluation of fractional devices, Lasers Surg. Med., vol. 41, pp. 634-642 (2009).

[5] H.-J. Laubach, Z. Tannous, R.R. Anderson, D. Manstein, Skin responses to fractional photothermolysis, Lasers Surg. Med., vol. 38, pp. 142-149 (2006).

RECENT PROGRESS IN INTERFERING FEMTOSEOCOND LASER PROCESSING

Yoshiki Nakata[1], Naoto Shimada[1], Yoshiki Matsuba[1], Keiichi Murakawa[1], Noriaki Miyanaga[1]
Tatsuya Shoji[2], Yasuyuki Tsuboi[2]
[1]*Osaka University, 2-6 Yamadaoka, Suita, Osaka, 565-0871Japan*
[2]*Osaka City University, 3-3-138, Sugimoto, Sumiyoshi, 558-8585 Japan*
nakata-y@ile.osaka-u.ac.jp

A variety of metamaterials can be fabricated in a single process using an interfering femtosecond laser technique. In the past papers, we have shown a variety of metamaterials such as nanowhisker [3,5], nanobump [2-5], MHA (metallic-hole array) [1,2]. In addition, a shape of meta-atom can be controlled by number, phase and amplitude shift of beams [4,6,7]. In the presentation, recent progress and representative results will be shown.

In interfering femtosecond laser processing a beam is split by a diffraction beam splitter, and 1st diffracted beams correlate on a surface of a target through a demagnifncation system [4,6,7]. The wavelength is 785 nm, and the pulsewidth is about 240 fs. In Fig. 1, SEM images of example metal metamaterials fabricated with different beam and target parameters are shown. Fig. 2 is the transmission spectrum of a MHA fabricated on 100 nm thick gold film. The right-top image is a part of MHA, and the spacing is s = 1.93 μm. The hole diameter is about 600 nm in this area. In the transmission spectrum, the calculated transmission peaks are indicated by dashed lines, and corresponding peaks appear at about 4 % longer wavelength than the dashed lines.

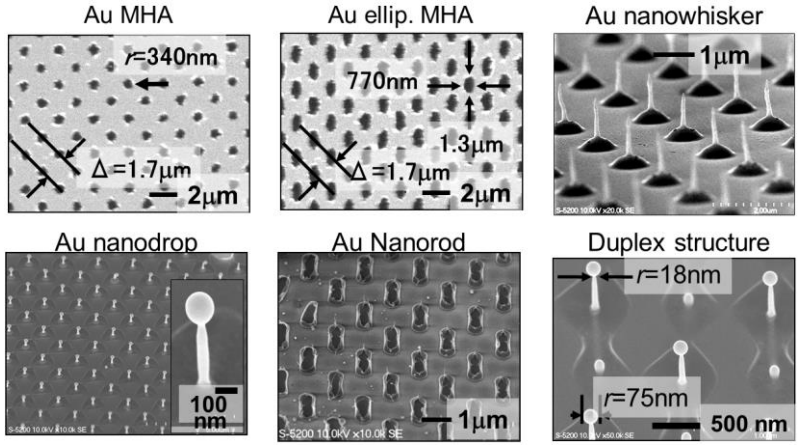

Fig. 1 a variety of metal metamaterials fabricated by a single shot of interfering femtosecond laser irradiation.

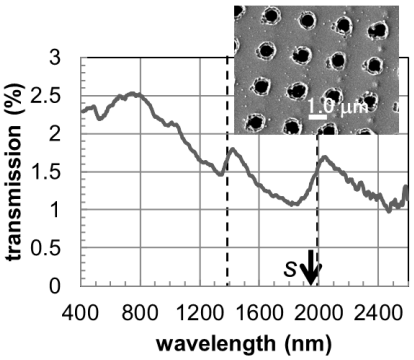

Fig. 2 transmission spectrum of gold MHA and SEM image.

References:

1. Y. Nakata et al., Fabrication of dot matrix, comb, and nanowire structures using laser ablation by interfering femtosecond laser beams, Appl. Phys. Lett. 81, pp. 4239-4241 (2002).
2. Y. Nakata et al., Nano-sized hollow bump array generated by single femtosecond laser pulse, Jpn. J. Appl. Phys. 42, L1452-L1454 (2003).
3. Y. Nakata et al., "Solid-liquid-solid process for forming free-standing gold nanowhisker superlattice by interfering femtosecond laser irradiation", Appl. Surf. Sci., 274, pp. 27-32, (2013).
4. Y. Nakata et al., "Mesoscopic nanomaterials generated by interfering femtosecond laser processing", Appl. Surf. Sci. 101, pp. 471-474 (2010).
5. Y. Nakata et al., Frozen water drops in the nanoworld, SPIE newsroom, DOI; 10.1117/2.1200906.1708. published online, (2009).
6. Y. Nakata et al., Design of interference using coherent beams configuring as a six-sided pyramid, Appl. Opt. 51, pp. 5004-5010 (2012).
7. Y. Nakata et al., Designing of interference pattern in ultra-short pulse laser processing, Appl. Phys. A, 112, pp. 191-196 (2013).

Photonic crystal mirrors: a cornucopia of nanopatterned structures for the taming of light at the wavelength scale

Rémy Artinyan, Chérif Belacel, Zhen Lin, Jean-Louis Leclercq, Ségolène Callard and Xavier Letartre

Université de Lyon, Institut des Nanotechnologies de Lyon (INL), UMR CNRS 5270, Ecole Centrale de Lyon, France, Xavier.letartre@ec-lyon.fr.

High index contrast periodic structures, or Photonic Crystal membranes (PCMs), can be exploited to perform an arbitrarily adjustable spatio-temporal molding of light at the wavelength scale. This tight control of photons is obtained through a shaping of resonant modes and a suitable adjustment of their coupling with propagative modes. In this talk, surface addressable (or above the light line) Bloch modes in photonic crystal membranes (PCMs) will be investigated. The concepts governing the properties of these modes will be first presented. It will be demonstrated that simple models can be considered to understand their behavior and, more specifically, their ability to capture photons during the desired lifetime. Bloch modes with a very large band width or a very high Q factor can be easily designed this way. The wide application range of these PCMs will be illustrated by different devices. Low Q Bloch modes will be used as efficient and broadband reflectors and exploited to realize compact and efficient vertical microcavity lasers with unprecedented functionalities [1]. In addition, it will be shown that this kind of mirrors can be bent to form a "photons cage" where light can be confined, even in low index materials, in the 3 directions of space. Applications for new classes of emitters and sensors will be envisaged [2].

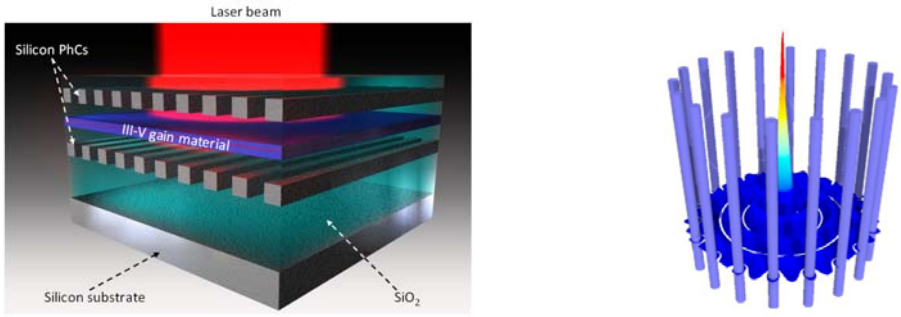

Figure 1: left: artistic representation of a PCMs based VCSEL. Right: a "photon cage" formed by bending a silicon/air PCM

Aknowledgement : The research leading to these results has received funding from the French National Research Agency (ANR project MOREMIR) and by the Labex IMUST of the University of Lyon (project REBECA).

References :

[1] C. Sciancalepore et al., IEEE Phot. Techn. Lett. 24, 455 (2012)

[2] C. Sieutat et al., Optics express 21, 20015 (2013)

Exciton states of the optical electrons of dielectric nanoparticles in dielectric matrix

Kulchin Yu.N., Dzyuba V.P., Amosov A.V.

Institute of Automation and Control Processes FEB RAS, Radio 5, 690041, Vladivostok, Russia

Far Eastern Federal University, Sukhanova 8, 690950, Vladivostok, Russia

kulchin@iacp.dvo.ru ; vdzyuba@iacp.dvo.ru

In recent years, experimental investigations of the nonlinear optical properties of dielectric nanocomposites containing small concentrations of dielectric nanoparticles showed that they [1–10 etc.] exhibit unique optical nonlinearity in low-intensity optical radiation fields. The anomalous nonlinear optical properties are as follows: (i) Great value of bandgap gave reason to think that the nonlinear response of nanocomposite media occurs under ultraviolet light but it is observed for visible and infrared light; (ii) Nonlinear response occurs at radiation intensities below 1 kW/cm2 and can be observed under pulsed and cw laser modes. It reaches a maximum and disappears with increasing intensity; (iii) It takes place if transmission spectra of nanoparticles array have the broad bands of light absorption that are absent for the bulk sample; (iiii) Nonlinear optical properties take place at frequencies lying within the absorption band of light.

The intensity threshold and nature of nonlinear response depend on characteristics of nanoparticles and matrix material as well as their size and shape. It was determined that dielectric nanoparticles have nonlinear response when the matrix has a static permittivity less than that of nanoparticles. This fact allows us to vary the parameters of response by changing nanocomposite components and nanoparticles concentration, size, and shape. The existence of nonlinear optical properties in dielectric nanocomposites points out that the electronic structure of nanoparticles dispersed in dielectric matrix differs significantly from the electronic structure of the bulk sample. Differences consist, first, of formation of the allowed energy levels for the charge carrier in the bandgap because the bandgap structure is connected with a complex form of nanoparticles and high density of surface defects in the crystal structure. Moreover, the electrons of nanoparticles should have broad band of exciton states. The report presents and analyzes the experimental and theoretical results showing that the dielectric nanoparticles have the exciton states of electrons with binding energy of several electron volts, which are excited by the weak optical laser radiation. Such materials with a wide spectrum of exciton states are important for creation: exciton lasers and optical emitters; receiving and emitting optical nano-antennas; control and processing information and signals; generation low-power optical solitons; optical computers etc.

1. Mikheeva O.P., Sidorov A.I. *Zh. Tekh. Fiz.*, **74** (6), 77 (2004) [*Tech. Phys*., **49** (6), 739 (2004)].
2. Yu. N. Kulchin, A. V. Shcherbakov, 2.V. P. Dzyuba, S. S. Voznesenskii, and G. T. Mikaelyan, “Nonlinear-optical properties of heterogeneous liquid nanophase composites based on high-energy-gap Al2O3 nanoparticles,” *IOP Quantum Electron* **38**(2), 154–158 (2008).
3. Yu. N. Kulchin, V. P. Dzyuba, and A. V. Scherbakov, “Optical transmittance spectra of insulator nanoparticles in bulk heterocomposites,” *Semicond*. **43**(3), 331–339 (2009).
4. V. P. Dzyuba, A. E. Krasnok, Yu. N. Kulchin, and I. V. Dzyuba, “A model of nonlinear optical transmittance for insulator nanocomposites,” *Semicond*. **45**(3), 295–301 (2011).
5. V. P. Dzyuba, A. E. Krasnok, and Yu. N. Kulchin, “Nonlinear refractive index of dielectric nanocomposites in weak optical fields,” *Tech. Fiz. Lett.* **36**(11), 973–977 (2010).
6. Yu. N. Kulchin, V. P. Dzyuba, and S. S. Voznesenskiy, “Threshold optical nonlinearity of dielectric composite,” in *Advances in Diverse Industrial Applications of Nanocomposites*, p. 261–288, Intech Open Access Publisher, Croatia (2011).
7. Vladimir Dzyuba, Valentin Milichko, Yurii Kulchina, Nontypical photoinduced optical nonlinearity of dielectric nanostructures. *J. Nanophotonics*, **5**,053528 (2011).
8. Dzyuba V., Kulchin Yu., Milichko V Effect of the shape of a nano-object on quantum-size states. *J. Nanopart. Res*., **14**, 1208 (2012).
9. V.A. Milichko, V.P. Dzyuba, Yu.N. Kulchin Anomalous optical nonlinearity of dielectric a nodispersions**Quantum Electronics* **43** (6) 567 – 573 (2013)
10. Vladimir Dzyuba, Yurii Kulchin andValentin Milichko Photonics of Heterogeneous Dielectric Nanostructures In Nanocomposites - New Trends and Developments Ebrahimi (Ed.), 2012 / ISBN: 978-953-51-0762-0 , InTech, Chapter 15.

All-optical polarization control in fibers for Telecom applications

P-Y. Bony[1], M. Guasoni[1], S. Pitois[1], P. Morin[1], D. Sugny[1], A. Picozzi[1], H. R. Jauslin[1], G. Millot[1], S. Wabnitz[2] and J. Fatome[1]

1- Laboratoire Interdisciplinaire Carnot de Bourgogne (ICB), UMR 6303 CNRS - Université de Bourgogne, 9 Av. Alain Savary, BP 47870, 21078 Dijon, France

2- Department of Information Engineering, Università di Brescia, Via Branze 38, 25123 Brescia, Italy

jfatome@u-bourgogne.fr

The all-optical polarization control of a light beam propagating in optical fiber is a crucial issue which could find important applications in optical networks. To this aim, the research has moved on the development of nonlinear methods in order to re-polarize an initially depolarized light [1-4]. In this contribution, we propose a novel approach which is based on the capability for an incident signal to self-organize its state of polarization (SOP) without any need of external control. We baptize this device as the Omnipolarizer [3]. It basically consists in a km-long telecom fiber in which a Watt-level input signal nonlinearly interacts with its own counter-propagating replica produced by means of a back-reflection at the fiber output (Fig.1). Two distinct operating regimes are reachable depending on the back-reflection coefficient. When it is larger than unity (i.e., the back-reflected light is amplified thanks to an EDFA), any arbitrary input signal SOP is attracted in output towards a specific SOP. In this configuration, the Omnipolarizer acts as a powerful ideal polarizer which enables to reach a very high degree of polarization (DOP) close to unity. A second polarization control function can be achieved when the back-reflection coefficient is below unity, here close to 0.5. In this case any arbitrary input SOP is then attracted in output towards a right or left circular state depending on the sign of its initial ellipticity. As a result, we obtain a discrete polarization beam splitter (PBS) which can digitally route the whole signal energy to either the right or left-circular SOP. The Omnipolarizer has been successfully tested in an error free transmission over an input On/Off Keying 40-Gbit/s signal which was initially scrambled over the entire Poincaré sphere (Fig.1).

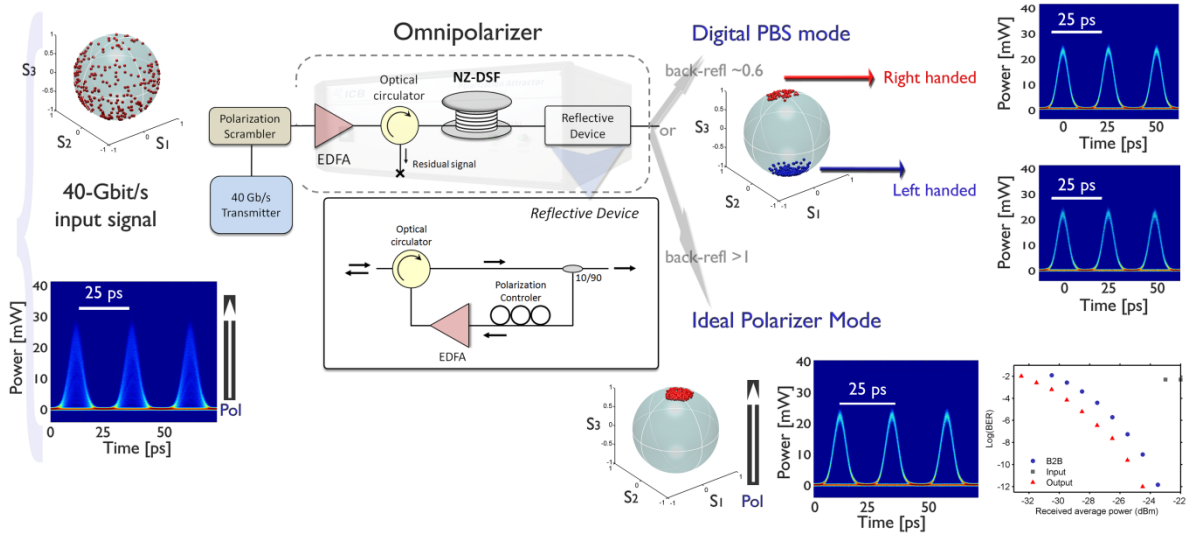

Figure 1 Experimental results obtained for the Omnipolarizer for an input signal power of 27 dBm. Depending on the back-reflected power, the device can act in two modes of operation: PBS or ideal polarizer.

[1] M. Martinelli, M. Cirigliano, M. Ferrario, L. Marazzi, and P. Martelli, Evidence of Raman-induced polarization pulling, Opt. Express, 17, pp. 947-955, (2009).

[2] P. Morin, J. Fatome, C. Finot, S. Pitois, R. Claveau, and G. Millot, All-optical nonlinear processing of both polarization state and intensity profile for 40 Gbit/s regeneration applications, Opt. Express, 19, pp. 17158-17166, (2011).

[3] J. Fatome, S. Pitois, P. Morin, D. Sugny, E. Assémat, A. Picozzi, H. R. Jauslin, G. Millot, V. V. Kozlov and S. Wabnitz, A universal optical all-fiber omnipolarizer, Sci. Rep., 2, 938 (2012).

[4] P.-Y. Bony, M. Guasoni, E. Assémat, S. Pitois, D. Sugny, A. Picozzi, H. R. Jauslin, and J. Fatome, Optical flip–flop memory and data packet switching operation based on polarization bistability in a telecommunication optical fiber, J. Opt. Soc. Am. B, 30, pp. 2318-2325, (2013).

Joint Influence of Cubic Nonlinearity and Thermally Induced Birefringence on the Radiation Polarization in High Peak Power Lasers

M. Kuzmina*, E. Khazanov, A. Stepanov

Institute of Applied Physics of the RAS, 46 Ulyanov Street, 603950 Nizhny Novgorod, Russia

kmsnn@mail.ru

Creation of laser systems possessing simultaneously high peak power and high average power is the promising trend in laser physics. One of the key problems to be solved in construction of such lasers is suppression of thermal effects restricting average power and nonlinear optical effects limiting peak power. This talk provides an overview of the recent results of investigation of the joint impact of thermal and nonlinear effects on the output polarization of powerful laser with high pulse repetition rate.

In media with cubic nonlinearity sufficiently intense laser radiation can cause a noticeable change in refractive index due to its dependence on the intensity. Cubic nonlinearity manifests itself as a well-known effect of polarization ellipse turn in the isotropic medium because of the nonlinear difference in the refractive indices of circularly polarized components [1,2]. Rotation angle of the polarization ellipse is dependent on the optical path, intensity of radiation and the polarization ellipticity.

The appearance of the induced by strong field birefringence leads to negative consequences in case of laser radiation propagation in a medium with a different type of birefringence, for example natural or thermally induced. Both cubic nonlinearity and birefringence introduce polarization distortions in the laser beam, giving rise to depolarization.

The active elements of laser amplifiers and magnetic elements of the Faraday isolator are examples of optical elements with thermally induced anisotropy. Such birefringence and the consequent increase of depolarization in these elements are successfully compensated in the absence of the cubic nonlinearity. However, it was shown theoretically and experimentally that the efficiency of the broadly employed method of depolarization compensation in active elements by means of a 90° polarization rotator decreases with increasing B-integral (nonlinear phase incursion). The contributions of both the effects are nonadditive in principle, as thermally induced birefringence depends neither on intensity, nor on laser field polarization, whereas anisotropy induced by cubic nonlinearity is a function of intensity and polarization. The magnitude of uncompensated depolarization in such a scheme is proportional to B^2 for arbitrary values of thermally induced phase difference δ. The dependence of depolarization γ on δ is essentially nonmonotonic. There exists a critical value δ_{cr} at which γ is maximal. Values of the rotator optimal angle providing significant decrease of the residual depolarization were numerically calculated.

The influence of cubic nonlinearity on the insulation value of the state-of-art schemes of Faraday isolator was also investigated. Three types of birefringence were taken into account: induced by strong field, circular (Faraday effect) and thermally induced. It was found out that for all schemes depolarization increase due to cubic nonlinearity is proportional to squared B-integral and for $B > 1$ this increase is an order of magnitude or more.

Wave plates are example of media with natural anisotropy. Dependence of depolarization degree Γ (fraction of energy in the polarization orthogonal to the polarization in the absence of nonlinearity) at the output of a quarter-wave plate of crystalline quartz on B-integral was obtained theoretically and experimentally. It was revealed that in such quarter-wave plate with thickness of 0.18 cm the depolarization value reaches 1% at the laser intensity of 370 GW/cm^2. It was shown that the use of the quarter-wave plate made from crystal DKDP can significantly reduce the negative impact of cubic nonlinearity: depolarization in this case does not exceed 0.2% for the intensity up to 2 TW/cm^2.

References

[1] A.L. Berkhoer, V.E. Zakharov, "Self Excitation of Waves with Different Polarizations in Nonlinear Media," Soviet J. of Experimental and Theoretical Physics, **31**, 486 (1970).

[2] D.V. Vlasov, V.V. Korobkin, R.V. Serov, "Nonlinear precession of elliptically polarized Gaussian beams," Soviet J. of Quantum Electronics **9**, 904 (1979).

Laser-induced Damage in Second Harmonic Generation by Periodically Poled $LiTaO_3$

O. A. Louchev,[1] H. Hatano,[2] N. Saito,[1] S. Wada,[1] and K. Kitamura[2]

1. Advanced Photonics Center, RIKEN, 2-1 Hirosawa, Wako, Saitama, 351-0198, Japan.

2. Division of Environment & Energy Materials, NIMS, 1-1 Namiki, Tsukuba, Ibaraki 305-0044, Japan

e-mail : oleglouchev@riken.jp

By presenting our experimental-theoretical study for ns pulsed second harmonics generation (SHG) in periodically poled lithium tantalate (LT) we suggest a specific mechanism providing an effective kinetic pathway for electron heating and damage generation existing in nonlinear crystals. In short, during SHG the initial temperature increase ΔT of few K caused by two-photon absorption in the rear of the crystal induces a high gradient of the spontaneous polarization P_s across the irradiated zone resulting in the onset of the electric field $E\approx 10$ kV/cm, which accelerates the free electrons produced by absorption to the energy of ≈10 eV, followed by the crystal damage [1,2].

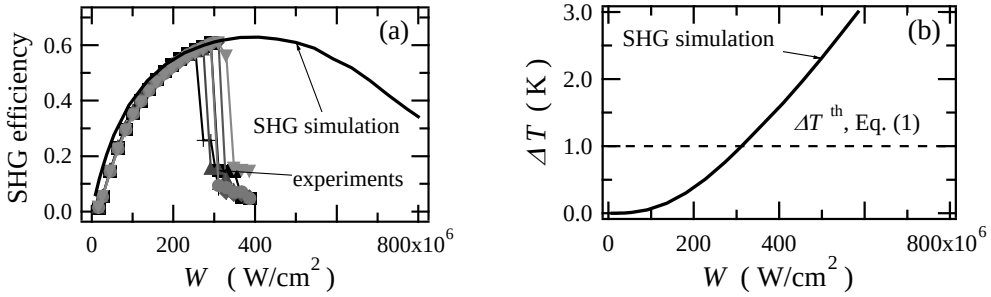

Fig.1 SHG efficiency data [1,2] and numerical simulation by complex non-linear frequency conversion model [3]: (a) SHG efficiency and (b) maximal temperature increase in operating crystal vs 1064 nm input power density.

The experimental data is obtained by using 1064 nm *Q*-switched Nd:YAG laser for the following parameters: crystal dimensions 3 mm (along the beam)x1x2 mm, beam radius 28 μm for e^{-2} fall of the intensity, repetition rate ν=6.8 kHz, pulse duration time τ_p=4.4 ns, the poled period Λ=8 μm and quasi-phase-matching temperature T_{QPM}=44 ^{0}C. The experimental data exhibits the threshold fall in SHG efficiency taking place at $W\approx 300$ MW/cm^2 and producing damage at the rear side of LT crystal [1]. Experimental data is shown together with the simulation results obtained by our model which rigorously integrates SHG formalism with the simulation of the temperature field in operating crystals [3]. The maximal temperature change, $\Delta T\approx 0.92$ K, found by our simulation for the damage threshold is described well by the following expression [1,2]:

$$\Delta T^{th} \approx \left(\frac{m_e \varepsilon_{cr}}{2}\right)^{1/2} \frac{\varepsilon\varepsilon_0}{|p_T| q_e \tau^*} \approx 1\ K \quad , \qquad (1)$$

where $\varepsilon_{cr}\approx 1.5E_g$ is the critical energy for impact generation, ε_0 is the vacuum permittivity, $\varepsilon=\varepsilon_{33}$ is the dielectric constant along P_s , $p_T=dP_s/dT$, τ^* is the electron-to-lattice energy transfer time of LT, m_e and q_e are the electron mass and charge.

A more detailed analysis given in our presentation shows (i) how laser-induced breakdown develops during single pulse and pulse repetition mode and, finally, (ii) allows us to find an explicit expression for the damage threshold which agrees well with the original experimental and published data for various materials [2].

[1] O. A. Louchev, H. Hatano, S. Wada, and K. Kitamura, "Optical breakdown threshold in nanosecond high repetition second harmonic generation by periodically poled Mg-doped $LiTaO_3$ crystal" , *Appl. Phys. Lett.* **103**, 091114 (2013).

[2] O. A. Louchev, H. Hatano, N. Saito, S. Wada, and K. Kitamura, "Laser-induced breakdown and damage generation by nonlinear frequency conversion in ferroelectric crystals: experiment and theory" , *J. Appl.. Phys.* **114,** 203101 (2013).

[3] O.A. Louchev and S. Wada, , "Numerical model and study of cascaded third harmonics generation in two-sectioned a periodically poled Mg-doped $LiTaO_3$ structure", *J. Appl. Phys.* **106**, 093106 (2009).

Identifying hidden substances by THz remote sensing: A realistic dream?

E. Hérault, F. Garet, and J.-L. Coutaz

IMEP-LAHC, UMR CNRS 5130, University of Savoie, 73 376 Le Bourget du Lac Cedex, France

emilie.herault@univ-savoie.fr

From the beginning of modern THz science, defence and security have been identified as potential fruitful applications of THz technology. Thanks to THz imagery, many people have dreamt to detect weapons and prohibited substances such as drugs or explosives at border or airport gates, even if those items are concealed under a cloth or in a bag. To reach this goal, the key point is often believed to be a powerful source or a noiseless detector. Fabrics, as thin dielectric materials, are considered to be more or less transparent, and thus just act as weak attenuators. We show here that diffraction, interferences or/and scattering occurring within fabrics, make difficult, if not impossible, the identification of hidden substances. We have studied the transmission of 13 different fabrics used to make the most common clothes (T-shirt, jeans, sport cloth, clean room overall…), and their impact of the THz spectra, recorded either in transmission or in reflection, of a pellet of organic material (glutamic acid) hidden by these fabrics. This panel of different material compositions (polyester, cotton, silk…) and of different weavings allows us to investigate the influence of various radiometric responses (absorption, but also diffusion, diffraction and interference) induced by fabrics when spectra are recorded in realistic conditions. Our experimental data were recorded up to 7 THz with a TAS7500 Advantest THz time-domain spectrometer.

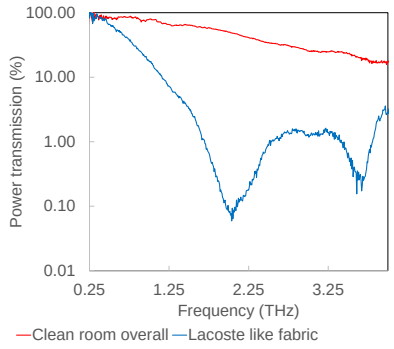

Fig. 1. Transmission spectrum of fabric samples.

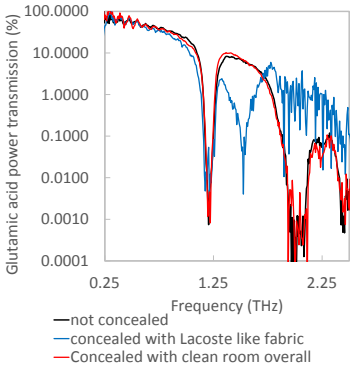

Fig. 2: Deduced glutamic acid transmission spectrum.

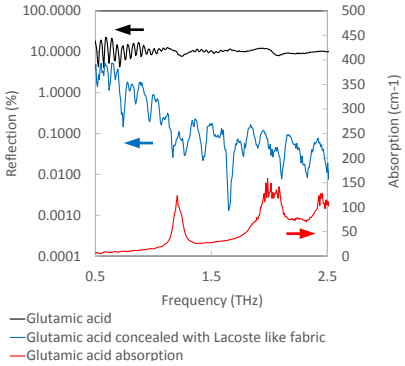

Fig. 3: Concealed and not concealed glutamic acid reflection spectrum.

Fig. 1 shows the transmission spectra of clean room overall and Lacoste-like fabric. Above 1.5 THz, i.e. in the range where interesting spectral lines of organic materials lie, most fabrics transmit less than 10 %. Fig. 2 presents the transmission spectrum of a pellet of pure glutamic acid covered by a cloth. The spectrum has been divided by the one of the cloth alone (Fig. 1), i.e. the curves correspond to the spectrum of the pellet as deduced from a measurement when the pellet is hidden by the cloth. For a fabric that is not diffracting or scattering, the spectrum of the pellet alone can be nicely retrieved from the measurements with a covered pellet. For other fabrics, diffraction, scattering or interferences make the spectra more complicated. Here, an interference feature at 1.5 THz could be misinterpreted as a spectral line. Nevertheless, in transmission, identification of the hidden substance is quite easy. The spectra, recorded in reflection, of the pellet alone and covered by a cloth, as well as the absorption spectrum of glutamic acid, are shown on Fig. 3. Even for the bare pellet, the strong absorption lines of glutamic acid result only in a weak variation of the reflection spectrum. When the pellet is covered by a cloth, the reflected THz beam crosses twice the fabric, which makes the signal very weak over 1 THz, and thus completely erases the spectral signature of the glutamic acid. For some clothes (not shown here), additional strong interference features make the reflection spectra unusable.

"Time-domain probe of THz nanostructure lasers"

J. Darmo, D. Bachmann, M. Martl, D. Dietze, V. Paeder, A.M. Andrews, G. Strasser, K. Unterrainer

Photonics Institute and Center for Micro&Nanostructures, Technische Universität Wien, A-1040 Vienna, Austria.

The generation of coherent THz pulses from femto-second sources has enormously progressed. The band-width, intensities, as well as the efficiency has increased by using advanced semiconductor emitters and non-linear processes. In this way the spectral range up to 100 THz can be covered by quasi single cycle THz pulses. In solids, the resonance energies of phonons, plasmons and impurity transition are within the THz range opening are large field for spectroscopy. In particular also the transition energies of semiconductor nano structures occur in the THz band. Thus few-cycle THz spectroscopy is the right tool to study these elementary transitions. Moreover, time-resolved THz spectroscopy allows phase-locked measurements – in particular phase-resolved detection.

Modern nano fabrication can be used to fabricate devices based on quantized transitions. The most prominent and sophisticated example for such multilayer structures to generate light are Quantum Cascade lasers (QCLs). Advanced design concepts of active regions as well as of waveguides persistently extend the lasing properties like frequency range, operating temperature power output, efficiency, tunability, multicolor concepts, and nonlinear effects.

THz spectroscopy allows unique measurements of Quantum-Cascade lasers. The knowledge of the phase of the THz emission provides fascinating insights into the quantum optical processes. In addition, these measurements enable the study of the gain band width, gain saturation and recovery as well as the observation of spatial hole burning. We will present the results of several different active regions which show quite different behavior due to the underlying quantum transport processes. We also investigate different waveguides where the difference in the confinement leads to substantial changes in the dispersion.

With high intensity THz pulses we can also explore the non-linear regime of intersubband transitions. The observation of two and three photon processes is encouraging for further THz non-linear effects in structures with large confinement. In meta-material coupled nanostructures we observe strong coupling und study its dependence on the THz field strength.

M. Martl et al., "Gain and losses in THz quantum cascade laser with metal-metal waveguide," Opt. Express 19, 733 (2011), doi: 10.1364/OE.19.000733.

J. Kröll, J. Darmo, S. Dhillon, X.Marcadet, M. Calligaro, C. Sirtori, K. Unterrainer, “Phase resolved measurements of stimulated emission in a laser“, Nature, 449, 698 (2007).

D. Dietze et al., “Efficient population transfer in modulation doped single quantum wells by intense few-cycle terahertz pulses”, New J. Phys. 15, 065014 (2013); doi:10.1088/1367-2630/15/6/065014

Sub-gigawatt Terahertz Source Based on Optical Rectification and Its Non-thermal Impact on In-vivo Mouse Brain Neural Cell

Li-Guo Zhu[1,2], Sen-Cheng Zhong[1,2], Tu-Nan Chen[1,3], Kun Meng[1,2], Qiao Liu[1,2], Zhao-Hui Zhai[1,2], Hua Feng[3], Ze-Ren Li[1,2], Jian-Heng Zhao[1]

1- Interdisciplinary Lab of Physics and Biomedicine, Institute of Fluid Physics, China Academy of Engineering Physics, Mianyang, Sichuan 621900, P. R. China

2- Terahertz Research Center, China Academy of Engineering Physics, Mianyang, Sichuan 621900, P. R. China

3- Department of Neurosurgery, Southwest Hospital, Third Military Medical University, Shapingba District, Chongqing, 400038, P. R. China

*Main author email address: **zhuliguo@tsinghua.org.cn***

With the development of terahertz (THz) pulsed source, several research groups recently demonstrated that pulsed THz source induce non-thermal effect on biology, such as disturbing gene expresses in mouse stem cell [1], perturbing wound healing process in mouse skin via downstream target genes [2], and down-regulating cancer-related gene on mouse skin cancer [3]. In order to realize THz non-thermal effect on biology, the peak-power of THz pulse used in these work was promoted to about 30MW, either by femtosecond (fs) laser-plasma interaction, or by fs-laser optical rectification in LiNbO3 (LN), or from a fs-laser driven accelerator.

In this talk, I'll present how we achieve a THz pulsed source with 0.29 GW peak-power driven by a terawatt (TW) fs-laser in LN via optical rectification (which, to our knowledge, is of the highest peak power with this method reported, and one order higher than recent reported [5]). A fs-second laser with peak-power of ~1.2 TW, beam size of ~4 cm, and pulsed duration of 45 fs was used to excite LN following the standard tilted wave front scheme [4]. A LN crystal with new geometry was designed to reduce large laser beam effect and keep the over-all conversion efficiency to 0.5%.

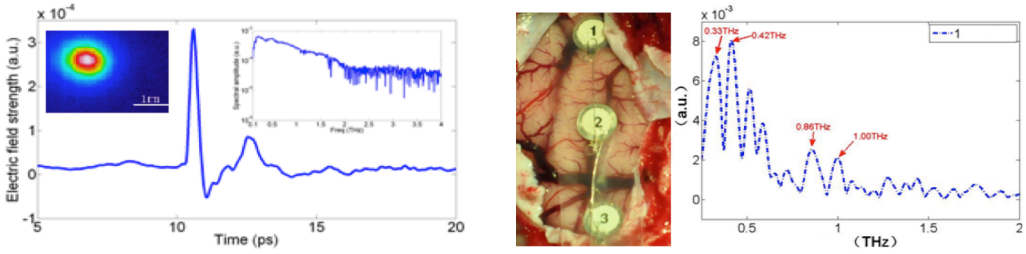

(a) (b)

Figure 1 (a) electric waveform, spectrum and beam profile of the THz pulsed source achieved in our experiment. (b) In-vivo living mouse brain stimulated by the 0.29 GW THz pulses and its response in THz spectrum.

In the second part, I'll demonstrate non-thermal influence of 0.19 GW peak-power THz pulses (with average power of ~2 mW, and repetition rate of 10 Hz) on mouse brain, which include in-vivo gene express in a mouse brain neural cell and perturbation on brain function. Gene expression perturbation was confirmed by standard microarray survey and reverse transcription polymerase chain reaction (RT-PCR) experiments. Heat shock proteins weren't affected, which demonstrates that THz pulse impact is non-thermal. Detailed optimization of the 0.19 GW THz source, experiment procedure and results on living mouse brain will be shown in my talk. Preliminary experiment on enhancement of THz power by cooling down LN crystal and passible THz induced gene toxicity on other living organs will be also discussed in my talk.

[1] B. S. Alexandrov, M. L. Phipps, L. B. Alexandrov, et al, Specificity and heterogeneity of terahertz radiation effect on gene expression in mouse mesenchymal stem cells, ***Scientific Reports*** 3, 1184 (2013).

[2] K.-T. Kim, J. Park, S. J. Jo, et al, High-power femtosecond-terahertz pulse induces a wound response in mouse skin, ***Scientific Reports*** 3, 2296 (2013).

[3] L. V. Titova, A. K. Ayesheshim, A. Golubov, et al, Intense THz pulses down-regulate genes associated with skin cancer and psoriasis: a new therapeutic avenue? ***Scientific Reports*** 3, 2363 (2013).

[4] J. Hebling, G. Almasi, I.Z. Kozma, et al, Velocity matching by pulse front tilting for large area THz-pulse generation. ***Optics Express*** 10, 1161-1166 (2002)

[5] S.-W. Huang, E. Granados, W. R. Huang, et al, High conversion efficiency, high energy terahertz pulses by optical rectification in cryogenically cooled lithium niobate, ***Optics Letters*** 38, 796-798 (2013).

[6] W. M. Freeman, S. J. Walker, K. E. Vrana, Quantitative RT-PCR: pitfalls and potential. ***BioTechniques*** 26, 112-125 (1999).

[7] A. De Maio, Heat shock proteins: facts, thoughts, and dreams. ***Shock*** 11, 1–12 (1999)

Simultaneous generation of nonlinear optical harmonics and THz radiation in air: polarization discrimination of various nonlinear contributions

Mikhail Esaulkov[1], Olga Kosareva[2], Nikolay Panov, Vladimir Makarov[2], Alexander Shkurinov[2]

1. Institute on Laser and Information Technologies of the Russian Academy of Sciencies (ILIT RAS). 140700, Svyatoozerskaya 1, Shatura, Russia
2. M.V.Lomonosov Moscow State University, 119991Leninskie Gory 1, Moscow, Russia
esaulkov_mich@mail.ru

Abstract: We experimentally observed generation of the second, the third optical harmonics and terahertz radiation in air during optical breakdown with a 120-fs laser pulse. The analysis of their polarization properties revealed unity of their nonlinear optical nature.

OCIS codes: (190.2620) Harmonic generation and mixing (190.4380) Nonlinear optics, four-wave mixing

1. Introduction

When femtosecond laser radiation is focused in the athmospheric air, gas acts like nonlinear optical medium. This leads to generation of optical harmonics, waves at sum- and difference frequencies at fairly small femtosecond laser pulse energies. In the case of simultaneous interaction of laser pulses at two frequencies (first and second harmonics) in the optical beam waist, a number of symmetry forbiddances are removed and both odd and even harmonic generation including terahertz (THz) radiation [1] become allowed.

The nature and the origin of nonlinear polarization in gases interacting with powerful laser radiation are quite complex. Along with many others, a major contribution is related to gas atoms which stay neutral after the interaction with intense laser radiation, and free electrons which are result of ionization of other part of atoms of the medium. These contributions can interact both constructively and destructively behaving differently in low-frequency emission properties, such as THz emission spectrum, directionality diagram and its polarization properties [2].

In this work we study experimentally the polarization of the second, the third optical harmonics and the broadband terahertz radiation generated during the interaction of a two femtosecond pulses with degenerated frequencies ω and 2 ω with air. While nonlinear polarization properties at second and third optical harmonics are defined mainly by the contribution of neutral atoms, the THz emission is in general described as the contribution of both neutral atoms and free electrons. We show that taking into account only the third-order nonlinear response of an isotropic medium neutral [3] (non-ionized) atoms is enough to describe the experimentally observed polarization properties of the newly generated third harmonic, the phase-dependent linear polarization of the wide-spectra pulsed THz radiation and the appearance of the crossed-polarized second harmonic radiation.

2. Experiment

In our experiments we used laser radiation from Ti:Sapphire regenerative amplifier (Spectra Physics Spitfire) with the energy up to 2 mJ per pulse, duration 120 fs, wavelength 797 nm and 1 kHz repetition rate. We separated the laser beam into two arms for independent control of intensity, polarization and time delay of the fundamental and second harmonic radiation. The second harmonic was generated using a I-type BBO crystal (thickness 0.3mm). After recombining the two beams with a dielectric mirror, a lens with f=10cm was used to focus the two-color radiation. Its focal region is the area of interaction where plasma channel is ignited and generation of optical harmonics and terahertz radiation takes place.

Optical radiation from the breakdown region was collimated with a quartz lens (f=10cm) and guided into the slit of Acton SpectraPro 500i monochromator coupled to a CCD camera for studying 3ω polarization or to a diffraction grating with 1200 slits/mm for studying the polarization of 2ω using a photodiode and lock-in amplifier.

The THz radiation was separated from the optical beam using a 0.35mm thick Si plate, then collimated and refocused using off-axis parabolic mirrors. The power of the THz radiation was measured with a Golay cell (Tydex GC-1P) able to detect radiation from 0 to 300 THz. A wire-grid analyzer was placed into the collimated THz beam to study its polarization. We stress that in all the experiments we kept the similar energies of the input ω and 2ω

radiation (0.25±0.01mJ/pulse and 0.05±0.005 mJ/pulse respectively) so that we could compare the data on different nonlinear processes under study.

3. Results

We investigated the polarization state of the 2ω radiation emitted from the beam focus in the case of the linear initial polarization of both ω and 2ω. The nonlinear interaction in the breakdown region leads to shift of the polarization of second harmonic radiation. If we place an analyzer crossed with the initial 2ω polarization, we see that for zero time delay between the ω and 2ω pulses the 2ω radiation passes through analyzer. We measured the energy of the 2ω radiation after the analyzer as a function of the angle ψ between initial ω and 2ω field vectors, the dependence is shown in the Fig.1.

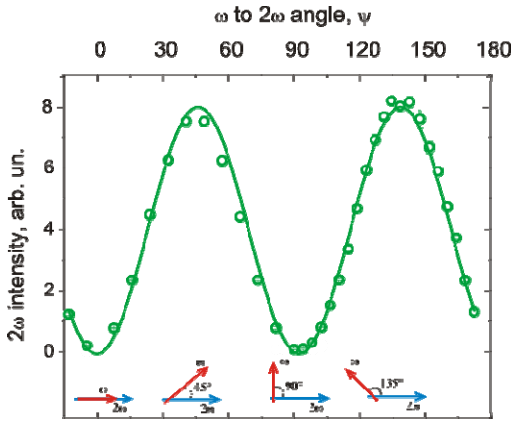

Fig. 1. Measured intensity of the 2ω radiation polarized orthogonally to the initial 2ω polarization vs angle ψ between electric fields of ω and 2ω pulse.

The Fig. 2 shows the experimental dependences of energies of THz radiation polarized along the y and x (along the 2ω polarization direction) axes respectively on the angle between ω and 2ω polarizations. The dependence is also symmetrical about ψ = 45º and similar to the observed dependence for second harmonic polarization change. The energy of x-polarized THz radiation has its maximal value when ω and 2ω polarizations are parallel and decreases as the angle ψ increases from 0 to 90º (the case of orthogonally polarized ω and 2ω beams).

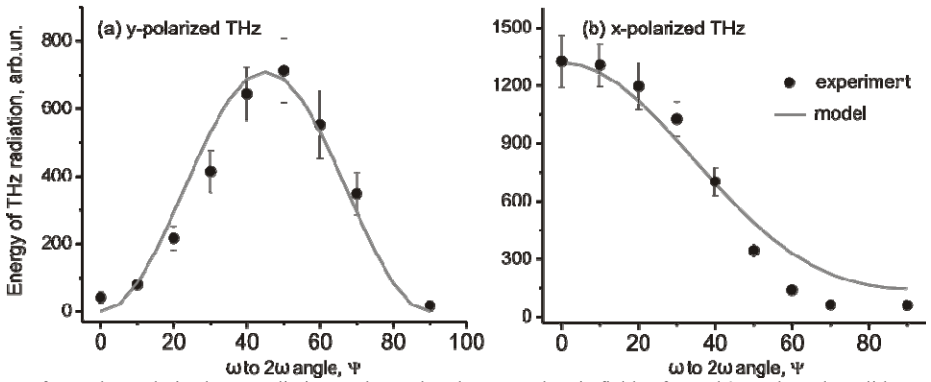

Fig. 2. Energy of y- and x- polarized THz radiation vs the angle ψ between electric fields of ω and 2ω pulse. The solid curves show the dependences of the x- and y-polarized THz energy in accordance with the theoretical four-wave mixing model.

We also studied the polarization state of the 3ω radiation resulting from nonlinear interaction of circularly polarized fundamental radiation and linearly polarized second harmonic radiation (along x axis). A λ/4 wave plate placed before the dichroic mirror was used to achieve the circular polarization of ω beam. Intensity of the input ω beam vs the analyzer angle is shown on Fig. 3 with red circles. In this configuration of the optical fields, the third harmonic radiation is generated only in the four-wave mixing process 3ω = 2ω + 2ω – ω. We observed the elliptically polarized 3ω radiation with the major axis of the ellipse directed along the electric field vector of 2ω pulse (see Fig. 3).

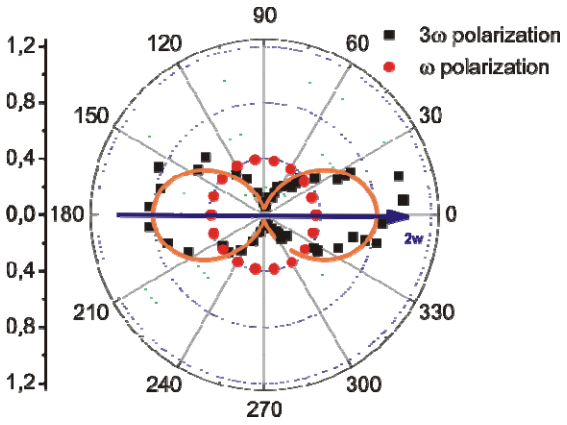

Fig. 3. Polarization of the third harmonic radiation (black squares) as compared with the polarization if the initial ω radiation (red circles) and the linear 2ω polarization direction (blue line). Orange solid line shows the simulated 3ω polarization

4. Discussion

For theoretical interpretation of the results, we propose that the observed polarization properties of the generated THz radiation and optical harmonics can be described using the third-order effective nonlinearity only and neglecting spatial and temporal dispersion. We add an assumption that the material dispersion is absent.

Under these assumptions, we show that the energy of 2ω radiation, polarized orthogonally to its initial direction, follows the sine-square dependence $W_{crossed}^{(2\omega)}(\psi) = W_{crossed}^{2\omega(\max)} \sin^2 2\psi$ on the angle 2ψ between the initial linear polarization directions of the ω to 2ω fields. The major contribution of the third order nonlinear response of neutrals is further confirmed by the similar sine-square dependence of the newly appearing terahertz radiation after the analyzer crossed to the initial 2ω field linear polarization direction.

If the initial ω field is circularly polarized and the 2ω field is linearly polarized, the newly appearing 3ω radiation is elliptically polarized with its major axis of the ellipse directed along the 2ω linear polarization direction. The terahertz field polarization in this case is linear. Variation of the phase difference φ between ω and 2ω fields leads to change in the terahertz field polarization direction without affecting its amplitude.

5. Conclusions

In conclusion, we have experimentally investigated simultaneous generation of three nonlinear-optical processes appearing in the course of interaction of the two-color femtosecond pulse with atmospheric air. We show that third-order nonlinear response of the neutral molecules of air can account for the observed polarization properties.

6. References

[1] J. Wynne, P. Sorokin. “Optical mixing in atomic vapors. Nonlinear infrared generation”. Ed. Y.R. Shen. Berlin: Springer-Verlag. 1977. P. 159-214

[2] A. V. Borodin et al., “Transformation of terahertz spectra emitted from dual-frequency femtosecond pulse interaction in gases”, Optics Letters, **38** (11), 1906-1908 (2013)

[3] M.N. Esaulkov et al., “Simultaneous generation of nonlinear optical harmonics and THz radiation in air: polarization discrimination of various nonlinear contributions”, accepted for Frontiers of Optoelectronics (2014)

[4] G. Gryaznov, V. Makarov, I. Perezhogin, and N. Potravkin. “Modeling of nonlinear optical activity in propagation of ultrashort elliptically polarized laser pulses”. Physical Review E, **89**, 013306-013316 (2014)

Terahertz time-domain spectroscopy of diabetic rat blood plasma

O. P. Cherkasova[1], M.M.Nazarov[2], I. N. Smirnova[3], A.A. Angeluz[4], A. P. Shkurinov[2, 4]

1-Institute of Laser Physics of SB RAS, pr. Lavrentyeva, 13/3, Novosibirsk, 630090 Russia

2-Institute on Laser and Information Technologies of RAS, 1 Svyatooserskaya St., Shatura, 142092

3-Graduate School of Engineering, Nagoya University, Furo-cho, Chikusa-ku, Nagoya, 464-8603, Japan

4-Lomonosov Moscow State University, Leninskie Gory, GSP-1, Moscow, 119991, Russia

e-mail: o.p.cherkasova@gmail.com

Diabetes is among the diseases with great impact on health and society, not only for its high prevalence but also for its chronic complications and high mortality, so the developing of diagnostic methods of this disease has high importance for medicine. For this purpose in the present work we study the spectral features of blood plasma using terahertz time-domain spectroscopy (THz-TDS) in case of healthy rats and rats with alloxan diabetes. Diabetes is characterized by high levels of blood glucose, blood lipid profile changes and elevated corticosteroid hormones [1], so we consider that biochemical disturbances in diabetes can contribute to the absorption and refraction spectra in terahertz frequency range.

The THz-TDS apparatus has been reported previously [2, 3]. The experiments were made both in the transmission geometry and using the attenuated total internal reflection (ATR) scheme with silicon right angle Dowe prism. The practical advantage of ATR scheme is in the large signal amplitude (|R| is close to 1) for absorbing media such as blood plasma or water. ATR scheme is very convinuent for solvents study. To measure the transmission spectra of blood plasma the Bruker cell with polystyrene windows separated by a 200 μm Teflon spacer was used. Both transmission (Fig.1) and ATR measurements detected difference of diabetic rats blood THz response.

We found that the amplitude of the blood plasma absorption and refraction spectra of the rats with diabetes reliably differs from those of the healthy rats and depends on diabetes severity. This difference of the spectra is most noticeable in the range 0.2-1.6 THz. This fact can be explained by the higher level of blood glucose, corticosterone and other components in the blood plasma of rats with severity (group 3) compare to the mild diabetes (group 2) and healthy species (group 1) (fig. 1).

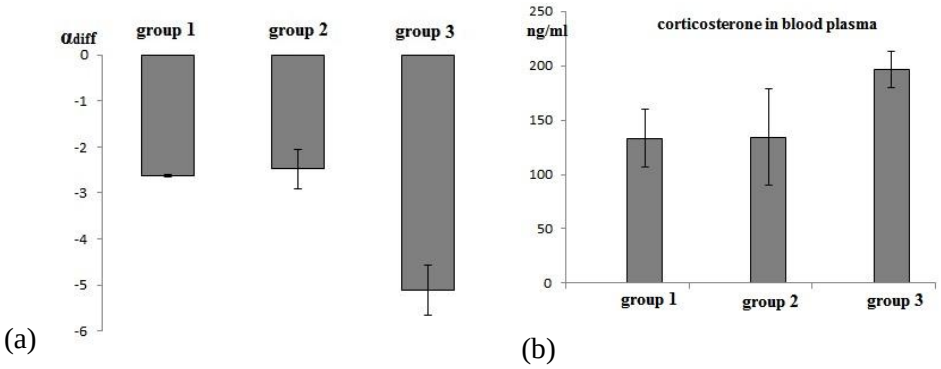

Figure 1. The differential absorption (α_{diff}) of rat blood plasma at 1.0 THz (a); corticosterone in rat blood plasma (b); group 1 – healthy rats, group 2 – rat with mild alloxan diabetes, group 3 – rats with heavy alloxan diabetes.

This work has been supported by RFBR (grant № 13-02-01364).

[1] O. P. Cherkasova, V. G. Selyatitskaya, "Adrenocortical and Renin-Angiotensin Systems in Dynamics of Experimental Diabetes", Biochemistry (Moscow) Supplement Series B: Biomedical Chemistry, vol. 7, № 1, pp. 90-94 (2013).

[2] I. N. Smirnova, D. A. Sapozhnikov, A. V. Kargovsky, V. A. Volodin, O. P. Cherkasova, R. Bocquet, A. P. Shkurinov, "Lowest-lying vibrational signatures in corticosteroids studied by terahertz time-domain and Raman spectroscopies Vibrational Spectroscopy", vol. 62, pp 238–247 (2012).

[3] M. M. Nazarov, A. P. Shkurinov, E .A. Kuleshov, V. V. Tuchin, "Terahertz time-domain spectroscopy of biological tissues", Quantum Electronics, vol. 38, pp. 647-654 (2008)

Thursday 9th October

The Role of Photonics in THz Technology

Kyung Hyun Park, Namje Kim, Kiwon Moon, Eui Su Lee, Il-Min Lee, Hyunsung Ko, Jeong-Woo Park, and Sang-Pil Han

THz Photonics Creative Research Center, ETRI Daejeon, 305-700, KOREA

khp@etri.re.kr

Terahertz (THz) systems have attracted great interest in their possibilities in a wide range of industrial applications such as wireless communications, spectroscopy, and sensing. Consequently, compact and low cost THz module gets more important to the wide fields of application. To realize a compact THz emitter module, high power semiconductor beating sources and antenna integrated photomixer can be desirably considered. Laser Diodes (LDs) emitting two lasing modes simultaneously are preferable because of their compactness, low power consumption, and narrow linewidth. By using semiconductor lasers, the system cost can be dramatically reduced. We developed micro-heater integrated single cavity dual-mode lasers (DMLs). The DMLs consist of two distributed feedback laser diodes (DFB LDs) of different emission wavelengths, sharing one optical cavity in common. This single-cavity design ensures co-polarized and collinear dual-mode emission, significantly simplifies the optical alignment, and reduces the number of required components. According to our research roadmap to realize one-chip THz emitter and detector, we developed several different types of photonic devices [1, 2]. Some of the selected between our own developed semiconductor beating lasers are shown in Fig.1.

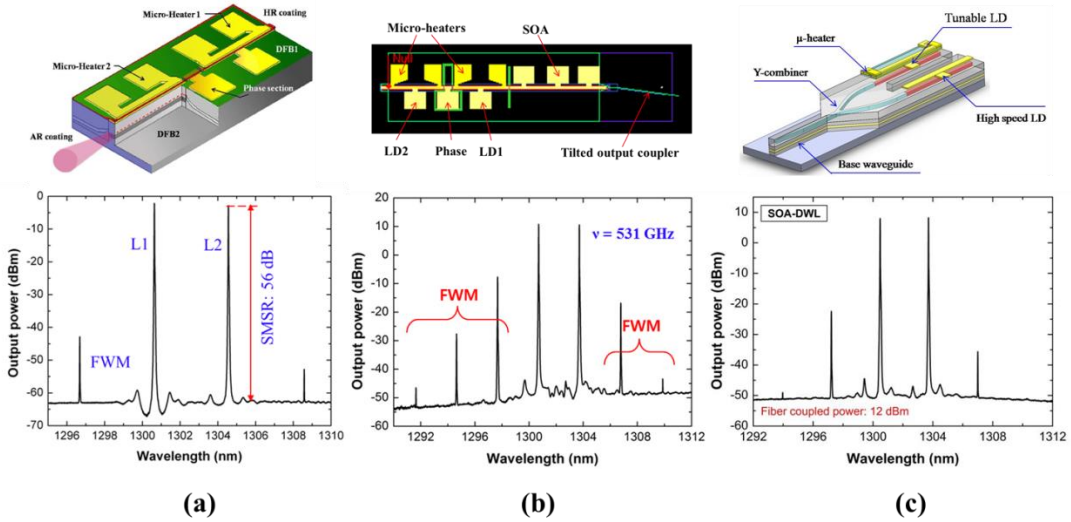

Fig.1. Semiconductor beating sources and its lasing spectrum. (a) 1.3 μm lasing wavelength dual-mode laser. (b) semiconductor optical amplifier (SOA) integrated DML. (c) spot-size converter integrated dual-wavelength laser.

We also proposed several different types of photomixers including the evanescently coupled waveguide photodiodes (ECPDs). Both of the molecular beam epitaxy (MBE) and the metalorganic chemical vapor deposition (MOCVD) system are utilized for the growth of photomixer materials. Experimental results are already published in elsewhere [3,4]. In this talk, our recent studies in the field of CW THz systems based on photonics technologies including beating sources, THz generating and detecting devices and of which applications such as THz imaging and thickness measurements will be briefly reviewed.

[1] N. Kim, H.-C. Ryu, D. Lee, S.-P. Han, H. Ko, K. Moon, J.-W. Park, M. Y. Jeon, and K. H. Park, "Monolithically integrated optical beat sources toward a single-chip broadband terahertz emitter," Laser Phys. Lett. 10., 085805 (2013).
[2] H.-C. Ryu, N. Kim, S.-P. Han, H. Ko, J.-W. Park, K. Moon, and K. H. Park, "Simple and cost-effective thickness measurement terahertz system based on a compact 1.55 μm λ/4 phase-shifted dual-mode laser," Opt. Express 20(23), 25990 (2012).
[3] S.-P. Han et al., "InGaAs Schottky barrier diode array detector for a real-time compact terahertz line scanner", Optics Express, 21(22), 255874(2013).
[4] K. Moon et al.,,"Low-temperature-grown InGaAs terahertz photomixer embedded in InP thermal spreading layer regrown by metalorganic chemical vapor deposition", Optics Lett., 38(24), 5466(2013).

Shaped light for imaging and manipulation

J. Nylk*[1,2], T. Vettenburg[1], Z. Yang[1], H.I.C. Dalgarno[1], C. Coll-Lladó[2], D.E.K. Ferrier[2], T. Čižmár[3], F. J. Gunn-Moore[2], K. Dholakia[1]

1- SUPA, School of Physics and Astronomy, University of St. Andrews,

North Haugh, St. Andrews, UK

2- School of Biology, University of St. Andrews, North Haugh, St. Andrews, UK

3- School of Medicine, University of St. Andrews, North Haugh, St. Andrews, UK

** jn78@st-andrews.ac.uk*

High resolution imaging of large biological specimens in a rapid and biologically friendly manner is a significant challenge in microscopy. Light sheet microscopy has revolutionised developmental biology and similar disciplines because it confronts this challenge and rapid, high contrast, volumetric imaging with minimal sample exposure is facilitated by planar illumination which is orthogonal to the fluorescence detection lens [1].

A fundamental limitation of light sheet microscopy with Gaussian beam illumination is the rapid divergence of the beam which prevents a uniformly thin light sheet, thus impeding high resolution imaging over a large volume. The use of Bessel beams for light sheet illumination has grown in popularity due to the propagation invariance of the Bessel beam [2], but its use must be combined with additional techniques such as multi-photon excitation, confocal scanning, or structured illumination (see for example [3]) to recover high contrast images.

I will present our recent work on the use of an Airy beam for light sheet illumination which gives isotropic high resolution imaging over a ten-fold greater field of view compared to a Gaussian light sheet. I will show that the intrinsic properties of the Airy beam make it ideally suited for light sheet imaging, and as such, can be readily implemented in the single-photon excitation regime requiring only a one-dimensional deconvolution to yield images of high contrast and high resolution [4].

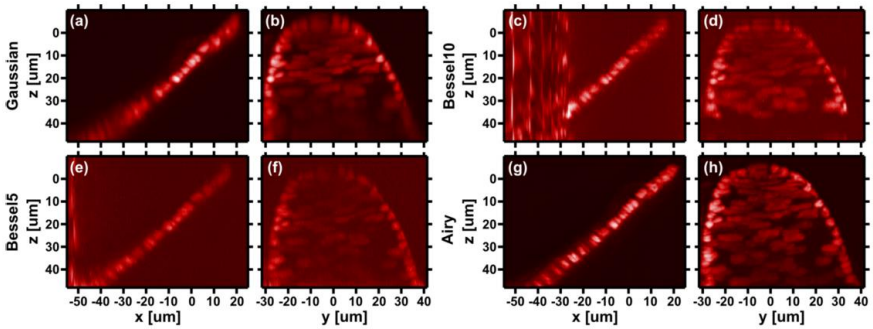

Figure 1. Comparison of image quality between various light sheet types imaging a volume at the dorsal end of the notochord in a fixed amphioxus. Nuclei are fluorescently labelled with propidium iodide. y-axis and x-axis projections, respectively for the case of (a,b) Gaussian, (c,d) Bessel10, (e,f) Bessel5, and (g,h) Airy beam illumination. Bessel10 denotes a Bessel beam with a propagation invariance of ±21μm from focus of a Gaussian beam, Bessel5 denotes a Bessel beam with propagation invariance of ±42μm.

Further developments will also be discussed, including an investigation into other, simpler optical approaches to generate an Airy beam, and the integration of optical tweezers into the light sheet microscope. This will allow precise control and manipulation for imaging specimens as well as novel approaches to tomographic imaging.

[1] Huisken, J. and Stainer, D.Y.R., Selective plane illumination techniques in developmental biology, Development, 136, 1963-1975, (2009).

[2] Fahrbach, F.O. and Rohrbach A.., A line scanned light-sheet microscope with phase-shaped self-reconstructing beams, Optics Express, 18, 24229-24244, (2010).

[3] Planchon, T.A., Gao, L., Milkie, D.E., Davidson, M.W., Galbraith, J.A., Betzig, E., Rapid three-dimensional isotropic imaging of living cells using Bessel beam plane illumination, Nature Methods 8, 417-423 (2011)

[4] Vettenburg, T., Dalgarno, H.I.C., Nylk, J., Coll-Lladó, C., Ferrier, D.E.K., Čižmár, T., Gunn-Moore, F.J., Dholakia, K., Light-sheet microscopy using an Airy beam, Nature Methods, 11, 541-544 (2014).

Non-invasive methods of imaging the human microcirculation

Martin. J. Leahy

[1]Tissue Optics & Microcirculation Imaging Facility, National University of Ireland, Galway, Ireland and National Biophotonics & Imaging Platform, Ireland.

Improper functioning of the microcirculation is a characteristic of many diseases such as diabetes mellitus, heart disease, peripheral vascular disease and arteriosclerosis. Hence the assessment of both the structural and dynamic properties of the capillaries in the upper dermis and the vessels which supply them are of vital importance.

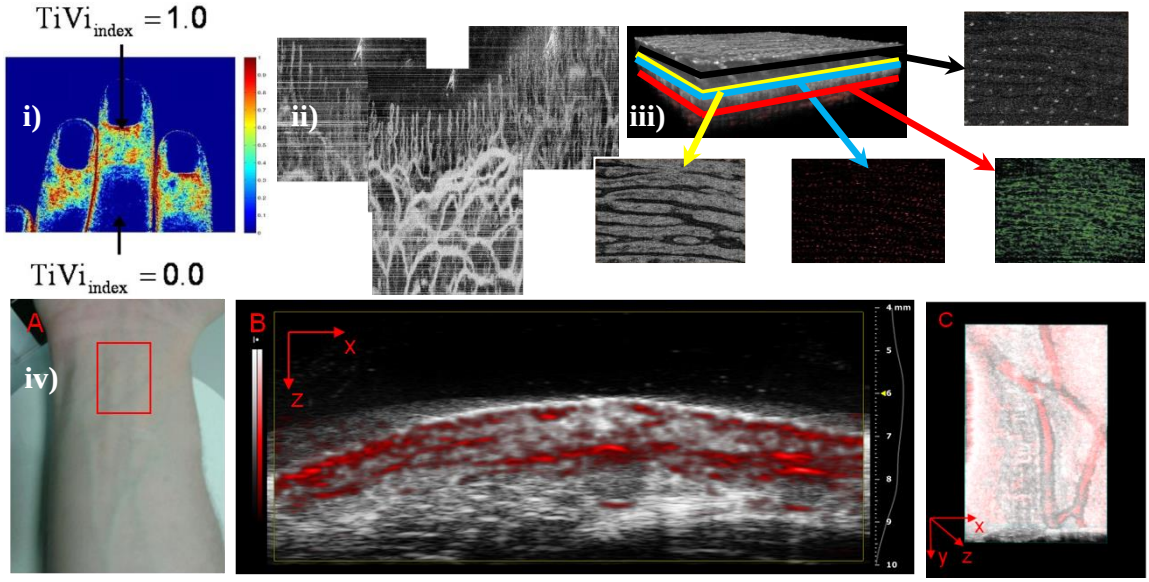

Figure 1. Imaging the microcirculation i) TiVi, ii) cmOCT of the nailfold plexus, iii) 3D cmOCT on the fingertip with structure and iv) 3D photoacoustic and ultrasound imaging of the volar aspect of human wrist.

We have developed 2D devices based on polarisation spectroscopy which output colour-coded maps which are sensitive to the concentration of red blood cells in the skin tissue. The hardware design consists of two orthogonally placed polarisation filters over the light source and sensor of a standard digital camera and utilises the video mode to provide an acquisition frequency of 15/30 Hz at a resolution of ~ 200 μm. We have also developed correlation mapping optical coherence tomography (cmOCT) to render the 3D microcirculation. To obtain microvascular maps without motion artefact, we used the full-field technique developed by Boccara and others and applied the cmOCT algorithm to the data. Since the depth is limited to one or two mm with OCT and much less with full-field OCT, we have recently begun to work with photoacoustic tomography. We believe that a reflection type probe, similar to existing clinical ultrasound, is most likely to

succeed in real clinical applications. Its advantages include ease of use, speed and familiarity for radiographers and clinicians.

References:

1. McNamara, P., O'Doherty, J., O'Connell, M.L., Henricson, J., Fitzgerald, B.W., Anderson, C., Nilsson, G.E., Toll, R. and Leahy, M.J., 2010. Tissue Viability (TiVi) Imaging: Temporal effects of local occlusion studies in the volar forearm. *J. Biophotonics*, **3**(1-2), 66-74. http://dx.doi.org/10.1002/jbio.200910061
2. Enfield, J., Jonathan, E. and Leahy, M.J., 2011. *In vivo* imaging of the microcirculation of the volar forearm using correlation mapping optical coherence tomography (OCT). *Biomedical Optics Express* **2** (5) 1184-1193.
3. Zam, A., Dsouza, R., Subhash, H.M., O'Connell, M., Enfield, J., Larin, K., Leahy, M.J. , 2013. Feasibility of correlation mapping optical coherence tomography (cmOCT) for anti-spoof sub-surface fingerprinting. *J. Biophoton.* **6** (9) , 663-667. http://dx.doi.org/10.1002/jbio.201200231.
4. McNamara, P.M., Subhash, H.M. and Leahy, 2013. In vivo full-field en face correlation mapping optical coherence tomography *J. Biomed. Opt.* **18** (12), 126008. http://dx.doi.org/10.1117/1.JBO.18.12.126008.

Tissue imaging and therapeutic effects at laser-induced nanoparticle luminescence, heating, and ROS-generation

V. Tuchin[1,2,3]

1 - Saratov State University named by N.G. Chernyshevsky, 83 Astrakhanskaya Street, Saratov 410012, Russia

2 - Institute of Precise Mechanics and Control, Russian Academy of Sciences, 24 Rabochaya Street, Saratov 410028, Russia

3 - University of Oulu, P.O. Box 4500, Oulu FI-90014, Finland

Main author email address: tuchinvv@mail.ru

Nanoparticle-mediated laser diagnostic and therapeutic technology of cancer and inflammatory diseases is of great interest as a novel modality realizing principles of *Theranostics* (therapy/diagnostics). The major principles of the technology were formulated in the special issue of *Journal of Biomedical Optics* in 2009 [1] and recent achievements were summarized in review paper [2]. To enhance cancer and inflammatory diseases by photothermal/PDT/photocatalytic treatment and to provide tissue and cell optoporation we are using different types of nanoparticles designed in many groups, including gold nanoparticles (GNPs) – bulk spheres (GNSps), nanoshells (GNShs), nanorods (GNRs), nanocages (GNCs), and nanostars (GNSts) (IBPPM RAS; IFAC, Italy; Aix-Marseille University, France; Duke University, USA), gold/carbon nanotubes (GNTs) (Univ. of Arkansas Med. Sci.), magnetic nanoparticles (MNPs) (Univ. of Arkansas Med. Sci., University of Oulu, and SSU), photocatalytic TiO_2 nanoparticles, nanowires, and nanopartical enriched gypsum (University of Oulu, Finland), nanocomposites – nanoparticle/photodynamic dye conjugates (IBPPM RAS), and upconversion luminescence nanoparticles (University of Oulu).

Photocatalytic, plasmonic, and upcoversion properties of nanoparticles will be considered in the framework of laser heating conditions [3]. Methods of laser-induced transcutaneous administration of nanoparticles for direct delivery to the region of interest, i.e. pathologically modified areas of the tissue will be presented and discussed. It will be demonstrated that antibacterial effect of titania-nanoparticle-gypsum-composites depends on several factors such as photocatalytic activity (ROS generation) of decorated and doped titania-nanofibers and increased light fluence caused by gypsum scattering. We will show that the enhancement of tissue permeability using laser multi-beam optoporation is a promising technique for accelerating delivery of nanoparticles to their target areas in the skin and other tissues. There will be also demonstrated that gold nanocomposite design is a promising platform for optical imaging and treatment at cell and tissue level, usage of upconversion nanoluminophores is an attractive tool for deep-tissue imaging, and nanosized extracellular vesicles generated by adipocytes at laser heating and photodynamic action is a new field for theranostics.

[1] V.V. Tuchin, R. Drezek, S. Nie, and V.P. Zharov (Guest Editors) Nanophotonics for Diagnostics, Protection and Treatment of Cancer and Inflammatory Diseases, *J. Biomed. Opt.* **14** (2) (2009).

[2] N.G. Khlebtsov, et al. Analytical and theranostic applications of gold nanoparticles and multifunctional nanocomposites, *Theranostics* **3**, 167-180 (2013).

[3] Yu.A Avetisyan, A.N. Yakunin, V.V. Tuchin, Novel thermal effect at nanoshell heating by pulsed laser irradiation: hoop-shaped hot zone, *J. Biophotonics* **5**, 734-744 (2012).

Detection of metabolic tumor status, using genetically encoded sensors and optical imaging

E.V. Zagaynova [1,2], M.V. Shirmanova [1], I.N. Druzhkova [1], M.M. Kuznetsova [1,2], L.B. Snopova [1], N.N. Prodanetz [1], V.V. Belousov [1,3], S.A. Lukyanov [1,3]

[1] *Nizhny Novgorod State Medical Academy, Russia*

[2] *Lobachevsky State University of Nizhny Novgorod, Russia*

[3] *Shemyakin–Ovchinnikov Institute of Bioorganic Chemistry RAS, Moscow, Russia*

ezagaynova@gmail.com

Introduction. The problem of all traditional chemotherapeutic drugs is the lack of specificity: they affect not only tumor cells, but the normal ones, first and foremost, the tissues with rapid proliferation. That is why a special attention should be paid to the search of medication with other mechanisms of action aimed at damaging the viability of a tumor cells. For example, fundamental differences of energy metabolism of a tumor cell from a normal one can be the base for the development of medications of a new generation aimed at the inhibition of glycolysis, damage of a structure or functions of mitochondria, system of pH regulation. It is supposed that the increased level of glycolysis in tumor cells is a relevant symptom of a malignant phenotype and a sign of invasiveness, and therefore it can be a prediction criterion of tumor development and its response to treatment [1]. In the result of the increased glycolytic activity in tumors there is formed a reverse gradient of pH. Intracellular pH of tumor cells is more alkaline compared to normal cells of the organism (7.12-7.65 at the norm: 6.99-7.2), and extracellular pH of a tumor is more acidic (6.2-6.9 at the norm: 7.3-7.4) [2]. The intracellular pH plays the main role in regulation of activity of glycolic enzymes and formation of the effect of multi-drug resistance. From the other hand, Co-factors of electron-transport chain – NADH and FAD are a relevant parameter of energy metabolism of a cell [3]. The intensive glycolysis (aerobic and anaerobic) typical of tumor cells causes changes in relative concentration of metabolic co-enzymes FAD and NADH. Due to the change of metabolism in tumor cells spatial distribution of FAD and NADH is also changed because other enzymes binding them are also involved [4]. **Materials and methods**. *Analysis of intracellular pH value in cancer cells with ratiometric genetically encoded sensor.* To analyze intracellular pH there were used cancer cell lines stably expressing a genetically encoded sensor of cytozolic localization. The sensor has two excitation peaks of fluorescence (at about 420 and 500 nm) which allows ratiometrically calculate pH value. In alkaline medium there is a proportional decrease of the peak at 420 nm and an increase of the peak at 500 nm. The advantage of ratiometric sensors is that the ratio does not depend on the amount of the expressed protein, artifacts of cell motion and shape change. Ratiometric assessment of a sensor signal was performed by fluorescence microscopy and macroimaging. There were developed methods of assessment of intracellular pH level in tumor cells and animal's tumors with a genetically encoded ratiometric sensor. *Analysis of endogenous metabolic co-factors NADH and FAD in tumor cells based on fluorescence intensity and lifetime estimation*. There were studied the change of fluorescence intensity and fluorescence lifetime of metabolic co-factors NADH and FAD in tumor cells. To achieve this there were developed the methods of visualization of metabolic co-factors of the respiratory chain in cancer cells *in vitro* and tumor tissue of animals by the method of two-photon fluorescence microscopy with temporal resolution. **Results**. In the in vitro system have been shown, that in more alkaline conditions excitation maxima of genetically encoded sensor at 420 nm decreased and at 500 nm increased, resulting in increase of the I_{500}/I_{420} ratio. The cells were injected subcutaneously to nude mice to generate tumors, and whole-body fluorescence imaging was performed *in vivo* to visualize the indicator emission at 520 nm. Calculation of the I_{500}/I_{430} ratio showed that the signal of the sensor in HeLa tumor is highly heterogeneous, which indicates differences in pHi value in a tumor tissue. The data of the fluorescence imaging were confirmed by histopathological investigation and hypoxia analysis on the tumor tissue sections. The differences in the fluorescence intensity and fluorescence lifetime of metabolic co-factors NADH and FAD in tumor and normal cells *in vitro* have been shown. Also the specific features of NADH and FAD concentration have been found during tumor progression in living mice.

1. C.V. Dang, Links between metabolism and cancer // Genes Dev. 2012 26: 877-890.

2. L.E. Gerweck, K.Seetharaman. Cellular pH Gradient in Tumor versus Normal Tissue: Potential Exploitation for the Treatment of Cancer. Cancer research. 1996. 56. 1194-1198.

3. A.A. Heikal, Intracellular coenzymes as natural biomarkers for metabolic activities and mitochondrial anomalies. Biomark Med. 2010 April ; 4(2): 241-263.

4. M.C. Skala, K.M. Riching, A.Gendron-Fitzpatrick, J. Eickhoff, K.W. Eliceiri, J. G. White, and N. Ramanujam, In vivo multiphoton microscopy of NADH and FAD redox states, fluorescence lifetimes, and cellular morphology in precancerous epithelia. PNAS, 104(49), 19494-19499, 2007

Dual Imaging System for Intraoperative Assessment of Positive Tumor Margins

C. Matei[1, 2], M. Patachia[1], S. Miclos[3], S. Dontu[3], D. Savastru[3], C. Achim[1, 2], A.M. Bratu[1], M. Petrus[1], S. Banita[1], M.A. Calin[3] and D.C. Dumitras[1]

1- Laser Department, National Institute for Laser, Plasma and Radiation Physics, 409 Atomistilor Street, PO Box MG-36, 077125 Magurele - Bucharest, Romania
2- University POLITEHNICA of Bucharest, 313 Splaiul Independentei, 060042 Bucuresti, Romania
3- National Institute for Research and Development in Optoelectronics, 409 Atomistilor Street, PO Box MG-5, 077125 Magurele - Bucharest, Romania

consuela.matei@inflpr.ro

Cancer is one of the high impact disease affecting the society health in terms of quality of life and incapacitation of active population. The high rate of social expenses related to the treatment of malignant diseases could be decreased by a sustained development of the fundamental research on both directions of prophylactic screening for early detection of tumoral formations and improvement of the treatment techniques.

In case of surgery, the most important aspect consists in the total resection of the tumor, but unfortunately, today, the margins of tumor infiltration could be assessed only by the post-surgical pathological examination. The studies proved that patients with a positive margin have a higher reccurence rate and a poorer survival rate than those with negative margins. This is the reason why, in the last years, the quest for *in-situ* optical detection methods was intensified. These new methods usually combines two optical imaging techniques with complementary characteristics in a single dual system allowing the surgeon to visualize the positive margins through the tissue during even the surgery, thus decreasing the patient risk to develope a primary site recurrence.

In our laboratories, we developed such a hybride experimental setup joining the spectral domain optical coherence tomography (SD-OCT) and the reflectance/fluorescence spectroscopy. Both techniques share the ability to simultaneously measure multiple wavelengths of reflected light across the spectrum, but offer different information about the tissue structure. The system includes a self-developed OCT arm and a commercial available hyperspectral imaging module. The SD-OCT system is equipped with a 1310 nm light source, which has a bandwidth of 80 nm and a maximum power of 20 mW, offering an axial resolution of 7 μm for the biological tissue. The hyperspectral imaging module is working in the spectral range 400 - 1000 nm, with a nominal spectral resolution of 2.73 nm. The CCD camera has a monochrome 2/3" sensor, being able to acquire 1.5 Mega pixel images at 11 fps.

We shall present the detailed design of our setup, mentioning the specific characteristics together with the software requirements, and reveal some preliminary results for *in-vitro* detection of tissue samples, at different wavelengths. Comments on the required setup improvements imposed by a future implementation in the clinical trial will be also made.

Loshchenov M.V.[1], Borodkin A.V. [1], Grachev P.V. [1], Savelieva T.A. [1], Linkov K.G. [1], Zelenkov P.V. [2], Gol'bin D.A. [2], Potapov A.A. [2], Filonenko E.V. [3], Loschenov V.B. [1]

1 Prokhorov Institute of General Physics, Moscow, Russia

2. Burdenko Institute of Neurosurgery, Moscow, Russia

3. Herzen Institute of Oncology, Moscow, Russia

Clinical experience in fluorescence diagnostics and photodynamic therapy control using laser imaging and laser spectroscopy technologies on photosensitized bio-tissues

We present a summary of clinical trials of the novel fluorescence imaging system carried out in two specialized Moscow clinics. The new fluorescence imaging system comprises of a powerful fluorescence excitation laser, dual-channel registration system, specialized LED white light source, and point of interest laser fiber optic spectrophotometer. The excitation wavelength for both imaging system and spectrometer system is 635 nm which allows deeper scanning comparing with other industry-available systems which use 400 nm excitation wavelength. The imaging system functions in overlay mode allowing the clinician observing the surface in natural colors mode with addition of color-coded fluorescence layer. Both fluorescence spectroscopy and fluorescence imaging provide possibility to estimate quantitive photosensitizer concentration. In different studies we used different photosensitizers including Fotosens (Aluminum-phthalocyanine), Alasens (5-ALA), Radachlorine (chlorine e6 derivative). The system was used in patients with different tumor types including neural system tumors, reproduction system tumors, skin tumors, and so on.

The results of the clinical experiments proved high sensitivity of the both fluorescence diagnostic systems and. The estimation of photosensitizer accumulation contrast using the imaging system highly correlates with the results of fluorescence spectroscopy carried out simultaneously. The photosensitizer accumulation is best observed with green color coding for open surgery and magenta color for skin tumor diagnostics. Photodynamic therapy control using the fluorescence imaging system allows monitoring of the light doze and provides photobleaching control as a photodynamic therapy efficacy indicator. Imaging system illumination and excitation systems do not interfere with spectroscopy measurements and both fluorescence diagnostic procedures could be carried out simultaneously.

Method of combined optical spectroscopy in neurooncology: theoretical basis and clinical experience

Savelieva T.A.[1], Loschenov V.B.[1], Kholodtsova M.N.[1], Grachev P.V.[1], Goryajnov S.A.[2], Potapov A.A.[2]

[1] *A.M. Prokhorov General Physics Institute of Russian Academy of Sciences, Moscow, Russia*

[2] *N.N. Burdenko Institute of Neurosurgery, Moscow, Russia*

Mail to: savelevat@gmail.com

Background and objectives. Actuality of this work is conditioned by the complexity of the biological media spectroscopic analysis due to their complex absorbers composition, effect of multiple scattering, as well as complex geometry of measurements carried out *in vivo*. In the neurooncology the problem of tumor delineation is particularly acute and requires the development of new methods of intraoperative diagnosis. Optical spectroscopy allows to identify various important diagnostic parameters non-invasively. 5-ALA induced protoporphyrin IX is often used as fluorescent tumor marker in neurooncology. Analysis of the concentration and degree of oxygenation of heme also allows determining the malignization level and it is often used as diagnostic criterion in the preoperative MRI. A significant change of light scattering by tumor tissues causes relevance of analysis of spectroscopic signal component caused by scattering. This paper presents an original method for the simultaneous analysis of diffuse reflectance and fluorescence spectra, allowing at one time to determine all the parameters listed above.

Materials and methods. In this paper stochastic numerical simulation of light propagation in strongly scattering biological media was used to create algorithm that satisfies the conditions of measurement. The developed algorithm for combined spectra analysis was verified using optical phantoms. Clinical studies involving 90 patients with intracranial glial tumors and 19 patients with meningiomas were carried out in the N.N. Burdenko Institute of Neurosurgery. For registration of the spectral dependences spectroscopic system LESA-01-BIOSPEC was used.

Results. The original spectra processing algorithm based on the approximation of numerical simulation of detected signal dependence on the main optical parameters - the absorption coefficient and the scattering coefficient – is developed and verified. Software and hardware is created, which allow to increase the sensitivity of intraoperative demarcation of tumors from 78 to 96% and specificity from 60 to 82% in comparison with the methods currently used in neurosurgical practice.

Live Dynamic Imaging of Developmental Defects in Mouse Models with Optical Coherence Tomography

I.V. Larina
Molecular Physiology & Biophysics,
Baylor College of Medicine,
One Baylor Plaza, Houston, TX 77030, USA

Our research is focused on development of methods for live imaging and dynamic characterization of early embryonic cardiovascular development in animal models of human diseases and using these methods to understand congenital defects in humans through multidisciplinary approaches, which include optical coherence tomography (OCT), vital fluorescent markers, confocal microscopy, live mouse embryo manipulations and static embryo culture, molecular biology, advanced image processing and computational modeling. OCT imaging of live early mouse embryos cultured on the imaging stage allows visualizing developmental events with spatial resolution of a few micrometers (less than a size of individual cells) and a frame rate of up to hundreds of frames per second. These features make OCT a unique tool for mammalian developmental research revealing highly valuable information, which is not accessible with any other imaging approach.

Optical Biopsy for Initial Diagnosis of Cutaneous Tumours – Clinical Applications

E. Borisova[1], E. Pavlova[2], M. Keremedchiev[2], Ts. Genova[1], A. Zhelyazkova[1], L. Angelova[1], P. Troyanova[2], T. Kundurjiev[3], L. Avramov[1]

1- Institute of Electronics, Bulgarian Academy of Sciences, 72, Tsarigradsko chaussee Blvd., 1784 Sofia, Bulgaria
2- University hospital "Queen Jiovanna-ISUL", 8 Bialo more str., 1527 Sofia, Bulgaria
3- Faculty of Public Health, Medical University-Sofia, 8, Bialo more Str., 1527 Sofia, Bulgaria

borisova@ie.bas.bg

This report generalized our four-year efforts on accumulation and development of autofluorescence and diffuse-reflectance spectral database for skin cancer diagnosis and differentiation for clinical practice, formatting optical biopsy method for initial skin cancer detection. We investigated more than 500 clinical cases to receive the spectral properties of basal cell (136 patients) and squamous cell carcinoma (28), malignant melanoma (41) and different cutaneous dysplastic and benign lesions. Excitation at 365, 385 and 405 nm using LEDs sources is applied to obtain autofluorescence spectra, and broad-band illumination in the region of 400-900 nm is used to detect diffuse reflectance spectra of all pathologies investigated. USB4000 microspectrometer (Ocean Optics Inc, USA) is applied as a detector and fiberoptic probe is used for delivery of the light.
In the case of in vivo tumor measurements spectral shape and intensity changes are observed that are specific for a given type of lesion. Autofluorescence origins of the signals coming from skin tissues are mainly due to proteins, such as collagen, elastin, keratin, their cross-links, co-enzymes – NADH and flavins and endogenous porphyrins. Spectral features significant into diffuse spectroscopy diagnosis of different cutaneous tumours are related to the effects of re-absorption of hemoglobin and its forms as well as melanin and its concentration in different pathologies. The spectral features in both spectroscopic modalities used depend from the lesion type and growth stage of the tumor and could be applied for differentiation algorithms and cancer diagnosis. Based on our results, we develop significant database and revealed specific features for a large class of cutaneous neoplasia, using about 30 different spectral peculiarities to differentiate cutaneous tumor and to evaluate the diagnostic accuracy, when optical spectroscopy of skin is applied in clinical environment. Sensitivity and specificity obtained exceed 90%, which make optical biopsy very useful tool for clinical practice.
These results are obtained in the frames of clinical investigations for development of significant "spectral features" database for the most common cutaneous malignant, dysplastic and benign lesions. In the forthcoming plans, our group tries to optimize the existing experimental system for optical biopsy of skin, and to introduce it and the diagnostic algorithms developed into clinical practice of University hospital "Queen Jiovanna-ISUL"- Sofia, based on the high diagnostic accuracy achieved under these investigations.

Acknowledgements: This work is supported by the National Science Fund of Bulgarian Ministry of Education, Youth and Science under grants #DMU-03-46/2011 and #DO-02-112/2008.

Laser modification of pore system in cartilage matrix – a novel approach for cartilage repair

E. Sobol[1], A. Shnirelman[2], O. Baum[1], V. Vinokour[3]

1-Institute on Laser and Information Technologies, Russian Academy of Sciences, Troitsk-Moscow, 142190, Russia
2-Department of Mathematics and Statistics, Concordia University, Montreal, H3G 1M8, Canada
3-Materials Science Division, Argonne National Laboratory, Argonne, Illinois 60439, USA

esobol@rambler.ru

The problem. More than 70% of the peoples in the world suffer from cartilage diseases of joints and spine. Since cartilage is an avascular tissue, the majority of cartilage metabolic processes is controlled with mass transfer of tissue water and solved substances through existing pore system. In degenerative changed cartilage drastic modification of the intercellular matrix structure occurs that results in disorganization of the micro-pore system, and as a sequence to worsened nutrition and cellular death [1]. Laser solution - precise laser control of the stress distribution in cartilage due to formation of pores in these tissues. Pore formation is a known mechanism of stress relaxation in solids [2]. Laser-induced formation of submicron size pores in cartilage matrix is one of the recently established factors promoting regeneration of cartilaginous tissues [1, 3]. Light scattering and optoacoustic techniques are effective for monitoring of pores arising in cartilage in the course of laser irradiation and therefore for creating feed-back control systems for laser technologies in medicine. Since there is an optimal range of the pore sizes [1], the actual task in this field is optimization of laser settings providing safe and effective laser treatment of biological tissues. The aim of the paper is to develop a theoretical model describing dynamics of the pore formation in biopolymers and allows optimizing laser settings. Cartilage is considered here as a nonlinear quasi-elastic medium. The Euler equations and boundary conditions are not considered, because both theoretical study and the numerical solution of the problem are based on the variational formulation [4]. We do no assumptions of the smallness of deformations; moreover, the model reveals the development of strong nonhomogeneity of the cartilage, even if in the initial moment it was nearly homogeneous, and consequently the emergence of strong concentrations of stresses and strains, i.e. large local deformations. So, we can't restrict ourself to any approximation of small deformations, like a linear or weakly nonlinear elasticity, and solve the completely nonlinear problem. We take into account that essential structural and metabolic unit of articular cartilage is a chondron (including a chondrocyte and its pericellular matrix) surrounded by territorial and interterritorial matrices with different chemical composition and mechanical properties [1]. In our model the chondrons formed a periodic (chessboard-like) system in the plane. The temperature field was defined as a spot with the maximal temperature at the center, and the minimal temperature at the periphery [2]. The stresses from the temperature extension were added to the preexisting internal stresses. The problem consisted of the elastic part which reduced to the direct minimization of the elastic energy at each moment, and the thermo destruction part where the rate of the bond destruction depended on the local temperature and strain via the Arrhenius formula [4]. The problem was solved by the finite element method. The following parameters have been varied: laser power and power density, laser pulse duration and pulse repetition rate, temperature gradient, optical and mechanical properties of the tissue, and tissue heterogeneity level. The presented theoretical model describes dynamics of the pore formation and allows optimizing laser settings for cartilage repair.

[1] E. Sobol et al, Lasers for medical applications: Diagnostics, therapy and surgery, Ed. by H.Jelinkova, Woodhead Publishing, Cambridge, UK, Chapter 21 Lasers in orthopedic surgery, 628-658 (2013).
[2] E. Sobol, Phase transformation and ablation in laser-treated solids, Wiley and Sons, N.Y. (1995).
[3] E. Sobol et al, Laser regeneration of cartilage, J. Biomed.Opt., **16** (8), 80 (2011).
[4] A. Shnirelman, et al , A new mechanism for stress relaxation in cartilage under laser heating, Laser physics 14(3), 404-408 (2004).

Depth-Resolved Shear Wave Imaging in Tissues using Optical Coherence Elastography

S. Wang[1], K. Larin[1,2]

1- Department of Physiology and Biophysics, Baylor College of Medicine, One Baylor Plaza, Houston, Texas, USA

2- Department of Biomedical Engineering, University of Houston, 4800 Calhoun Rd, Houston, Texas, USA

klarin@uh.edu

The characteristics of shear (lamb) wave propagation in cornea can be of great importance for the quantitative measurement of corneal viscoelasticity. Here we investigate the use of SWI-OCT to assess the lamb wave dispersion in an *ex vivo* rabbit cornea. Spectral analysis is conducted on the corneal displacement profile obtained from SWI-OCT (Fig 1). The resulted amplitude spectrum is used to estimate the frequency range that is available for the measurement of phase velocity. The distance-dependence of the phase from lamb wave propagation is reconstructed and presented for typical frequency components (Fig 2). Obtained results indicate that the lamb wave dispersion curve agrees well with the analytical approximation (Fig 3) and demonstrate the feasibility of using SWI-OCT to study the dispersion of lamb wave propagation in cornea.

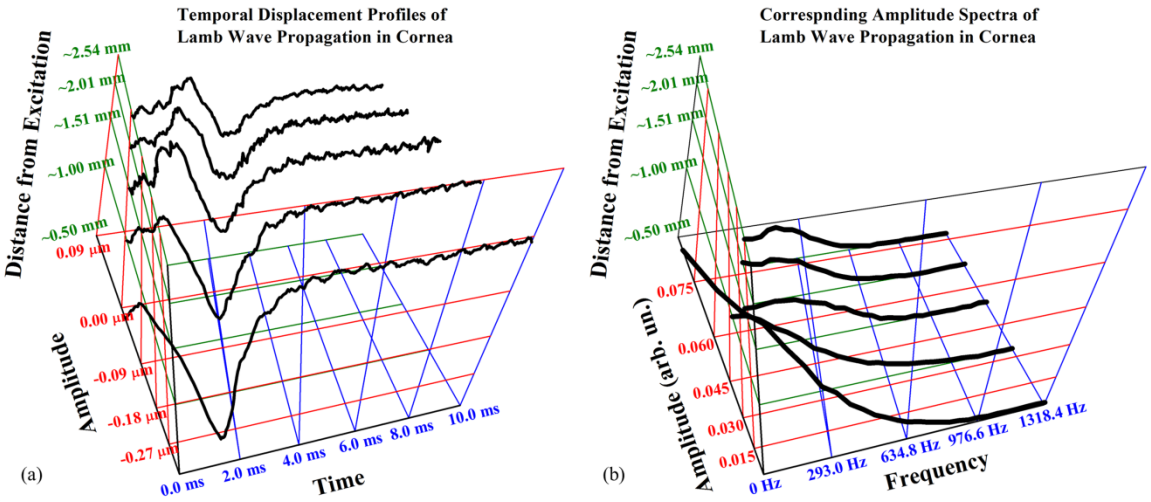

Figure 1: Typical (a) displacement profiles along the lamb wave propagation in cornea and the (b) corresponding amplitude spectra.

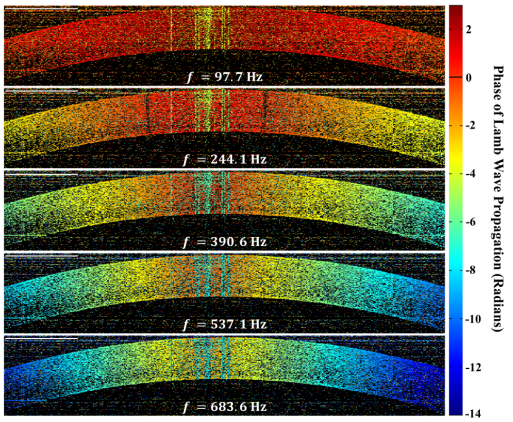

Figure 2: 2-D depth-resolved phase map at five typical frequencies for lamb wave propagation in cornea. The air-puff excitation is at the position around the center.

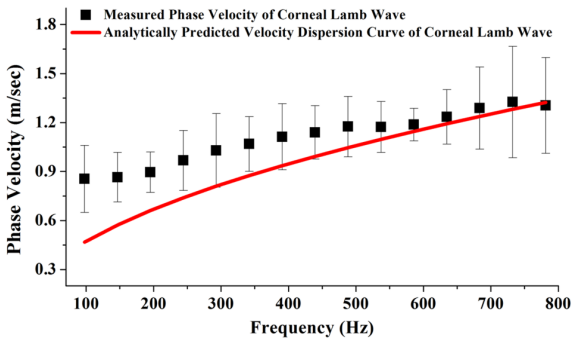

Figure 3: Experimentally measured phase velocity of lamb wave in cornea compared with the analytical approximation of the lamb wave dispersion curve.

Selective photoactivity of porphyrin- polymer complexes against Gram-negative and Gram-positive bacteria

A. B. Solovieva[1], N. A. Aksenova[2], N. N. Glagolev[2], A. B. Shekhter[2]

1- N.N.Semenov Institute of Chemical Physics Russian Academy of Science, Kosygin str., Moscow, 119991, Russia
2-1st I.M.Sechenov Moscow State Medical University, 8 ,Trubeckaya str., 8, cmp. 2 , 119991, Moscow, Russia

ann.solovieva@gmail.com

Growing resistance of microorganisms to antibiotics, increasing the number of superinfections causes need to find new ways to treat inflammatory processes in particular, in otolaryngology, dentistry, surgery for the treatment of purulent wounds, gastroenterology. Valuable alternative to antibiotic therapy may be antimicrobial photodynamic therapy (APDT), rapidly developing in recent years. APDT objects are anaerobic and aerobic Gram + and Gram- bacteria, as well as yeast and filamentous fungi. Photodynamic therapy (PDT) is one of the modern and perspective methods for treatment of wounds. The method is based on the introduction of photosensitizers (PS) in infected cells and tissues, followed by irradiation of the tissues with light of a certain wavelength. The most active and non-toxic PS – porphyrin compounds (PPS). Triplet-excited molecules PPS accumulate in cell membranes and can transfer excitation energy to oxygen molecules, with the formation of singlet oxygen, the active oxidant.

Previously, we found that PPS can form complexes with some amphiphilic polymers (AP) in water solutions. Such complexes are more active than the initial porphyrins in 1.5-2 times in the model photooxidation processes and in 10-30 times by the PD action on tumor cells and tumors in laboratory animals [1]. It was also shown that such complexes were more active than initial porphyrins by PDT of festering wounds [2].

In this study, we would like to use of complexes PPS with amphiphilic polymers for selective APDT. We investigated the PD-action of complexes Photoditazin (PhZ) with Pluronic F127 and Polyvinylpyrrolidone (PVP) on Gram-negative E.coli and Gram-positive S.anzeus bacteria in culture of primary human fibroblasts, which allocated from skin biopsies of healthy patients. Growth medium with a complex PhZ-AP was used as a control. The cells were stained with Ziehl-Nilsson. The number of microorganisms was evaluated in five fields of view (40.x) under the light microscope. It was found that in the presence of complexes PhZ-PVP upon photoexcitation occurs only growth inhibition of Gram-negative organisms.

Interestingly that activity of PVP appears at its low concentrations in a medium (0.05%). If the PVP concentration is increased up to 0,025% the modulating impact of the polymer on phototoxicity Photoditazin dramatically reduced. At the same time, complexes PhZ - Pluronic F127 in PD-exposure have not shown selectivity for E.coli and S.anzeus. In particular, complex of PhZ-PVP ~ 10 times more active than the system PhZ-F127 on E.coli and ~ 15 times than that of pure PhZ.

Thus, selective antimicrobial activity of complexes photodithazine - polyvinylpyrrolidone against Gram-negative bacteria E.coli was found. This opens up the possibility of creating drugs based on complexes of PPS - AP to selectively antimicrobial photodynamic therapy as a new treatment of infectious and inflammatory diseases. The mechanism of our complexes selectivity is still unclear. It is possible that observed in previous experiments high antimicrobial photoactivity of complexes PhZ-AP in the PD-treatment of purulent wounds was achieved by specific binding of hydrophobic groups AP with fragments of cell walls of bacteria.

This work was funded by Russian Foundation of Basic Research, Projects 13-02- 12422, 13-02-00934.

1. A. B. Solovieva, N. N. Glagolev, A. V. Ivanov, etc. Russian patent № 2314806, 2008.
2.A. B. Solovieva, Berlin A.A, Tolstih P.I., etc., Russian patent, 2457873, 2011.

Characterization of fresh water centric diatom frustules (*Stephanodiscus hantzschii sp.*): a type of biogenic photonic crystals

A. Gogoi[1], N. Mazumder[2], P. P. Nath[3], G. A. Ahmed[4] and A. K. Buragohain[5]

1- Department of Physics, Jagannath Barooah College, Jorhat 785001, Assam, India
2- W.M. Keck Center for Cellular Imaging (KCCI), University of Virginia, Charlottesville, VA 22904, USA
3- Department of Physics, Guwahati College, Guwahati-781021, Assam, India
4- Department of Physics, Tezpur University, Tezpur 784028, Assam, India
5- Department of Molecular Biology and Biotechnology, Tezpur University, Tezpur 784028, Assam, India

Main author email address: ankurgogoi@gmail.com

Diatoms are a group of unicellular micro algae with protoplasts enclosed in a nano-porous silica cell wall called frustule that exhibit unique optoelectronic and photonic properties. Importantly, there are over 200000 species of these photosynthetic algae with worldwide distribution [1] and are responsible for 20 – 25% of global oxygen production by photosynthesis process [2]. The diversity of such highly ordered and periodic nanostructures extends possibilities for their use in nanofabrications of a multitude of devices having wide range of potential areas of application, such as in photonics, optoelectronics, microelectronics, biomedical technology, etc [1 – 3].

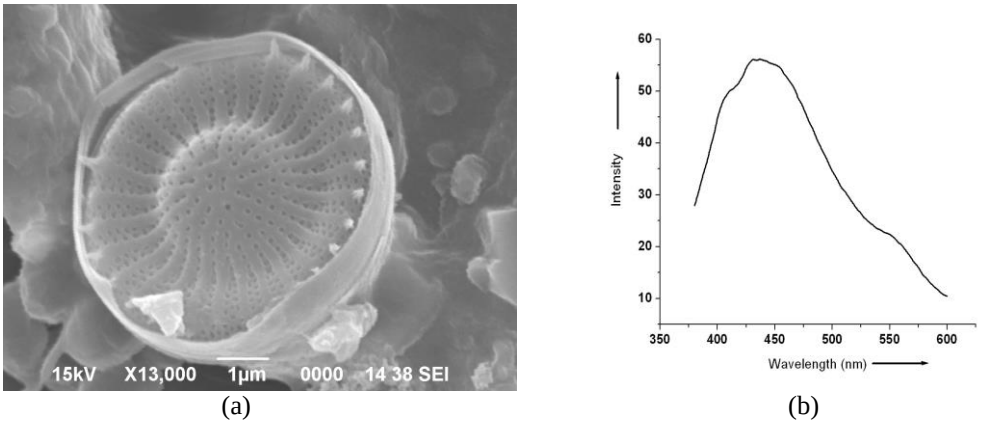

(a) (b)

Figure 1. (a) Scanning Electron Microscopy (SEM) image of centric diatom frustules (*Stephanodiscus hantzschii sp.*). (b) Photoluminescence (PL) spectroscopy of the diatom frustules (excitation wavelength 350 nm).

In this work, fresh water diatoms were grown in the laboratory and the frustules were extracted from these diatoms by treating with aqueous HCl acid. Scanning electron microscopy (SEM) of diatom frustules were studied to identify the different species of fresh water diatoms and to investigate their morphological differences. From energy dispersive X –ray spectroscopy (SEM-EDS) and X-ray diffraction (XRD) analysis it was confirmed that the frustules isolated from diatoms are composed mainly of Si in the form of amorphous SiO_2. A blue photoluminescence (PL) band centered at 435 nm was observed when the frustules were excited at UV wavelengths. The strong blue PL obtained here indicates the diatom to be a potential candidate for efficient luminescent devices. The chemical structural analysis of the porous silicon surface of diatom frustules were carried out by means of Fourier transform infrared (FTIR) spectroscopy which clearly showed characteristic peaks for diatom biosilica, including Si-O-Si stretching vibration at 1060 cm^{-1} and 775 cm^{-1}.

[1] A. Gogoi, A. K. Buragohain, A. Choudhury and G. A. Ahmed, Laboratory measurements of light scattering by tropical fresh water diatoms, J. Quant. Spectrosc. Radiat. Transfer, vol. 110, pp. 1566–1578, (2009).
[2] Katie Bentley, Eileen J. Cox and Peter J. Bentley, Nature's Batik: A Computer Evolution Model of Diatom Valve Morphogenesis, J. of Nanoscience and Technology, vol. 5, pp. 25-34, (2005).
[3] E. De Tommasi *et al*., Optics with diatoms: towards efficient, bioinspired photonic devices at the micro-scale, Proc. SPIE 8792, Optical Methods for Inspection, Characterization, and Imaging of Biomaterials, 87920O (2013).

Self-organization and nanostructuring in SiGe layers induced by pulsed laser annealing

N.A. Sobolev [1,5*)], G.D. Ivlev [2)], P.I. Gaiduk [2,3)], H. Presting[4)]

1) Departamento de Física and I3N, Universidade de Aveiro, 3810-193 Aveiro, Portugal

2) Belarusian State University, Nezavisimosti Ave 4, Minsk 220030, Belarus

3) Department of Physics and Astronomy / Interdisciplinary Nanoscience Center, Aarhus University, The iNANO House, Gustav Wieds Vej 14, DK-8000 Aarhus C, Denmark

4) Daimler Research & Development Ulm, Wilhelm-Runge-Straße 11, 89081 Ulm, Germany

5) National University of Science and Technology "MISiS", 119049 Moscow, Russia

*) Email: sobolev@ua.pt

Due to their enhanced light absorption and improved carrier transport properties, SiGe nanostructures are promising for applications in photovoltaics and high-frequency electronics. A short review of structural transformations and modification of electronic properties induced by pulsed laser annealing in SiGe layers on Si substrates and short period SiGe superlattices is presented in this talk. The samples were treated by 80-ns pulses of a ruby laser in a wide range of energy densities. The induced changes were monitored *in situ* by time-resolved reflectivity and *ex situ* by scanning electron microscopy, Raman scattering and atomic force microscopy. Above a certain energy density threshold, a self-organization phenomenon is observed: a system of quasiregular rectangular grains with linear dimensions of about 100 nm develops on the sample surface. The results are discussed within the framework of fast solid-liquid-solid phase transitions.

Laser Ignition of Engines: Status, Current Problems, Solutions

E. Wintner[1], H. Kofler[1,2], A.K. Agarwal[3]
[1]*Photonics Institute, Vienna University of Technology, Gusshausstrasse 27, 1040 Wien, Austria*
[2]*D. Swarovski KG, Swarovskistrasse 30, 6112 Wattens, Austria*
[3]*Indian Institute of Technology Kanpur, Engine Research Laboratory, Kanpur 208016, India*

ernst.wintner@tuwien.ac.at

Non-resonant laser plasma ignition is the most likely candidate for a successful commercial system of laser ignition. A satisfying technical solution is achieved via a longitudinally diode-pumped passively Q-switched (Cr^{4+}:YAG) Nd^{3+}:YAG laser capable of emitting ~1ns-pulses of at least 20mJ [1,2]. This type of solid-state laser confectioned in an engine-compatible form can be called a laser sparkplug. Early versions of this concept comprised a high-power diode pump laser (quasi-cw power >500 W @ 808nm with ~500µs duration) placed remote from the engine to avoid detrimental influences of temperature, vibrations, pollution etc. In this case only the solid-state laser is exposed to the elevated temperature in the vicinity of the cylinder walls (<100°C).

Recently, mainly cost-oriented considerations, but also technical advances, led to a change of concept from fiber-based remote pumping via edge emitter arrays to the use of newly developed so-called power VCSELs. Thereby the symmetry of pump laser arrays is in the focus of attention: edge emitter arrays usually consist of one row of some 20 emitters (aperture around 1 x 5 µm) with ~50-100 µm periodicity, i.e. a very elongated arrangement of light sources. Collimation to form a round pump beam represents some challenge applying the laws of classical optics. Opposed to that, VCSELs are 2-dimensionally arranged (e.g. [3]). Hence the problem of collimation optics is much more relaxed. Additionally, direct mounting of the pump laser onto the laser sparkplug will improve simplicity and eventually cost, provided operation at elevated temperature due to direct mounting on the cylinder head of an engine can be tolerated.

The change of operation temperature has at least threefold impact on performance: the output power will be reduced; the lifetime of the device will shrink and the emission wavelength will become slightly longer. Mode characteristics might also vary, however this does not follow such a clear pattern. Typical specifications: changing from 20°C to 85°C @ 50A current will result in a drop of the maximum output from ~50W to ~25W, i.e. to one half [3]! The lifetime of VCSELs can lie above 1 Mio. hours (corresponding to >100 yrs) decreasing exponentially, however, with rising temperature [3]. This may lead to <1/10 of this time span for a realistic temperature rise still remaining sufficient.

Under engine-like operation conditions, the laser sparkplug will work at temperatures up to 120°C and hence the question of crystal temperature influence on laser performance had to be investigated [2]. A clear dependence of the Q-switched output pulse energy could be measured in different open and monolithic setups. Consequences of this and other results will be discussed in more detail in the conference and proceedings papers.

[1]. H. Kofler, E. Schwarz, E. Wintner, "Experimental development of a monolithic passively Q-switched diode-pumped Nd:YAG laser", Eur. Physical Journal D **58**, 209-218 (2010).
[2]. H. Kofler, "Development of a laser spark plug and comparative testing", PhD Thesis, Vienna University of Technology, 2009.
[3] Introduction to vertical-cavity surface-emitting diode laser (VCSEL) technology: http://princetonoptronics.com/technology/ /technology.php.

COLOR MARKING BY LASER OXIDATION

V.P. Veiko, G.V. Odintsova, A.A. Slobodov

Saint–Petersburg National Research University
Of Information Technologies, Mechanics & Optics
(veiko@lastech.ifmo.ru)

Heating of metal surface in air, as known, leads to its oxidation. This process becomes controlled due to local laser action, i.e. it is possible to produce a predetermined thickness of interference films [1].

Authors of presented work developed the technology of laser-induced formation of colorful images on metal surfaces [2]. Color is induced by action of fiber Yb-laser IR-radiation. It appears due to interference effects in the oxide films and intrinsic color of oxide. Color formation process was investigated theoretically and experimentally. For instance, the composition of nascent oxide films was revealed, the dependence between processing characteristics and color of a surface in the given local region was found. Selected processing parameters provide visually equilibrium coloration of a material. For the purpose of a unique identification of the received color by the international XYZ system, spectrophotometric and colorimetric study was conducted. On the base of resulting data, color charts were prepared for presented materials. Moreover, in an attempt of introduction into the industry, the software for CLM technology was developed.

This technology can be applied in an instrument making, which includes a medical equipment, in a mechanical engineering, for a marking of collectors' weapons, in an advertising business, in the process of development of decorative and applied arts objects and others (Fig).

Acknowledgements: the work is supported by the Agreement with RSF № 14–12–00351.

References:

1. Arzuov M. I., Barchukov A. I., Bunkin F. V., Kirichenko N. A., Konov V. I., Luk’yanchuk, B. S. Influence of interference effects in oxide films

on the kinetics of laser heating of metals // Quantum Electronic. 1979. Vol. 6. P. 281-284

2. Veiko V. P., Slobodov A. A., Odintsova G. V. Availability of methods of chemical thermodynamics and kinetics for the analysis of chemical transformations on metal surfaces under pulsed laser action // Laser Physics. 2013. Vol. 23. P. 066001.

Nuclear-chemical processes under laser ablation of metals in aqueous mediums

S.F Timashev[1, 2], A.V. Simakin[3], G.A. Shafeev[3]

1- Institute of Laser and Information Technologies, Russ. Academy of Sciences, Troitsk, Russia.
2- National Research Nuclear University MEPhI, Moscow, Russia
3- Wave Research Center of A.M. Prokhorov General Physics Institute, Russ. Academy of Sciences, Moscow, Russia

serget@mail.ru

A brief overview of the results [1-5] to initiate nuclear reactions under laser ablation of metals in aqueous media under the influence of picosecond laser pulses with a peak intensity $J_E \sim (10^{10} - 10^{13})$ W/cm^2, on orders less than is necessary for direct initiation of nuclear processes, $J_E \sim (10^{18} - 10^{19})$ W/cm^2, is presented. It is shown that in these conditions significantly (by orders of magnitude) increase in the rate of decay of radioactive nuclei (on the example of the decay of uranium-238) , initiates the process of nuclear transmutation (for example, the conversion of mercury-196 nuclei in the gold nucleus-197), carried out a nuclear fusion of light elements (for example, tritium nuclei). Under the effect of such pulses the liquid at the liquid-metal interface was vaporized, so that a low-temperature plasma was formed in the resultant vapor-filled spaces. As demonstrated in this paper, the cause of the nuclear transformations observed in the above-mentioned works (see also [6, 7]) could be the inelastic weak interaction of electrons with the nuclei (with the birth of the neutrino – antineutrino pair), if the high (for chemical scale) kinetic energy E_e of the electrons in the plasma being formed reached ~ 5-10 eV. The latter reflected in the definition of these processes as nuclear and chemical. As a result of the first stage of the inelastic week interaction, which is the emission of a neutrino (an irreversible process!), the state of nuclear matter into the nucleus is formed in the unbalanced state of “internal shake-up” (if the nucleus is not radioactive as K-capture one), and it can not provide the basic (standard) way – as a set of a certain number of nucleons. This state is a reactive to a broad class of nuclear transformations.

[1] G. A. Shafeev, F. Bozon-Verduraz, M. Robert. Experimental evidence of transmutation of Hg into Au under laser exposure of Hg nanodrops in D_2O. Physics of Wave Phenomena. vol. 15, no. 3, pp. 131–136 (2007).
2. A.V. Simakin, G.A.Shafeev. Initiation of nuclear reactions under laser irradiation of Au nanoparticles in the aqueous solution of uranium salts. Applied Physics A, vol. 101, no. 1, pp. 199-203 (2010).
[3] G.A. Shafeev, Laser-induced nuclear decays in Uranium isotopes. In: Uranium: Characteristics, Occurrence and Human Exposure. Eds. A.Ya. Vasiliev and M. Sidorov. Nova Sci. Publishers. Chapter 4. pp. 117-153 (2012).
[4] G.A. Shafeev, A.V. Simakin, F. Bozon-Verduraz, M. Robert. Excitation of high energy levels under laser exposure of suspensions of nanoparticles in liquids. Applied Surface Science. vol. 254, pp. 1022-1026 (2007).
[5] E.V. Barmina, P.G. Kuzmin, S.F. Timashev,G.A. Shafeev. Laser-induced synthesis and decay of Tritium under exposure of solid targets in heavy water: http://arxiv.org/abs/1306.0830
[6] S.F. Timashev, A.V. Simakin, G.A. Shafeev. Nuclear-chemical processes under laser ablation of metals in aqueous mediums (“cold synthesis” problems). Russian J. Phys. Chem. A, vol. 88, no. 11 (2014).
[7] S.F. Timashev. Physical vaccum as a system manifesting itself on various scales – from nuclear physics to cosmology: http://arxiv.org/abs/1107.1799v7

Optimization of multispectral synchrotron photoluminescence at sub-microscale to image heterogeneity of historical metals.

Tatiana Séverin-Fabiani[1,2], Mathieu Thoury[2,1] , Luc Robbiola[3], Benoit Mille[4], Matthieu Réfrégiers[2] and Loïc Bertrand[1,2]

[1] IPANEMA, USR3461, CNRS, Ministère de la Culture et de la Communication, BP 48 St Aubin, F-91192 Gif-sur-Yvette cedex, France
[2] SOLEIL synchrotron, BP48 Saint-Aubin, F-91192 Gif-sur-Yvette cedex, France
[3] Laboratoire TRACES – UMR 5608, Université de Toulouse II - Le Mirail, Maison de la Recherche, 5 allées Antonio MACHADO, 31058 Toulouse Cedex 9
[4] C2RMF, UMR171, CNRS, Palais du Louvre - Porte des Lions, 14 Quai François Mitterrand, 75001 Paris, France

Main author email address: tatiana.severin-fabiani@synchrotron-soleil.fr

Novel imaging approaches based on synchrotron UV/visible photoluminescence (PL) allow studying a variety of ancient materials at sub-microscale [1]. Particularly, deep UV enables accessing the complex heterogeneity of PL signatures at high resolution of materials highly absorbent in the UV. PL studies at a macroscopic scale are often inadequate to characterize distinct phases or crystalline forms present at multiple spatial scales [2]. Synchrotron (SR) source, similar to free electron laser (FEL), provides major advantages for analysing such heterogeneous materials. One critical interest of the SR source at the DISCO beamline is the continuous excitation range from the DUV (200 nm / 6.2 eV) to the visible (600 nm / 2.1 eV). Excitation-emission matrix photoluminescence spectra are essential to fully characterize the various compounds present in our systems. To perform such a study, flux optimization in the full range is performing.

Corroded layers in copper-based archaeological artefacts are notoriously challenging to characterize because of their heterogeneous structure at the microscale due in particular to the presence of multiple phases and partial amorphous character [3]. Within this project, synchrotron PL micro-imaging was further optimized to characterize the multiple corrosion phases formed during the long-term alteration processes of copper-based archaeological artefacts. PL signatures were studied at high spatial resolution to get information on the nanoscale structure and PL properties of these complex materials Copper and tin oxides, often encountered in natural patinas, exhibit semiconducting properties, which were exploited for characterisation, respectively in the 3.6 and 2.1 eV energy ranges. In order to tackle both the great variability of corrosion layers dimensions, ranging from tens of micrometers to few millimeters, and their crystalline heterogeneity, we exploited the spatial dynamics determined by the lateral resolution of 150 nm over millimeter-size field of views, available at the DISCO synchrotron beamline. The excitation tunability as well as the emission spectral selectivity allowed to excite and detect PL from the various Sn- and Cu- based alteration products between 200 to 600 nm and from 320 to 1100 nm, respectively. The flux stability of the SR source is a crucial asset to to allow intercomparison of PL signature, with high signal-to-noise ratio, of weakly luminescent materials. . Compared to OPO systems, the flux available at the DISCO beamline (10^{-11} to 10^{-12} ph/s) is low enough to limit beam damages on precious historical samples. Promising first results were obtained on a corpus of copper-based artefacts by coupling the spatial and spectral information collected at sub-microscale.

The correlation between PL spatial and spectral information at high resolution provides new tools to characterize the heterogeneity of corrosion phases. The ability to characterize semiconductor materials heterogeneity at sub-microscale, such as what was recently been achieved for ZnO, TiO_2 and ZnS;$BaSO_4$, opens new ways to study corroded metal artefacts [2].

[1] M. Thoury, J.-P. Echard, M. Refregiers, B. Berrie, A. Nevin, F. Jamme and L. Bertrand. « Synchrotron UV-visible multispectral luminescence micro-imaging of historical samples ». Anal. Chem., **83(5),** pp.1737-1745 (2011).
[2] L. Bertrand, M. Refregiers, B. Berrie, J.-P. Echard and M. Thoury. « A multiscalar photoluminescence approach to discriminate among semiconducting historical zinc white pigments. », Analyst, **138(16),** pp. 4463-4469 (2013).

[3] P. Piccardo, B. Mille, L. Robbiola, « Tin and copper oxides in corroded archaeological bronzes », Corrosion of Metallic Heritage Artefacts, Eds. P. Dillmann, G. Beranger, P. Piccardo and H. Matthiessen, Woodhead Pub., UK, Chap. 14, 2007.

Relativistic optics using engineered plasmas

S. Monchocé[1], S. Kahaly[1], A. Leblanc[1], V. Floquet[1], Ph. Martin[1], F.Quéré[1], T. Ceccotti[1], P. Monot[1], L. Videau[2], P. Combis[2], M. Raynaud[3], A. Macchi[4], O. Klimo[5]

1- Commissariat à l'Energie Atomique /IRAMIS/SPAM, F-91191 Gif-sur-Yvette, France
2- Commissariat à l'Energie Atomique, DAM, DIF 91297 Arpajon Cedex, France
3- Commissariat à 'Energie Atomique /IRAMIS/ LSI, CNRS, EP, 91128 Palaiseau Cedex, France
4- Dipartimento di Fisica ''Enrico Fermi,'' Universita` di Pisa, Largo Bruno Pontecorvo 3, I-56127 Pisa, Italy
5- FNSPE, Czech Technical University in Prague, CR-11519 Prague, Czech Republic

pascal.monot@cea.fr

We will show in this talk how engineered plasma can be used to modify solid target responses to ultra-intensity laser irradiation. This will be illustrated following two distinct processes: ionic acceleration and high order harmonic generation. We will focus on two different types of plasma property adjustments, creating smooth controlled gradient density [1], or generating periodic modulations of the surface thanks to the use of conventional grating or to interference patterns.

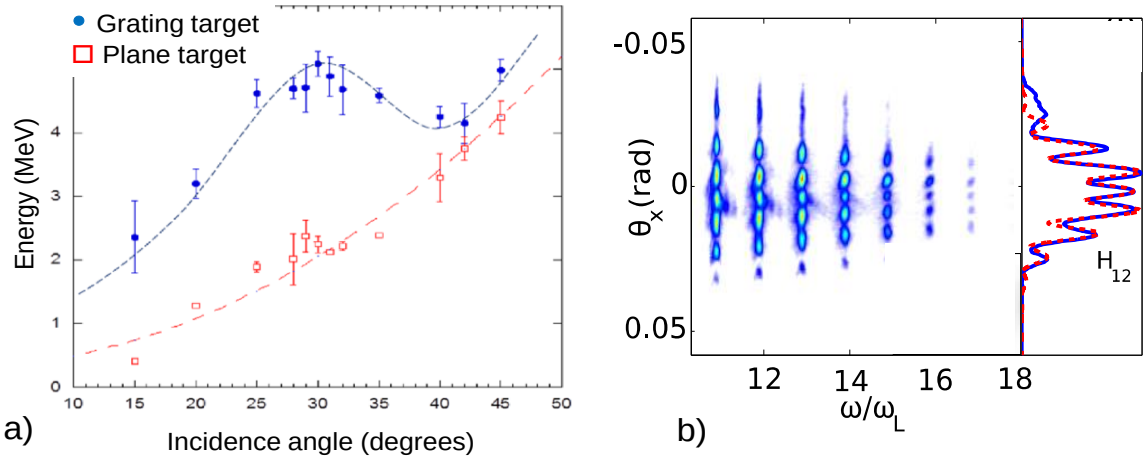

FIG. 1 . a) maximum proton energies as a function of the incident angle with and without grating. b) high order harmonics spatial pattern and corresponding 12th harmonic profile.

As shown on Fig.1 a), enhancement of laser-target coupling has been observed in the relativistic regime of ultrahigh intensity ($I > 10^{19} W/cm^2$) using a manufactured grating. The use of Ultrahigh Contrast pulses ($>10^{12}$) allowed us to demonstrate a maximum increase by a factor of 2.5 of the cutoff energy of protons produced by target normal sheath acceleration with respect to plane targets, around the incidence angle expected for the resonant excitation of surface plasma waves [2].
A more versatile approach for optically-controlled spatial structuring of overdense plasmas generated at the surface of initially plain solid targets were developed using the interference pattern generated from two low intensity pulses. This technic allows for fine adjustments of the density gradient length and spatial step.
We have reported on Fig.1 b) the diffraction profile of High Order Harmonics generated by an UHC & UHI pulse onto the modulated plasma. We will show how these gratings can be used to determine the source size and wavefront properties of the high-order harmonic beams [3].

[1] S. Kahaly et al., Phys. Rev. Lett. 110, 175001 (2013), "Direct Observation of Density-Gradient Effects in Harmonic Generation from Plasma Mirrors"
[2] T. Ceccotti et al., Phys. Rev. Lett. 111, 185001 (2013), "Evidence of Resonant Surface-Wave Excitation in the Relativistic Regime through Measurements of Proton Acceleration from Grating Targets"
[3] S. Monchocé et al., Phys. Rev. Lett. 112, 145008 (2014),"Optically-controlled solid-density transient plasma gratings",

Multiterawatt Hybrid (Solid/Gas) Femtosecond Systems of Visible Range

L. Mikheev[1], V. Losev[2]

[1]*P.N.Lebedev Physics Institute, Leninsky Prospekt 53, 119991, Moscow, Russia,*
[2]*Institute of High Current Electronics, Akademichesky Prospect 2/3, 634055, Tomsk, Russia,*

e-mail: mikheev@sci.lebedev.ru

A novel hybrid concept of multiterawatt femtosecond systems operating in the visible spectral range will be presented along with experimental results demonstrating record peak power in the visible and considerable promise of the approach to designing these systems based on a XeF(C-A)-amplifier optically driven by e-beam-to-VUV-radiation converter (see Figure 1). Potential applications of these systems will also be discussed with main emphasis on the advantage of the visible radiation for the realization of the recombination mechanism of soft X-ray laser excitation in plasma.

Figure1. Photo of the XeF(C-A) amplifier optically driven by e-beam-to-VUV-radiation converter (THL-100 femtosecond system, Tomsk, Russia).

Optimization of the Vulcan 20 PW chirp compensated OPCPA front end

A S Wyatt*, P Oliveira, Y Tang, M Galimberti, I N Ross, I O Musgrave, C Hernandez–Gomez, J Collier

Central Laser Facility, STFC Rutherford Appleton Laboratory, UK

email: adam.wyatt@stfc.ac.uk

In order to reach laser intensities in the multi petawatt to exawatt (10^{15}-10^{18} W) level, ever increasing pulse energies and decreasing pulse durations, coupled with an enhanced contrast ratio, are required. Optical parametric chirped pulse amplification (OPCPA) supports large bandwidths, is tunable, allows for high energy densities, and pulse contrast on the nanosecond scale is enhanced since the spontaneous parametric fluorescence remains within the pump intensity envelope.

The Vulcan 20 PW front end is based on a novel collinear chirp compensated (CP-) OPCPA [1]: broadband chirped pump and signal pulses are mixed in LBO such that at any given time the instantaneous frequency of the signal is phase matched with the instantaneous frequency of the pump, currently resulting in an idler bandwidth spanning over 150 nm (figure 1), limited by the signal stretcher bandwidth. This collinear scheme eliminates angular dispersion in the idler and utilizes the full bandwidth available from Ti:Sapph chirped pulse amplifiers. The idler will be subsequently stretched to nanoseconds and amplified further in LBO and KD*P to reach the 20 PW level. Since the resulting spontaneous parametric fluorescence is also chirped, this can be compressed along with the idler, thus significantly increasing the contrast ratio.

The spectral phase of the idler is determined by the spectral phase of the pump and signal, and as the bandwidth of the idler increases, it becomes increasingly more difficult to fully compensate the high order spectral phase of the generated idler to achieve close to bandwidth limited pulse durations. Additional phase aberrations during the subsequent stretching, amplification and propagation of the idler limits the pulse duration further. Here we demonstrate how spectral shaping of both the pump and signal can lead to bandwidth limited pulses and potentially compensate for chromatic aberration generated further downstream in the amplification chain and provides a degree pulse shaping capabilities.

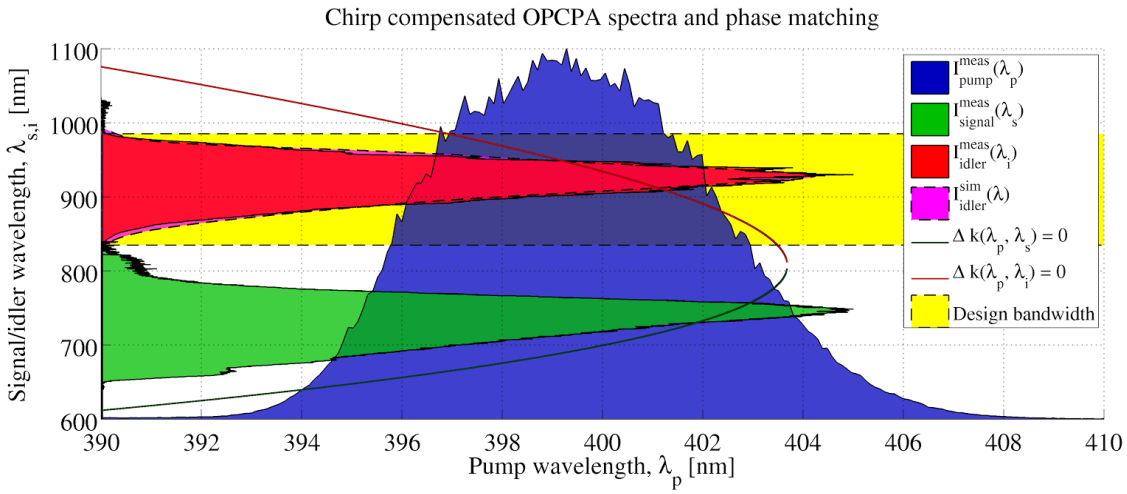

Figure 1 | Phase matching curves and measured pump, signal idler and simulated idler spectra for the Vulcan picosecond CP-OPCPA front end. The design bandwidth is currently 150 nm centred at 910 nm, since this can be amplified further in KD*P, and can support compression down to 15 fs. Further optimization of the system has the potential to reach over 200 nm.

[1] Y. Tang et al, Optical parametric chirped-pulse amplification source suitable for seeding high-energy systems, Optics Letters, Vol. 33, Issue 20, pp. 2386-2388 (2008)

Millijoule, femtosecond, near infrared, ultra-high contrast frontend for a Petawatt-scale diode-pumped solid state laser

Hartmut Liebetrau[1], Marco Hornung[1,2], Andreas Seidel[1], Marco Hellwing[1], Sebastian Keppler[1], Joachim Hein[1,2] and Malte C. Kaluza[1,2]

1- Institute of Optics and Quantum Electronics, Max-Wien-Platz 1, 07743 Jena, Germany
2- Helmholtz Institute Jena, Fröbelstieg 3, 07743 Jena, Germany

Main author email address: Hartmut.Liebetrau@uni-jena.de

We demonstrate the capability of the double CPA-scheme (DCPA) [1] in combination with cross-polarized wave generation (XPW) [2] to generate seed pulses of high quality, regarding temporal contrast and pulse duration, for the Petawatt-class, all-diode pumped solid state laser (DPSSL) POLARIS at the Helmholtz Institute in Jena.
The double-CPA architecture is implemented by adding a picosecond Öffner-type stretcher before the first frontend amplifier, where the pulses are stretched to about 20 ps, allowing the oscillator pulses to be amplified to more than 2 mJ at a center wavelength of 1030 nm. A grating compressor after the amplifier recompresses the pulses to 130 fs, which makes it possible to apply the temporal filtering via XPW in a BaF_2 holographic-cut crystal, in a single crystal setup.
As it can be seen in Figure 1(a) the output energy of the XPW signal exceeds 100 µJ with an internal conversion efficiency of at least 12%. Thus, the second amplifier can be seeded with the same energy as without the DCPA stage, allowing for a direct comparison of the achieved contrast improvement. In Figure 1(b) the green and the black curves show the 3rd order cross-correlation (Sequoia, Amplitude

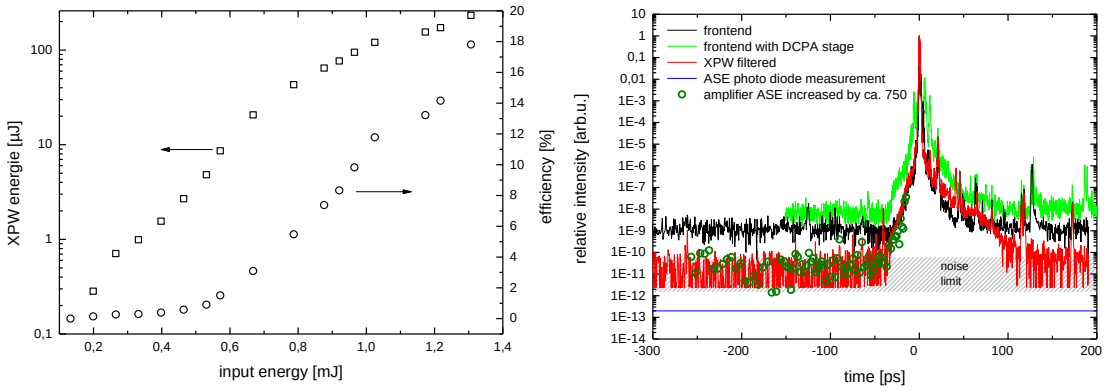

(b)

Figure 1 (a) Output energy and internal conversion efficiency of the XPW signal (b) 3rd order cross-correlation measurements of the frontend pulses with and without XPW filtering.

Technologies) traces of the unfiltered pulses of the frontend with and without the ps-CPA stage, respectively. The red curve shows the temporal intensity contrast (TIC) of the XPW filtered pulses where the ASE contrast dropped below the detection limit of the correlator at 30 ps before the main pulse. Measuring the ASE energy with a calibrated photodiode [3] results in a TIC of $2 \cdot 10^{-13}$ for the ASE level. This is validated by cleaning a pulse with an artificially increased ASE by a factor of 750. As indicated by the dark green circles in Fig. 1(b), the ASE level is still below the detection limit of the Sequoia. Thus with the double CPA stage including the XPW filter, the ASE-contrast was increased by more than 4 orders of magnitude,
To the best of our knowledge, this magnitude of ASE suppression via XPW is shown for the first time for pulses at 1030 nm and the ASE intensity contrast is the best achieved so far for a high-power-DPSS laser system.

[1] M. P. Kalashnikov, E. Risse, H. Schonnagel, and W. Sandner, "Double chirped-pulse-amplification laser: a way to clean pulses temporally," Optics Letters 30, 923–925 (2005)
[2] G. I. Petrov, O. Albert, J. Etchepare, and S. M. Saltiel, "Cross-polarized wave generation by effective cubic nonlinear optical interaction," Optics Letters 26, 355–357 (2001)
[3] S. Keppler, M. Hornung, R. Bödefeld, A. Sävert, H. Liebetrau, J. Hein, and M. C. Kaluza, "Full characterization of the amplified spontaneous emission from a diode-pumped high-power laser system ," Optics Express 22, 11228-11235 (2014)

Quasi-flat-top pulse generation in a powerful Nd:glass laser operating in the saturation regime

A. Kuzmin, E. Khazanov, A. Shaykin, I. Shaykin

Institute of Applied Physics of the Russian Academy of Sciences,
Russia, 603950 Nizhny Novgorod, 46 Ulyanov Street

alexeyhsgap@yandex.ru

Generation of quasi-flat-top pulses is an urgent problem in a number of applications in laser physics. As an example it is worth mentioning high-power Nd:glass lasers which radiation is used after the second harmonic generation for pumping Ti:sapphire or parametric amplifiers of chirped pulses. In the first case the quasi-flat-top pulse shape in contrast to Gaussian one provides the maximal efficiency of the second harmonic generation. In the second case we additionally get an increase in the parametric amplifier efficiency, as well as a reduction of the amplified radiation spectral distortions.

The high efficiency of the laser and the high pulse energy mean that the latter is comparable with the saturation energy of the laser amplifiers. In this regime the output pulse shape significantly differs from that of the input pulse because the leading edge of the pulse propagates through the medium with greater population inversion and is amplified stronger than the trailing edge. The stronger the saturation, the greater the distortion of the pulse, and the more difficult the tailoring the appropriately shaped input pulse. This is particularly urgent in pump lasers of parametric amplifiers, in which the pulse duration is small enough (about 1ns), thus the possibilities of pulse shaping are limited by the operating speed of control electronics. In practice high-power pump lasers for parametric amplifiers usually have a quasi-Gaussian pulse shape [1]. For quasi-Gaussian pulses the shape distortions are usually insignificant, and the saturation mainly leads to the temporal shift of the pulse maximum.

In our paper we propose a method that allows significant reduction of the pulse shape distortions in a laser amplifier that operates in the saturation regime. The idea of the method consists in decomposing the input pulse into two or more replicas, which leads to significant reduction of pulse shape distortions and diminishes the influence of the cubic nonlinearity, preventing small scale self-focusing, which is the major factor limiting the output energy of the laser. This means a possibility to increase the laser output energy without enlarging the amplifiers aperture. Our calculations of the output pulse parameters of the multistage Nd:glass amplifier, used to pump the parametric petawatt laser [1], proof the efficiency of the proposed method. The output aperture of the Nd:glass amplifier is 100mm, the total small-signal gain is 4×10^6, the input pulse energy is 10mJ for the output one is 300J. The model input pulse was chosen to be a 1ns in duration part of the 8.3ns FWHM Gaussian pulse. This part can be cut out by means of a commercially available Pockels cell having switching time of about 0.1ns. We have estimated that for a single input pulse the ratio of intensities at the leading edge and the trailing one should exceed 30. It means that this pulse should be cut out of the initial Gaussian one at the instant $t_c = 45$ns before its maximum. Practically this leads to great losses due to cutting out, and also to a significant difference of the resulting pulse shape from the desired one, because in such large temporal interval t_c the shape of real pulse can strongly differ from Gaussian. However, in the case of two replicas of the input pulse the ratio mentioned above does not exceed 6, and t_c is much smaller. Besides, the shapes of the output pulses are much closer to the desired flat-top one.

The aspects of practical implementation of the proposed method in PEARL-10 laser facility (10PW stage of the project XCELS [2] that is under construction in our institute) will be also discussed during the talk.

[1] V.V. Lozhkarev, G.I. Freidman, V.N. Ginzburg, E.V. Katin, E.A. Khazanov, A.V. Kirsanov, G.A. Luchinin, A.N. Mal'shakov, M.A. Martyanov, O.V. Palashov, A.K. Poteomkin, A.M. Sergeev, A.A. Shaykin, I.V. Yakovlev, Compact 0.56 petawatt laser system based on optical parametric chirped pulse amplification in KD*P crystals, Laser Physics Letters, vol. 4, pp. 421-427 (2007).
[2] www.xcels.iapras.ru

High Bandwidth measurement and control of FM-AM modulation

S. Montant, V. Moreau, J. Luce

CEA – CESTA, 15 avenue des sablières CS60001, 33116 Le Barp Cedex, France

sebastien.montant@cea.fr

Spectral broadening is required on high power lasers chain like the NIF or the LMJ to avoid Stimulated Brillouin Scattering (SBS) in the laser chains and to smooth the focal spot along the pulse duration [1]. Spectral broadening is obtained by sinusoidal temporal phase modulation. However the spectral broadening is non-homogenous. To reach performances required the spectral broadening must be large. But the spectral bandwidth of the laser chain is limited by the third harmonic conversion and by the limited spectral bandwidth of the Nd:glass laser amplifier. Hence the spectral bandwidth reduction induced in the laser chain leads to temporal shape distortion through the so-called FM to AM conversion [2]. As the frequency modulation is at high frequency, the temporal modulation induced by the FM-AM conversion can be at frequency more than 100 GHz.
So temporal diagnostics which characterize the FM to AM conversion need a bandwidth as high as possible. To obtain a precise measurement of the temporal profile of laser pulse, we perform a precise characterisation of spectral response of the temporal diagnostic setup. In the presentation we show this characterisation of the 33 GHz bandwidth temporal diagnostic setup (Figure 1a).

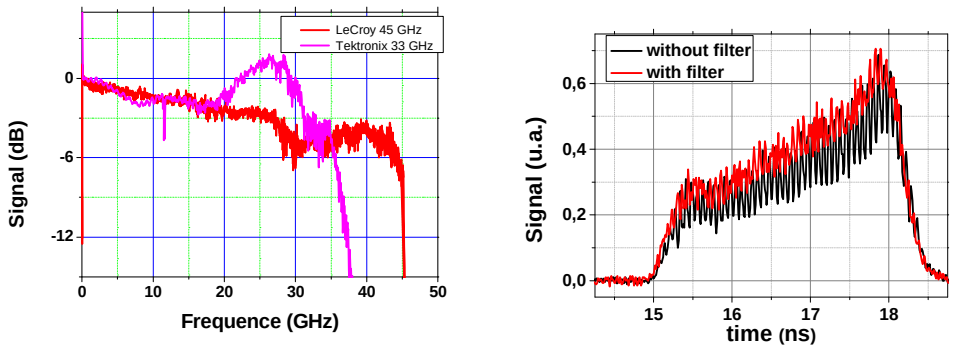

(a) (b)

Figure 1 (a) Spectral response of our 33(purple line) and 45 GHz (red line) bandwidth temporal diagnostics. (b) Distortion of temporal profile induced by FM to AM conversion without (black line) and with spectral filter (red line).

Many effects may generate FM to AM conversion [3]. Hopefully, for the LMJ a significant number of effects are simply due to linear spectral filters and thus they can be compensated thanks to inverse transfer functions. In this talk we will present the different spectral filter used and the performance obtained. These filters have been used on LIL high power chain, the prototype of the LMJ. The amplitude and stability performance of the FM to AM compensation is evaluated (Figure 1b) in amplitude and with a decomposition of harmonic modulation in the electrical spectrum. This evidences new performance constraint on the pre amplifier module

[1] S. H. Glenzer, et al, Sciences **327**, 1228 (2010).
[2] J. E. Rothenberg, D. F. Browning, and R. B. Wilcox, Proc. SPIE **3492**, 51 (1999).
[3] S. Hocquet, D. Penninckx, E. Bordenave, C. Gouédard, and Y. Jaouën, Appl. Opt. **47**, 3338 (2008).

Improved Nonlinear Cross-Polarized Wave Generation in Crystal of 42m Point Group Symmetry

M. Kuzmina, E. Khazanov

Institute of Applied Physics of the RA S, 46 Ulyanov Street, 603950 Nizhny Novgorod, Russia

kmsnn@mail.ru

Cross-polarized wave (XPW) generation, observed in a medium with cubic nonlinearity in which linearly polarized wave is converted to a perpendicular one, is one of promising methods of temporal contrast improvement of femtosecond optical pulses. In this talk we overview some schemes of XPW generation and propose high-efficient XPW generation in DKDP crystal assuming the plane waves model.

A scheme that consists of two plane-parallel plates made of uniaxial crystals was considered. We assumed the model medium with weak linear birefringence and isotropic cubic nonlinearity. This approach means that the phase difference between the ordinary and extraordinary waves on the plate thickness does not exceed $\delta = 0.5\pi$. The third-order nonlinear susceptibility tensor $\chi^{(3)}$ coincides with the one in case of isotropic medium. The relative orientation of the crystals is such that in the absence of effects associated with cubic nonlinearity the output polarization of the laser radiation is linear. Maximum efficiency of the XPW generation η was obtained by varying the inclination angle φ of the electrical field vector **E** with respect to the optical axis of the first crystal, δ and nonlinear phase incursion (B-integral) in each of the crystals; δ is the same in both crystals. Maximum η is equal to 37% when the total for the whole scheme B = 4 (Fig. 1a).

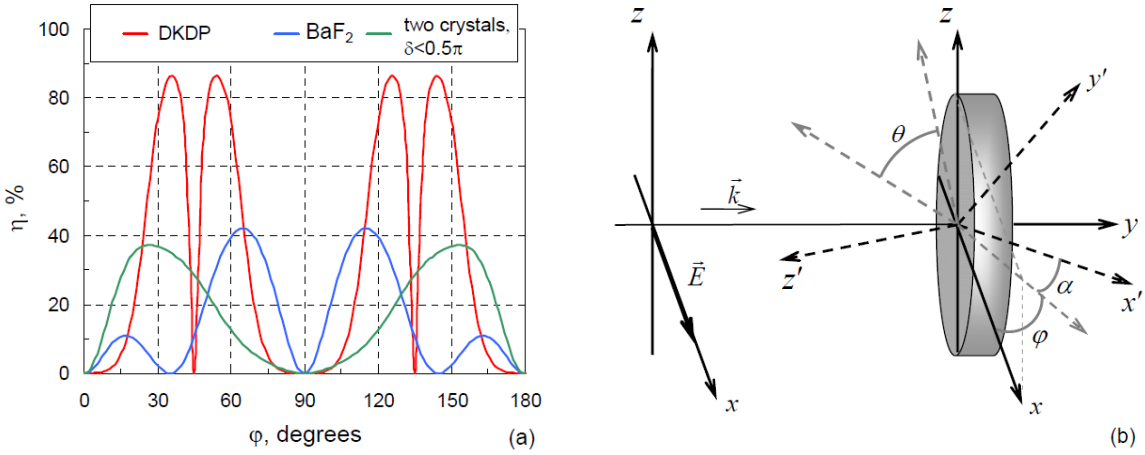

Figure 1. Dependence of XPW generation efficiency η on angle φ in the scheme of two plates made of uniaxial crystals with $\delta < 0.5\pi$ when total B = 4, in schemes with BaF_2 and DKDP crystals for B = 2 (a). Definition of angles (φ, θ, α), (x,y,z) – light propagation basis (b).

Generation efficiency of the XPW in a DKDP crystal of 42m point group symmetry dependence on the orientation of the crystal was studied. Crystal orientation was specified by three angles (φ, θ, α), defining the mutual arrangement of the coordinate system associated with the polarization of the laser radiation and the coordinate system associated with the crystallographic axes of the crystal (Fig. 1b). The XPW generation efficiency was considered with the help of a system of differential equations, describing linear birefringence; nonlinear processes such as self-phase and cross-phase modulation and generation of orthogonally polarized wave; diffraction effects were omitted. The case when the optical axis z' of the crystal is oriented along the axis of radiation propagation ($\theta = 90°$, $\alpha = 0°$) was analyzed. According to Fig. 1a maximum of η equal to 85% can be achieved for certain values of the angle φ when B = 2. The maximum of η in the scheme with the commonly used cubic crystal BaF_2 with optimal orientation [101] is equal to 42% (Fig. 1a). Thus, even the simplest orientation of DKDP crystal provides a more efficient generation of the XPW that can be due to the greater difference in values of the diagonal and nondiagonal components of $\chi^{(3)}$ in DKDP crystal as compared with BaF_2.

Generation and Application of mJ-level Ultrashort Terahertz Pulses

G. Almási[1,2], Z. Tibai[1], L. Pálfalvi[1], J. A. Fülöp[2], J. Hebling[1,2]

1- University of Pécs, Institute of Physics, Pécs, Hungary
2- MTA-PTE High-Field THz Research Group, Pécs, Hungary

hebling@fizika.ttk.pte.hu

The development of intense THz sources in the last decade (see Fig. 1.a) enabled many new applications. THz pulse energy on the 1-μJ, and peak electric field on the 100-kV/cm level opened up nonlinear THz spectroscopy studies a few years ago [1].
Using $LiNbO_3$ (LN) as nonlinear optical material and titled-pulse-front-pumping (TPFP) significant further increase of the THz pulse energy was experimentally demonstrated (see Fig. 1.a), approaching very recently 0.5 mJ [2]. According to numerical calculations, using cryogenic cooling of LN, pump pulses with optimal duration, and contact grating technique [3], generation of THz pulses with 10-mJ-level energy and 10 to 100 MV/cm peak electric field will be possible in the next years [4].
These unprecedented THz pulses will open the door for important new applications such as improving attosecond pulse generation [5], manipulation of relativistic electron bunches including acceleration, longitudinal compression, and undulation [6,7], as well as laser-plasma-generated proton bunch post-acceleration and monochromatization [8].
As an example, Fig. 1b shows the electric field distribution in a THz-pulse-driven double-dielectric-grating electron accelerator, while Fig. 1c depicts the evolution of the electron energy along the accelerator for a few different injection phases of the electrons relative to the driving THz field. In the simulation two 0.7-THz pump pulses (see Fig. 1b), each of 2 MV/cm field amplitude, were assumed. The calculation predicts 1.07 MV/cm average acceleration gradient. Please notice that, because of their larger wavelength and longer oscillation period, using THz pulses with 0.1 to 3 THz frequency for driving such type of accelerator can result clear acceleration and high device throughput, contrary to the case of using 800 nm driving laser [9].

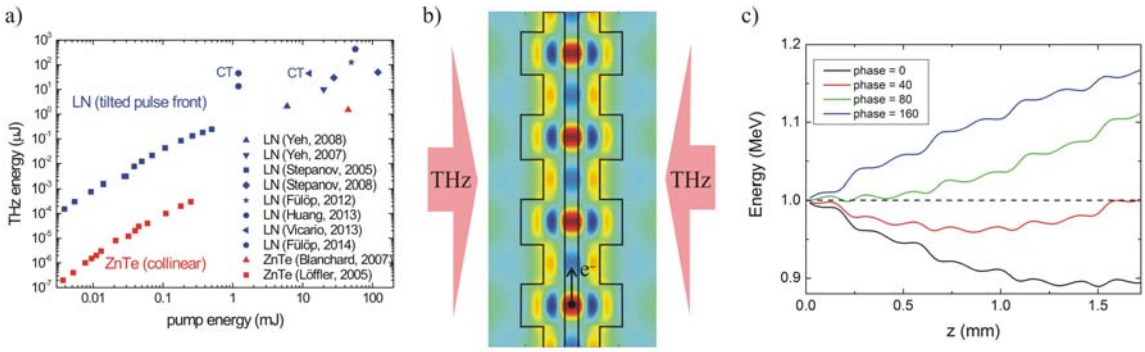

Figure 1. Generated THz pulse energy vs. pump energy (a), electric field distribution in a THz pulse drived double dielectric grating accelerator (b), and the simulated energy of an electron injected with a few different phase (c).

[1] M. C. Hoffmann et al., Impact ionization in InSb probed by terahertz pump-terahertz probe spectroscopy, Phys. Rev. B 79, 161201 (2009)
[2] J. A. Fülöp et al., Efficient generation of THz pulses with 0.4 mJ energy, Optics Express, submitted (2014).
[3] L. Pálfalvi et al., Novel setups for extremely high power single-cycle terahertz pulse generation by optical rectification, Appl. Phys. Lett. 92, 171107 (2008).
[4] J. A. Fülöp et al., Towards generation of mJ-level ultrashort THz pulses by optical rectification, Optics Express 19, 15090 (2011).
[5] K. Kovács et al., Quasi-phase-matching high-harmonic radiation using chirped THz pulses, Phys. Rev. Lett. 108, 193903 (2012).
[6] J. Hebling et al., Optical manipulation of relativistic electron beams using THz pulses, arXiv1109.6852v1 (2011).
[7] L. J. Wong et al., Compact electron acceleration and bunch compression in THz waveguides, Optics Express 21, 9792-9806 (2013).
[8] L. Pálfalvi et al., Evanescent-wave proton postaccelerator driven by intense THz pulse, Phys. Rev. Spec. Top. Accel. and Beams 17, 031301 (2014)
[9] E. A. Peralta et al., Demonstration of electron acceleration in a laser-driven dielectric microstructure, Nature 503, 91-94 (2013)

Surface plasmon polariton studies in the terahertz range: A state of the art review

B. A. Knyazev[1,2], V. V. Gerasimov, I. A. Kotelnikov[1,2], A. K. Nikitin[3]

1- Novosibirsk State University, 2 Pirogova St., 630090 Novosibursk, Russia
2- Budker Institute of Nuclear Physics SB RAS, 11 Lavrentyeva Ave., 630090 Novosibirsk, Russia
3- Scientific and Technology Center for Unique Instrumentation, Moscow RAS, 117342, Russia

ba_knyazev@phys.nsu.ru

Surface plasmon polaritons (SPPs) attract growing attention in modern photonics, in particular, because of the feasibility of realizing two- and three-dimensional all-optical integration circuits [1]. Such devices are of special interest in the terahertz (THz) range for communication systems, chemical and biological sensors and material study. Characteristics of SPPs are well investigated in the visible and near-infrared regions [2], but experiments in the terahertz range yielded contradictory results and reveal some discrepancies with theory. Because of a weak coupling of THz SPPs to metal surfaces, so called "designer surface plasmons" on subwavelength structures with freely tailorable dispersion seem to have become a main stream in the surface plasmonics. However, the fields, where the "true plasmons" appear or are employed, apparently, exist. In this paper we will review our recent experiments with true THz SPPs on plane and curved metal-dielectric-air interfaces and compare the results with theory and with the results of experiments performed during the past 35 years.

Our experiments have been carried out using monochromatic radiation of the Novosibirsk free electron laser at a wavelength of 130 μm, whereas most of recent experiments (see, e. g., [3-5]) have been performed using the time-domain technique. It is instructive to compare all these results with the results obtained in 1970-80th using monochromatic far-infrared molecular lasers [6-7]. Since different groups applied different detection techniques, we have tried via comparative analysis to collect the results which seem to be reliable.

A number of problems is crucial for designing terahertz-based communication and circuits. First, a free wave has to be coupled to a metal surface with an acceptable efficiency to produce a SPP. Gratings, prisms, waveguides and diffraction methods were applied by different authors. There is still no clear evidence, which technique is most effective in THz, but after testing all of them we have selected the "end-fire-coupling" technique: laser beam diffraction on a sample edge. Second task is collection of data on the propagation length, which are important for plasmon waveguiding, for THz SPPs on different interfaces at a wide wavelength range. Though the data are rather fragmentary, they clearly evidence that in the THz region the propagation length is obviously less (or even much less!), than the Drude theory predicted. Experiments have shown that even a thin dielectric layer on a metal drastically couple SPP to the surface and decrease the propagation length, and in this case the SPP obviously became a true plasmon. We observed also that the SPP out-of-plane decay length was closed to a value predicted by the Drude theory. Third important problem is moving SPP along curved surfaces. To date, a noncontradictory theory for SPP travelling azimuthally along a cylindrical surface has not been developed. We will clarify the problem at the conference presentation. The forth problem under discussion is SPP "jumping" across air gaps, which is promising for information transmission between electrically isolated pieces of plasmonic integrated circuits. We observed SPP jumps at a distance as large as 100 mm.

[1] A. V. Zayats and I. I. Smolyaninov, Near-field photonics: surface plasmon polaritons and localized surface plasmons, J. Opt. A: Pure Appl. Opt., vol. 5, pp. S16-S50, (2003).
[2] S. A. Maier, Plasmonics: fundamentals and applications (Springer Verlag, New York, LLC), (2007).
[3] Jeon Tae-In and Grischkowsky D., THz Zenneck surface wave THz surface plasmon propagation on a metal sheet, Appl. Phys. Lett. Vol. 88, art. No 061113, 4 pp. (2006).
[4] Nazarov M. and Coutaz J.-L., THz surface waves propagation on metals with sub-wavelength structure and grating reliefs, J. Infrared Terahz Waves, vol. 32, pp. 1054-1073, (2011).
[5] Nazarov M., Coutaz J.-L., Shkurinov A. and Garet F., THz surface plasmon jump between two metal edges, Optics Communications, vol. 277, pp. 33-39, (2007).
[6] Begley D. L., Alexander R. W., Ward C. A., Miller R. and Bell R. J., Propagation distances of surface electromagnetic waves in the far infrared, Surface Sci., vol. 81, pp. 245-251, (1979)
[7] Koteles E. S. and McNeill W. H., Far infrared surface plasmon propagation, Int. J. Infrared Milli Waves, vol. 2, pp. 361-371, (1981).

Nonlinear effects of strong THz fields

S. Tzortzakis[1,2]

1. *Institute of Electronic Structure and Laser (IESL), Foundation for Research and Technology - Hellas (FORTH), P.O. Box 1527, GR-71110 Heraklion, Greece*
2. *Department of Materials Science and Technology, University of Crete, GR-71003, Heraklion, Greece*

e-mail: stzortz@iesl.forth.gr

Gas-plasma strings from 2-color femtosecond laser filaments constitute one of the most convenient and promising sources of pulsed terahertz (THz) radiation. It is one of the approaches that allow one to achieve at the same time ultrabroadband THz spectra and very high amplitudes of THz electric fields. Such sources present major advantages for applications of sensing, spectroscopy, imaging, and nonlinear optics.

Here we present experimental and theoretical results on the spatial and temporal THz emission properties from 2-color filaments and we study the induced THz nonlinearities in transparent media. Exciting spatiotemporal effects are revealed enriching the era of THz nonlinear optics.

Acknowledgements: This work was supported by the Aristeia project “FTERA” (grant no 2570), co-funded by the European Social Fund (ESF) and National Resources and partially supported by the EU FP7 “Laserlab III” project.

Nonlinear optics in the electrostatic limit at terahertz frequencies

Pernille Klarskov[1], Abebe T. Tarakegne[1], Krzysztof Iwaszczuk[1], Andrew C. Strikwerda[1], Stewart J. Clark[2], Peter Uhd Jepsen[1]

1- Department of Photonics Engineering, Technical University of Denmark, DK-2800 Kongens Lyngby, Denmark

2- Department of Physics, University of Durham, Durham DH1 3LE, United Kingdom

puje@fotonik.dtu.dk

Nonlinear optics is most often described in the multiphoton picture, where the energies of individual photons can be added or subtracted, or the energy between photons can be redistributed, in sum-frequency, difference-frequency, and parametric generation processes, respectively. However, it is well known that if the light intensity is sufficiently high, this multiphoton picture of nonlinear optics is no longer valid. This regime is known as extreme nonlinear optics, and is characterized by laser fields strong enough to compete with the atomic fields of the solid that the light field interacts with. Until now extreme nonlinear optics has been limited mainly to atomic systems (i.e. gas jets), as solid-state materials suffer permanent damage before high enough intensities of the laser field can be reached. We have recently demonstrated experimentally and numerically that by using intense light fields at long wavelengths, corresponding to THz frequencies, it is now possible to enter the realm of extreme nonlinear optics without damaging the sample under study.

A strong THz field can drive low-frequency modes in molecular crystals in a highly nonlinear fashion that is best described by strong-field physics, where the interatomic potential is strongly modified by the driving field. This is in stark contrast to weak field interaction where the absorption is simply given by the linear phonon spectrum of the material. With the aid of quantum mechanical molecular dynamics simulations it has been demonstrated that a strong THz field modifies the potential so strongly that tunneling of the ions in the crystal between lattice points becomes a real possibility. The implication of this is that the strong THz pulse rattles the cage of the crystal so hard that it can fall apart in a nonthermal manner, i.e. dependent on whether the THz field is resonant with phonon modes or not. In more complicated molecular crystals such as sucrose, where several vibrational modes are closely spaced, this nonlinearity leads to strong coupling between the modes.

In a somewhat similar process we have discovered that strong THz fields can rip electrons out of metals via a tunneling process. The electrons are emitted in the form of an ultrafast electron “bullet” which is extremely bright compared to other pulsed electron sources. The emitted electrons can initiate physical and chemical processes in the immediate environment of the metal surface, for instance by ionizing atmospheric nitrogen, and thus create a nitrogen plasma on a time scale faster than 1 picosecond.

Interaction of Terahertz Radiation with Nanostructured Objects on a Surface

M. Esaulkov[1], A. Kaul[3], A. Makarevich[3], I. Ozheredov[2], P. Solyankin[2], A. Shkurinov[3]

(List of authors in 11 point, centred and bold: the presenting author underlined)

1- Institute on Laser and Information Technologies of the Russian Academy of Sciences, Shatura, Moscow Region 40700 RUSSIA

2- Department of Physics and International Laser Canter, Lomonosov Moscow State University, Moscow 19992 RUSSIA

3- Department of Chemistry, Lomonosov Moscow State University, Moscow 19992 RUSSIA

In the paper we present the results of study of basic regularities of interaction of terahertz frequency range electromagnetic radiation (0.1-10 THz) with functional materials that exhibit properties of phase transitions. The paper is focused on the development of the materials and on the basis of these materials the photocontrollable detectors and sensors operating in the terahertz frequency range.

So far, all published studies concerning the interaction of terahertz radiation with thin films of metals, were limited by gold films in the absence of vacuum. Other metals are rarely aroused the interest of researchers because of oxidation under atmospheric conditions. This work fills this gap - as the characteristics of different metals, and by type of external conditions.

Similar studies in the terahertz range under controlled chemical and morphological state of the surface under ultra high vacuum and the absence of oxidation by atmospheric oxygen films have not been conducted to date. In addition, virtually unexplored opportunities to improve the efficiency of nonlinear optical generation of terahertz radiation by converting the optical radiation under the reflection from metal films and nanostructures.

Interaction of strong THz fields with solids and liquids

S.Bodrov[1,2], A. Kiselev[1], Yu. Mal'kov[1], A.Murzanev[1], Yu. Sergeev[1], A. Stepanov[1,2], D. Yashunin[1]

1 – Institute of Applied Physics RAS, 603950 Russia, Nizhny Novgorod, Uljanov Str., 46

2- Nizhny Novgorod State University, 603950 Russia, Nizhny Novgorod, Gagarin Av., 23

step@ufp.appl.sci-nnov.ru

In our report we consider the interaction of single-cycle THz pulses with an amplitude of electric field up to 300 kV/cm with liquids, semiconductors and metals. Optical birefringence in liquids induced by strong THz field due to Kerr effect was investigated. Visualization of THz near-field close to the metal tip was demonstrated. Peculiarities of optic second harmonic generation from the surface of semiconductor and metal samples in the presence of strong THz radiation also were the subject of our interest.

Wireless links in the THz range using UTC photodiodes

P. Latzel[1], F. Pavanello[1], G. Ducournau[1], E. Peytavit[1], D. Bacquet[2], P. Szriftgiser[2], M. Zaknoune[1], X. Wallart[1], J.-F. Lampin[1]

1- Institut d'Electronique de Microélectronique et de Nanotechnologie (IEMN), UMR CNRS 8520, Université de Lille 1, Avenue Poincaré, F-59652 Villeneuve d'Ascq cedex, France
2- Laboratoire de Physique des Lasers Atomes et Molécules (PhLAM), UMR CNRS 8523, Université de Lille1, F-59655 Villeneuve d'Ascq cedex, France

jean-francois.lampin@isen.iemn.univ-lille1.fr

Free space communications with huge data capacity have become a key point for the development of mobile access, services, and network technologies convergence. Wireless links using emerging terahertz technologies have several advantages since it allows more data rate than millimeter waves and it is more robust against scintillation, dielectric obstacles, and fog than near-infrared links. Here we demonstrate the use of infrared lasers for terahertz wave generation and wireless data transmission. This down-conversion is done thanks to the photomixing of two CW lasers lines in a large bandwidth uni-travelling photodiode (UTC-PD) connected to an antenna (a "photomixer"). This approach (fig. 1a) has the advantage of using standard 1.5 µm modulators that allows very high data rates up to 40 Gbit/s and more.
In this presentation we will show a 400 GHz wireless link that was used to investigate data rates up to 46 Gbit/s [1]. We will show also a 600 GHz hotspot for HDTV transmission at 1.7 Gbit/s [2]. In each case a photomixing photonic transmitter and a large bandwidth heterodyne receiver are used. We show that thanks to the high sensitivity of the receiver very small THz power are needed (µW or less).

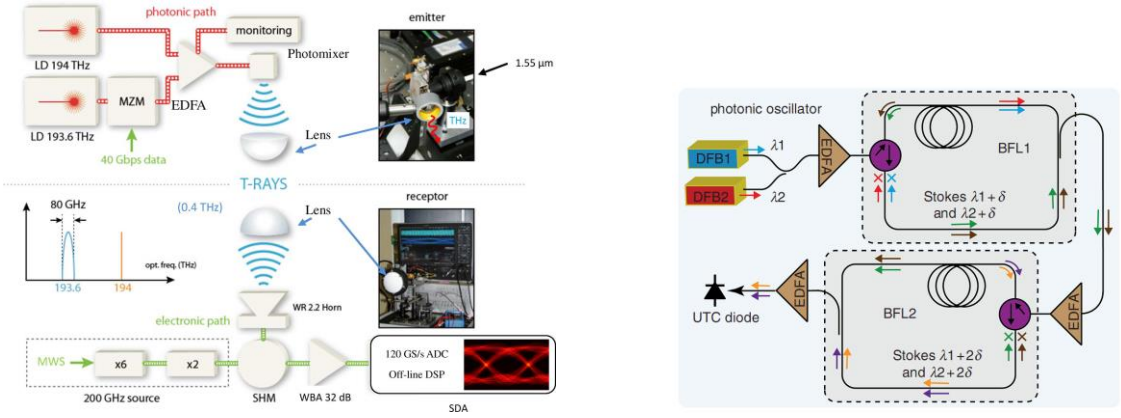

(a) (b)

Figure 1 (a) Schematic of the data transmission setup at 0.4 THz. (b) Schematic of the cascaded dual-frequency Brillouin fibre lasers.

With the photomixing approach, the linewidth of the generated THz beatnote is directly linked to the linewidth of the two laser lines. In the standard set-up we use two DFB laser diodes and generate a THz line with about 1 MHz linewidth. We will show that it is possible to reduce this linewidth by pumping Brillouin lasers with standard DFB [3]. Recently, by using a cascaded dual-frequency Brillouin lasers scheme (fig. 1b) we have obtained a linewidth <100 Hz at 1014.7 GHz [4]. This approach can be used to improve the quality of the beatnote and to allow vector modulation data transmission.

[1] G. Ducournau *et al.*, Ultrawide-bandwidth single-channel 0.4 THz wireless link combining broadband quasi-optic photomixer and coherent detection, IEEE Transactions on Terahertz Science and Technology, vol. 4, pp. 328-337, (2014).
[2] G. Ducournau *et al.*, High-definition television transmission at 600 GHz combining THz photonics hotspot and high-sensitivity heterodyne receiver, Electronics Letters, vol. 50, pp. 413-415, (2014).
[3] G. Ducournau *et al.*, Highly coherent terahertz wave generation with a dual-frequency Brillouin fiber laser and a 1.55 µm photomixer, Optics Letters, vol. 36, pp. 2044-2046, (2011).
[4] G. Ducournau *et al.*, Cascaded Brillouin fibre lasers coupled to unitravelling carrier photodiodes for narrow linewidth terahertz generation, Electronics Letters, vol. 50, pp. 690-692, (2014).

Nanometer Plasma Field Effect Transistors for Detection of Terahertz Radiation

W.Knap, D.But, N.Diakonova, F.Teppe, D.Coquillat,

L2C & TERALAB Montpellier University &CNRS, 34950 Montpellier, France

***Abstract*—Two-dimensional electron plasma in nanometer size field effect transistors can oscillate in Terahertz (THz) frequencies, far beyond transistors fundamental cut-of frequencies [1]. We propose an overview of some important and recent results concerning THz detection by nanometer field effect transistors. The subjects were selected in a way to show physics related limitations and advantages rather than purely technological/engineering improvements of nanometer Field Effect transistors working as Terahertz detectors.**

TWO -dimensional electron plasma in nanometer size field effect transistors can oscillate in Terahertz (THz) frequencies, far beyond transistors fundamental cut-of frequencies. Interest in using nanometer field effect transistors (FETs) for THz applications was initiated in the early '90s by the theoretical work of Dyakonov and Shur who predicted that the channel of a FET could act as a resonator for plasma waves and that THz radiation can be efficiently rectified FET. Rectification and detection of THz radiation is also possible in the non-resonant case, (low electron mobility) when plasma waves decay at the distance smaller than the channel length. Typical length of this region ranges from 30nm to 300nm [3]. Therefore, both resonant and nonresonant plasma wave THz detection requires nanometer scale FETs. For recent reviews see [1] and [2].

The real large scale interest in using FETs as THz detectors started around 2004 after first experimental demonstration of sub-THz and THz detection in silicon CMOS FETs [3,4]. Both pioneering works have clearly stated importance of Si- CMOS FETs which present the advantages of room temperature operation, very fast response times, easy on-chip integration with read-out electronics and high reproducibility leading to straight-forward array fabrication. We propose a review of the most important and recent results on terahertz detection using nanometer size FETs. The subjects were selected in a way to stress physical limits of FET detectors and possible new developments [5-9].

We would like to address the basic physics related problems like power dependence of the photoresponse [2], temperature dependence, of the response [5], and helicity sensitive detection [6].

Until now, most of the work on nanometer FETs detectors considered mainly THz imaging applications. We show also the progress in the application of nanometer FETs as detectors in THz wireless communication [7]. Finally we would like to present results from THz detection by grapheme transistors [8] and discuss possible developments of future THz detectors using nanowires.

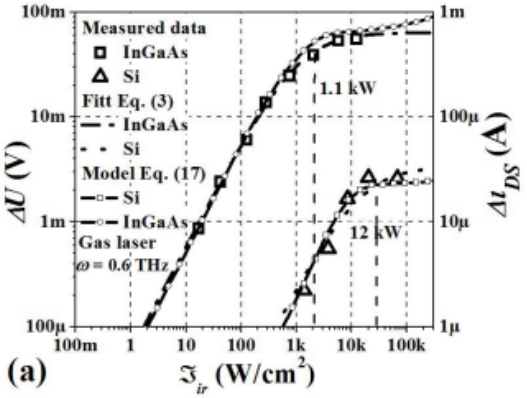

Fig. Photoresponse of FETs based on InGaAs (HEMT) and Si (MOSFET in Table I) as a function of radiation intensity. The radiation frequency is 0.6 THz. Nonlinear and saturation regions of detections are seen for intensities above 1kW/cm^2 [After Ref.9].

REFERENCES

[1] W. Knap and M. I. Dyakonov, 'Field effect transistors for terahertz applications' in D. Saeedkia, Handbook of terahertz technology for imaging, sensing and communications, Cambridge, Woodhead Publishing, 121-155(2013)

[2] W Knap, S Rumyantsev, M S Vitiello, D Coquillat, S Blin, M Shur, F Teppe, A Tredicucci and T Nagatsuma Nanometer size field effect transistors for terahertz detectors Nanotechnology 24 (2013)

[3] Knap W, Teppe F, Meziani Y, Dyakonova N, Lusakowski J, Boeuf F, Skotnicki T, Maude D, Rumyantsev S, Shur M S Plasma wave detection of sub-terahertz and terahertz radiation by silicon field-effect transistors Applied Physics Letters 85 675 (2004)

[4] Tauk R, Teppe F, Boubanga S, Coquillat D, Knap W, Meziani Y M, Gallon C, Boeuf F, Skotnicki T, Fenouillet-Beranger C, Maude D K, Rumyantsev S, Shur M S Plasma wave detection of terahertz radiation by silicon field effects transistors: Responsivity and noise equivalent power Applied Physics Letters 89 253511 (2006)

[5] Klimenko O A, Knap W, Iniguez B, Coquillat D, Mityagin Y A, Teppe F, Dyakonova N, Videlier H, But D, Lime F, Marczewski J, and Kucharski K Temperature enhancement of terahertz responsivity of plasma field effect Transistors J. Appl. Phys. 112, 014506 (2012)

[6] Drexler C, Dyakonova N, Olbrich P, Karch J, Schafberger M, Karpierz K, Mityagin Yu, Lifshits M B, Teppe F, Klimenko O, Meziani Y M, Knap W and Ganichev S D 2012 Helicity sensitive terahertz radiation detection by field effect transistors J. Appl. Phys. 111 124504 (2012)]

[7] Blin S, Teppe F, Tohme L, Hisatake S, Nouvel P, Coquillat D, Penarier A, Torres J, Knap W, Nagatsuma T Plasma-Wave Detectors For Terahertz Wireless Communication IEEE El. Dev. Lett. 33 1354 (2012)

[8] Vicarelli L, Vitiello M S, Coquillat D, Lombardo A, Ferrari A C, Knap et al . Graphene field-effect transistors as room-temperature terahertz detectors, Nature Materials 11 865(2012)

[9] D.But et al Power dependence of THz photoresponse of field effect transistors submitted to J.Appl .Phys.February 2014

Terahertz plasmons in active graphene: diffusion pumping concept

M. Morozov[1], A. Davoyan[2], I. Moiseenko[3], V. Popov[1,3]

1- Kotelnikov Institute of Radioeng. and Electr. RAS, Saratov branch, Zelenaya, 38, Saratov, Russia, 410019
2- University of Pennsylvania, Philadelphia, Pennsylvania 19104, USA.
3- Saratov State University, Astrakhanskaya, 83, Saratov, Russia, 410012.

mikkym@mail.ru

Graphene, due to its unique properties [1], is one of the promising materials for creating compact THz lasers [2] and plasmonic amplifiers [3-5]. Proposed concepts of the THz graphene lasers and plasmon amplifiers employ the optical pumping of graphene. However, because graphene absorbs only 2.3% of incident optical pump power [6], the optical pumping technique limits the efficiency of THz graphene lasers. The concept of THz graphene laser with diffusion pumping was proposed in [7]. In this case, a population inversion in graphene is created by ambipolar carrier diffusion from a wide-gap optically pumped semiconductor substrate.

In present paper, we study the amplification of plasma waves (plasmons) propagating in graphene pumped by carrier diffusion from a semiconductor substrate.

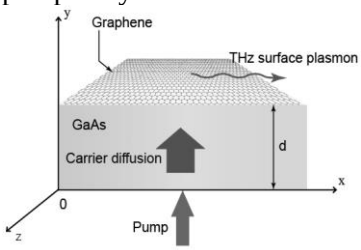

Figure 1 Schematic view of the graphene based THz plasmon amplifier.

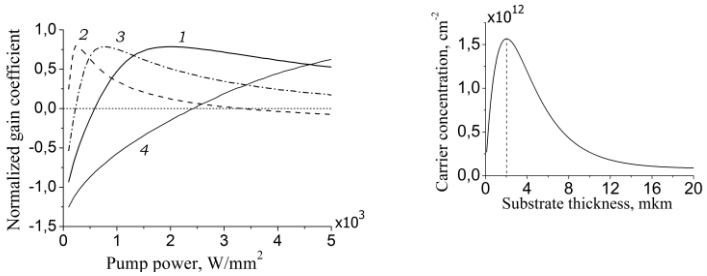

Figure 2 Plasmon gain vs the optical pump power for different substrate thicknesses 0.1 μm (curve *1*), 2 μm (curve *2*), and 7μm (curve *3*). Curve *4* corresponds to direct optical pumping of graphene (zero substrate thickness). The inset shows the variation of the carrier density in graphene as a function of the substrate thickness.

A schematic view of the proposed plasmon amplifier is shown in Fig.1. A monolayer graphene is deposited on a semiconductor substrate having thickness *d*. Charge carriers generated in semiconductor by optical illumination diffuse toward graphene and captured in it, creating the population inversion in graphene.

Fig. 2 shows the plasmon gain (normalized to plasmon wavelength) versus pump power for different substrate thicknesses. Plasmon frequency is fixed at 5 THz. If the thickness of substrate is comparable to the ambipolar diffusion length in semiconductor, the population inversion in graphene reaches its maximum (see inset in Fig. 1) providing the maximal plasmon gain. It is worth mentioning that an order of magnitude greater optical pump power is needed to reach the same plasmon gain for direct optical pumping of graphene (curve *4* in Fig. 1).

The work has been supported by the Russian Foundation for Basic Research (Grant No. 13-02-12070).

[1] K. S. Novoselov, V. I. Fal'ko, L. Colombo, et al. A roadmap for graphene. Nature, 490, pp. 192 – 200, (2012).
[2] V. Ryzhii, A. A. Dubinov, T. Otsuji, V. Mitin, M. S. Shur. Terahertz lasers based on optically pumped multiple graphene structures with slot-line and dielectric waveguides. J. Appl. Phys., 107, pp. 054505-1 – 054505-5, (2010).
[3] A. A. Dubinov, V. Ya. Aleshkin, V. Mitin, T. Otsuji, V. Ryzhii. Terahertz surface plasmons in optically pumped graphene structures. J. Phys.: Condens. Matter, 23, pp. 145302-1 – 145302-8 (2011).
[4] V. V. Popov, O. V. Polischuk, A. R. Davoyan, V. Ryzhii, T. Otsuji, M. S. Shur. Plasmonic terahertz lasing in an array of graphene nanocavities. Phys. Rev. B, 86, pp. 195437-1 – 195437-6 (2012).
[5] V. V. Popov, O. V. Polischuk, S. A. Nikitov, V. Ryzhii, T. Otsuji, M. S. Shur. Amplification and lasing of terahertz radiation by plasmons in graphene with a planar distributed Bragg resonator. J. Opt., 15, pp. 114009-1 – 114009-8 (2013).
[6] R. R. Nair, P. Blake, A. N. Grigorenko, K. S. Novoselov. *et al.*. Fine Structure Constant Defines Visual Transparency of Graphene. Science, 320, p. 1308 (2008).
[7] A. R. Davoyan, M. Yu. Morozov, V. V. Popov, A. Satou, T. Otsuji. Graphene surface emitting terahertz laser: Diffusion pumping concept. Applied Physics Letters, 103, pp. 251102-1 – 251102-5 (2013).

New Scientific opportunities using Coherent Synchrotron Radiation

E. Roussel[1,2], C. Szwaj[1,2], C. Evain[1,2], S. Bielawski[1,2], S.Tammaro[3], O.Pirali[3,4] L. Manceron[3], J. B Brubach[3], M.A. Tordeux[3], M. Labat[3], J.P. Ricaud[3], M. E. Couprie[3], , G.Mouret[5], J-F Lampin[6], G. Ducournau[6], A. Cuisset[5], F.Hindle[5] & P. Roy

(Dated: July 21, 2014)

1-Laboratoire PhLAM, UMR CNRS 8523, Université Lille 1, 59655 Villeneuve d'Ascq, France
2- Centre d'Etude Recherches et Applications (CERLA), 59655 Villeneuve d'Ascq, France
3- Synchrotron SOLEIL, L'Orme des Merisiers, Saint-Aubin, BP 48, 91192 Gif-sur-Yvette Cedex, France
4- Institut des Sciences Moléculaires d'Orsay, UMR8214 CNRS – U. Paris-Sud, Bât. 210, 91405 Orsay, France
5- LPCA, Université du Littoral côte d'opale, 189A Avenue Maurice Schumann, 59140 Dunkerque, France
6- IEMN, Avenue Poincaré-Cité Scientifique, 59652 Villeneuve D'Ascq

Pascale.roy@synchrotron-soleil.fr

Recently, an unprecedented high power source of THz radiation was made scientifically available: coherent synchrotron radiation (CSR) [1-3]. This radiation produced from relativistic electron bunches of picosecond duration opens up new territory in the THz range with intensities up to 4 orders of magnitude higher than previous sources. Its huge potential can however be hampered by its stability which is critically affected by accelerator and electron bunches properties. Investigating these intrinsic instabilities remained up to now an open problem because of the extreme speed of the phenomena, implying to record picosecond signals at MHz acquisition rates. We will show how this was recently made possible by adapting a photonic technique, called time-stretch, which allows to slow-down" the signal prior to recording [4]. As a result we will demonstrate the possibility to look continuously at electron bunch emission with sub-psec resolution. We will also describe new scientific opportunities made possible by CSR in particular, high rate terahertz spectroscopy, as well as ultra-high resolution spectroscopy based on heterodyne mixing technique [5].

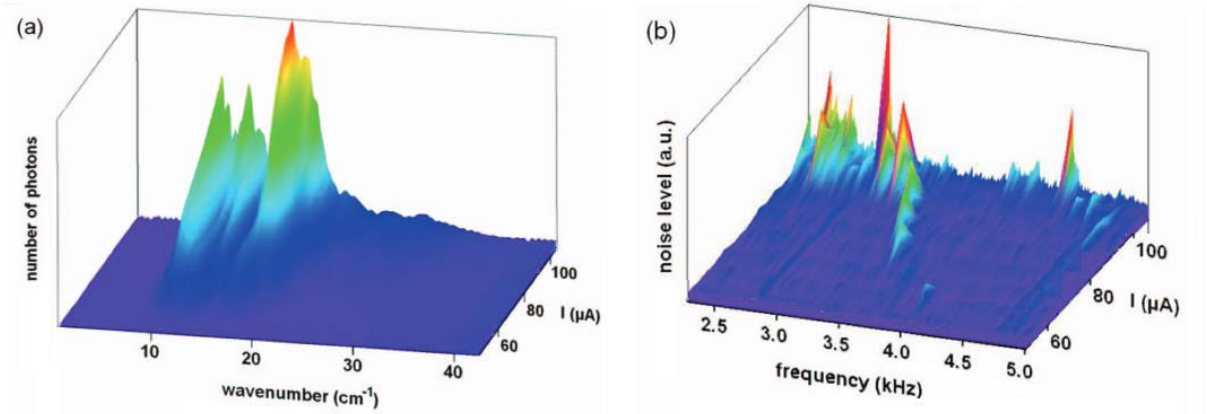

Figure 1: Spectral distribution of the CSR Intensity measured for various bunch currents showing the appearance of CSR for I bunch=55μA (a) and strong instabilities at precise frequencies measured for higher bunch current (b). The THz CSR signal fluctuates at frequencies in the kHz range, resulting in localized artifacts in the Fourier Transform Interferometry spectra.

[1] G. Stupakov and S. Heifets, Phys. Rev. ST Accel. Beams,5, 054402 (2002).
[2] J. M. Byrd, W. P. Leemans, A. Loftsdottir, B. Marcelis, M. C. Martin, W. R. McKinney, F. Sannibale, T. Scarvie, and C. Steier, Phys. Rev. Lett., 89, 224801 (2002).
[3] M. Abo-Bakr, J. Feikes, K. Holldack, G. Wustefeld, and H.-W. Hubers, Phys. Rev. Lett., 88, 254801 (2002).
[4] F. Coppinger, A. Bhushan, and B. Jalali, IEEE Trans. on Microwave Theory and Techniques, 47, 1309 (1999).
[5] D. Burghoff, T. Kao, N. Han, C. Wang, I. Chan, X. Cai, Y. Darren J. Hayton, J-R. Gao, J. L. Reno, and Q. Hu, Nature Photonics (2014)

Friday 10th October

Development of the PETAL laser facility and its applications in physics

D. Batani[1], J.-L. Miquel[2], N. Blanchot[3]

1- Univ. Bordeaux, CEA, CNRS, CELIA UMR5107, F-33400 Talence, France
2- CEA, DAM, DIF, F-91297 Arpajon, France
3-CEA, DAM, CESTA, BP 2, F-33114 Le Barp, France

batani@celia.u-bordeaux1.fr

A new era of plasma science started with experiments on the National Ignition Facility (NIF) in the US, which will be soon followed by the Laser Mégajoule (LMJ) in France.
Such facilities, whose main objective is to reach nuclear ignition by imploding deuterium-tritium targets using high-energy laser beams, will provide a unique tool not only for ICF physics but also for basic science fields such as high energy density physics (HEDP), laboratory astrophysics, planetary science, nuclear and particle physics.
A petawatt short pulse laser is in construction to be added to the ns pulse beams of LMJ. This is the PETAL system (PETawatt Aquitaine Laser), under construction on the LMJ site near Bordeaux (France), with the ultimate goal of reaching 7 PW (3.5 kJ with 0.5 ps pulses). The LMJ/PETAL facility will be open to European Research groups for academic access starting in 2017. In this phase, PETAL will provide 1 kJ in 0.5 ps and will be coupled to the first two LMJ Quads as shown in the figure.

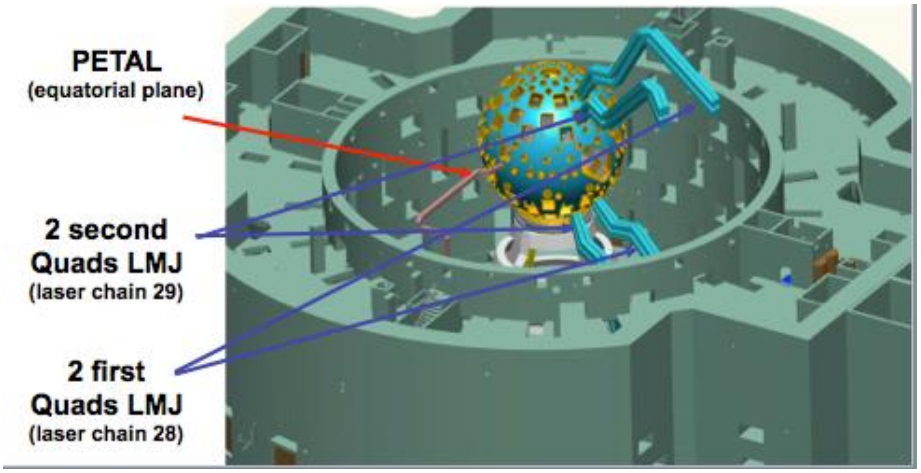

PETAL is aiming at providing secondary sources of particles and radiation to diagnose high energy density plasmas generated by the LMJ beams. An additional project, Petal+, has been funded by the French National Research Agency (ANR) and managed by the University of Bordeaux and it is addressed to design and provide diagnostics dedicated to experiments with the PETAL laser beam.
Within this project, three types of diagnostics are planned: proton spectrometry, electron spectrometry and X-ray spectrometry. Because of the characteristics of the PETAL beam, these diagnostics need to cover a large dynamical range. The goal of these diagnostics will be to assess the characteristics of the secondary sources produced with PETAL, as well as the performance of PETAL itself. Further diagnostics will be installed in the future on the LMJ/PETAL facility to allow HEDP experiments.
During the presentation to the conference, the status of the PETAL and Petal+ projects will be presented in detail, as well as the main lines of the scientific program to be investigated on the LMJ/PETAL facility.

MONITORING OF PDT: WHAT IS THE BEST FOR CLINICAL PRACTICE

Sergey Gamayunov [2,3,4], Ksenia Korchagina[3], Ilya Turchin [1,4], Pavel Subochev [1,4], Sergey Kuznetsov[3,4], Vitaliy Terekhov[2] and Natalia Shakhova [1,3,4]

[1] Institute of Applied Physics RAS, Nizhny Novgorod, Russia
[2] Nizhny Novgorod Oncologic Clinic, Nizhny Novgorod, Russia
[3] Nizhny Novgorod State Medical Academy, Nizhny Novgorod, Russia
[4] N.I. Lobachevsky State University of Nizhny Novgorod, Nizhny Novgorod, Russia

Introduction

PDT is an actively developing technique for treatment of malignant tumors[1]. For optimization of PDT procedure monitoring of the tissue reaction is required[2]. The main requirements for monitoring techniques are high information content in combination with noninvasiveness. Currently the main candidates for using in PDT monitoring are fluorescent imaging [2], optical coherence tomography (OCT)[2,3] , Laser Doppler flowmetry (LDF)[4] and photoacustic imaging[5].

The aim of the study is to demonstrate the capability of each of the above methods and suitability of multimodal approach to control PDT in clinical practice.

Materials and methods

The study was performed at the Nizhny Novgorod Oncologic Clinic. More than 250 patients with skin cancer treated by PDT were enrolled in the study. Fluorescence imaging, spectroscopy, different modes of OCT (standard and PS OCT), and LDF were employed for monitoring. *Ex vivo* optoacoustic images of skin tumors were obtained. Comparative analysis of data was performed.

Results

Analysis of diagnostic data revealed the ability of fluorescence imaging and spectroscopy to evaluate photosensitizer (PS) accumulation and its photobleaching which can be employed for prognosis of immediate and long-term results. OCT allows evaluating the changes in tissue structure in real time in the course of PDT procedure which can be employed for early monitoring of efficacy of the selected regimes. PS OCT is promising for diagnosing of skin cancer recurrence in scar. LDF is suitable for monitoring of the changes in vascular component of PDT action. Development of multispectral optoacustic imaging will allow to determine tissue oxygen status before procedure and to control it in course of treatment, and also to estimate vascular component of PDT action.

In conclusion: comparative analysis revealed complementarity of the employed techniques rather than their competition; multimodal approach in PDT monitoring is the method of choice for clinical application; further development and advancement of monitoring techniques are required.

Acknowledgements: the study was supported by the Government of Russian Federation (agreement # 14.B25.31.0015), RFBR (project 14-02-00753/14) and Nizhny Novgorod N.I. Lobachevsky State University (agreement # 02.B.49.21.0003).

1. Patrizia Agostinis et al. Photodynamic therapy of cancer: an update. CA Cancer J Clin. 2011 Jul-Aug; 61(4): 250–281.

2. Jonathan P. Celli et al. Imaging and Photodynamic Therapy: Mechanisms, Monitoring, and Optimization. Chem Rev. 2010 May 12; 110(5): 2795–2838.

3. Standish BA, Yang VX, Munce NR, Wong Kee Song LM, Gardiner G, Lin A, Mao YI, Vitkin A, Marcon NE, Wilson BC. Doppler optical coherence tomography monitoring of microvascular tissue response during photodynamic therapy in an animal model of Barrett's esophagus. Gastrointest Endosc. 2007 Aug;66(2):326-33.

4. Enejder A.; Klinteberg C.; Wang I.; Andersson-Engels S.; Bendsoe N.; Svanberg S.; Svanberg, K. Blood Perfusion Studies on Basal Cell Carcinomas in Conjunction with Photodynamic Therapy and Cryotherapy Employing Laser-Doppler Perfusion Imaging Acta Dermato-Venereologica . Jan2000, Vol. 80 Issue 1, p19-23

5. Wang LV, Hu S. Photoacoustic tomography: in vivo imaging from organelles to organs. Science. 2012 Mar 23;335(6075):1458-62.

Impact of Nanodiamonds on Red Blood Cells Studied by Laser Techniques

A.V. Priezzhev[1,2,*], A.E. Lugovtsov[2], V.B. Koshelev[3] and O.E. Fadyukova[3],
[1]International Laser Center, [2]Physics Faculty and [3]Faculty of Medicine of Lomonosov Moscow State University, Leninskye Gory 1, Moscow, 119991, Russia
and
C.-L. Cheng[4], Y.-C. Lin[4] and E.B. Perevedentseva[4]
[4]National Dong Hwa University, Hualien, Taiwan

[*]e-mail: avp2@mail.ru

Diamond nanoparticles – nanodiamonds (ND) attract much attention due to their intrinsic properties of nontoxicity and biocompatibility. However possible effects of these nanoparticles on biological structures starting from molecular and cellular levels, including blood components, have not been fully assessed so far. The aim of this work was to study the effect of ND on the microrheologic characteristics of human and rat blood at *in-vitro* incubation of blood samples with ND and *in-vivo* incubation after intravenous administration of ND into live rats.

In our previous work [1], we studied various effects of ND on the components of blood plasma. The adsorption of blood plasma proteins on ND was analysed using UV-visible absorption measurements. We showed, in particular, that the adsorption of blood plasma proteins albumin and γ-globulin on ND sized 5 and 100 nm leads to structural transformations of the adsorbed molecules and, consequently, to a significant decrease in the protein functional activity. We also found that the influence of 5-nm ND on the protein structure and functions is more significant than that of 100-nm ND. We also studied the influence of ND on the oxygenation states and microrheological properties of red blood cells (RBC) *in-vitro* [2]. Measurements were facilitated using laser scanning fluorescence and Raman scattering spectroscopy, dynamic and diffuse light scattering techniques, and laser diffractometry. Diffuse light scattering from freshly drawn whole blood samples after their incubation with ND was used to study the effect of ND on the kinetics of RBC spontaneous aggregation and shear-induced disaggregation. Diffraction of laser beam on diluted suspensions of RBC before and after incubation with ND was implemented for quantitative measurements of the effect of ND on the ability of RBC to deform when subjected to shear stress in a flow cell. Optical trapping with laser tweezers was used to study the interaction of individual RBCs suspended in autologous plasma and/or in solutions of various macromolecules and ND. All measurements were performed *in-vitro*.

Here we report on the latest results of our research, which combines our *in-vitro* and *in-vivo* expertise in cellular and in whole blood and animal models using state of the art laser methods and instruments. Importantly, we show that the ND in their as-prepared form and in physiological condition neither cause hemolysis nor affect the cell viability. Neither the oxygenation/deoxygenation states are altered when the ND interact with RBC. However, in some cases the ND affect the microrheologioc properties of RBC such as their ability to change their shape under shear stress as well spontaneous aggregation and shear–induced disaggregation parameters. This may be due to the ND sticking to RBC membrane as well as due to adsorption of blood plasma proteins on their surfaces, which we recorded by various laser techniques. The effects are particle size, concentration and surface functionalization dependent.

The obtained results imply that controlling the blood (micro) rheologic properties is necessary during the ND application in the *in-vivo* experiments and clinical trials. Different techniques based on laser interaction with particles can be efficiently used for this purpose. We believe that this conclusion is true for all nanoparticles designed for biomedical applications albeit their administration into the organism is to be performed via blood flow. Further *in-vivo* experiments are of crucial importance for testing the results obtained in *in-vitro* conditions.

The authors acknowledge the financial support of the Taiwan-Russia collaboration project (grants RFBR-12-02-92008_NSC and NSC-101-2923-M-259-001-MY3).

[1] E.V. Perevedentseva, F.Y. Su, T.H. Su, et al. *Quant. Electron.,* **40**(12), 1089-1093 (2010).
[2] Y.-C. Lin, L.-W. Tsai, E. Perevedentseva, et al. *J. Biomed. Opt.*, **17**(10), 101512 (2012).

Fluence-compensated optoacoustic image reconstruction for quantitative imaging

T. Petrosyan, G. Held, S. Preisser, G. Akarcay, M. Jaeger, M. Frenz

Institute of Applied Physics, University of Bern, Sidlerstrasse 5, CH-3012 Bern
frenz@iap.unibe.ch

Spectral optoacoustic (OA) imaging enables spatially-resolved measurement of the local blood oxygenation level, due to the different optical absorption spectra of oxygenated and deoxygenated blood. Wavelength-dependent optical attenuation in the bulk tissue, however, distorts the spectral OA signal of the blood and thus renders absolute oxygenation measurements challenging. We present a novel method to correct for this spectral distortion, which does not require a-priori knowledge about the optical properties of the bulk tissue. For this purpose the irradiation position is scanned over the tissue surface. In that way, the changing OA signal amplitude of embedded absorbers as a function of different light propagation distances enables a sampling of the fluence distribution and thus the reconstruction of the effective optical attenuation coefficient of the bulk medium. For a proof of principle this method was tested in phantom experiments, where cylindrical inclusions, filled with indocyanine green (ICG), were used as embedded absorbers in a strongly light scattering bulk medium (Intralipid).

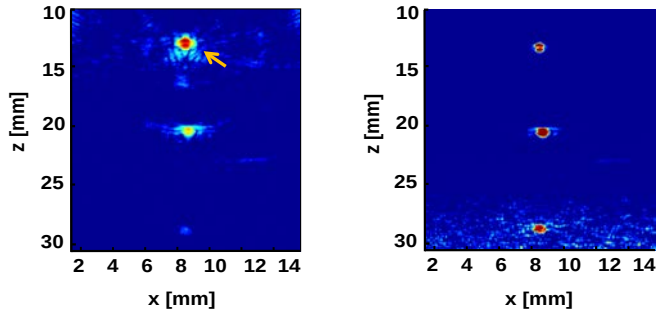

Figure 1: OA image of a strongly light scattering phantom, embedding three cylindrical inclusions as optical absorbers at a depth of 12 mm, 20 mm and 28 mm, a) OA signal amplitude decreases with increasing depth, due to optical attenuation; arrow indicates upper cylindrical absorber inside phantom. b) Knowledge about the effective optical attenuation of the bulk medium renders to compensate for the wavelength dependent fluence decay resulting in the same signal amplitude for all three absorbers.

Figure 1a shows an OA image of the phantom with the three inclusions located perpendicular to the imaging plane, indicating the decrease in signal amplitude with increasing depth, due to optical attenuation in the bulk medium. A stepwise moving of the irradiation location relative to the fixed position of the cylindrical absorbers renders a sampling of the fluence distribution, based on the changing OA signal amplitude of the embedded absorbers as a function of different light propagation distances. By fitting a simplified model for light propagation in strongly scattering media to the measured data points, describing the fluence distribution for different propagation distances, we were able to reconstruct the effective optical attenuation coefficient of the bulk medium. Our phantom results show good agreement with reference measurements of optical properties using diffuse optical tomography (DOT). The ensued characterization of the surrounding bulk medium in terms of effective optical attenuation, allows compensating for the wavelength dependent fluence attenuation. Fig. 1b shows the OA image of the investigated phantom after correction for the optical fluence attenuation in the bulk medium. This technique is a promising approach for effective attenuation compensation in real-time clinical OA imaging.

Optical elastography – Imaging tissue stiffness at high resolution

D. D. Sampson[1,2], K. M. Kennedy[1], S. Es'haghian[1], L. Chin[1], A. Curatolo[1], P. R. T. Munro[1], R. A. McLaughlin[1], B. F. Kennedy[1]

1- Optical+Biomedical Engineering Laboratory, School of Electrical, Electronic & Computer Engineering, The University of Western Australia

2- Centre for Microscopy, Characterisation & Analysis, The University of Western Australia

Email: David.Sampson@uwa.edu.au

The mechanical interactions of cells play an important role in how they grow, differentiate and migrate. Impairment in a cell's capacity to respond to mechanical forces contributes to diseases such as cancer[1], and to differences in biomechanical properties manifested on length scales from the sub-cellular, to the tissue microenvironment, to whole organs.

At the extremes of the length scale, methods for probing tissue mechanics are well established. On the cellular and sub-cellular scale, cell mechanics may be probed by atomic force microscopy and traction force microscopy[2]. On the scale of whole organs, tissue mechanics may be probed by medical elastography methods[2, 3]. Such methods are relatively underdeveloped on the intermediate scale, between cells and whole tissues, in the length scale range 10 micrometres to 1 millimetre[4]. On this scale, these methods promise new information on the mechanical heterogeneity of tissues with implications for the understanding of cells in their three-dimensional native environment as well as potential in a range of medical applications in cancer, cardiovascular and eye disease.

We have been developing micro-elastography methods based on compressive loading of whole tissues and measurement of the resulting displacement using three-dimensional optical coherence tomography[5-9]. By utilizing the same signal processing approach used to measure fluid flow, it is possible to sense displacements with order 100-picometre resolution, which enables exquisitely small variations in mechanical properties to be detected. Without recourse to inverse methods, such methods have generally been used to present elastograms based on local strain. We will present elastograms of malignant and normal breast, lung, lymph node and muscle tissues. Recently, we have shown how to measure surface stress (Fig. 1)[10] and, thus, provide a means to provide images of elastic modulus.

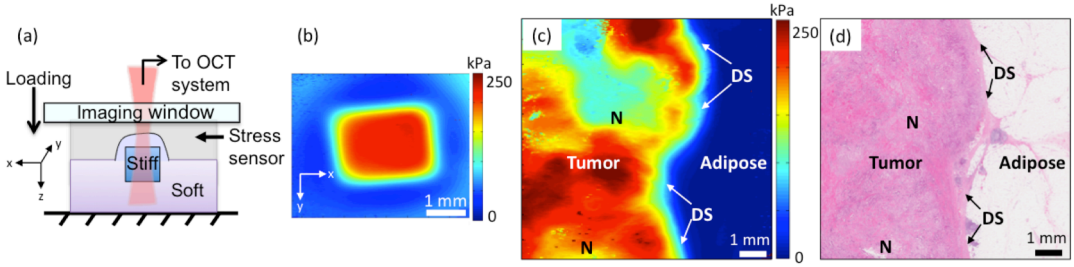

Figure 1: (a) Setup for measuring stress in optical elastography; (b) Stress map of an inclusion phantom; (c) stress map of freshly excised human breast tissue comprising a region of invasive tumor and a region of healthy adipose, and (d) corresponding histology.

[1] S. Kumar and V. Weaver, "Mechanics, malignancy, and metastasis: The force journey of a tumor cell," *Cancer and Metastasis Reviews,* vol. 28, pp. 113-127, 2009.

[2] K. J. Parker, M. M. Doyley, and D. J. Rubens, "Imaging the elastic properties of tissue: The 20 year perspective," *Physics in Medicine and Biology,* vol. 56, pp. R1-R29, 2011.

[3] Y. K. Mariappan, K. J. Glaser, and R. L. Ehman, "Magnetic resonance elastography: A review," *Clinical Anatomy,* vol. 23, pp. 497-511, 2010.

[4] B. F. Kennedy, K. M. Kennedy, and D. D. Sampson, "A review of optical coherence elastography: Fundamentals, techniques and prospects," *IEEE Journal of Selected Topics in Quantum Electronics,* vol. 20, p. 7101217, 2014.

[5] B. F. Kennedy, T. R. Hillman, R. A. McLaughlin, B. C. Quirk, and D. D. Sampson, "In vivo dynamic optical coherence elastography using a ring actuator," *Optics Express,* vol. 17, pp. 21762-21772, 2009.

[6] B. F. Kennedy, X. Liang, S. G. Adie, D. K. Gerstmann, B. C. Quirk, S. A. Boppart, and D. D. Sampson, "In vivo three-dimensional optical coherence elastography," *Optics Express,* vol. 19, pp. 6623-6634, 2011.

[7] B. F. Kennedy, S. H. Koh, R. A. McLaughlin, K. M. Kennedy, P. R. T. Munro, and D. D. Sampson, "Strain estimation in phase-sensitive optical coherence elastography," *Biomedical Optics Express,* vol. 3, pp. 1865-1879, 2012.

[8] K. M. Kennedy, C. Ford, B. F. Kennedy, M. B. Bush, and D. D. Sampson, "Analysis of mechanical contrast in optical coherence elastography," *Journal of Biomedical Optics,* vol. 18, p. 121508, 2013.

[9] K. M. Kennedy, R. A. McLaughlin, B. F. Kennedy, A. Tien, B. Latham, C. M. Saunders, and D. D. Sampson, "Needle optical coherence elastography for the measurement of microscale mechanical contrast deep within human breast tissues," *Journal of Biomedical Optics,* vol. 18, p. 121510, 2013.

[10] K. M. Kennedy, S. Es'haghian, L. Chin, R. A. McLaughlin, D. D. Sampson, and B. F. Kennedy, "Optical palpation: Optical coherence tomography-based tactile imaging using a compliant sensor," *Optics Letters,* vol. 39, pp. 3014-3017, 2014.

Laser Assessment of Human and Rat Blood Microrheology Alterations in Diabetes Mellitus

A.E. Lugovtsov[1], A.V. Priezzhev[1,2], V.D. Ustinov[3], M.A. Kormacheva[2], V.B. Koshelev[4], O.E. Fadyukova[4], M.D. Lin[4]
[1]*International Laser Center and* [2]*Physics Department,*
[3]*Faculty of Computational Mathematics and Cybernetics and* [4]*Faculty of Basic Medicine of M.V. Lomonosov Moscow State University,*
Leninskye Gory 1, Moscow, 119991, Russia
e-mail: anlug@bmp.ilc.edu.ru

Diabetes mellitus (DM) is a systemic disease that is gaining higher and higher social problem due to the quickly growing number of Earth population suffering from it and due to severe alterations of vitally important systems of the human organism involved including the cardiovascular system. The major long-term DM complications are related to the damage to blood vessels and capillaries (causes microangiopathy) and impairment of blood rheological properties. This leads to doubling the risk of cardiovascular diseases. It is obvious that control and monitoring of DM complications is very important, in particular microrheological and rheological parameters. The rheological parameters are mostly related to the deformability and aggregation properties of red blood cells (RBCs), which are expected to be impaired in DM patients. The main goal of this work was to estimate the alterations of these parameters for rat and human blood in case of non-insulin-dependent DM (NIDDM) and insulin-dependent DM (IDDM).

In this work, we conducted measurements based on laser aggregometry and diffractometry techniques. Laser diffractometry is a convenient, fast and relatively simple technique for measuring the RBCs deformability. The essence of this technique is in obtaining and subsequent analysis of the diffraction patterns from a highly diluted suspension of RBCs at rest and shear flow [1]. Dependence of the diffraction pattern elongation on shear stress characterizes the ability of RBCs to deform. Laser aggregometry technique allows to study the kinetics of the spontaneous aggregation (time dependence of light intensity backscattered from a sample of whole blood in the rest) and shear-induced disaggregation (shear stress dependence of light intensity backscattered from a sample of whole blood under shear flow) of RBCs for obtaining characteristic times of linear (T1) and three-dimensional (T2) aggregates formation, as well as hydrodynamic strength of RBCs [2]. All experimental measurements were performed with human blood drawn from patients with IDDM (N=8), NIDDM (N=10) and practically healthy volunteers (N=10), as well as with rat blood drawn from healthy animals (N=8) and from rats with experimentally induced DM (N=8).

The experimentally obtained results show that the microrheological properties are impaired in case of DM diseases. For instance, the ability of human RBCs to deform in shear flow decreases by about 8-10 % (in cases of both IDDM and NIDDM) in comparison with that in the control group. It has been shown that the reduction of RBCs deformability in case of DM is mainly related with the increasing of RBCs membranes rigidity. The parameter T2 decreases by about 20-25 % (in cases of both IDDM and NIDDM) in comparison with that in the control group while the parameter T1 increases by about 20% in case of NIDDM and about 60 % in case of IDDM. Microrheological alterations in the blood of DM rats are quantitatively different from those in human DM patients. This may be due to the fact that DM rats do no suffer from accompany diseases and complications characteristic of human DM patients.

This work was partially supported by RFBR grants № 12-02-01329 and № 13-02-01373.

[1] S.Yu. Nikitin, A.V. Priezzhev, and A.E. Lugovtsov, [Laser diffraction by the erythrocytes and deformability measurements], Advanced Optical Flow Cytometry: Methods and Disease Diagnoses, Edited by Valery V. Tuchin, Published by Wiley-VCH Verlag GmbH & Co., pp. 133-154 (2011).
[2] A.V. Priezzhev, N.N. Firsov, J. Lademann, [Light backscattering diagnostics of RBC aggregation in whole blood samples], Chapter 11 in Handbook of Optical Biomedical Diagnostics, Editor V. Tuchin, Washington: SPIE Press, pp. 651 – 674 (2012).

Ultrafast Laser Produced Non-equilibrium Warm Dense Matter

Y. Y. Tsui

Department of Electrical & Computer Engineering, University of Alberta, Edmonton, Alberta T6G 2V4, Canada.

tsui@ece.ualberta.ca

When a high intensity ultrashort laser pulse is absorbed by a solid target, a two temperature warm dense matter with electron temperature of several electron volts, ion temperature near room temperature and density remains as solid is formed initially in less than a picosecond. During the subsequent several picoseconds the electron temperature reduces and ion temperature rises and the heated target eventually disassembles into an expanding plasma. The ultrashort laser produced warm dense matter which lies in between the condense matter and plasma states is related to two forefront research areas in materials science under extreme conditions, namely, the warm dense matter science [1] and the high energy density physics[2].

In this talk, I will first present results of our study on the time evolution of AC conductivity of two temperature warm dense gold [3]. In the experiment, freestanding 30nm-thick gold foils are excited by 400nm, 45fs (FWHM) laser pulses to energy densities up to ~4MJ/kg. Temporal evolution in AC conductivity of the resulting state is determined from simultaneous measurements of reflection and transmission of a chirped pulse probe at 800nm. This yields two important benchmarks for comparison with theory. The conductivity value at the end of the femtosecond laser pulse is a measure of its dependence on electron temperature as the ions remain cold. Subsequent changes then provide a measure of conductivity as a function of both electron and ion temperatures as thermal equilibration between electron and ion progresses. These data are compared with ab-initio quantum simulations.

In the second part of the talk I will present our initial measurement results of ultrashort x-ray probing warm dense aluminium [4]. Ultrashort duration betatron x-ray radiation results from the acceleration of relativistic electrons inside high intensity laser wakefield cavities. The femtosecond pulse duration and the synchronization properties make Betatron radiation an ideal probe for investigating the dynamic properties of laser produced warm dense matter. Study of the ionization state of material in the non-equilibrium warm dense regime is a significant challenge at present. However, time-dependent x-ray measurements of K-shell absorption lines allows the ionization states of warm dense matter to be measured. We have employed ultrashort betatron radiation as a spectroscopic probe to temporally resolve the ionization states of warm dense aluminum. A Kirkpatrick-Baez Microscope was used to focus the radiation around the 1.5 keV photon energy range onto a 50-nm free-standing aluminum foil that was heated by a synchronized 800 nm laser pump pulse. By dispersing the K-shell absorption spectra in this range using a flat KAP bragg crystal spectrometer, we observed the ionization states of warm dense aluminum as a function of time and heating pulse fluence.

[1] Ng et al., "Idealized Slab Plasma Approach for the Study of Warm Dense Matter", Laser Part. Beams 23, 527 (2005).
[2] Davidson et al., "Frontiers in High Energy Density Physics: The X-Games of Contemporary Science" National Academy of Sciences Report, National Acad. Press, ISBN: 0-309-51360-X (2003).
[3] Chen et al., "Evolution of ac Conductivity in Nonequilibrium Warm Dense Gold", Phys. Rev. Lett. 110, 135001 (2013).
[4] Mo et al, "Laser Wakefield Generated X-ray Probe for Femtosecond Time-resolved Measurements of Ionization States of Warm Dense Aluminum", Rev. Sci. Instrum 84 , 123106 (2013).

Relativistic intensity sub-5-femtosecond laser pulses and their applications

L. Veisz[1], D. Rivas[1], G. Marcus[1], X. Gu[1], D. Cardenas[1], J. Xu[1], J. Mikhailova[1], A. Buck[1,2], T. Wittmann[1], C. M. S. Sears[1], D. Herrmann[3], O. Razskazovskaya[2], V. Pervak[2], F. Krausz[1,2]

1- Max-Planck-Institut für Quantenoptik, Hans-Kopfermann-Strasse 1, 85748 Garching, Germany
2- Ludwig-Maximilians-Universität München, Am Coulombwall 1, 85748 Garching, Germany
3- Lehrstuhl für BioMolekulare Optik, Department für Physik, Ludwig-Maximilians-Universität, Oettingenstrasse 67, 80538 München, Germany

laszlo.veisz@mpq.mpg.de

The continuous development of pulsed light sources with ultra-high intensity lead to a novel principle, the optical parametric synthesizer (OPS), which provides unparallelled gain bandwidth supporting quasi-single-cycle pulse duration [1]. The Light Wave Synthesizer 20 (LWS-20) system is the first light source based on OPS principle providing few-fs pulses at ultra-relativistic intensities. The basic infrastructure of the system includes an optically synchronized 80 ps Nd:YAG pump laser from EKSPLA and a kHz Ti:Sa multipass Femtopower amplifier from Femtolasers, both seeded from a common broadband Ti:Sa Rainbow oscillator from Femtolasers. The spectrum of the kHz laser pulses are broadened in a hollow-core fiber filled with 2 bars of Neon to provide a seed source. A carefully designed grism stretcher and a custom made Dazzler from Fastlite elongate the pulses to 67 ps and four consecutive OPS stages are amplifying them. After the last amplifier an energy about 100 mJ is achieved and a spectrum in the range of 580-1020 nm supporting 3.9 – 4.3 fs or sub-two optical cycle pulse duration depending on the application. The pulses are compressed in bulk glasses (100 mm Quartz and 2x80 mm SF57) and four specially designed chirped mirrors. Temporal characterization is realized with a home-made DazScope as well as a single shot autocorrelator and FROG. A compressed duration of sub-5 fs and 80 mJ energy is routinely obtained (Fig. 1. demonstrates 4.5 fs).

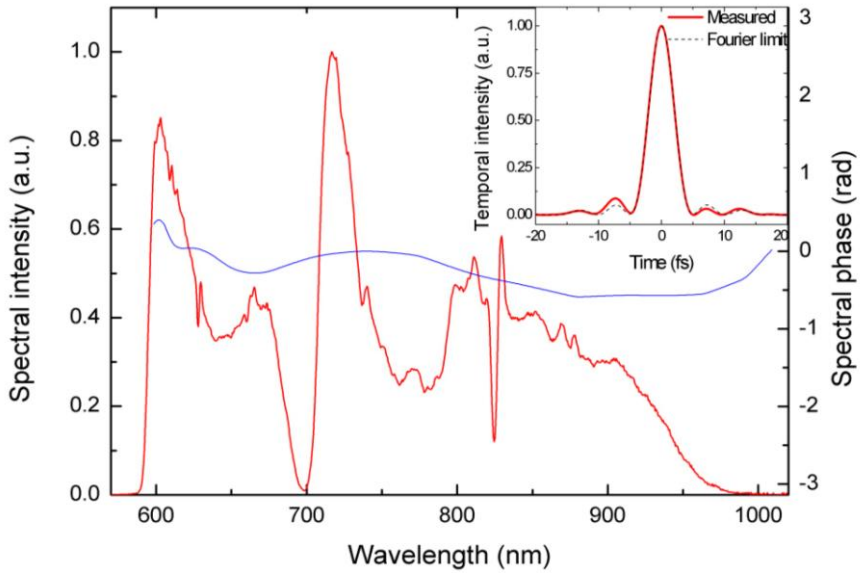

Figure 1. Typical spectral intensity (red) and phase (blue) of LWS-20. Inset: corresponding temporal intensity with 4.5 fs FWHM duration (red) and Fourier limited temporal intensity (dashed black).

Carrier envelope phase tagging using a single-shot phase meter is implemented in the system. Two main applications are pursued with this system: (1) generation of intense isolated attosecond XUV pulses in laser – solid-density-plasma interaction [2] or in gas medium [3]; (2) acceleration of relativistic femto- to attosecond electron bunches in a laser-plasma accelerator [4]. These unique sources open up the route to nonlinear X-ray science and attosecond electron diffraction.

[1] D. Herrmann et al., "Approaching the full octave : Noncollinear optical parametric chirped pulse amplification with two-color pumping", Opt. Express 18, 18752 (2010).
[2] G. Tsakiris, K. Eidmann, J. Meyer-ter-Vehn, and F. Krausz, "Route to intense single attosecond pulses", New J. Phys. 8, 19 (2006).
[3] F. Krausz, and M. Ivanov, "Attosecond Physics", Rev. Mod. Phys. 81, 163 (2009).
[4] K. Schmid et al., "Few-cycle laser-driven electron acceleration", Phys. Rev. Lett. 102, 124801 (2009).

High field physics at ALLS: from electron acceleration to x-ray coherent imaging

S. Fourmaux[1], A. Lachapelle[1], S. Payeur[1], A. Saraf[1], K. Otani[1,2], P. Antici[1], S. MacLean[1,2], J C Kieffer[1]

1- INRS-EMT, Varennes, Qc, Canada
2- IQC, Waterloo University, Ont. Canada

kieffer@emt.inrs.ca

I will present our most recent results obtained with the 200TW laser facility at ALLS on the acceleration of electrons and applications using the laser Wakefield Acceleration (LWFA) concept and by direct laser field acceleration (DLFA).

Using LWFA, we recently demonstrated for the first time the generation of betatron radiation with energies in excess of 10 keV and a sufficient number of photons (10^9) to achieve phase contrast imaging in a single laser shot. We describe here our most recent progresses in both the X-ray source developments and phase contrast imaging of complex interfaces in anisotropic materials. A full characterization and assessment of the betatron phase contrast imaging beam line has been realized and will be presented and discussed.

For the DLFA, we are focusing a high peak power beam, 3J in 30fs, radially polarized, using a transverse magnetic mode (TM01), on gaz targets and electrons are accelerated to multi-MeV energies by the intense longitudinal field produced in an intensity range of 10^{21} W/cm^2 – $2x10^{22}$ W/cm^2. We describe the various diagnostics used in these experiments, our most recent progresses and the perspectives of this program.

Time-resolved XANES as an atomic-level diagnostic of non-equilibrium transition from solid to Warm Dense Matter

F. Dorchies[1], J. Gaudin[1], C. Fourment[1], P.-M. Leguay[1], B. Chimier[1], O. Peyrusse[1], V. Recoules[2], B. Holst[2], P. Combis[2], L. Videau[2], P. A. Heimann[3], B. I. Cho[3], K. Engelhorn[3], T. Tschentscher[4], C. Ozkan[4], M. Nakatsutsumi[4], M. Harmand[5], S. Toleikis[5], M. Störmer[6], B. Nagler[7], H. J. Lee[7], E. Galtier[7]

1- Univ. Bordeaux, CNRS, CEA, CELIA, Talence, France
2- CEA-DAM-DIF, Arpajon, France
3- Lawrence Berkeley National Laboratory, Berkeley, USA
4- European XFEL, Hamburg, Germany
5- DESY, Hamburg, Germany
6- Helmholtz zentrum Geesthacht, Geesthacht, Germany
7- SLAC National Accelerator Laboratory, Menlo Park, USA

dorchies@celia.u-bordeaux1.fr

The advent of femtosecond lasers has shed new light on non-equilibrium high energy density physic. The ultrafast energy absorption by electrons and the finite rate of their energy transfer to the lattice creates non-equilibrium states of matter, triggering a new class of non-thermal processes in solids of primordial importance in material science, as well as resulting in warm dense matter (WDM) which finds implication in astrophysics and fusion.

We have developed an original approach to study the dynamical interplay between electron and ion at the atomic scale. It is based on time-resolved x-ray absorption near-edge spectroscopy (TR-XANES) measurements, giving access to the short-range disordering together with the electronic structure modification.

Two experiments are presented. The first one has been performed on a full-optical-laser device at CELIA, and reveals the ultrafast short-range disordering in warm dense aluminum [1]. The second one has been performed on the x-ray free electron laser (XFEL) at LCLS. Besides the demonstration of TR-XANES on XFEL within few x-ray pulses [2], this last provides new insight on evolution of the electron density of state (DOS) of molybdenum during its transition from solid to WDM.

The sample expansion is controlled by Fourier Domain Interferometry (FDI) optical measurements [3], coupled with hydrodynamic simulations of the femtosecond-laser-heated samples. XANES spectra, and related electron and ion structures, are supported by *ab initio* Quantum Molecular Dynamic (QMD) calculations.

[1] P.-M. Leguay *et al*., *Ultrafast short-range disordering of femtosecond-laser-heated warm dense aluminum*, Physical Review Letters **111**, 245004 (2013).
[2] J. Gaudin *et al*., *Towards simultaneous measurements of electronic and structural properties in ultra-fast x-ray free electron laser absorption spectroscopy experiments*, Scientific Reports **4**, 4724 (2014).
[3] F. Deneuville *et al*., *Sub-picosecond and nanometer scale dynamics of aluminum target surface heated by ultrashort laser pulse*, Applied Physics Letters **102**, 055002 (2013).

Femtosecond laser-induced damage of optical thin film materials, from the UV to the IR

Laurent Gallais, Dam-Bé Douti and Mireille Commandré
Aix Marseille Université, CNRS, Centrale Marseille, Institut Fresnel UMR 7249, 13013 Marseille, France

laurent.gallais@fresnel.fr

The laser damage resistance of optical components is a main concern for the development of high power short and ultrashort pulse lasers. In these laser systems, there are enormous technological challenges to produce multilayer optical coatings that can limit pulse lengthening, spectral distortion and exhibit high laser-induced damage thresholds (LIDT). Progress on this particular topic requires available experimental data on the LIDT of optical coating materials and fundamental knowledge of the laser damage mechanisms [1-3]. Despite common characteristics with bulk materials, the laser damage of dielectric thin films has peculiarities that need to be taken into account: specific optical, mechanical, thermal, and electronic properties affecting the resistance of components under laser exposition, these properties being very dependent on the deposition conditions.
In the presentation we will report on our recent experimental and numerical work on the LIDT of various thin film optical materials and the dependence of the LIDT with material parameters (intrinsic properties, manufacturing conditions, defects) and laser wavelength. The experimental investigation has been conducted with 100 to 600fs pulses, at different wavelengths from the UV to the NIR. Single and multiple pulses (up to 10e6) have been considered. The experimental data are compared to a numerical model that describes the ionization process in dielectric materials. The model is based on the Keldysh photo-ionization theory and the description of impact ionization by the multiple-rate-equation [4]. Using this approach, the dependence of laser-breakdown with the photon energy can be simulated and the relative importance of the ionization processes can be derived depending on material properties and irradiation conditions.

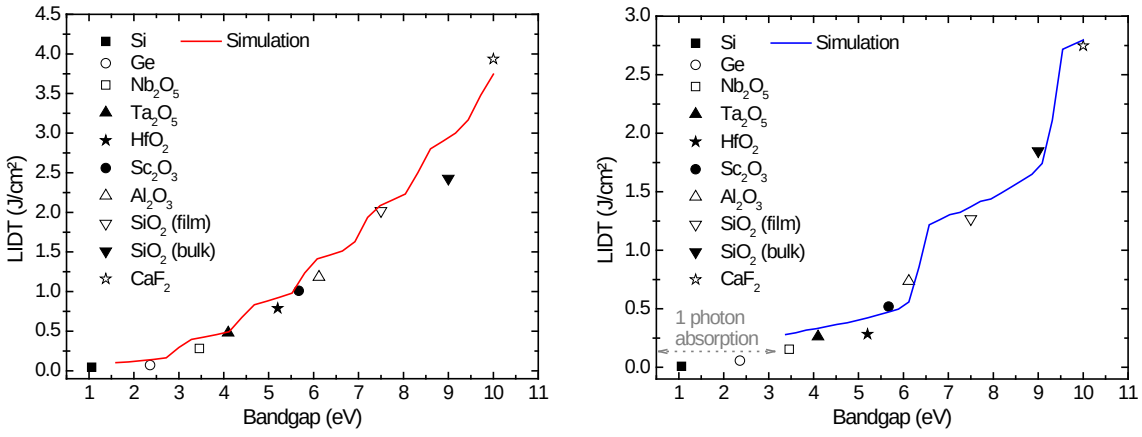

Figure 1: single pulse LIDT of optical materials measured at 100fs / 800nm (a) and 400nm (b). Results of numerical simulations are compared to experimental data.

[1] M. Mero, J. Liu, W. Rudolph, D. Ristau and K. Starke, Scaling laws of femtosecond laser pulse induced breakdown in oxide films, Physical Review B, vol. 71, pp. 115-109, (2005).
[2] L. Gallais and M. Commandré, Laser-induced damage thresholds of bulk and coating optical materials at 1030 nm, 500 fs, Applied Optics 53, A186 (2014)
[3] N. Šiaulys, L. Gallais and A. Melninkaitis, Direct holographic imaging of ultrafast laser damage process in thin films, Optics Letters 39, 2164 (2014).
[4] B. Rethfeld, Unified Model for the Free-Electron Avalanche in Laser-Irradiated Dielectrics, Physical Review Letters, vol. 192, pp. 187401, (2008).

Laser-induced damage thresholds of high-reflective coatings for PW lasers

Adrien Hervy[1, 2, 3, *], Gilles Chériaux[2], Laurent Gallais[3], Daniel Mouricaud[1]
Olivier Uteza[4], Raphael Clady[4], Marc Sentis[4], Antoine Fréneaux[5]

[1]Reosc (SAFRAN Group), 91280 Saint-Pierre-du-Perray, France
[2]Laboratoire d'Optique Appliquée, ENSTA, Ecole Polytechnique, CNRS UMR 7639, 91761 Palaiseau cedex, France
[3]Aix Marseille Université, CNRS, Centrale Marseille, Institut Fresnel, UMR 7249, 13397 Marseille, France
[4]Aix Marseille Université, CNRS, LP3 UMR 7341, 13288 Marseille, France
[5]Laboratoire d'Utilisation des Lasers Intenses, Ecole Polytechnique, 91128 Palaiseau Cedex, France

[*]adrien.hervy@reosc.com

The peak power handling capability of ultra-short pulse lasers is main concern for new facilities, like those for the French *APOLLON 10P*, and European *Extreme Light Infrastructure* (ELI) projects. Indeed, these last generation lasers require large (Ø 1m) and resistant optical components with optimized thin-films coatings. In this context and in the framework of a joint project, LOA, Fresnel Institute and Reosc are working together to develop high performance coatings for ultra-short pulse laser applications.

In the femtosecond regime, the damage of dielectric materials can be understood as a result of electronic processes. The electronic structure of materials is then particularly significant. As a consequence of these processes it is possible to increase the Laser-Induced Damage Threshold (LIDT) by adjusting the Electric Field Intensity (EFI) distribution in the stack of High-Reflective (HR) coatings [1]. LIDT of many currently used oxides, often deposited by Ion-Beam Sputtering (IBS), are well known and a correlation with the band gap energy was shown [2].

With these results we decided to study the LIDT of oxides-made stacks with Electron Beam Deposition (EBD) processes compatible with 1-meter class optics. Several dielectric (MLD) and hybrid metal-multidielectic stacks were design and coated at Reosc.

Samples were irradiated at Fresnel Institute by a 500fs KYW:Yb pulsed laser delivering 1mJ at 1030nm [3], at the LOA by a 40fs (resp. 150ps) Ti:Sa pulsed laser delivering 1.5mJ (resp. 3mJ) in a Gaussian spectrum 20nm FHWM centered at 790nm and at the LP3 by a 11fs Ti:Sa pulsed laser delivering 50µJ in a Gaussian spectrum 130nm FHWM centered at 790nm [4]. Irradiated areas are optically inspected under a Nomarski microscope and any visible modification of the surface is considered as damage. A statistically distribution of the damages gives the LIDT as the mean of the highest fluency class undamaged and the lowest fluency class damaged. Single pulse and multi pulses tests were performed.

We present on one hand the measured spectral characteristics of the coated samples like reflectivity and Group Delay Dispersion (GDD) and on the other hand the LIDT tests results. Moreover, we discuss about the relationship between this results, the intrinsic LIDT of used materials and the electric field distribution inside the stacks (eq. 1).

$$LIDT_{stack} = \min\left(\left|\frac{E_{inc}}{E_{max}}\right|^2 * LIDT_{intrinsic}\right)_{materials} \quad (1)$$

References

[1] G. Abromavicius, R. Buzelis, R. Drazdys, A. Melninkaitis, and V. Sirutkaitis, "Influence of electric field distribution on laser induced damage threshold and morphology of high reflectance optical coatings," Laser-Induced Damage in Optical Materials, , vol. 6720, p. 67200Y–67200Y–8, 2007.

[2] L. Gallais and M. Commandré "Laser-induced damage thresholds of bulk and coating optical materials at 1030 nm, 500 fs," Appl. Opt. **53**, A186-A196, 2014.

[3] B. Mangote, L. Gallais, M. Zerrad, F. Lemarchand, L.-H. Gao, M. Commandré, M. Lequime "A high accuracy femto-/picosecond laser damage test facility dedicated to the study of optical thin films," Review of Scientific Instruments, 83, 013109, 2012.

[4] B. Chimier, O. Uteza, N. Sanner, M. Sentis, A.-T. Itin, P. Lassonde, F. Legare, F. Vidal, J.-C. Kieffer "Damage and ablation thresholds of fused silica in femtosecond regime: relevant physical criteria and mechanisms," Phys. Rev. B. **84**, 094104-10, 2011.

Femtosecond laser filamentation: a tool from micro-nano surface structure fabrication to microwave energy guiding

H. Tao, Y. Ren, M. Alshershby, X. Gao, Z. Hao and J. Lin

Changchun University of Science and Technology, Changchun 130022, China
E-mail: linjingquan@cust.edu.cn

Femtosecond laser filamentation in air has been intensively investigated during the past few years. The attractive properties of the femtosecond filament such as intensity clamping along the filament, great improvement in conductivity of a filament over free space and many others allow for the filament finding applications in various fields. In this presentation, we would like to give our recent simulation and experimental results on carrying microwave energy with plasma waveguide formed by filaments. Particularly, we will focus on two configurations of filament microwave transmission lines: single and double plasma transmission lines. The results show that both plasma transmission lines "waveguides" can provide a considerable enhancement of microwave energy transmission relative to freely propagating in air[1-2]. In the meantime, we will also discuss the fabrication of micro-and nano-structures on non-planar metal surface using femtosecond laser filament, and we find that the filament-processed spherical Al surface has a strong light-trapping ability from UV to IR (0.2-2.5 μm), This result demonstrates that filament fabricating method can be used to process a non-planar surface without the complexity of a 4-axis sample control [3]. The successful use of laser filamentation in those fields enable it a promising tool from manipulating material surface function to directed transmitting electromagnetic energy wirelessly.

[1] Mostafa Alshershby, Zuoqiang Hao and Jingquan Lin Appl. Phys.Lett. 204101 (2013)
[2] Yu Ren, Mostafa Alshershby, Zuoqiang Hao and Jingquan Lin, Phys.Rev.E, 013104(2013)
[3] Haiyan Tao, Jingquan Lin et al., Appl. Phys. Lett, Vol.100, 201111(2012)

Acknowledgements: This project was supported by the 973 program (2013CB922404); the National Natural Science Foundation of China under grant nos. 11274053, 11074027, 61178022; the Research Fund for the Doctoral Program of Higher Education of China (nos. 20122216120009, 20122216110007, and 20112216120006).

Air lasing induced by tunnel ionization: from molecular physics investigation to remote sensing application

Jinping Yao[1,*], Haisu Zhang[1], Jielei Ni[1], Wei Chu[1], Bin Zeng[1], Guihua Li[1], Chenrui Jing[1], Hongqiang Xie[1], Huailiang Xu[2], and Ya Cheng[1]

[1]*State Key Laboratory of High Field Laser Physics, Shanghai Institute of Optics and Fine Mechanics, Chinese Academy of Sciences, Shanghai 201800, China*

[2]*State Key Laboratory on Integrated Optoelectronics, College of Electronic Science and Engineering, Jilin University, Changchun 130012, China*

[*]*E-mail address: jinpingyao@siom.ac.cn*

Abstract: We report on generation of high-brightness, high-gain, and wavelength-switchable lasers in remote air based on femtosecond laser filamentation. The air laser is enabled by instantaneous buildup of population inversion in the molecular ions which are produced by tunnel ionization of molecules in the pump laser fields. We show that this novel phenomenon offers not only opportunities for investigating quantum wavepacket dynamics of molecules based on ultrafast spectroscopy, but also possibilities for detecting multiple pollutants in the atmosphere.

1. Introduction

It was discovered recently that exposure of molecules to ultrashort intense laser pulses can result in instantaneous population inversion in the tunnel-ionized molecular ions, which in turn initiates lasing actions in varies kinds of molecules such as N_2 [1-7], CO_2 [8], and mixed gases [9]. The lasing action induced by femtosecond laser filamentation shows characteristics of linear polarization, high gain and low divergence as well as potential of remote sensing applications [1]. Therefore, it may provide a new strategy to meet the pressing needs of various environmental issues from monitoring global warming and stratospheric ozone depletion to early detection of nuclear reactor radiation leak and biological threat agents in air. Moreover, the air lasing mentioned above uniquely involves a series of ultrafast processes, which begins with a tunnel ionization of the molecules on the attosecond time scale, followed by the population inversion establishment on the femtosecond time scale, and ends up with the amplification of the seed pulses on the picosecond time scale. Therefore, the air laser can be employed as a novel tool for investigation of ultrafast molecular physics in the strong field regime [3,7,10].

In this contribution, we will discuss the mechanism behind the observed ultrafast air laser, manipulation and optimization of the air laser characteristics, and application of the air laser signals as probes for investigating coherent rotational wavepacket dynamics of molecules.

2. Experimental results

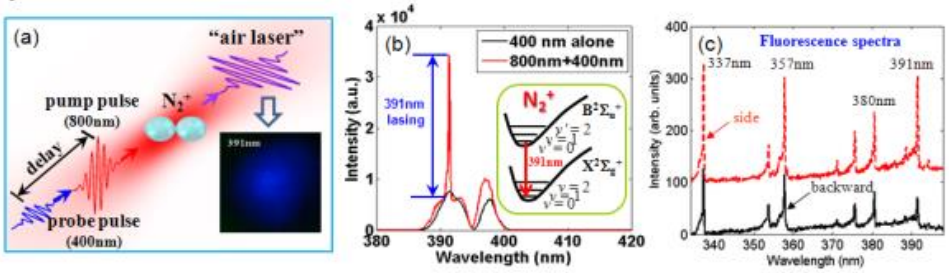

Fig. 1 (a) Experimental schematic to generate the air laser with a two-color pump-probe scheme. Inset: The spatial profile of the air laser. (b) Measured spectra of the probe pulse with (red line) and without (black line) the pump pulse. Inset: Energy level diagram of N_2^+ corresponding to the 391 nm lasing. (c) Typical fluorescence spectra of neutral and ionized nitrogen molecules recorded in backward and side directions. Note that the intensity of air laser measured in the forward direction is at least two orders of magnitude higher than the fluorescence signal measured in the backward and side directions.

Most of our experiments are performed with a Ti:sapphire laser system (Legend Elite-Duo, Coherent, Inc.), providing 1 kHz, 40 fs, ~6 mJ, 800 nm laser pulses. The laser beam is split into two arms: one is used as the pump and the other passes through a BBO crystal to produce ~400 nm probe pulses with the polarization direction perpendicular to the pump pulses. As shown in Fig. 1(a), an intense pump pulse at 800 nm and a weak probe pulse at 400 nm with a variable delay are collinearly focused into a chamber filled with nitrogen gas to generate the air laser

[2-4]. The spatial profile of the air laser is shown in inset of Fig. 1(a). Typical air laser spectra captured by a grating spectrometer (Shamrock 303i, Andor) are presented in Fig. 1(b). It can be clearly seen that in the absence of the pump pulse, the spectral profile of the probe pulse appears smooth. In contrast, when the pump pulse is sent into the molecular system ahead of the probe pulse, a strong, narrow-bandwidth emission located at ~391 nm appears on the top of the probe spectrum, indicating amplification of the probe pulse at ~391 nm. The ~391 nm lasing corresponds to the transition from the electronic state $B^2\Sigma_u^+$ (v'=0) to $X^2\Sigma_g^+$ (v=0), as indicated in inset of Fig. 1(b). For comparison, we also present the fluorescence spectra measured in the backward and side directions, as shown in Fig. 1(c). Since the probe pulse at 400 nm always propagates in the forward direction, the spectra recorded in the backward and side directions do not show any lasing peak as the ~391 nm lasing in Fig. 1(b), in which only fluorescence lines with comparable intensities from both ionized and neutral nitrogen molecules are observed. It is noteworthy that the air laser measured in the forward direction is at least two orders of magnitude stronger than the fluorescence signal measured in the backward and side directions. The unexpected lasing action can be explained as follows. By exposure to intense pump pulses, molecules can be first tunnel-ionized and then a population inversion can be instantaneously established between the excited and ground electronic states of N_2^+. Meanwhile, the probe pulse provides a seed for stimulated emission. Due to the presence of seeding effects, the air laser shows characteristics of high gain, linear polarization and low divergence.

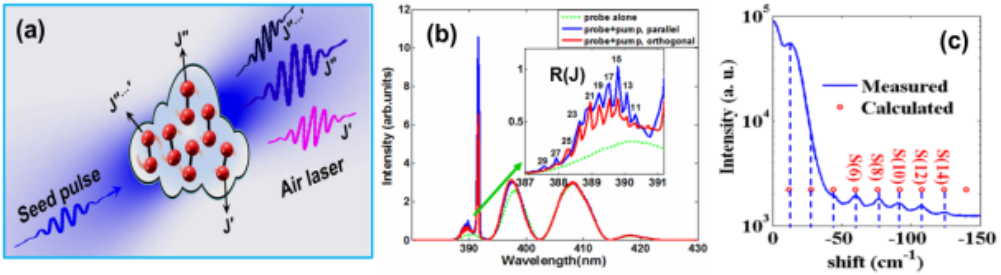

Fig. 2 (a) Diagram of molecular rotational states encoded in an air laser spectrum. (b) The forward probe pulse spectra captured with the polarization direction of the probe pulse parallel (blue line) or perpendicular (red line) to the pump pulse. The inset shows the enlarged R-branch spectrum, and the numbers label the upper rotational levels. (c) Measured Raman spectrum (blue line) induced by intense lasing emission at ~428 nm, and calculated Raman peaks in neutral nitrogen with a rotational constant B = 1.998 cm^{-1} (red circle).

The air lasing driven by two-color fields provides a promising tool for probing molecular dynamics by performing pump-probe measurement. When the intense 800-nm pulses interact with N_2 molecules, molecules are ionized and meanwhile a rotational wave packet is created in the molecular ions. The rotational states distribution of the coherent wave packet can be faithfully mapped onto the frequency-resolved laser spectrum, as illustrated in Figs. 2(a) and (b) [3]. From the frequency-resolved laser spectrum, one can remotely characterize and reconstruct the rotational wave packet of molecules in a single-shot detection manner. More surprisingly, it is found that an intense air laser beam can induce impulsive rotational Raman scattering from neutral nitrogen molecules in a femtosecond laser filament [7], as shown in Fig. 2(c). The impulsive rotational Raman fingerprint signals are observed with a maximum conversion efficiency of ~0.8%. Our observation provides a promising way of remote identification and location of chemical species in atmosphere by rotational Raman scattering of molecules.

3. Conclusion

In summary, we have experimentally demonstrated remote air lasers with intense femtosecond laser pulses. We show that the air lasers provide not only new insights in strong-field molecular physics but also new opportunities for remote nonlinear spectroscopy applications.

[1] J. Yao, B. Zeng, H. Xu, G. Li, W. Chu, J. Ni, H. Zhang, S. L. Chin, Y. Cheng, and Z. Xu, Phys. Rev. A **84**, 051802(R) (2011).
[2] J. Yao, G. Li, C. Jing *et al.*, New J. Phys. **15**, 023046 (2013).
[3] H. Zhang, C. Jing, J. Yao *et al.*, Phys. Rev. X **3**, 041009 (2013).
[4] J. Ni, W. Chu, C. Jing *et al.*, Opt. Express **21**, 8746 (2013).
[5] Y. Liu, Y. Brelet, G. Point, A. Houard, and A. Mysyrowicz, Optics Express **21**, 22791 (2013).
[6] D. Kartashov, S. Alisauskas, A. Baltuska, A. Schmitt-Sody, W. Roach, and P. Polynkin, Phys. Rev. A **88**, 041805(R) (2013).
[7] J. Ni, W. Chu, H. Zhang, B. Zeng, J. Yao, G. Li, C. Jing, H. Xie, H. Xu, Y. Cheng, and Z. Xu, arXiv:1402.5515 (2014).
[8] W. Chu, B. Zeng, J. Yao, H. Xu, J. Ni, G. Li, H. Zhang, F. He, C. Jing, Y. Cheng, and Z. Xu, Europhy. Lett. **97**, 64004 (2012).
[9] J. Ni, W. Chu, H. Zhang *et al.*, Opt. Express **20**, 20970 (2012).
[10] O. Graydon, Nature Photonics, **8**, 3 (2014).

DIAMOND DEPOSITION IN OPEN AIR USING LASER RESONANT VIBRATIONAL EXCITATION OF PRECURSOR MOLECULES

Y.F. Lu

Department of Electrical Engineering, University of Nebraska-Lincoln, Lincoln, NE 68588-0511, USA

*ylu2@unl.edu

Abstract

In this study, we explored laser resonant vibrational excitations for promotion of energy efficiency in chemical reactions, for enhancement of diamond deposition, and for control of chemical reactions. The research mainly focused on resonant vibrational excitations of precursor molecules using lasers in combustion flame deposition of diamond, which led to: 1) promotion of chemical reactions; 2) enhancement of diamond growth with higher growth rate and better crystallizations; 3) steering of chemical reactions which lead to preferential growth of {100}-oriented diamond films and crystals; and 4) mode-selective excitations of precursor molecules toward bond-selective control of chemical reactions.

Diamond films and crystals were deposited in open air by combustion flame deposition through resonant vibrational excitations of precursor molecules, including ethylene (C_2H_4) and propylene (C_3H_6). A kilowatt wavelength-tunable CO_2 laser with spectral range from 9.2 to 10.9 μm was tuned to match vibrational modes of the precursor molecules. Resonant vibrational excitations of these molecules were achieved with high energy efficiency as compared with excitations using a common CO_2 laser (fixed wavelength at 10.591μm). With resonant vibrational excitations, the diamond growth rate was increased; diamond quality was promoted; diamond crystals with lengths up to 5 mm were deposited in open air; preferential growth of {100}-oriented diamond films and single crystals was achieved; mode-selective excitations of precursor molecules were investigated toward control of chemical reactions.

Estimation of the wave process formed on the melt surface during laser cutting of steel

A.V. Dubrov, Yu. N. Zavalov, V. D. Dubrov
Institute on Laser and Information Technologies of Russian Academy of Sciences, Shatura, Moscow Region, Russia

E-mail address: dubrovav@gmail.com

To analyse the metal melt flow entrained by the auxiliary gas jet in the process of laser cutting, the use of the integral model [1] is suggested which accounts for hydrodynamic instability development. Gas jet effect on the liquid film stability is taken into account through pulsations of pressure and shear stress on the interfacial surface. The calculation of pulsations was performed using the "Model D*" [2]. The unperturbed values of pressure gradient and shear stress with dependence on the auxiliary gas pressure were estimated according to [3]. The study of dispersion relations shows the presence of a local maximum of the increment which corresponds to the waves of maximum growth. For the common laser cutting conditions the highest increment belongs to the waves with the length of about 100 mm. The time of the instability development is about several ms what is substantially less than the characteristic time t^* of laser cutting.

Figure 1 shows the dependences of dimensionless phase velocity c and increment b on the wave length l. It can be seen that $l(c)$ is a two-valued function. It is known from the wave theory [4] that the interaction between the waves travelling at similar velocity can be more effective than between the waves with different velocities. So one can consider the mechanism of long-wave mode amplification which is in virtual resonance with the waves of maximum growth caused by velocities equality. Selection of a growing resonant mode is schematically shown on figure 1. It is important to note that the instability development time of the resonant mode is also less than t^*.

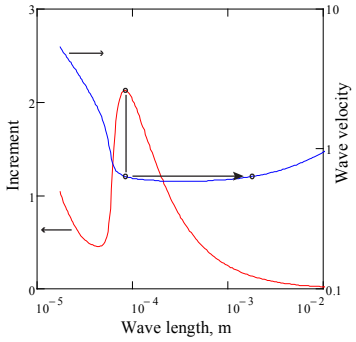

Figure 1 Dependences of dimensionless phase velocity and increment on the wave length. Selection of the resonant mode. CO2, steel 3mm, p=0.25MPa, Vcut = 53mm/s

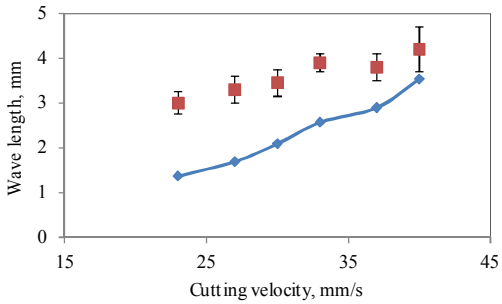

Figure 2 Theoretical (line) and experimental (dots) dependences of the wave length on the cutting velocity. CO2, steel 6mm, p=0.45MPa

We previously performed [5] the experimental study by optical correlation method of the waves on the melt surface in the process of laser cutting of steel sheets with thicknesses of 3 and 6 mm. The development of nonlinear waves with the length of 2–4 mm was discovered. The experimental dependences of wave lengths on the process parameters are similar to those calculated from the presented model, taking into account the assumptions made (figure 2).

So, the calculations performed show that long waves form on the melt surface during the laser cutting process, what is consistent with the experimental results.

Acknowledgements: The reported study was partially supported by RFBR, research project № 13-08-00987

[1] S. V. Alekseenko and V. E. Nakoryakov, Instability of a liquid film moving under the effect of gravity and gas flow, Int.J. of Heat and Mass Transfer, v. 38, pp. 2127–2134 (1995).
[2] J. C. Asali and T. J. Hanratty, Ripples generated on a liquid film at high gas velocities, International journal of multiphase flow 19.2: 229-243. (1993)
[3] K. Chen, Y. L. Yao, V. Modi, Gas jet–workpiece interactions in laser machining. Journal of manufacturing science and engineering 122.3: 429-438. (2000)
[4] G. B. Whitham, Linear and nonlinear waves (Vol. 42). (John Wiley & Sons). (2011).
[5] A.V. Dubrov, Yu. N. Zavalov, and V. D. Dubrov, Evaluation of Speed of Melt Evacuation in the Technology of Laser Cutting of Metals by the Optical Correlation Method, Technical Physics Letters, Vol. 40, No. 6, pp. 511–514, (2014)

Effect of high power CO_2 and Yb:YAG laser radiation on the characteristics of TIG arc in atmospherical pressure argon and helium

Shikai WU*, Rongshi XIAO

Institute of Laser Engineering, Beijing University of Technology, Beijing 100124, China

*Corresponding author. Email address: wushikai@bjut.edu.cn (Shikai. WU)

Abstract Laser hybrid welding is receiving intensive study all over the world because of its unparalleled advantages, and a profound understanding of the laser-arc interaction can further improve the processes. The effects of laser radiation on the characteristics of the DC tungsten inert gas (TIG) arc were investigated by applying a high power slab CO_2 laser and a Yb:YAG disc laser. Experiment results reveal that the arc voltage-current curve shifts downwards, the arc column expands, and the arc temperature rises while the high power CO_2 laser beam vertically interacts with the TIG arc in argon. With the increase of the laser power, the voltage-current curve of the arc shifts downwards more significantly, and the closer the laser beam impingement on the arc is to the cathode, the more the arc voltage decreases. Moreover, the arc column expansion and the arc temperature rise occur mainly in the region between the laser beam incident position and the anode. However, the arc characteristics seldom change in the cases of the CO_2 laser-helium arc and YAG laser-arc interactions. The reason is that the inverse bremasstrahlung absorption coefficients are greatly different due to the different electron densities of the argon and helium arcs and the different wave lengths of CO_2 and YAG lasers.

Key words: CO_2 laser, YAG laser, TIG arc, arc atmosphere, Arc Configuration, inverse bremsstrahlung absorption

High Fundamental Repetition Rate Fiber Laser Using a 45°-Tilted Fiber Grating

Zuxing Zhang, Chengbo Mou, Zhijun Yan, Kaiming Zhou, Lin Zhang, and Sergei Turitsyn
Aston Institute of Photonic Technologies, Aston University, Aston Triangle, Birmingham, United Kingdom, B4 7ET
z.zhang13@aston.ac.uk

Abstract: We demonstrate a high fundamental repetition rate erbium-doped fiber laser with all-fiber-integrated configuration. A novel scheme using a 45°-tilted fiber grating as in-fiber polarizing element is employed to increase the repetition rate of the fiber laser. Pulses with fundamental repetition rate of 245 MHz and pulse duration of 103 fs are achieved from the compact ring laser cavity.
OCIS codes: (060.3735) Fiber Bragg gratings; (140.3510) Lasers , erbium; (140.4050) Mode locked lasers

1. Introduction

High repetition rate femtosecond fiber lasers with the compact configuration and robust operation are in demand for applications in various fields, such as optical frequency metrology, high-speed optical sampling and telecommunication. A possible approach to reach higher repetition rate in passively mode-locked fiber lasers is harmonic mode locking, but the inherent timing jitter and accompanying power fluctuations make development of stable lasers a very challenging problem. It is desirable to operate laser at a high fundamental repetition rate by stringently controlling the cavity dimensions and gain fiber characteristics. High fundamental repetition rate fiber lasers have been demonstrated using semiconductor saturable absorber mirror (SESAM) [1], and single-wall carbon nanotube (SWCNT) [2]. However, the achieved pulse duration was at the picosecond scale. The nonlinear polarization evolution (NPE) technique does not require extra mode-locking elements inserted into the cavity making it possible to build a compact setup with high fundamental repetition rate.

The development of high fundamental repetition rate fiber lasers based on the NPE has attracted recently a great deal of attention. Taking the advantage of hybrid component, a 503 MHz fundamental repetition rate ytterbium-doped fiber laser incorporating a wavelength–division-multiplexing collimator was reported in [3]. A 234 MHz fundamental repetition rate erbium-doped fiber ring laser operated in strong normal dispersion regime using a polarization beam splitter as both the pump input coupler and the fiber laser output coupler was demonstrated [4]. However, these designs share the same feature that several free-space components are used inside the laser cavities, which is not desirable for a robust operation. Introducing highly-doped gain fiber, fundamental repetition rates up to 235 MHz in an Er^{3+}/Yb^{3+} co-doped phosphate glass fiber laser has been realized [5]. However, use of a gain fiber with high doping concentration and high gain coefficient greatly increases the cost. Here, we demonstrate the implementation of all-fiber-integrated high fundamental repetition rate fiber laser by using a 45°-tilted fiber grating as in-fiber polarizing element.

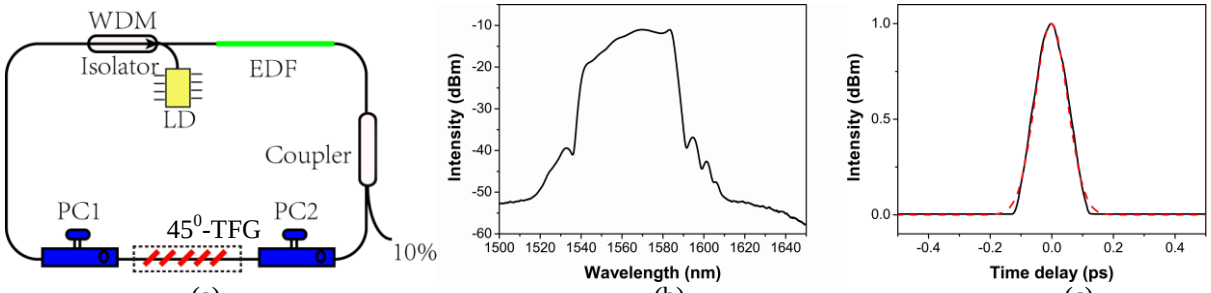

(a) (b) (c)

Fig. 1 (a) schematic of high fundamental repetition rate mode-locked erbium-doped fiber laser with polarizing fiber grating, (b) output optical spectra, (c) autocorrelation trace (black line) and its Gaussian fitting (red dotted line) after out-cavity compression.

2. Experimental setup and results

The all-fiber ring cavity is shown in Fig. 1(a). To minimize the cavity length, a 32-cm-long erbium-doped fiber (EDF) with group velocity dispersion (GVD) of about 69 ps^2/km at 1560 nm and peak absorption of around 150 dB/m at 1530 nm is used as the gain medium in the cavity. To simplify and shorten the cavity, a hybrid of polarization-insensitive isolator and wavelength-division multiplexer (WDM), is implemented. The pump laser at 976 nm, which is provided by two 976 nm laser diodes combined via a polarization beam combiner is injected into the pump port of the hybrid, and then reflected to the common port. A 90:10 fiber coupler is employed to tap 10% of laser power out of the cavity. Two in-line polarization controllers (PC) are used to adjust the polarization state of propagation light inside the cavity. The 45°-tilted fiber grating inscribed in a standard telecom fiber (SMF28) using the standard phase mask scanning technique and a 244 nm UV source from a CW

frequency doubled Ar^+ laser, is the key component to build a short, compact laser cavity. In principle, physics of operation is very similar to a pile of plate polarizer which based on the Brewster angle therefore radiating out s-light and preserving p-light for propagation [6]. In-fiber structure is a vital feature of the polarizing fiber grating, therefore its physical length inserted into the laser cavity can be very short. Beside the EDF, the rest standard single-mode fiber (SMF) inside the cavity including all fiber pigtails is ~0.51 m. The net GVD of the laser cavity is ~0.01 ps^2.

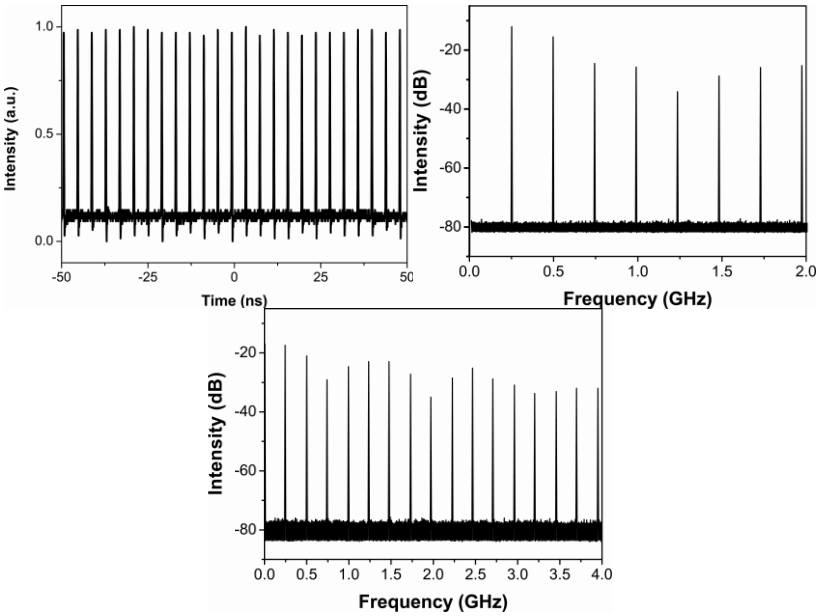

(a) (b) (c)

Fig. 2 (a) Output pulse train, measured RF spectra with 2-GHz span and 1-kHz resolution bandwidth (b) and with 4-GHz span and 3-kHz resolution bandwidth (c).

Adjusting the PCs at an appropriate state, self-start mode locking was achieved at a pump power of 710 mW. Once the mode-locked pulse has been generated, the laser is stable and the average output power is 23.2 mW. The optical spectrum of output pulse is shown in Fig. 1(b), having a 3-dB width of 40 nm. The output pulses were measured by an autocorrelator and the pulse duration after out-cavity compression with SMF is estimated to be 103 fs (assuming Gaussian fitting) as shown in Fig. 1(c), corresponding to a time-bandwidth product (TBWP) of 0.51. The output pulse train is also recorded by an oscilloscope, as shown in Fig. 2(a), and the time separation is 4.1 ns, which agrees with the corresponding number calculated using the cavity length. Figure 2(b) shows the radio frequency (RF) spectrum with a 2-GHz span and 1-kHz resolution bandwidth, and obviously the fundamental repetition rate is 245.3 MHz. The signal-to-noise ratio (SNR) is about 70 dB, indicating that the laser is operating with relatively low amplitude noise. A broader harmonics spectrum is also shown in the Fig. 2(c) with 4-GHz span and 1-kHz resolution bandwidth. A high signal-to-noise ratio is maintained at high harmonic repetition rate, although there appears slight modulation probably due to Q-switch instability. The laser is stable under laboratory condition for >24 hours. The repetition rate could be further enhanced though adopting gain fiber with higher doping concentration.

3. Conclusions

In conclusion, using a 45°-tilted fiber grating as a polarizing element we have implemented a novel high fundamental repetition rate fiber laser with all-fiber-integrated configuration. A fiber laser mode-locked at the fundamental rate generating 103-fs pulses at 245 MHz is demonstrated.

Support of the Marie Curie IIF project DISCANT is acknowledged.

4. References

[1] J. J. McFerran, L. Nenadović, W. C. Swann, J. B. Schlager, and N. R. Newbury, "A passively mode-locked fiber laser at 1.54μm with a fundamental repetition frequency reaching 2 GHz," Opt, Express 15, 13155-13166 (2007)

[2] A. Martinez and S. Yamashita, "Multi-gigahertzrepetition rate passively mode-locked fiber lasers using carbon nanotubes ," Opt, Express 19, 6155-25417 (2011)

[3] A. Wang, H. Yang, and Z. Zhang, "503MHz repetition rate femtosecond Yb:fiber ring laser with an integrated WDM collimator," Opt, Express 19, 25412-25417 (2011)

[4] L. M. Zhao, C. Lu, H.Y. Tam, P. K. A. Wai, and D. Y. Tang, "High fundamental repetition rate fiber lasers operated in strong normal dispersion regime," IEEE Photon. Technol. Lett. 21, 724-726 (2009)

[5] X. Wei, S. Xu, H. Huang, M. Peng, and Z. Yang, "Compact all-fiber ring femtosecond laser with high fundamental repetition rate," Opt, Express 20, 24608-24613 (2012)

[6] C. B. Mou, H. Wang, B. G. Bale, K. M. Zhou, L. Zhang, and I. Bennion, "All-fiber passively mode-locked femtosecond laser using a 45 degrees-tilted fiber grating polarization element," Opt. Express 18, 18906-18911 (2010)

Session
Poster I

Session Poster I : Tuesday 7th October : 16h45 – 18h15

S1-P1 : A. Potlov, Express inhomogeneity detection in turbid media

S1-P2 : L. Taskina, Quality assessment of fermented dairy products by Raman spectroscopy

S1-P3 : M. Pietrus, Ethylene and ammonia traces measurements from healthy humans with different diets by LPAS technique

S1-P4 : M. Veres, Surface-enhanced Raman spectroscopy of carbon-based nanomaterials

S1-P5 : E. Axente, Compositional analyses of indium zinc oxide thin films by spectroscopic techniques

S1-P6 : C. Shakher, Digital Holographic Interferometry for Measurement of Natural Convective Heat Transfer Coefficient Along the Surface of Heated Wire

S1-P7 : E.A. Obraztsova, Optical Spectroscopy of Sulfur-Doped GaSe Crystals

S1-P8 : S. Kutrovskaya, Laser formation of collodial alloys of the noble nanoparticles and deposition of the microclusters on the glass substrate

S1-P9 : A. Antipov, Investigation of laser-induced hydrodynamic processes at laser ablation materials in liquid

S1-P10 : G. Shandybina, Accumulation effects during femtosecond laser microstructuring of monocrystalline silicon surface

S1-P11 : P. Lorenz, Generation of mechanical and electrical interconnection of micro devices by laser embossing of undercut structures

S1-P12 : S. Zabotnov, Femtosecond Laser Fabrication of Silicon Nanocrystal Ensembles for Bioimaging and Solar Energy

S1-P13 : K. Allakhverdiev, Confocal Raman, PL, and Fluorscence Lifetime Imaging Microscopy of Gallium Selenide Crystals – an Outstanding NLO Material

S1-P14 : A. Mouskeftaras, Space-time study of microplasmas inside semiconductors

S1-P15 : V. Mazhukin, Overheated metastable states in metals irradiated by pulsed laser

S1-P16 : Bin Liu, Pre-processing of corrugated and porous metal surfaces by picosecond laser irradiation for thermal spraying

S1-P17 : M. Boudhib, Analysis of aerosols via calibration-free laser-induced breakdown spectroscopy

S1-P18 : A. Nagy, Classification of aerosol particles by laser light scattering

S1-P19 : N. Fedorov, Femtosecond laser impact ionization of quartz

S1-P20 : S. Guizard, Femtosecond laser induced modification of dielectric materials: Experimental investigation of fundamental mechanisms

S1-P21 : D. Zadorin, Synthesis of silicon nanoparticles by pulsed laser ablation in organic liquids

S1-P22 : K. Viskontas, Criteria for Widely Tunable and Long-Term Operation of Mode-Locked All-Fiber Oscillator

S1-P23 : N. Kozlova, The influence of thermal treatment on the luminescence of lanthanum – gallium tantalate crystals

S1-P24 : O. Egorova, Er-Yb co-doped cladding pumped fiber laser with phosphate core and silica cladding

S1-P25 : A. Brenier, Active Q-switching of the dual-wavelength Nd:$YGd_2Sc_2Al_2GaO_{12}$ ceramic laser

S1-P26 : D. Grojo, Bessel-like photonic nanojets from engineered nanospheres for the fabrication of ultra-high-density porous membranes

S1-P27 : I. Ivascu, Photoacoustic Detection of Air Pollutants within Urban Area

S1-P28 : Yu. Morozov, Intracavity singly-resonant OPO pumped by GaSb-based semiconductor disk laser

S1-P29 : M. Kuzmina, Joint Influence of Cubic Nonlinearity and Thermally Induced Birefringence on the Radiation Polarization in High Peak Power Lasers

EXPRESS INHOMOGENEITY DETECTION IN TURBID MEDIA

A. Potlov, S. Proskurin

Tambov State Technical University
106 Sovetskaya St, Tambov, Russia
spros@tamb.ru

A method for rapid detection of absorbing inhomogeneity in a strongly scattering medium having the properties of a biological tissue before the image reconstruction is described based on the principles of diffuse optical tomography [1]. The method is based on preliminary processing of a three-dimensional surface obtained from the set of time-resolved data in the Cartesian coordinate system, followed by its conformal transformation into two surfaces in the cylindrical coordinate system. A specific feature of the method is the use of late-arriving photons, scattered and diffusely transmitted through an optically turbid object. The method includes the following steps: (I) LAP each TPSF standardized to LAP of TPSF for minimum angle; (II) the resulting normalized function approximated by straight lines; (III) based on LAP of TPSF for minimum angle built reference function; (IV) normalized function is modified (increasing or decreasing of curvature) with the additional factor of display; (V) performed the transition from the Cartesian coordinates to the cylindrical coordinates and the resulting functions are visualized. This method has been implemented as a specialized software product in LabVIEW programming environment. The results of its work for the homogeneous and inhomogeneous cases are shown in Figure 1a and 1b, respectively.

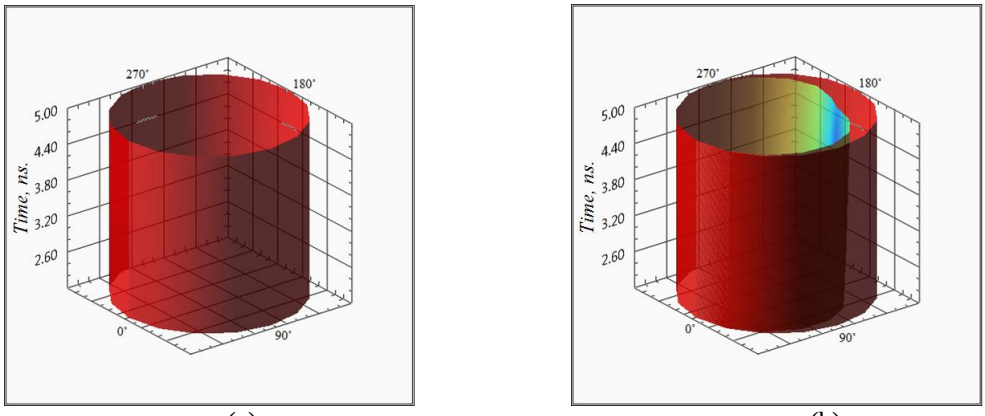

(a) (b)

Figure 1 Three-dimensional representation of the TPSF in a cylindrical coordinate system for the homogeneous (a) and inhomogeneous (b) cases

This approach is simple and reliable, and particularly suitable to visualization relatively large inhomogeneities (about 20 mm in diameter). This is generally corresponds to many clinical cases, since the region of angiogenesis (pathological formation of new blood vessels) that surrounds a real tumor a few millimeters in diameter has the size of a few centimeters. Due to the fact that the absorption coefficient of blood and tumor is significantly higher than in normal tissues, they will be as single relatively large pathological inhomogeneity for the DOT system [2].

The proposed method can be used in time-resolved DOT for express detection [3] of hematoma, tumors, cysts, etc. in the diagnostics of brain structures (and, optionally, in yet another promising application of DOT - mammography diagnostics). Conformal mapping LAP of TPSF in a cylindrical coordinate system does not require high-performance computing and works in real time mode.

[1] S.G. Proskurin, A.Yu. Potlov, S.V. Frolov Detection of an absorbing heterogeneity in a biological object during recording of scattered, Biomedical Engineering, Vol. 46, №6, pp.219-223, (2013)
[2] A.Y Potlov., S.G. Proskurin, S.V. Frolov Three-dimensional representation of late arriving photons for the detection of inhomogeneous in diffuse optical tomography, Quantum Electronics, Vol. 44, №2, pp. 174–181, (2014)
[3] S.G. Proskurin, A.Y. Potlov Early- and late-arriving photons in diffuse optical tomography, Photonics & Lasers in Medicine, Vol.2, Iss.2, pp. 139-146, (2013)

Quality assessment of fermented dairy products by Raman spectroscopy

Timchenko E.V.[1], Taskina L.A.[1], Rodina A.V. [1], Tregub N.V. [1]

[1] *S.P. Korolyov Samara State Aerospace University (National Research University)*

Vorobjeva.82@mail.ru, retuo@mail.ru

An important component of the diet for average healthy person is a dairy product. The dairy products are complex medium, which mainly consist from water, protein, carbohydrates, fats and numerous other trace elements. Due to molecular structure, intra-and intermolecular interactions in food medium, the physicochemical properties of these components define the final characteristics of food product [1].

The food quality assessment includes the chemical, biological and microbiological factors such as the food medium instability, related with irreversible chemical and enzymatic reactions, as well as the processes of vital activity of bacteria, which influence at product shelf life.

This paper presents the experimental study results for quality control of dairy product with different fat content and various manufacturers using Raman spectroscopy. The investigated food products throughout the entire experiment were isolated in refrigerating chamber, where a temperature conditions were constant (+4 ÷ -6 ^{0}C). Raman spectroscopy has been implemented by a high-resolution digital spectrometer Shamrock sr-303i (focal length of 303 mm) with ANDOR DV-420A-OE integrated digital camera (1024*256). 785 nm laser source was used for excitation of Raman spectrum. This system provides a spatial resolution up to 1 mm. Registration error was +0.2 nm. The processing of Raman spectra was calculated by «Wolfram Mathematica»'8 tool.

The research results are the following:

1) Raman spectra features of dairy products with different manufacturers and different fat content were obtained;
2) The results of spectral characteristics for dairy products with different types of food excipients were presented;
3) The intensity increase of bands 1060 cm^{-1} and 1443 cm^{-1} in process of "souring" milk products was observed. This observation is corresponds of symmetric stretching ν (C–C) in fatty acids and vibration CH^2 groups, respectively. Also, there was a significant intensity decline of bands 634, 1005 cm^{-1}.

[1] S. Gallier, K.C. Gordon, R. Jiménez-Flores, D.W. Everett, Composition of bovine milk fat globules by confocal Raman microscopy, International Dairy Journal, 21, 402-412, (2011).

Ethylene and ammonia traces measurements from healthy humans with different diets by LPAS technique

M. Petrus[1], C. Popa[1,2], A.M. Bratu[1], C. Matei[1,2], M. Patachia[1], S. Banita[1] and D.C. Dumitras[1]

1- Department of Lasers, National Institute for Laser, Plasma and Radiation Physics, 409 Atomistilor St., PO BOX MG-36, 077125, Bucharest, Romania

2 - University POLITEHNICA of Bucharest, 313 Splaiul Independentei St., Bucharest, Romania

e-mail: mioara.petrus@inflpr.ro

Exhaled breath is a mixture of more than a thousand molecules, some of which are present at parts per billion (ppb) or even parts per trillion (ppt) concentration levels [1]. These molecules provide a unique breath profile of the health condition and have endogenous and exogenous origins. The sources of endogenous molecules are normal and abnormal physiological processes, whereas the sources of exogenous molecules are: inspiratory air, ingested food and beverages, or any exogenous molecule that has entered the body by other routes (e.g. dermal absorption) [2]. The concentrations of some of the exhaled molecules can be used as biomarkers for the identification and monitoring of human diseases or wellness states [3].

Laser photoacoustic spectroscopy (LPAS) [4,5] is a fast and precise technique of breath biomarkers measurements. Laser Photoacoustic Spectroscopy method (LPAS) is a very powerful investigation technique which is capable of measuring trace gas concentration at sub ppb level [4,5].

We determined the ethylene and ammonia concentration in healthy humans with different diets (mixed, vegetarian, raw vegan [6] and Dukan [7] diet). Analysis of ethylene and ammonia traces from the human breath may provide information about the severity of oxidative stress and metabolic disturbances in the human body. Ethylene from human breath is a biomarker of oxidant stress and can be directly attributed to biochemical events surrounding lipid peroxidation [8]. Lipid peroxidation is the free-radical-induced oxidative degradation of polyunsaturated fatty acids, where biomembranes and cells are thereby disrupted, and causing cell damage and cell death. Ammonia is the natural by-product of protein metabolism, and is associated with several important disease states. Since protein metabolism is fluid and changeable based on many factors (e.g., recent food consumption, exercise, medications, pH, etc), ammonia levels are dynamic, and this likely leads to pathogenic consequences in some conditions (e.g., liver cirrhosis) [2].

Ethylene and ammonia were measured using LPAS method on a group of healthy subjects with different diets (mixed, vegetarian, raw vegan and protein diet). The measurements of ammonia were in the range 72 – 3500 ppbV and ethylene in the range 39.3 – 1080 ppbV. We observe a significant variation of ethylene concentration in subjects with variation of diet (mixed diet to raw vegan diet and mixed diet).

Our measurements were performed to observe the behavior of the human organism to different diets. Breath test is noninvasive, easily repeated, and does not have the discomfort or embarrassment associated with blood tests. LPAS system is a fast and sensitive trace gas detector and will play an important role in exhaled breath analysis. Measurements of human biomarkers in exhaled breath using LPAS method technique capable of measuring trace gas concentration at sub ppb level, promise to revolutionize the manner in which diagnostics are carried out today and may soon lead to rapid diagnostics.

[1] R. A. Dweik, A. Amann, "Exhaled breath analysis: the new frontier in medical testing", Journal of Breath Research 2(3), (2008)
[2] T. H. Risby, S. F. Solga, "Current status of clinical breath analysis", Applied Physics B: Lasers and Optics 85, 421- 26, (2006)
[3] T. Risby, F. K. Tittel, "Current Status of Mid-Infrared Quantum and Interband Cascade Lasers for Clinical Breath Analysis", Optical Engineering 49(11), 000000-1 (2010).
[4] R. Cernat, C. Matei, A.M. Bratu, C. Popa, D.C.A. Dutu, M. Patachia, M. Petrus, S. Banita, D.C. Dumitras, "Laser photoacoustic spectroscopy method for measurements of trace gas concentration from human breath", Rom. Rep. Phys, 62 (3): 610-616 (2010).
[5] C. Popa, D.C.A. Dutu, R. Cernat, C. Matei, A.M. Bratu, S. Banita, D.C. Dumitras, "Ethylene and ammonia traces measurements from patients' breath with renal failure via LPAS method", Appl. Phys. B, 105:669-674 (2011)
[6] http://www.vegan-raw-diet.com/
[7] http://www.hivehealthmedia.com/skinny-french-dukan-diet/
[8] G.J. Handelman, Blood Purif., Karger Publication, 21 (46) (2003).

Surface-enhanced Raman spectroscopy of carbon-based nanomaterials

M. Veres, L. Himics, S. Tóth, M. Koós, A. Nagy, D. Oszetzky, A. Kerekes, Sz. Kugler, A. Czitrovszky

Wigner Research Centre for Physics, Hungarian Academy of Sciences, PO Box 49., Budapest, Hungary, H1525
veres.miklos@wigner.mta.hu

During the last decades from an exotic, rarely used experimental technique Raman spectroscopy was turned into a mainstream materials characterization tool. In addition to the novel coherent light sources and developments in optical, detection and data processing equipment, the discovery of novel Raman spectroscopic methods was the main driving force of this success. Special techniques, like resonant, surface-enhanced, tip-enhanced or spatially offset Raman scattering increase the sensitivity of the method to the detection of single molecules and its spatial resolution well below the diffraction limit – to the nanometer scale.

Surface-enhanced Raman spectroscopy (SERS) utilizes the amplification of Raman scattering by a factor of 10^{10}–10^{11}. This is achieved by the local enhancement of the electromagnetic field of the exciting and/or scattered light through surface plasmons excited on the surface of metal nanoparticles or nanostructures.

The high sensitivity of SERS can be utilized in materials characterization, including carbon-based nanostructures. It can provide information on the local structure and structural transformations, impurities, surface structure of nanoparticles and thin films. We have used SERS in different configurations to study carbon-based nanomaterials including amorphous carbon thin films, nanocystalline diamond, nanotubes, polymers and graphene. SERS-active agents in form of gold nanoparticles, nanostructured gold films and patterned surfaces were tested with different excitation energies. The enhancement of the different agents was tested on polymeric nanoparticle model material. In addition, correlations between the SERS spectra and the sample parameters were determined. Comparison of the information on bonding configuration of the surface, provided by SERS, with that of the bulk, obtained by normal Raman spectra allows to study the structural differences of the two regions.

Compositional analyses of indium zinc oxide thin films by spectroscopic techniques

E. Axente[1], J. Hermann[2], G. Socol[1], C.R. Luculescu[1], A.C. Galca[3], D. Pantelica[4], and V. Craciun[1]

1- Laser-Surface-Plasma Interactions Laboratory, National Institute for Lasers, Plasma and Radiation Physics, RO - 077125, Măgurele, Romania
2- LP3, CNRS - Aix-Marseille University, Luminy, Marseille, France
3- Laboratory of Multifunctional Materials and Structures, National Institute of Materials Physics, RO - 077125, Măgurele, Romania
4- National Institute of Physics and Nuclear Engineering Horia Hulubei, RO - 077125, Măgurele, Romania

emanuel.axente@inflpr.ro

Flexible and transparent electronics, solar cells and sensors are among the most promising potential applications for amorphous oxides. Recently, high quality amorphous indium zinc oxide (IZO) thin films deposited by pulsed laser deposition exhibited optical transmittance higher than 85%, resistivities of about 5-7×10^{-4} Ω cm and electron mobilities in the 47-54 cm^2/V s range [1]. Since the optical and electrical properties, as well as the cost of these films depend on the In/(In+Zn) values, the growth of films with variable composition, is paramount for optimization studies and for further developments. However, due to materials complexity, the conventional "step by step" analyses are time consuming and expensive. A viable solution to overcome these drawbacks would be the thin films synthesis by a combinatorial approach. Here, Combinatorial Pulsed Laser Deposition technique was used for the synthesis of IZO compositional libraries in a single-step process [2].
Calibration-free Laser-Induced Breakdown Spectroscopy was chosen for the monitoring of the thin films elemental composition, in view of further *in-situ* and real-time technological developments and process control in case of amorphous oxides fabrication. Indeed, in addition to sampling flexibility in terms of size and shape of the sample to be analyzed, LIBS investigations could be performed in ambient air, at atmospheric pressure [2].

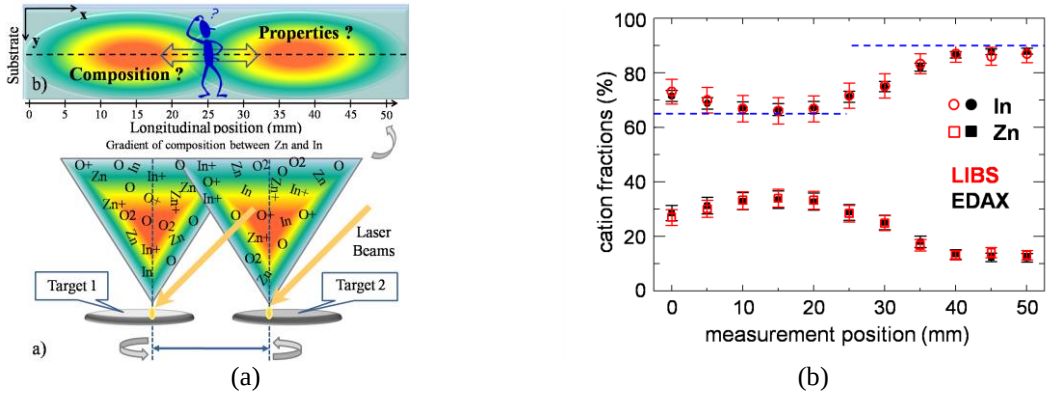

(a) (b)

Figure 1 (a) Schematic representation of the combinatorial pulsed laser deposition setup. The analyses were performed in eleven discrete measurements positions along the longitudinal direction of the sample as shown by the dashed line (b) atomic fractions measured by LIBS (empty red symbols) and EDAX (filled black symbols) along the longitudinal direction of the sample.

The results were compared to values obtained by complementary techniques using energy dispersive X-ray spectroscopy, spectroscopic ellipsometry, X-ray fluorescence and Rutherford backscattering spectrometry. A good agreement between LIBS and EDAX results has been obtained, the LIBS measurement accuracy being estimated to 5%. Complementary measurements using XRF and RBS have been performed in view of samples homogeneity investigations and elemental concentration validation. Our results demonstrated that LIBS analysis based on plasma modeling has great potential in view of further implementation as an efficient inspection tool during amorphous oxides fabrication.

[1] G. Socol, M. Socol, N. Stefan, E. Axente, G. Popescu-Pelin, D. Craciun, L. Duta, C.N. Mihailescu, I.N. Mihailescu, A. Stanculescu, D. Visan, V. Sava, A.C. Galca, C.R. Luculescu, V. Craciun, Applied Surface Science 260, 42 (2012).
[2] E. Axente, J. Hermann, G. Socol, L. Mercadier, S. A. Beldjilali, M. Cirisan, C. Luculescu, C. Ristoscu, I. Mihailescu and V. Craciun, J. Anal. At. Spectrom., 29 (3), 553 – 564, (2014).

Digital Holographic Interferometry for Measurement of Natural Convective Heat Transfer Coefficient Along the Surface of Heated Wire

Varun Kumar[1], Manoj Kuamr and Chandra Shakher*

Laser Applications and Holography Laboratory, Instrument Design Development Centre, Indian Institute of Technology Delhi, Hauz Khas, New Delhi -110016

[1]varunphy@gmail.com, * cshakher@iddc.iitd.ac.in

Measurement of temperature profile around axisymmetric objects such as cylinders, and the measurement of local heat transfer coefficient has been investigated extensively [1]. It is useful in industry to investigate the flow performance in cylindrical channels, and measurement of temperature profile in and around the gaseous flame of burners. Numbers of methods like classical interferometry, shearing interferometry, holographic interferometry, moiré deflectometry, laser speckle technique, Talbot interferometry and Lau phase interferometry have been investigated and well developed and are being widely used for measurement of temperature field. Recently digital holographic interferometry (DHI) has been studied for measurement of temperature in gaseous flames [2-10].

This paper presents measurement of local convective heat transfer coefficient (h) along the surface of electrically heated vertical wire using digital holographic interferometry. Experimental results are presented for different heating conditions of wire. The results indicate that the local convective heat transfer coefficient decreases as height increases from bottom to top of wire due to the growth of thermal boundary layer. DHI is more precise, accurate and robust technique in comparison to other interferometric techniques because both amplitude and phase can be calculated from single digital hologram.

[1] W. Hauf, and U. Grigull, Optical Methods in Heat Transfer, in Advances in Heat Transfer, (Academic Press, New York 1970).
[2] D. Wilkie and S. A. Fisher, Measurement of temperature by Mach-Zehnder interferometry, Proc. Inst. Mech. Eng. 178, pp. 461–472, (1963).
[3] Priti Singh, Mohd. Shoeb Faridi and Chandra Shakher, Measurement of temperature of an axisymmetric flame using shearing interferometry and Fourier fringe analysis technique", Optical Eng. **43**, pp. 387-392 (2004).
[4] D. L. Reuss, Temperature measurement in a radially symmetric flame using holographic interferometry, Combust. Flame, **49**, pp. 207–219, (1983).
[5] C. M. Vest, *Holographic Interferometry*, (John Wiley & Sons, New York 1979).
[6]E. Bar-Ziv, S. Sgulim, O. Kafri, and E. Keren, Temperature mapping in flames by moire deflectometry, Appl. Opt. **22**, pp. 698-705, (1983).
[7] C. Shakher and A. K. Nirala, Measurement of temperature using speckle shearing interferometry, Appl. Opt. **33**, pp. 2125–2127, (1994).
[8]C. Shakher and A. J. P. Daniel, Talbot interferometry with circular grating for the measurement of temperature in axisymmetric gaseous flames, Appl. Opt. **33**, pp. 6068–6072, (1994).
[9] M. Thakur, A. L. Vyas, and C. Shakher, Measurement of temperature and temperature profile of an axisymmetric gaseous flames using Lau phase interferometer with linear grating, Opt. Lasers Eng. 36, pp. 373–380, (2001).
[10] S. Sharma, G. Sheoran, and C. Shakher, Investigation of temperature and temperature profile in axi-symmetric flame of butane torch burner using digital holographic interferometry, Opt. Lasers Eng. **50**, pp. 1436-1444, (2012).

Optical Spectroscopy of Sulfur-Doped GaSe Crystals

E.A.Obraztsova[1,2,3], K.A. Kokh[4,5,6], V.V. Atuchin[5,6,7], E.D. Obraztsova[2]

[1]- M.M. Shemiakin & Yu.A.Ovchinnikov Institute of Biooganic Chemistry, RAS
[2]- A.M.Prokhorov General Physics Institute, RAS
[3]- National University of Science and Technoligy "MISIS"
[4] – Sobolev Institute of Geology and Mineralogy, SB RAS, Novosibirsk, Russia
[5]- Novosibirsk State University, Novosibirsk 630090, Russia
[6]- Tomsk State University, Tomsk 634050, Russia
[7]- Institute of Semiconductor Physics, SB RAS, Novosibirsk 630090, Russia

Gallium selenide is a layered chalcogenide semiconductor crystal. Each layer of GaSe consists of four monoatomic sheets of Se-Ga-Ga-Se atoms. Inside such tetralayers, Ga and Se atoms are bonded covalently. The tetralayers are connected predominantly by van der Waals forces, so the interlayer coupling is relatively weak.

GaSe crystal is an excellent material for non-linear optical applications due to its structural, electronic and optical properties. In this work we have studied the optical and electronic properties of GaSe crystals doped by sulfur atoms in order to controllably tune its bandgap.

Typical Raman spectra of the gallium selenide crystals with the increasing amount of sulfur are shown in Fig.1. Introduction of sulfur leads to widening and shift to higher frequencies of the Raman bands. It can be explained by increasing number of defects in the resulting structure.

In the same time fluorescence emission spectra demonstrated in Fig.2 show a clear shift to the higher frequencies from 620 nm (for the initial GaSe crystals) to approximately 550 nm (for the material containing 11% of sulfur atoms).

We have thus demonstrated modification of the optical properties of gallium selenide crystals by a Se/S substitution. Previously the sulfur doping was demonstrated to lead to improvement of other physical properties of these crystals. We expect that our approach is an easy and efficient way to tune the optical properties of GaSe.

This work was supported by the RF president grant for young researchers MK-6201.2014.2, grant of Russian ministry of science and education G3431.0061 and by RAS research programs.

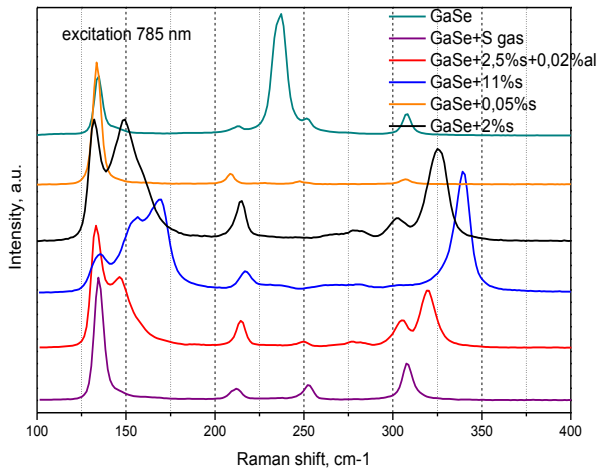

Figure 1. The Raman spectra of GaSe crystals with an increasing amount of sulfur introduced (0,05%, 2%, 2,5%, 11% and of a low-doped sample obtained by a gas-phase doping). The excitation wavelength 785 nm

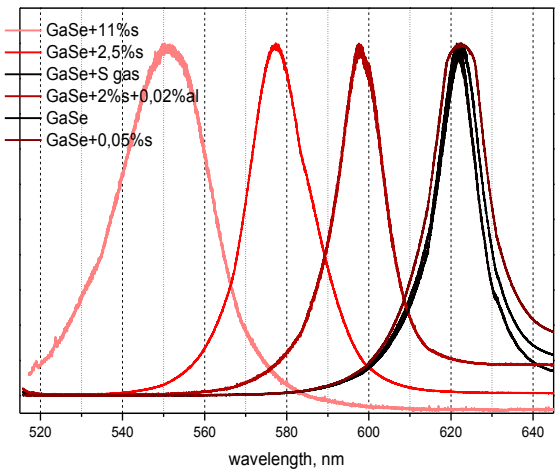

Figure 2. The fluorescence emission spectra of GaSe crystals with an increasing amount of sulfur introduced (0,05%, 2%, 2,5%, 11% and low-doped sample obtained by gas-phase doping).

Laser formation of collodial alloys of the noble nanoparticles and deposition of the microclusters on the glass substrate

A. Antipov[1], S. Arakelian[1], S. Kutrovskaya[1], A. Kucherik[1], T. Itina[2]

[1]*Department of Physics and Applied Mathematics, Stoletovs' Vladimir State University,*

Gorky st. 87, Vladimir, 600000 Russia

Phone: +7(4922) 479621

Fax: +7(4922) 333369

E-mail: 11stella@mail.ru

[2] *Hubert Curien Laboratory Bat. F, 18 rue Benoit Lauras, 42000, Saint-Etienne, France*

tatiana.itina@gmail.com

Laser ablation of solid targets in the liquid medium widly used method for fabrication nanostructures with various compositions such as metals, alloys, oxides, carbides, hydroxides, etc. At the same time a great advantage of the method is the possibility to re-irradiate the suspended nanomaterials that can be applied to further modify their size, shape, and composition. In the past two decades, with the rise of nanoscience, laser ablation has been broadly applied and developed for the synthesis of noble metal nanostructures such as gold (Au), silver (Ag), platinum (Pt) and palladium (Pd) or their alloys. Bimetallic structures of these metals have improved physical and chemical stability and selectivity compared with isometric structures. The bimetallic complex is related to change the optical properties, in particular transmission and absorption, depending on the nanoparticles (NPs) size and composition. Separate direction of controlling the optical properties of such nanostructures formation of clusters with variable morphology.

Promising method of obtaining bimetallic clusters is the laser formation of colloidal alloys. In this work we used two different schemes of laser ablation in liquid (water, ethanol, etc.):

a) Au, Ag colloidal systems formation were obtained by CW-laser (λ = 1.06 μm, I ~ 10^6 W/cm^2, t =10 min). (λ = 1.06 μm, I ~ 10^6 W/cm^2, t =10 min). Particle size in the colloidal solution is approximately 8 nm. After that, two colloidal systems were mixed and NPs were deposited on the SiO_2 substrate by 2 different methods: LDNC and droplet deposition with pinning effect.

b) the Au target was irradiated by the fs-laser (λ = 1.06 μm, I ~ 10^{13} W/cm^2, t=1 min), after that, Ag-target was placed into the Au NPs colloidal system and irradiated. In the result, the colloidal system with Au-Ag (100 nm) clusters was formed.

The morphological properties of deposited nano-clusters were investigated using atomic force microscopy (AFM) and scanning electron microscopy (SEM). It was found that the transmission spectra of the resulting structures depend on the concentration of gold and silver nanoparticles in the colloidal solution.

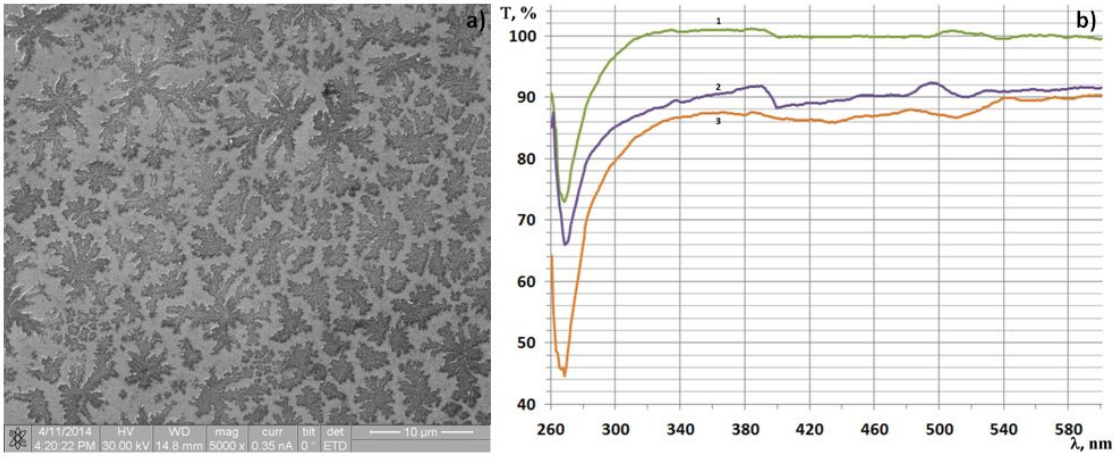

Figure 1 REM-images of deposited bimetal cluster (a) and Transmission spectra of deposited cluster for various mass ration of Au and Ag particles in colloidal solution: 1- 1(Au):1(Ag); 2 -1:3;; 3 - 3:1.

Investigation of laser-induced hydrodynamic processes at laser ablation materials in liquid

A. Antipov[1], S. Arakelian[1], S. Kutrovskaya[1], A. Kucherik[1], A. Osipov, T. Itina[2]

[1]*Department of Physics and Applied Mathematics, Stoletovs' Vladimir State University,*

Gorky st. 87, Vladimir, 600000 Russia

Phone: +7(4922) 479621

Fax: +7(4922) 333369

E-mail: 11stella@mail.ru

[2] *Hubert Curien Laboratory Bat. F, 18 rue Benoit Lauras, 42000, Saint-Etienne, France*

tatiana.itina@gmail.com

Laser ablation in liquids is a perspective method of forming nanoparticles. Morphologies properties of the nanoparticles are producing during the laser ablation of solids in liquids, depending on many parameters (laser wavelength, pulse duration, the energy density of the beam on the target, a kind of fluid, etc.). Short and ultrashort pulse duration lasers are usually used for the material ablation. In this case the cluster formation processes is significantly enhanced, at the same time to the material ejection mechanism in the liquid volume the shock waves action is added, which changes the distribution function of particles size. Furthermore laser ablation by nanosecond pulse duration melts target surface, which leads to emission in the volume of the colloid liquid droplets of the melt. When the femtosecond laser radiation is used a significant effect on the particle distribution function has a secondary fragmentation of particles. Due to the interaction of laser radiation with a liquid supercontinuum is observed which leads to the effective absorption of laser radiation which is realized for the particles with different diameters.

The paper presents the results of investigation of the formation of noble metal nanoparticles when irradiated to continuous/quasi-continuous laser radiation of moderate intensity of metal targets (Au, Ag) placed in the liquid. By using diagnostic system - "laser monitor" of laser -induced gas-hydrodynamic processes studied in real-time scale. The formation of convective flows and the formation of gas bubbles were observed. The dependence of the particle sizes on the conditions of laser radiation and selection of the liquid phase is demonstrated.

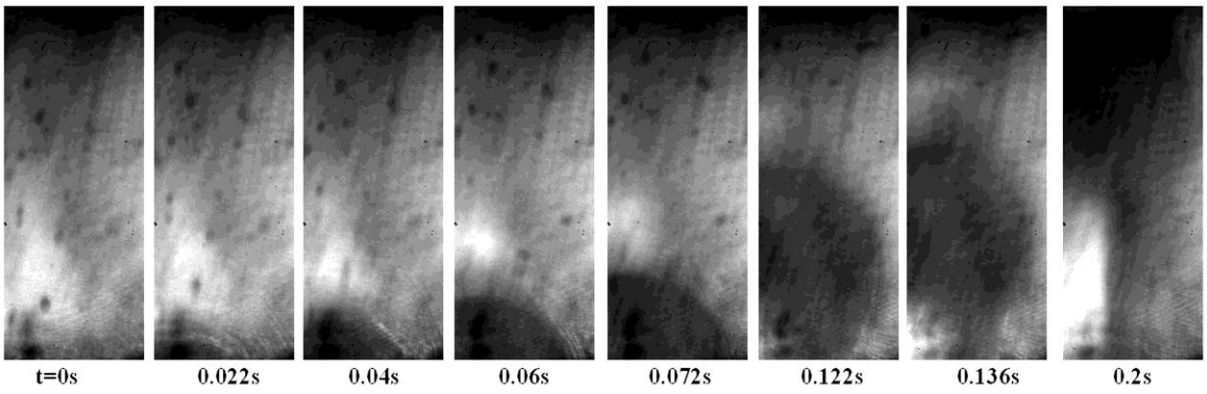

Figure 1 Images by "laser monitor" demonstrated the process of the gas bubble formation in glycerin by irradiation of ms-laser radiation with pulse duration 20ms and energy 0.5J

Accumulation effects during femtosecond laser microstructuring of monocrystalline silicon surface

I. Guk, G. Shandybina, E. Yakovlev

ITMO University. 49 Kronverksky pr., 197101 St.Petersburg, Russia

email:corchand@gmail.com

During laser processing of materials usually multi-pulse regime is used, as the most productive. The effect of heat accumulation from pulse to pulse can play important role in the final result. Study of accumulation effects in femtosecond laser technology of microstructuring of semiconductors is of particular interest. Since electronic processes and processes in lattice subsystem is divided by time, the accumulation effects can have different nature and affect each other. Moreover form experimental data it is known, that the pulse repetition rate in different regimes of femtosecond laser structuring vary over a wide range of 10 Hz to 80 MHz.

In the report the results of quantitative evaluations of accumulation effects during femtosecond laser structuring of silicon surface are presented for discussion. The calculations used numerical-analytical method, in which the dynamics of electronic processes and the lattice heat are simulated by numerical method, and cooling stage is described on the basis of analytical solution. This method significantly reduces the time required for the calculations.

There is used a numerical model of femtosecond excitation of silicon [1], in which the spatial and temporal variations in the concentration of nonequilibrium carriers is determined by two-photon absorption of light quanta, carrier diffusion, their thermalization due to electron-electron collisions and external electron emission. Heating model is based on the two-temperature model, which takes into account the change of the heat capacity of the electron gas.

It is assumed that accumulation effect is due to the change of the absorption coefficient from pulse to pulse due to the processes of transformation of the band structure stimulated by local heating.

In the lattice subsystem accumulation effect is associated with the surface component of the absorptivity. Strengthening of its contribution is due to the fact that during the regimes of microstructuring, excitation of the surface polaritons reduces reflectivity and increases from pulse to pulse the transformation coefficient of the incident wave into surface.

The calculation results were compared with experimental data on femtosecond microstructuring of silicon. The important role of the surface component of the absorptivity and the relations between the accumulation effect, flux density and repetition rate of femtosecond pulses is shown.

[1] R. Dyukin, G. Martsinovskiy, O. Sergaeva, G. Shandybina V. Svirina, E. Yakovlev, In book Laser Pulses – Theory, Technology and Applications, ed. by I. Peshko, Chapter 7, Rijeka: InTech, pp. 197-218, 2012.

[2] M. Libenson, V. Makin, S. Pudkov, Surface electromagnetic waves in optics, L.: LHSTP, 24 p, 1990.

Generation of mechanical and electrical interconnection of micro devices by laser embossing of undercut structures

M. Ehrhardt, P. Lorenz, J. Zajadacz, L. Bayer, R. Fechner, K. Zimmer

1- Leibniz-Institute of Surface Modification, Permoserstr. 15, D-04318 Leipzig, Germany

klaus.zimmer@iom-leipzig.de

Localised mechanical and electrical connections of micro devices without thermal loading have great importance in various sectors of micro technology. Micro structures with undercuts in combination with moulding are promising approaches to realize interlocking components that enable a tight fit at the micron level. In precede published paper (e.g.[1]) it has been shown that dovetail-like structures prepared from Si which were filled with PDMS (polydimethylsiloxane) by moulding are able to generate a geometric interlocking between two parts of micro systems components. The force required for separation was evaluated quantitatively; it amounts from 13.7 N to 30.2 N for the 2 x 2 cm² undercut geometries. Although this techniques works well further optimisation for specific applications are required. Special requirements are for example to generate a joint between two micro systems component with a size of tens of micrometer with a specific geometry at a specific point at the micro systems. Additional, demands are e.g. to produce a mechanical interlock with an electric conductive materials.

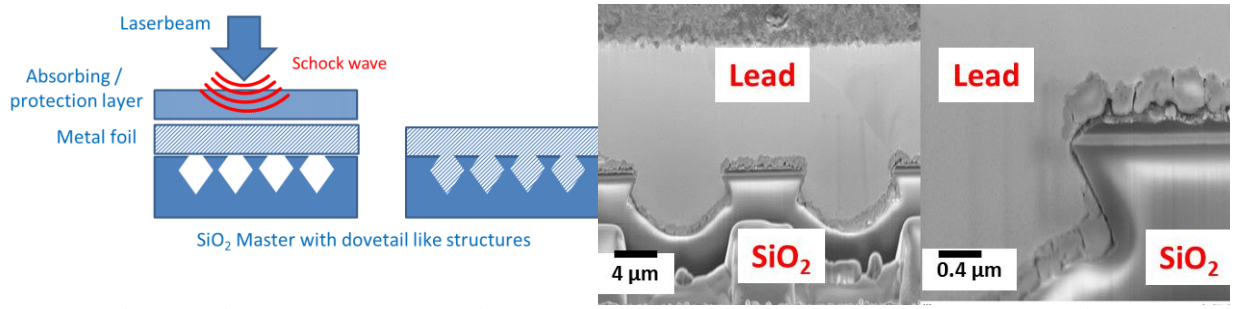

Figure 1 (left) Sketch of the laser embossing process for the geometrical interlocking of a dovetail-like structure with a lead foil. (right) SEM image of cross section of a dovetail-like structured which is interconnected with a lead foil due to the laser embossing process.

In the present study it will be shown that laser embossing is a promising technique to fulfill these requirements. Laser embossing is none thermal laser process which uses laser induced shock wave for forming of ductile materials like lead or copper [2]. A KrF Laser (wavelength 248 nm, pulse duration 25 ns) was used to emboss lead foils into dovetail-like structures prepared from SiO_2. The dovetail-like structures were generated by a special reactive ion beam etching process [3].
After the laser embossing process the generated join was investigated with scanning electron microscope in combination with focused ion beam (FIB) in order to investigate the embossing quality in dependency of the laser parameter used. In order to characterise the embossing process the laser induced shock wave pressure are correlated with the laser parameter used.

[1] Zajadacz, J., et al., Measurement and simulation of the pull-off strength at the separation of miniaturized 3D connectors consisting of silicon masters with undercuts and PDMS replicas. Microelectronic Engineering, 2013. 101: p. 31-36.
[2] Ehrhardt, M., P. Lorenz, and K. Zimmer, Laser Microembossing of Thin Copper and Silver Foils with UV Excimer Laser. Lasers in Engineering, 2012.
[3] Zimmer, K., et al., Fabrication of optimized 3D microstructures with undercuts in fused silica for replication. Microelectronic Engineering, 2012. 98: p. 163-166

Femtosecond Laser Fabrication of Silicon Nanocrystal Ensembles for Bioimaging and Solar Energy

S.V. Zabotnov[1,2], F.V. Kashaev[1], D.M. Zhigunov[1], P.A. Perminov[2], A.V. Emelyanov[2], P.A. Forsh[1,2], L.A. Golovan[1], P.K. Kashkarov[2,1]

[1]M.V. Lomonosov Moscow State University, 1/2 Leninskie Gory, Moscow, 119991 Russia
[2]Russian Research Center "Kurchatov Institute", 1 Kurchatov square, Moscow, 123182 Russia

e-mail: zabotnov@physics.msu.ru

Silicon nanostructures attract attention of researchers owing to a variety of useful properties. Particularly, the silicon nanocrystal ensembles are biocompatible and biodegradable at proper conditions [1]. Also silicon nanocrystal formation inside amorphous hydrogenated silicon (a-Si:H) allows to sufficiently improve electrophysical properties of such system from the point of view of solar energy applications [2]. The aim of our work is a demonstration of femtosecond laser radiation potentials for fabrication of photoluminescent markers and solar cells based on silicon nanocrystals.

We used an Cr:forsterite laser (1.25 μm, 150 fs) with regenerative and multipass amplifiers (pulse energy up to 4 mJ) to irradiation of monocrystalline silicon and a-Si:H.

In the first case the irradiation was realized in the ablation regime and took place in gaseous inert helium to avoid formation of undesirable oxygen, hydrogen or other bonds with the silicon atoms. As a result we obtained a fraction of silicon nanoparticles with the small size (1 – 10 nm) and high degree of crystallinity accordingly to atomic force microscopy and Raman spectroscopy data. Such nanocrystals possess visible photoluminescence in the red region (see Fig. 1 (a)) and are promising as photoluminescent markers in biotissues since the radiation occurs inside so-called "diagnostic transparency window" (700 – 1100 nm).

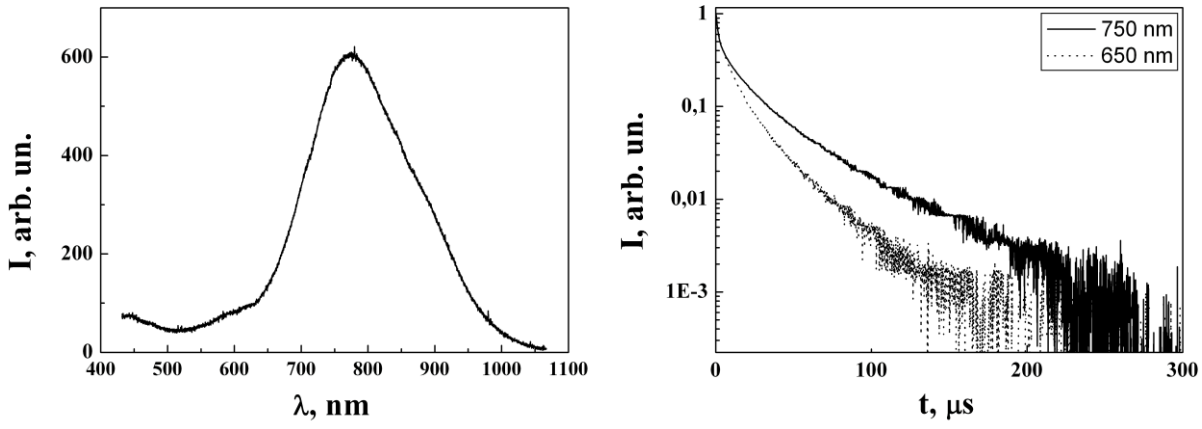

Figure 1. Photoluminescence spectrum (a) and kinetics (b) of silicon nanocrystal ensembles fabricated via laser ablation in helium at 1 bar.

The photoluminescence decay kinetics have non-exponential character (see Fig. 1 (b)) and so the recombination mechanism for charge carriers differs from excitonic one.

The laser irradiation of a-Si:H surfaces is another way to formation of the silicon nanocrystal ensembles when the Si-H bonds are destructed in the strong electromagnetic field and the crystallization takes place. In our work we have reached the crystallinity content up to 90 % at proper conditions. The nanocrystal presence increases the conductivity of such structures up to 4 – 5 orders in comparison with a non-irradiated a-Si:H film. The formed tandem amorhous-nanocrystalline structures seems promising as a base for solar cells.

This work was supported by the Russian Foundation for Basic Research (project 14-22-01086) and the Ministry of Education and Science of Russia.

[1] J.-H. Park, L. Gu1, G. von Maltzahn, et al., Biodegradable luminescent porous silicon nanoparticles for in vivo applications, Nature Materials, vol. 8, pp. 331 – 336, (2009).

[2] K. Yamamoto, A. Nakajima, M. Yoshimi, et al., A high efficiency thin film silicon solar cell and module, Solar Energy, vol. 77, pp. 939 – 949, (2004).

Confocal Raman, PL, and Fluorescence Lifetime Imaging Microscopy of Gallium Selenide Crystals – an Outstanding NLO Material

K. Allakhverdiev[1,2], S. Zahner[3], L. Kador[3], E. Salaev[4], F. Huseyinoglu[2]

1- Azerbaijan National Academy of Aviation, Bina 25th km, 1045 Baku, Azerbaijan
2- TÜBİTAK, Marmara Research Center, Materials Institute, P.K. 21, 41470 Gebze/Kocaeli, Turkey
3- Institute of Physics and Bayreuther Institut für Makromolekülforschung (BIMF), University of Bayreuth, 95440 Bayreuth, Germany
4- Azerbaijan National Academy of Sciences, Institute of Physics, 370073 Baku, Azerbaijan

kerim.allahverdi@tubitak.gov.tr kerim.allahverdi@gmail.com

The highly anisotropic gallium selenide (GaSe) possesses several outstanding physical properties: A very high nonlinear-optical (NLO) susceptibility $\chi^{(2)}$, wide transparency range (0.65 – 18 μm), high power threshold for optical damage, and a sufficiently large birefringence for phase-matched second-harmonic generation (SHG) in its transparence range [1]. Crystals of GaSe had previously been studied with confocal Raman and photoluminescence (PL) micro-spectroscopy [2-4]. Raman measurements with a cw HeNe laser (632.8 nm) had shown that the material emits a strong PL signal which is mainly blue-shifted from the laser line and has a quadratic dependence on laser intensity. The experimental data led to the conclusion that the mechanism behind the nonlinear PL most probably comprises two consecutive one-photon transitions involving an exciton state rather than direct two-photon absorption (TPA) or SHG in the laser focus [1-4].

Recently, GaSe crystals were studied with fluorescence lifetime imaging microscopy in the frequency domain using as excitation source a frequency-doubled cw Nd:YAG laser modulated at frequencies between 25 and 50 MHz [5]. The non-zero PL lifetime leads to a change of the relative modulation amplitude (m) and a phase lag (ϕ) of the luminescence with respect to the excitation. Data points of different spots on the sample show strong inhomogeneities and form looping structures in the polar plot. The analysis of the data indicates that the same exciton state(s) appear to be involved in both absorption and PL emission of GaSe [5].

An overview of all existing data encompassing Raman, PL, and fluorescence lifetime imaging microscopy of GaSe will be presented in this report. It will be shown that confocal micro-spectroscopy is a powerful tool for the identification and investigation of the physical properties of highly anisotropic (quasi two-dimensional) materials containing different crystal polytypes.

[1] K .R. Allakhverdiev, "Two-dimensional $A^{III}B^{VI}$ Semiconductors. Properties and Applications", *J. Optoel. Advanced Mater.*, **1**, 197 (2009).
[2] Y. Fan, M. Bauer, L. Kador, K. R. Allakhverdiev, and E. Yu. Salaev, "Photoluminescence Frequency Up-conversion in GaSe as Studied by Confocal Microscopy", *J. Appl. Phys.*, **91**, 108 (2002).
[3] Y. Fan, T. Schittkowski, M. Bauer, L. Kador, K. R. Allakhverdiev, and E. Yu. Salaev, "Confocal Photoluminescence Studied on GaSe Single Crystals", *J. Lumin.* **98**, 7 (2002).
[4] C. Perez Leon, L. Kador, K. R. Allakhverdiev, T. Baykara and A. A. Kaya, "Comparison of the Layered Semiconductors GaSe, GaS, and $GaSe_{1-x}S_x$ by Raman and Photoluminescence Spectroscopy", *J. Appl. Phys.* **98**, 103103 (2005).
[5] S. Zahner, L. Kador, K. R. Allkahverdiev, E. Yu. Salaev, and M. F. Huseyinoglu, "Fluorescence Lifetime Imaging Microscopy and Polar-Plot Analaysis of Gallium Selenide Crystals", *J. Appl. Phys.* **115**, 043504 (2014).

Space-time study of microplasmas inside semiconductors

Alexandros Mouskeftaras[1,*], Andrei Rode[2], Raphael Clady[1], Marc Sentis[1], Olivier Utéza[1], David Grojo[1,+]

1- Aix-Marseille University, CNRS, LP3 UMR 7341, F-13288, Marseille, France

2- Laser Physics Centre, Research School of Physics and Engineering, Australian National University, Canberra ACT 0200, Australia

*mouskeftaras@lp3.univ-mrs.fr ; +grojo@lp3.univ-mrs.fr

In the past decade, several works have been presented in the field of three dimensional (3D) laser-induced modification of transparent crystals (e.g. fused silica). This is made possible thanks to the fact that ultrashort laser pulses, when focused, allow reaching the peak intensities necessary for non-linear ionization[1] and subsequent breakdown at photon energies well below the bandgap energy. However, very few studies have focused on semiconductor crystals such as Ge, Si[2] or ZnSe and this is mainly due to the complications associated with the need for high-energy, near-to-mid infrared laser light pulses to penetrate deep inside the material. Furthermore, no experimental proof of direct, laser-induced modification in these solids has been given until now. Thus, there is increasing interest over the understanding and control of the energy deposition mechanisms in these crystals.

We have performed bulk damage threshold experiments in a wide range of materials and for different pulse durations (50 fs - 300 fs), wavelengths (1.3 µm and 2.2 µm) and focusing conditions (NA=0.3-0.85) only to show the impossibility to induce any modification in the above mentioned semiconductors by direct single Gaussian pulse focusing.

Next, we aim at bringing insight to the issue of ultra fast laser-semiconductor interaction. In particular, we focus our investigations on the initial ionization stage and the temporal evolution of the transient optical properties in the solid. In our experimental setup, tightly focused (NA=0.3) 50 fs and of few nJ laser pulses at 1.3 µm are used to generate a microplasma inside silicon and other semiconductors. Then we study the spatial and temporal evolution, for different excitation levels, of this microscale plasma using an infrared, pump and probe transmission imaging technique. In parallel, we have performed pump self-absorption measurements in the same conditions to estimate the deposited energy inside the solid. Our findings suggest a self-limited character of the excitation associated with beam energy depletion, thus failing to raise the deposited energy density to threshold levels for material modification.

[1]Grojo, D., Leyder, S., Delaporte, P., Marine, W., Sentis, M., &Utéza, O. (2013). Long-wavelength multiphoton ionization inside band-gap solids. *Physical Review B*, *88*(19), 195135

[2]Leyder, S., Grojo, D., Delaporte, P., Marine, W., Sentis, M., &Utéza, O. (2013). Non-linear absorption of focused femtosecond laser pulses at 1.3 µm inside silicon: Independence on doping concentration. *Applied Surface Science*,*278*, 13-18.

Overheated metastable states in metals irradiated by pulsed laser

V.I. Mazhukin, A.V. Shapranov, M.M. Demin, V.E. Perezhigin

Keldysh Institute of Applied Mathematics, Russian Academy of Sciences, Moscow, Russia
e-mail: vim@modhef.ru

The impact of ultrashort superpower laser pulses on highly absorbing condensed media accompanied by appearance of rapid phase transitions (melting, evaporation) and related overheated metastable states. There are two mechanisms of melting and evaporation: heterogeneous and homogeneous. Heterogeneous mechanism is characterized by exact phase boundary with an excess of free energy. Homogeneous mechanism is realized in some overheated region which is a prerequisite for the release of energy by volume.

Temperature and velocity of phase fronts are determined by solving the corresponding variants of the Stefan problem [1,2]. Characteristics of homogeneous melting/evaporating mechanisms such as the maximum degree of overheating of solid/liquid phase and the rate of change of the mass of the new phase are determined by solving atomistic models [3].

The evolution of homogeneous evaporation of the liquid phase, which is manifested in the form of phase explosion, spinodal decomposition and supercritical material expansion analyzed in detail in [4,5].

In this paper we analyzed the manifestations of limit overheating of the solid phase, Fig. 1 and the rate of heterogeneous melting.

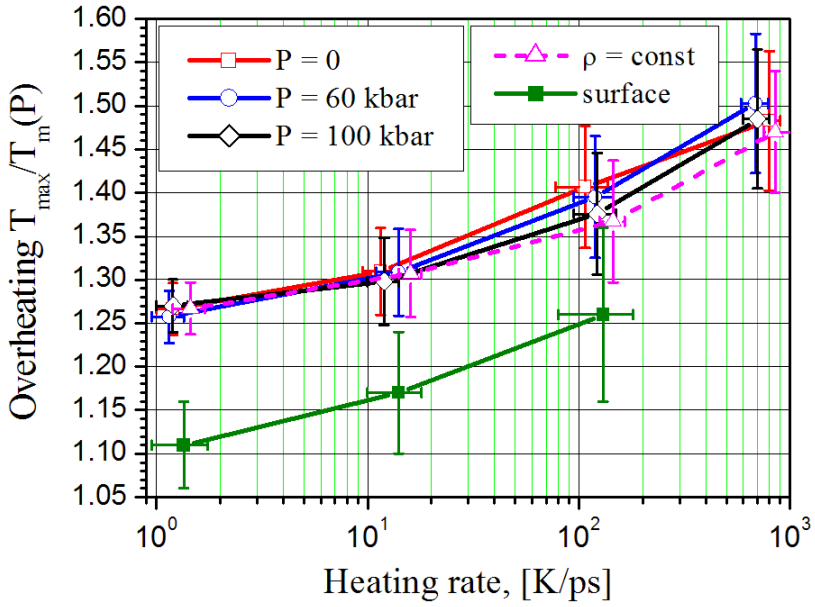

Fig.1 Limit overheating of the solid phase in the volume and on the surface.

This work was supported by RFBR projects Nos 12-07-00436, № 13-07-00597.

[1] A.A. Samokhin “First-order phase transitions induced by laser radiation in absorbing condensed matter” Proc. Institute of General Physics (USSR: Academy of Sciences) 13, 1990.
[2] V.I.Mazhukin. Laser Pulses – Theory, Technology, and Applications. InTech, Croatia, Chapter 8, 2012.
[3] C. Wu, L.V. Zhigilei “Microscopic mechanisms of laser spallation and ablation of metal targets from large-scale molecular dynamics simulations” . Appl. Phys A 114, p.11 2014.
[4] V.I.Mazhukin, A.A. Samokhin, M.M.Demin, A.V.Shapranov. Modeling of nanosecond laser vaporization and explosive boiling of metals. Mathematica Montisnigri. 2014, vol. 29, pp. 68 - 90.
[5] V.I.Mazhukin, A.A. Samokhin, M.M. Demin,A.V.Shapranov. Explosive boiling of metals upon irradiation by a nanosecond laser pulse. Quantum Electronics. 2014, vol.44, № 4, pp. 283–285.

Pre-processing of corrugated and porous metal surfaces by picosecond laser irradiation for thermal spraying

Bin Liu, Wenjun Wang, Xuesong Mei

State Key Laboratory for Manufacturing System Engineering

Xi’ an Jiaotong University, Xi’ an, China 710054

swdhlb@stu.xjtu.edu.cn，wenjunwang@mail.xjtu.edu.cn

Surface structure fabrication by ultrashort laser has been paid serious attention because it can manufacture structures with sub-spot size and can provide greater flexibility in fixing the position of ablated areas[1], which can widely improve the surface properties of materials in the fields of physics and chemistry. In application of thermal sprying, Lamraoui et al.[2] have reported a new process to improve the substrate-coating adherence: pre-preparation of surface structure on substrate. This pre-processing technique is designed to generate the undulating nature of the metal/ceramic interface for better interlocking adhesion, may produce out-of-plane stresses responsible for in-service failure of thermal barrier coatings (TBCs)[3].

For the better coating performance, the laser fabrication of the micro/nano-sized structures on the metal surface has been intensively studied. Some pit holes are often observed during fabrication of corrugated surface. For investigation of the mechanisms involved in the formation of microscale porous from corrugated structure, the influence of key structuring parameters has been analyzed using a multi-pulse irradiation in [4]. The holes of porous surface in center of ablated crater are shown in Figure1 (a).

For further exploring the performance of the porous structure surface should be achieved, a study is presented about preparation of porous structure in large-area on the 304 stainless steel target surface induced by a picosecond Nd:van regenerative amplified laser, operating at 1064 nm. The evolution of surface topography towards large amplitude sub-focal corrugations and pores is achieved with a triangle scanning path, controlled by peak irradiation fluence and scan spacing (distance between successive scan lines), as shown in Figure1 (b). The unambiguous influence of different laser parameters like the laser length, power, focusing distance, scanning velocity and overlapping spacing on the porous geometry and surrounding deposits helps to prepare the large-area porous structure surface with a high reproducibility. A further study of performance of thermal coating on laser texturing substrate is to prove the integrated laser/plasma spray techniques to increase coating/substrate adhesion, to reduce coating residual stresses, to improve coating cohesion.

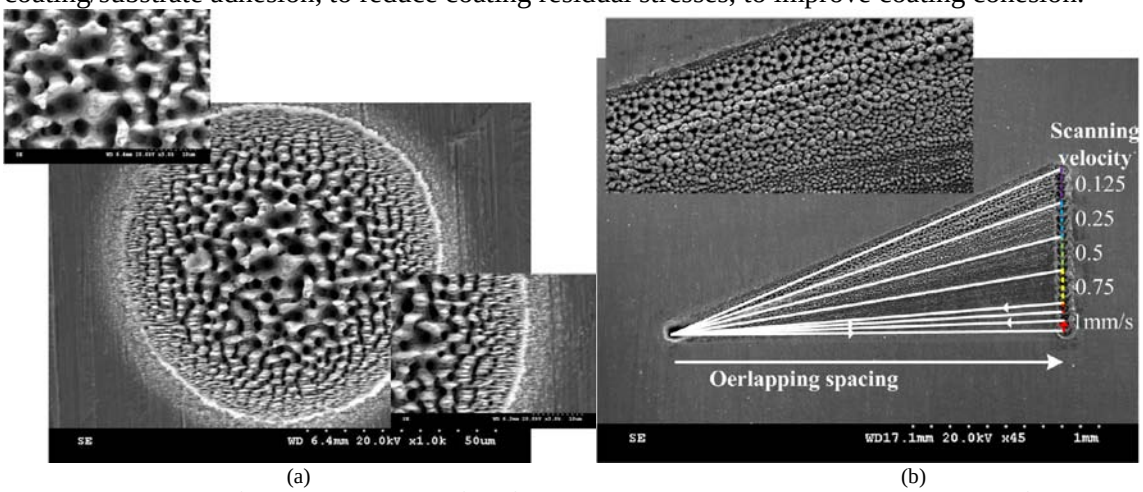

(a) (b)

Figure 1 (a) SEM images of micro- porous on the surface of ablated craters irradiated by laser pulses. (b) SEM image of general morphology view with beam scanning scheme and magnified high porosity onset areas. Holes in center or near edge of ablated crater were respectively shown as left or right -hand inset SEM images in (a). Scanning velocity vectors were orthogonal, with their directions shown in (b)

[1] W. Wang, X. Mei, and G. Jiang, Control of microstructure shape and morphology in femtosecond laser ablation of imprint rollers, International Journal of Advanced Manufacturing Technology, vol. 41, pp. 504‑512(2009).

[2] A. Lamraoui , S. Costil, C. Langlade, C. Coddet. Laser surface texturing (LST) treatment before thermal spraying: A new process to improve the substrate-coating adherence , Surface & Coatings Technology ,Vol.205. S164-S167(2010).

[3] Nitin P. Padture, Maurice Gell,Eric H. Jordan, Thermal Barrier Coatings for Gas-Turbine Engine Applications, Science 296, 280 (2002).

[4] Bin Liu, Wenjun Wang, Gedong Jiang, Xuesong Mei, Formation of Porous Structure with Subspot Size under the Irradiation of Picosecond Laser Pulses, Journal of Nanomaterials,vol.2013, Article ID 301301, 9 pages, (2013).

Analysis of aerosols via calibration-free laser-induced breakdown spectroscopy

M. Boudhib[1], J. Hermann[2], L. Boufendi[3], O. Le Bihan[1], E. Fréjafon[1], C. Dutouquet[1]

[1]*INERIS, DRC/CARA/NOVA, Parc technologique Alata, BP2, 60550 Verneuil-en-Halatte, France*
[2]*LP3, CNRS - Aix Marseille University, 163 Av. de Luminy, 13288 Marseille, France*
[3]*GREMI, CNRS-Orleans University, 14 Rue d'Issoudun, 45067 Orléans, France*

E-mail : christophe.dutouquet@ineris.fr

Large-scale industrial production of nanoparticles requires quality control through measurements of the size distribution and chemical composition [1]. For this purpose, new on-line monitoring techniques allowing real-time and in-situ characterization have to be developed. Producing composite nanoparticles elaborated from several chemical elements requires an instantaneous and in-situ stoichiometry control.

In this context, laser-induced breakdown spectroscopy (LIBS) is a promising technique. LIBS consists in focusing a powerful laser pulse on a material (solid, liquid, gas, nanoparticle flow) whose elemental composition is to be determined. The strong heating of the sample at the focusing spot leads to the ignition of a plasma. Simultaneous detection of all the elements is then achieved through optical emission spectroscopy. The LIBS technique has already been tested at INERIS for on-line monitoring, monitoring of heavy metal particle emission in the exhaust duct of a foundry and for controlling work environment. Thus, experiments aiming at determining the stoichiometry of aerosols using a calibration-free LIBS technique have been carried out.

The experimental setup consists of an analysis cell coupled to a LIBS optical setup. A vortex mixer has been used to suspend alumina Al_2O_3 micrometric particles. The suspended particles are then flowed through the cell using an inert gas (argon/helium). Laser pulses of 5 ns duration originating from a Q-switched Nd:Yag laser (1064nm) were focused inside the analysis cell on the aerosol flux where the plasma was generated. The LIBS signal was collected from the plasma using a telescope and spectra containing lines of aluminium Al and oxygen O were recorded using an echelle spectrometer coupled with an intensified charge-coupled device detector. The recorded spectra were then compared to theoretical spectra calculated for a plasma in the Local Thermodynamic Equilibrium [2] (figure 1).

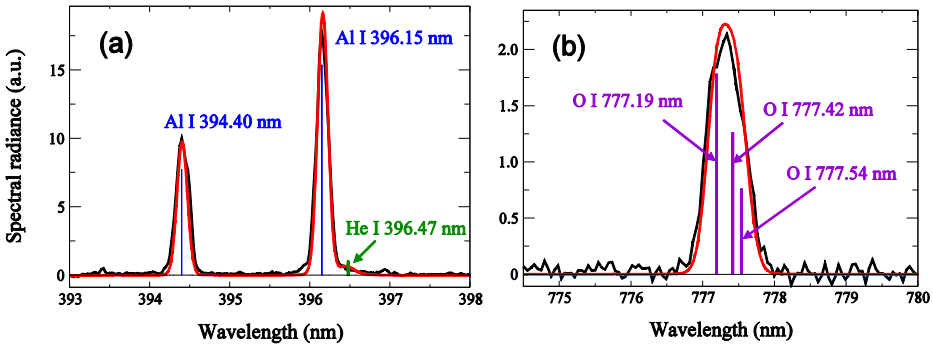

Figure 1 Measured (black lines) and computed spectral radiance (red lines) used for the determination of elemental composition of alumina particles

We demonstrate that the stoichiometric composition of the alumina particles can be deduced from the best agreement between measured and computed spectra if the experimental conditions were properly chosen. These preliminary experiments show that stoichiometry of alumina particles may be determined on-line without resorting to calibration with standards.

[1] T. Amodeo, C. Dutouquet, F. Tenegal, B Guizard, H. Maskrot, O. Le Bihan, E. Fréjafon, On-line monitoring of composite nanoparticles synthesized in a pre-industrial laser pyrolysis reactor using Laser-Induced Breakdown Spectroscopy, Spectrochimica Acta part B, 63, pp. 1183-1190. (2008)

[2] L. Mercadier, J. Hermann, C. Grisolia, A. Semerok, Diagnostics of nonuniform plasmas for elemental analysis via laser-induced breakdown spectroscopy: demonstration on carbon-based materials, Journal of Analytical Atomic Spectrometry, 28, pp. 1446-1455. (2013)

Classification of aerosol particles by laser light scattering

A. Nagy[1], A. Czitrovszky[1], W.W. Szymanski[2]

[1]*Wigner Research Centre for Physics, H-1121 Budapest, Konkoly Thege M. st. 29-33. Hungary*

[2]*Faculty of Physics, University of Vienna, A-1090 Vienna, Boltzmanngasse 5, Austria*

nagy.attila@wigner.mta.hu

We have developed a new optical method for the determination of different physical properties of aerosol particles suspended in the ambient air based on elastic light scattering on single particles (Szymanski et al. 2002). Comprehensive numerical analysis and laboratory tests were performed to study the reliability of the method (Nagy et al. 2007). A mobile prototype instrument were built so that we can study the method in field measurement campaigns and compared the results with other devices (TL-APC, Grimm-OPC, Magee Sc. Aethalometer, etc.).

In the frame of Jedlik Ányos project the Dual Wavelength Optical Particle Spectrometer (DWOPS) was utilized in 3 different longer measurement campaigns that aims to develop a new method/model for identification of different aerosol sources having different origin (anthropogenic - industrial, combustion/traffic, agricultural, etc.) (Fig. 1.). The main advantage of the new method is that with a short (several minutes) sampling time the contamination sources could be determined without further time consuming and expensive laboratory analyses. Fig. 2 shows the results obtained using DWOPS and Aethalometer instruments where the data from different instruments are presented. We have extracted and presented the number concentration and the absorbing fraction of particles (absorbing - imaginary refractive index are larger then 0.1) from the DWOPS data.

The results of the measurement campaigns show that the counting efficiency of the instrument is similar to the counting efficiency of other commercially available instruments. The time series of the absorbing fraction of the particles behave differently in different size ranges.

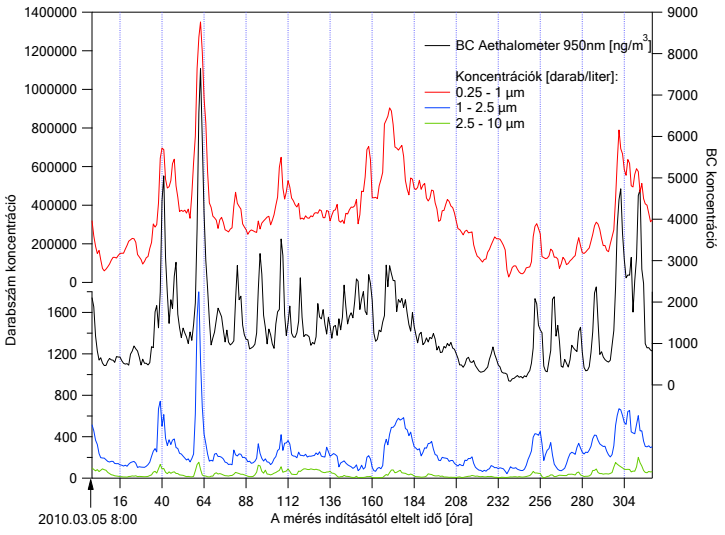

Figure 2. Some results of the measurement campaign

This work was supported by the TéT_10-1-2011-0725 project.

[1] Szymanski, W.W., Nagy, A., Czitrovszky, A., Jani, P. (2002). A new method for the simultaneous measurement of aerosol particle size, complex refractive index and particle density, *Measurement Science and Technology*, 13, 303-307.

[2[Nagy, A., Szymanski, W.W., Golczewski, A., Gál, P., Czitrovszky, A. (2007) Numarical and experimental study of the performance of the Dual Wavelength Optical Particle Spectrometer (DWOPS) (2007), *Journal of Aerosol Science*, vol. 38 issue 4. pp. 467-478.

Femtosecond laser impact ionization of quartz.

N.Fedorov[1], G.Geoffroy[1], G.Duchateau[1], L.Barilleau[1], P.Martin[1], S.Guizard[2], S.Klimentov[3].

1- CELIA, Université Bordeaux, 351 cours de la Libération 33405 Talence, France

2- LSI,IRAMIS,CEA,Saclay, Ecole Polytechnique, 91191, Saclay, France

3- GPI-RAS, Vavilova 38, 117942, Moscow, Russia

fedorov@celia.u-bordeaux1.fr

During last ten years a developing of femtosecond technological lasers gave a big progress in micromachining of materials. There are still some problems in this domain, thus as sub diffraction limit structuring, drilling of a long channel etc. To control these processes we need to understand in details all the mechanisms of ablation. How energy transfer from laser pulse to melt and sublimate the material. We were interested in micromachining of dielectrics, in particular, of silica, as a glass is the most used dielectric in industry.

To describe an ablation of dielectric usually use a model with following steps: multiphoton excitation of electrons, heating and multiplication by impact ionization to reach a critical density and ablation. [1]

The principal aim of this work is to study fundamental processes of electrons heating by laser pulse. To effectuate this study we have realized two types of experiments using Ti:Sapphire femtosecond laser systems: interferometry experiments [2] which can give us concentration and type of electronic excitation and photoemission experiment [3] to measure kinetic energy of excited electrons. Both type of experiments are pump-probe, two colors measurements: the initial concentration of electrons in conduction band was created by third harmonic of Ti:Sapphire laser (266nm). These electrons were heated by fundamental laser radiation (800nm) with various delays. From interferometry experiments we've got time resolved measurements of electronic concentration created by UV and IR laser pulses. Photoemission experiments gave us kinetic energy spectra of electrons. Scanning by delay between two laser pulses we can study time evolution of electronic excitations.

To describe these experimental results, we've developed a model which describes multiphoton absorption, interaction of electrons in conduction band with photons and phonons. Comparison of experimental and theoretical results and quantitative parameters of interaction will be present.

[1] S.Guizard, Femtosecond Laser Ablation of Dielectrics: Experimental studies of Fundamental Processes CLEO Europe , CM5 P.2 (2011)
[2] P.Martin, Subpicosecond study of carrier trapping dynamics in wide-band-gap crystals. Physical Review B, 55(9), 5799. (1997)
[3] S.Guizard Time resolved two-colour VUV-IR photoemission in wide band gap dielectrics. Physica Status Solidi (c), 2(1), 223-227. (2005).

Femtosecond laser induced modification of dielectric materials: Experimental investigation of fundamental mechanisms.

Stéphane Guizard[1*], Gautier Vilmart[1], Alexandros Mouskeftaras[1+], Sergey klimentov[2],

1. Laboratoire des Solides Irradiés, CEA-IRAMIS, CNRS, Ecole Polytechnique, 91128 Palaiseau, France,
2. General Physics Institute of the Russian Academy of Sciences, Vavilova St 38, 11991 Moscow, Russia.

* Corresponding author : stephane.guizard@cea.fr
[+] Now at Laboratoire Laser Plasmas et Procédés Photoniques (LP3) Aix-Marseille University, CNRS, LP3 UMR 7341, F-13288, Marseille, France.

Abstract: Laser processing and machining of dielectrics is a growing field, involving increasingly complex laser temporal and spatial pulse shaping. Predicting and modeling the optimum pulse characteristic for a given application requires a detailed knowledge of all the elementary events involved during the interaction. To understand and observe these physical mechanisms in detail, we carry out time resolved experiments, using spectral interferometry as a probe. Thus we can measure in real time the excitation density achieved in the solid and the following relaxation of excited carriers. Since many processes (non-linear excitation, impact ionization, modification of pulse shape and propagation) arise during the pump laser pulse itself, usual pump-probe experiments as not capable to distinguish and directly observe them. To encompass this difficulty, we used a flexible double pump scheme, allowing modulating the excitation density and carrier healing steps. We have been able to derive the following conclusions: - The appropriate criteria to determine the ablation or damage threshold is the amount of deposited energy in the solid, not the density of carriers. The latter, measured at breakdown threshold, decreases with increasing pulse duration. - We report the first direct observation of laser induced impact ionization/avalanche. This phenomena is a hypothesis in a huge number of publication, but was never demonstrated. More important, we show that it is not connected to the optical breakdown, occurring far above the threshold for damage/ablation. Finally, the most interesting result is that it does not take place in all materials. The possible reason for this selective occurrence of impact ionization will be discussed.

Synthesis of silicon nanoparticles by pulsed laser ablation in organic liquids.

D.A.Zadorin[1] , V.I. Krasovskii[1]

Center of Natural sciences

[1]A.M. Prokhorov General Physics Institute of the Russian Academy of Sciences

zadorin@mail.com

The results of silicon nanoparticles synthesis using pulsed laser ablation in toluene are presented. Pulsed Nd:YAG laser (λ = 1.06 um, τ ~20 ps, pulse energy W ~ 10 mJ.). Organic medium were taken to prevent the oxidation processes in nanoparticles. Obtained colloid demonstrate bright green luminescence peak with center near 570 nm under 395 nm diode pumping. The average size of nanoparticles and the sizes distribution were calculated from photoluminescence spectrum peak position of. The particles formation mechanism and conditions are discussed.

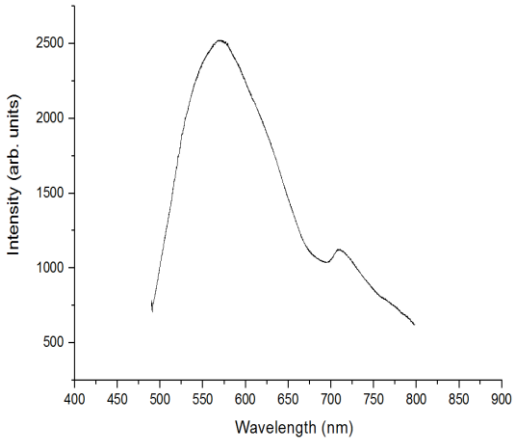

Figure 1. Photoluminscence spectrum of silicon particles colloid after ablation.

Criteria for Widely Tunable and Long-Term Operation of Mode-Locked All-Fiber Oscillator

K. Viskontas[1,2], N. Rusteika[1,2]

1- Center for Physical Sciences and Technology, Savanoriu Ave. 231, LT-02300 Vilnius, Lithuania
2- Ekspla uab, Savanoriu Ave. 231, LT-02300 Vilnius, Lithuania

karolis.viskontas@ar.fi.lt

In this paper, we introduce a picoseconds Yb-doped fiber oscillator with wide wavelength tunability (1020 – 1080 nm) and long operation time (~6000 h). To achieve mode-locking, high bandwidth $In_xGa_{1-x}As$ quantum well (QW) based semiconductor saturable absorber mirror (SESAM) and chirped fiber Bragg grating (FBG) were used. Incorporation of an all-fiber tunable filter with ~1 nm bandwidth and ~0.1 nm tuning resolution resulted in almost gradually adjustable output wavelength. For practical applications, the long term experiment of mode-locked fiber oscillator was performed. It was found, SESAM was the only device, limiting operation time. The non-linear reflectivity measurements after the long term tests indicated that the most likely mechanism of SESAM degradation was the modification of the InGaAs QW structure. By reducing a thermal load on SESAM, an expected life-time was increased ten-fold.

For operational wavelength of the Yb-doped fiber lasers (typically 1000 – 1100 nm), $In_xGa_{1-x}As$ QW based semiconductor saturable absorber mirror is a common choice [1]. Due to a wide operating bandwidth of anti-resonant cavity SESAM, single chip covers almost all region of Yb-doped gain medium [1, 2]. The low intensity and high intensity reflectivity spectrum of SESAM are shown in

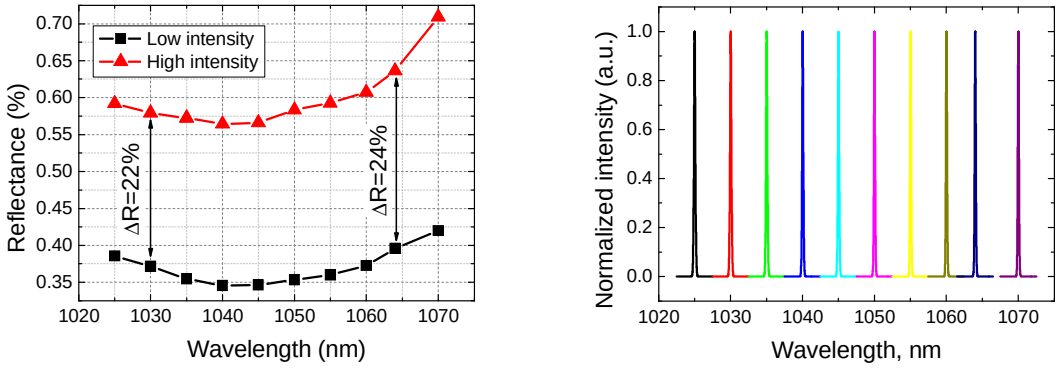

(a) (b)

Figure 1 (a) Reflectance of SESAM at low and high intensity. (b) Output spectrums of mode-locked fiber oscillator at different positions of tunable filter.

Figure 1a. The modulation depth of the absorber remains almost constant over wide wavelength region. It is very important as a modulation depth has to be much higher for fiber lasers to ensure their stable operation with a strong optical gain and large resonator losses [1]. The output spectrums of mode-locked fiber oscillator at different filter positions are shown in Figure 1 b.

[1] O. Okhotnikov, A. Grudinin, and M. Pessa, Ultra-fast fibre laser systems based on SESAM technology: new horizons and applications, New J. Phys., vol. 6(177), pp. 1-22, (2004).
[2] U. Keller et al., Semiconductor saturable absorber mirrors (SESAMs) for femtosecond to nanosecond pulse generation in solid-state lasers, IEEE J. Sel. Top. Quantum Electron, vol. 2, pp. 435 (1996).

THE INFLUENCE OF THERMAL TREATMENT ON THE LUMINESCENCE OF LANTHANUM – GALLIUM TANTALATE CRYSTALS

N.S. Kozlova[1], O.A.Buzanov[2], I.S. Didenko[1], A.P.Kozlova[1], A.V. Siminel[3], N.A. Siminel[1]
[1]*National University of Science and Technology "MISIS", Moscow, Russia*
[2]*Company Fomos-Materials, Moscow, Russia*
[3]*Istitute of Applied Physics of the Academy of Sciences of Moldova, Chisinau, Republic of Moldova*
kozlova_nina@mail.ru

Lanthanum – gallium tantalate crystal $La_3Ga_{5.5}Ta_{0.5}O_{14}$ (langatate - LGT) is a crystal belongs to the lanthanum – gallium silicate family. The space group of symmetry is P321. These crystals are grown with the Czochralski method.

The main object of this report is the complex investigation of the single crystal obtaining conditions (the growth atmosphere) and post-growth treatment influence on optical and luminescent properties of LGT crystals. All samples were investigated with methods of optical spectroscopy, optical microscopy and X-ray photoelectron spectroscopy before and after annealing.

The experiment required the use of the polar cut samples made from crystals grown in the argon (Ar) and argon with oxygen ($Ar+O_2$) atmospheres. The influence of different growth atmospheres on LGT crystals optic transmission spectra was investigated. Decrease of oxygen concentration in growth atmosphere leads to the considerable improvement of their optical properties. [1]

Isothermal annealing was carried out at temperatures 1000 ^oC within 4 hours in the air conditions. Annealing in air leads to more intensive coloration. The luminescent properties of the same samples were investigated. Influence of annealing on luminescence intensity is significant.

Results of the luminescent properties of langatate single crystals grown in different atmospheres were investigated. Wide luminescence bands were observed with a maximum at ~450 nm.[2] The luminescence was excited with third harmonic of YAG:Nd^{3+} laser with energy of 2mJ at 300 K.

Obtained results are evidence of the isothermal annealing having a profound effect on both optical properties and surfaces states of polar cuts of $La_3Ga_{5.5}Ta_{0.5}O_{14}$ crystals. It depends on the growth atmosphere. Extra luminescence bands are not observed after annealing mentioned above. The luminescence bands intensity changed significant. Essential increase of the luminescence bands intensity for the samples grown in the (Ar +(~0,5%) O_2) is observed whereas the luminescence bands intensity for the samples grown in the (Ar +(~2%) O_2) decreases.

References

1. O.A. Buzanov, E.V. Zabelina, N.S. Kozlova “Optical properties of Lanthanum – Gallium Tantalate at Different Growth and Post-Growth Treatment Conditions” Crystallography Reports, Vol. 52, № 4, pp. 691-696. (2007)
2. Luminescent properties of lanthanum-gallium tanatalate crystals. Book of abstracts The 21th annual International Conference on Advanced Laser Technologies ALT’13 Budva, Montenegro September 16–20, p.251, Paper LS-P-8 (2013)

Er-Yb co-doped cladding pumped fiber laser with phosphate core and silica cladding

O.Egorova[1], S. Semjonov[1], E. Dianov[1], B. Denker[2], B. Galagan[2], S. Sverchkov[2]

1- Fiber Optics Research Center, Russian Academy of Sciences, 38 Vavilov Street,119333 Moscow, Russia
2-General Physics Institute, Russian Academy of Sciences, 38 Vavilov Street,119991 Moscow, Russia

egorova@fo.gpi.ru

We present an optical fiber with an Er-Yb co-doped phosphate-glass core and silica cladding as well as cladding pumped laser. Phosphate core permits to achieve high doping level of rare earth ions. Silica cladding provides high mechanical strength as well as protection of phosphate glass from air moisture and permits easy splicing with silica fibers.

The fiber preform was fabricated using a rod-in-tube technique using phosphate glass with 1.7 cm^{-3} of ytterbium and 1.3 cm^{-3} of erbium ions concentration [1] as a core rod material and silica tube as a cladding. The preform was drawn into the fiber with a low refractive index polymer coating to form pump cladding. The fiber core was multimode with numerical aperture of 0.32 and diameter of 13.5 μm, cladding has a square shape for better pump absorption with dimensions of 100x100 μm. The small-signal cladding absorption of ytterbium was 0.65 dB/cm at 975 nm. The erbium core absorption at the 1535 nm was 1.5 dB/cm. The manufactured fiber was mechanically strong enough for handling. Splicing the composite fiber with silica fibers proved possible without bubble formation in the core.

The laser resonator was formed by the cleaved fiber ends, each providing 4% reflections. A semiconductor laser diode array at 980 nm was used for end pumping of the fiber. Using 50 cm of the fiber slope efficiency of 28 % with respect to the launched pump power has been obtained. Slope efficiency with respect to the absorbed pump power reached 39 %. Due to high doping level of phosphate core the optimal fiber length was several times less than the optimal length of a similar silica fiber [2].

[1] G. Karlsson, F. Laurell, J. Tellefsen, B. Denker, B. Galagan, V. Osiko, and S. Sverchkov, "Development and characterization of Yb-Er laser glass for high average power laser diode pumping," Applied Physics **B 75**, 41-46, (2002).
[2]J. Nilsson, S.U. Alam, J.A. Alvarez-Chavez, P.W. Turner, W.A Clarkson, and A.B. Grudinin, "High-power and tunable operation of erbium-ytterbium co-doped cladding-pumped fiber laser," IEEE J. Quantum Electronics **39**, 987-994, (2003).

Active Q-switching of the dual-wavelength Nd:$YGd_2Sc_2Al_2GaO_{12}$ ceramic laser

A. Brenier, G. Alombert-Goget, Y. Guyot

Institut Lumière Matière, UMR5306 Université Lyon 1-CNRS, Université de Lyon, 69622 Villeurbanne cedex, France

alain.brenier@univ-lyon1.fr

Nd- or Yb-doped laser ceramics as YAG or other garnets have reached a level of quality equivalent to single crystals, including high transparency, high laser damage thresholds, and excellent thermal and mechanical properties [1]. Some spectroscopic properties of the Nd^{3+}:$YGd_2Sc_2Al_2GaO_{12}$ ceramics have been studied [2] exhibiting a laser emission at 1060.8 nm in CW.

We present the active Q-switching with an acousto-optic modulator of a diode-pumped Nd:$YGd_2Sc_2Al_2GaO_{12}$ garnet ceramics laser. The laser beam is constituted by a dual-wavelength emission located near 1059.3 3 ("cold" line) and 1061.6 nm 3 ("hot" line). The temporal overlap of the two pulses obtained at the two different wavelengths is established by focusing the laser beam inside a nonlinear crystal, leading in addition to the second harmonic generation of each wavelength, to their sum-frequency generation. More, the time-resolved spectroscopy of the laser output and the temporal evolution of the pulses from two fast photo-detectors confirm the simultaneity of the dual-wavelength pulses. This result is promising for THz generation from difference-frequency mixing.

The two-wavelength laser power was measured at different repetition rates. The obtained pulse energies are increasing versus the absorbed pump power (Figure 1 (a)). At 4 kHz and 1.85 W absorbed pump power, we obtained 63 µJ/pulse, this value being intentionally limited to prevent any optical damages of the coatings. The pulses widths are visualized in Figure 1 (b). The relative intensity of the two pulses is expected to change because they originate from two Nd sublevels in Boltzman equilibrium. Just above the laser threshold, the "hot" line is hardly seen (Figure 1(c), but it quickly grows when increasing the pump power. The relative energy of the two lines can be adjusted by the control of the pump power (Figure 1 (d)).

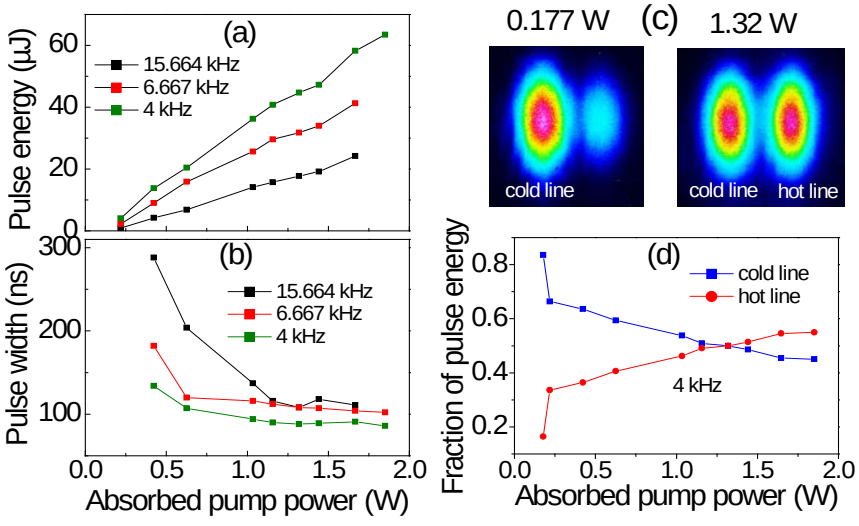

Figure 1 (a) Laser pulse energy; (b) laser pulse width versus the absorbed pump power at different repetition rates of the AO modulator; (c) images of the wavelength-separated laser beams for two different absorbed pump powers; (d) fraction of pulse energy in each wavelength-separated beam versus absorbed pump power.

[1] A. Ikesue, Nat. Phot. 2, 721 (2008).
[2] H. Okada, M. Tanaka, H. Kiriyama, Y. Nakai, Y. Ochi, A. Sugiyama, H. Daido, T. Kimura, T. Yanagitani, H. Yagi, N. Meichin, Opt. Lett. 35, 3048 (2010).

Bessel-like photonic nanojets from engineered nanospheres for the fabrication of ultra-high-density porous membranes

D. Grojo[1], G. Baravaglio[2], L. Boarino[2], C. Constantinescu[1], P. Delaporte[1], N. De Leo[2], M. Laus[3], A. Lionti[1], N. Sandeau[4], K. Sparnacci[3]

1- Aix-Marseille University, CNRS, LP3 UMR 7341, F-13288, Marseille, France
2- INRIM, NanoFacility, Division Electromagnetism, I-10135 Torino, Italy
3- Department of Sci. and Tech., Univ. of Eastern Piedmont Amedeo Avogadro, I-15121 Alessandria, Italy
4- Aix-Marseille University, CNRS, Centrale Marseille, Institut Fresnel, UMR 7249, 13013 Marseille, France

Main author email address: grojo@lp3.univ-mrs.fr

A photonic nanojet is an extremely narrow local field that spurts from the rear surface of a transparent sphere with size exceeding the wavelength. With sphere downscaling to the sub-wavelength level, the effect progressively vanishes and the intense field becomes highly localized. Our experiments show that there are two ways in which photonic nanojets can be obtained with sub-micrometer diameter spheres.

The first and obvious option is to decrease the wavelength. Using a 193-nm wavelength nanosecond laser, we illuminate spheres with well-controlled diameters from 260 nm. The spheres are assembled into monolayers at the surface of oxidized silicon substrates so that ablation with the nanojets produces periodically-porous silica membranes [1,2].

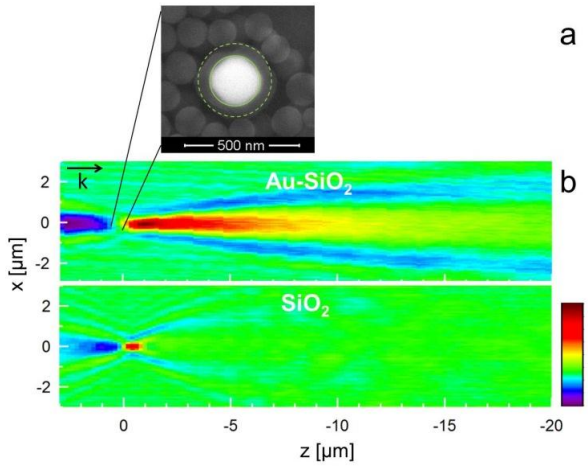

Figure 1 **:** (a) SEM image of synthesized core-shell (CS) spheres made with a gold core of 220-nm diameter surrounded by a silica shell (~ 70 nm). (b) Measurements of photonic jets from sub-wavelength spheres comparing the response of the core-shell spheres with a plain silica sphere of similar size (D = 350 nm).

The second way relies on nanosphere engineering. Using a modified Stöber method, we synthesize core-shell gold-silica nanospheres. What is essential in our sphere design is to use a light-blocking core to produce a Bessel-like nanojet and increase the apparent length of the scattered field [3]. As shown in fig. 1, we produce and image photonic nanojets at 400-nm wavelength. We show that photonic nanojets similar to those observed with micrometer scale conventional dielectric spheres can be obtained with engineered spheres of only 320-nm diameter. Photonic nanojets from nanoscale spheres must allow ultra-high-density periodic light matter interactions opening routes for new laser nanofabrication and optical diagnostic technologies.

[1] D. Grojo, L. Boarino, N. De Leo, R. Rocci, G. Panzarasa, P. Delaporte, M. Laus, K. Sparnacci, Size-scaling of mesoporous silica membranes produced by nanosphere mediated laser ablation, Nanotechnology 23 (2012) 485305
[2] A. Pereira, D. Grojo, M. Chaker, Ph. Delaporte, D. Guay, M. Sentis, Laser-fabricated porous alumina membrane (LF-PAM) for the preparation of metal nanodot arrays, Small, 4 (2008) 572-575
[3] D. Grojo, N. Sandeau, L. Boarino, C. Constantinescu, N. De Leo, M. Laus, K. Sparnacci, Bessel-like photonic nanojets from core-shell sub-wavelength spheres, Optics Letters, Accepted (2014) Doc. ID 211164

Photoacoustic Detection of Air Pollutants within Urban Area

I. R. Ivascu [1,2], C. E. Matei[1], M. Patachia[1], A. M. Bratu[1] and D. C. Dumitras [1,2]

[1] Department of Lasers, National Institute for Laser, Plasma, and Radiation Physics, 409 Atomistilor St., PO Box MG-36, 077125 Magurele, ROMANIA,

[2] Physics Department, Faculty of Applied Sciences, University "Politehnica" of Bucharest, 313 Splaiul Independentei, Bucharest - 060042, ROMANIA

ioana.ivascu@inflpr.ro

The benefits of the modern society brought by the high development of the industry and economy were accompanied by additional problems regarding the inherent environmental pollution. The continuous development of urban areas, in some cases, together with the surrounding industrial platforms, adds every day new sources of pollution due to people activity, construction of new buildings and technical facilities, enlarged transport network and increased car traffic. All of these activities have as result various pollutant residues with a major negative impact on the air quality and consequently on the people health. From this perspective, an appropriate monitoring of the air quality becomes a stringent concern for the authorities in order to detect potential pollution risk and to maintain a proper environment within urban agglomeration.

In this paper we present our results regarding pollutant trace gas detection based on the laser photoacoustic spectroscopy, one of the most sensitive techniques available today, being able to measure gas concentrations at sub-ppb levels (partial pressure of 10^{-10} atm) [1]. The experimental set-up employs as source a tunable CO_2 laser with a wavelength spectrum that covers the molecular absorption spectra of our target pollutants [2] mainly represented by ethylene, ethanol, methanol and ammonia. Exploiting their molecular absorption characteristics with respect to the CO_2 laser spectrum we measure the concentration of each particular trace gas in the air samples collected from various urban sites such as Bucharest underground network, including stations and cars during the rush hours, a heavy traffic street node or down town streets. The obtained results are valuable for monitoring the air quality from urban sites that present a high risk of pollution. This study could be also extended for controlling the indoor atmosphere of industrial or food storage spaces.

Acknowledgements: This work was supported by a grant of the Romanian Ministry of Education, CNCS – UEFISCDI, project PN-II-RU-PD-2012-3 - 0207.

[1] D. C. Dumitras *et al.*, Infrared Phys. Technol., Vol. 53(5), 308-314 (2010).

[2] P. L. Meyer, M. W. Sigrist, Rev. Sci. Instrum. 61, 1779-1807 (1990).

Intracavity singly-resonant OPO pumped by GaSb-based semiconductor disk laser

Yu. A. Morozov[1], M. Yu. Morozov[1], V. I. Kozlovsky[2], O. G. Okhotnikov[3]
1 - Kotelnikov Institute of RadioEngineering & Electronics (Saratov Branch), Russian Ac. Sci. 38 Zeleonaya Str. 410019, Saratov, Russia
2 - P. N. Lebedev Physical Institute, Russian Ac. Sci., 53 Leninsky Ave., 119991, Moscow, Russia
3 - Optoelectronics Research Centre, Tampere Univ. of Techn., P.O. Box 692, FIN-333101 Tampere, Finland

yuri.mor@rambler.ru

Many of gaseous chemical substances exhibit absorption lines in the mid- and far-infrared spectral region and can be detected with the use of spectroscopic techniques. Compact, room temperature sources of high spectral purity operating over this region are therefore of great demand. Among variety of optical sources suitable for high-resolution spectroscopy, continuous-wave singly-resonant OPOs (SROs) are of particular importance [1]. The SROs, however, need tens-of-watt pumping lasers in order to overcome the threshold of parametric generation. This threshold could be reduced if an SRO is placed within a high-finesse cavity of a pumping laser. In particular, such the intracavity SRO (ICSRO) was demonstrated with a neodymium laser [2]. Unfortunately, an ICSRO pumped by a neodymium laser appears to show pronounced relaxation oscillations of output intensity because laser active medium exhibits a long lifetime of excited state. To avoid this disadvantage, the pumping of the ICSRO by a semiconductor disk laser (SDL) has been proposed by D. Stothard *etal* [3]. Their device includes two dog-leg cavities: one for laser optical field (the pump with wavelength of 1.05 μm) and other for the signal radiation (1.6 μm). The cavities were separated by a dichroic beamsplitter having a high reflectivity for the signal and transparent for the pump. It should be noted that the approach [3] could be hardly adapted to an ICSRO with closer wavelengths of the pump and signal, i.e. with longer idler's wavelength, because sophisticated dichroic beamsplitter required.

Recently, we have proposed a novel type of the continuous-wave ICSRO pumped by a SDL [4]. One of the primary goals was to build a fairly compact device. Unlike to the ICSRO [3], a single plano-concave cavity both for the pump and the signal down-converted wave has been used thus avoiding the need for a dichroic beamsplitter and allowing the miniature ICSRO (~15 mm long) to be built.

In this paper, we report a modification of the approach [4] imposed by utilizing the SDL which is based on GaSb material system (emission wavelength ~ 2 μm). First, in order to ensure high-Q cavity for both the pump (1.98 μm) and signal (2.25 μm) wavelengths, we apply the concept of a double-band reflector [5] to the distributed Bragg mirror of the laser. Second, the primary pump beam at wavelength 808 nm is assumed to pass *through* a few millimeter long nonlinear crystal of quasi-phase-matched GaAs towards the gain region of the SDL. Such an approach allows to place the nonlinear crystal close to the laser chip where the laser and signal beams are tightly focused.

The mathematical model of the ICSRO is based on that developed in [6] for the analysis of a three-wave nonlinear interaction in the dual-wavelength vertical external cavity surface-emitting laser [7].

This study was supported by RFBR grant No.13-02-12070-OFI_M.

[1] Solid-state mid-infrared laser sources, T. Sorokina, K. L. Vodopyanov, Eds.(Springer-Verlag Berlin Heidelberg), Chapter 11, (2003).

[2] D. Stothard, M. Ebrahimzadeh, M. Dunn, Low pump threshold, continuous-wave, singly resonant, optical parametric oscillator, Opt. Lett., vol.23, pp. 1895-1897, (1998).

[3] D. Stothard, J. Hopkins, D. Burns, M. Dunn, Stable, continuous-wave, intracavity, opical parametric oscillator pumped by a semiconductor disk laser (VECSEL), Opt. Express, vol.17, pp. 10648-10658, (2009).

[4] Yu. A. Morozov, M. Yu. Morozov, Intracavity singly-resonant optical parametric oscillator pumped by a semiconductor disk laser, Proc. of 6-th Intern. Conf. on Adv. Optoel. and Lasers (CAOL'2013), Crimea, Ukraine, pp.100-101, (2013).

[5] S. Calvez, D. Burns, and M. D. Dawson, Optimization of an optically pumped 1.3-μm GaInNAs vertical-cavity surface-emitting laser,, IEEE Phot. Techn. Lett., vol. 14, pp. 131-133, (2002).

[6] Y. A. Morozov, M. Y. Morozov, Intracavity nonlinear frequency down-conversion in a continuous-wave operation regime of a dual-wavelength vertical-external-cavity surface-emitting laser, IEEE Journ. of Sel. Top. in Quantum Electronics, vol. 19, p. 1702105-1-1702105-5, (2013).

[7] T. Leinonen, Y. A. Morozov, A. Harkonen and M. Pessa, Vertical external-cavity surface-emitting laser for dual-wavelength generation, IEEE Phot. Techn. Lett., vol.17, pp. 2508--2510, (2005).

Joint Influence of Cubic Nonlinearity and Thermally Induced Birefringence on the Radiation Polarization in High Peak Power Lasers

M. Kuzmina*, E. Khazanov, A. Stepanov

Institute of Applied Physics of the RAS, 46 Ulyanov Street, 603950 Nizhny Novgorod, Russia

kmsnn@mail.ru

Creation of laser systems possessing simultaneously high peak power and high average power is the promising trend in laser physics. One of the key problems to be solved in construction of such lasers is suppression of thermal effects restricting average power and nonlinear optical effects limiting peak power. This talk provides an overview of the recent results of investigation of the joint impact of thermal and nonlinear effects on the output polarization of powerful laser with high pulse repetition rate.

In media with cubic nonlinearity sufficiently intense laser radiation can cause a noticeable change in refractive index due to its dependence on the intensity. Cubic nonlinearity manifests itself as a well-known effect of polarization ellipse turn in the isotropic medium because of the nonlinear difference in the refractive indices of circularly polarized components [1,2]. Rotation angle of the polarization ellipse is dependent on the optical path, intensity of radiation and the polarization ellipticity.

The appearance of the induced by strong field birefringence leads to negative consequences in case of laser radiation propagation in a medium with a different type of birefringence, for example natural or thermally induced. Both cubic nonlinearity and birefringence introduce polarization distortions in the laser beam, giving rise to depolarization.

The active elements of laser amplifiers and magnetic elements of the Faraday isolator are examples of optical elements with thermally induced anisotropy. Such birefringence and the consequent increase of depolarization in these elements are successfully compensated in the absence of the cubic nonlinearity. However, it was shown theoretically and experimentally that the efficiency of the broadly employed method of depolarization compensation in active elements by means of a 90° polarization rotator decreases with increasing B-integral (nonlinear phase incursion). The contributions of both the effects are nonadditive in principle, as thermally induced birefringence depends neither on intensity, nor on laser field polarization, whereas anisotropy induced by cubic nonlinearity is a function of intensity and polarization. The magnitude of uncompensated depolarization in such a scheme is proportional to B^2 for arbitrary values of thermally induced phase difference δ. The dependence of depolarization γ on δ is essentially nonmonotonic. There exists a critical value δ_{cr} at which γ is maximal. Values of the rotator optimal angle providing significant decrease of the residual depolarization were numerically calculated.

The influence of cubic nonlinearity on the insulation value of the state-of-art schemes of Faraday isolator was also investigated. Three types of birefringence were taken into account: induced by strong field, circular (Faraday effect) and thermally induced. It was found out that for all schemes depolarization increase due to cubic nonlinearity is proportional to squared B-integral and for $B > 1$ this increase is an order of magnitude or more.

Wave plates are example of media with natural anisotropy. Dependence of depolarization degree Γ (fraction of energy in the polarization orthogonal to the polarization in the absence of nonlinearity) at the output of a quarter-wave plate of crystalline quartz on B-integral was obtained theoretically and experimentally. It was revealed that in such quarter-wave plate with thickness of 0.18 cm the depolarization value reaches 1% at the laser intensity of 370 GW/cm^2. It was shown that the use of the quarter-wave plate made from crystal DKDP can significantly reduce the negative impact of cubic nonlinearity: depolarization in this case does not exceed 0.2% for the intensity up to 2 TW/cm^2.

References

[1] A.L. Berkhoer, V.E. Zakharov, "Self Excitation of Waves with Different Polarizations in Nonlinear Media," Soviet J. of Experimental and Theoretical Physics, **31**, 486 (1970).

[2] D.V. Vlasov, V.V. Korobkin, R.V. Serov, "Nonlinear precession of elliptically polarized Gaussian beams," Soviet J. of Quantum Electronics **9**, 904 (1979).

Session
Poster II

Session Poster II: Thursday 9th October : 16h30 – 18h

S2-P1 : L. Taskina, Raman spectroscopy for demineralization degree control of bone implants

S2-P2 : V. Mikhalevskiy, Synthesis of magnetic thin films of GaSb doped with MnSb clusters using pulsed laser deposition

S2-P3 : O. Novodvorskii, The optical and magnetic properties of Si1-xMnx films produced by the PLD method

S2-P4 : O. Khramova, Synthesis of thin films of CdS on amorphous substrates by the PLD method

S2-P5 : L. Parshina, Influence of the plume energy on the SnO_2:Sb films characteristics by using the PLD droplet-free method

S2-P6 : A. Lorusso, Structural and morphological properties of Nb thin films grown by pulsed laser deposition

S2-P7 : P. Lorenz, Fabrication and application of nanosecond laser-generated surface nanostructures on polyimide

S2-P8 : V. Levdansky, Formation of Aerosol Particles by Physical and Chemical Vapor Deposition in Field of Laser Radiation

S2-P9 : S. Vinogradov, Atomic-force microscopy of silver iodide nanocrystals under laser stimulated surface optical sensitization

S2-P10 : A. Osipov, Method of deposition nanoparticles from small colloidal drop

S2-P11 : J. Mlynczak, Spectroscopic and Pulse Generation Investigation of Co_{2+}:MALO Saturable Absorber as Separate Sample and as Thermally Bonded with Active Media

S2-P12 : O. Sergeeva, Variations in electrical response of thin-film multilayer structure based on PZT to the modulated laser irradiation

S2-P13 : T. Sokolova, Laser Forming of Micropeaks on Curved Surfaces of Glass-Carbon Plates

S2-P14 : M. Grigoryeva, Pore collapse dynamics in coatings under the laser annealing

S2-P15 : A. Samokhin, Modeling of Nanosecond Laser Vaporization of Metals. In Near Critical Region

S2-P16 : Dong Bizhe, Numerical Simulation of Laser Welding Deformation of Auxiliary Heat Source Controlled Aluminum Alloy Sheet Plate

S2-P17 : C. Shakher, Measurement of Temperature and Temperature Profile of Gaseous Flames using Holo-Shear Lens

S2-P18 : T. Vasile, THz Hadamard Transform Imager

S2-P19 : E. Gaižauskas, THz Generation by Combined One- and Two-photon Resonant Excitations in an Ensemble of Three Level Quantum Systems

S2-P20 : K. Fedorova, Behavior of aqueous lysozyme solution when it's heated

S2-P21 : O. Cherkasova, The study of surface enhanced Raman scattering of steroids

S2-P22 : I. Sergeeva, The interaction of cesium with globular proteins in model and native serum solutions of healthy and cancer patients by static light scattering (SLS)

S2-P23 : M. Gongalsky, Photoluminescent silicon nanoparticles in water suspension stabilized by dextran coating

S2-P24 : V. Makarov, Aluminum phthalocyanine crystal nanoparticles for fluorescence diagnosis and photodynamic therapy

S2-P25 : M. Sinyaeva, The investigation of nanoparticles application for teeth enamel microdamages diagnostics

S2-P26 : P. Grachev, The device for simultaneous stereotactic surgery and spectroscopic control

S2-P27 : L. Osminkina, Photoluminescence, bioimaging and sonosensitising properties of nanoparticle suspensions prepared from silicon nanowires

S2-P28 : A. Pacholski, Pointing stability challenges after 25-m beam propagation under vacuum on CETAL laser facility

S2-P29 : O. Utéza, Test-bench for laser damage experiments with sub-15 fs ultrashort pulses

S2-P30 : Y. Azamoum, Generation and characterization of a sub-picosecond laser-based hard X-ray Kα source with a high pulse repetition rate

Raman spectroscopy for demineralization degree control of bone implants

Timchenko E.V.[1], Timchenko P.E.[1], Taskina L.A.[1], Volova L.T.[2], Ponomareva Y.V. [2], Pershutkina S.V. [1]

[1] *S.P. Korolyov Samara State Aerospace University (National Research University)*
[2] *Experimental Medicine and Biotechnology Institute of the Samara State Medicine University*

retuo@mail.ru

For regenerative processes optimization at replacement of bone defects the allogeneic implant with different demineralization degree is necessary [1]. The demineralization degree control is an important part in production and carried out using biochemical methods, which takes a lot of time and therefore are not widespread.

This paper presents the results of experimental studies of donor bone samples with different mineralization degrees using Raman spectroscopy. Raman spectra were obtained for various non demineralized and demineralized bone biomaterial of different donor types (rat, rabbit and human). The result shown, that the demineralization process can be quantified controled with introduced relationships "mineral / organic matrix" and "carbonate / phosphate".

Raman bands 950–962 (PO_4^{3-} (ν1)), 1065–1070 (CO_3^{2-} (ν1)) and 1665 cm^{-1} (amide I) were evaluated. Finally, in demineralized bone (cancellous 86% at 5 minutes and 98% at 20 minutes of demineralization) a sharp decline of band 950–962 cm^{-1} was observed. A similar decline was occurred at 1065–1070 cm^{-1} with the advent of dominant band 1079–1090 cm^{-1} corresponding to the hydrated amorphous state CO_3^{2-} (ν1) [2].

As a result, the variation of ready implant parameters is inevitable at joint demineralisation of heterogeneous donor material and caused by natural differences in the initial parameters of primary donor material. This can decrease the rate of regeneration and the transplantation efficiency of bone implants.

[1] I.A. Kirilova, Demineralized bone graft as a stimulator of bone formation: modern concepts, J. Spine Surgery, 3, pp. 105-110, (2004).
[2] K.A. Esmonde-White, G.S. Mandair, F. Raaii, J.A. Jacobson, B.S. Miller, A.G. Urquhart, M.D. Morris, B.J. Roessler, Raman Spectroscopy of Synovial Fluid as a Tool for Diagnosing Osteoarthritis, J. Biomed. Opt., 14(3), 034013, (2009).

Synthesis of magnetic thin films of GaSb doped with MnSb clusters using pulsed laser deposition

V.A. Mikhalevskiy[1], O.A. Novodvorsky[1], A.V. Shorokhova[1], O.D. Khramova[1], L.S. Parshina[1], S.F. Marenkin[2], I.V. Fedorchenko[2], B.A. Aronzon[3], A.B. Davydov[3], A.V. Kochura[4]

[1]The Institute on Laser and Information Technologies of the Russian Academy of Sciences, 1 Svyatoozerskaya St., Moscow Region, Russia, 140700
[2]Kurnakov Institute of general and inorganic chemistry of the Russian Academy of Sciences, 31 Leninsky prospect, Moscow, Russia, 119991
[3]The P.N. Lebedev Physical Institute of the Russian Academy of Sciences, 53 Leninsky Prospekt, Moscow, Russia, 119991
[4]Southwest State University, 94 50 let Oktyabrya, Kursk, Russia, 305040

email address: uhr@inbox.ru

Thin films of $A^{III}B^{V}$ semiconductors doped with manganese nano-scale clusters are of great interest for spintronics. They could be applied in such spintronic devices as spin valves [1].
In this paper, the possibility of the synthesis of thin films of the ferromagnetic semiconductor materials using pulsed laser deposition (PLD), the composition of the films obtained in relation to the composition of the target , the homogeneity, the surface roughness, conductivity, resistivity, concentration and mobility of charge carriers, magnetic properties of the films were studied. Films of the GaSb-MnSb system having thicknesses of 80-130 nm were synthesized on the oriented sapphire substrates by PLD method with the mechanical separation of droplets [2]. Film composition corresponds to the composition of the target, which was made of a eutectic GaSb-MnSb system [3]. The films were homogeneous with a surface roughness at the nano level according to the electron and scanning probe microscopy (Figure 1). They are characterized by p-type conductivity. The electrical properties of the films depended on the deposition process conditions. The best examples of films had a resistivity $7 \cdot 10^{-3}$ Ohm·cm, the concentration of $8.1 \cdot 10^{19}$ cm^{-3} and mobility of charge carriers $1 \cdot 10^{2}$ $cm^2 \cdot V^{-1} \cdot s^{-1}$. Films synthesized on substrate heated up to 300 °C are characterized by a negative magnetic resistance. Evaluation of the coercive force dependence showed that the films are soft magnetic materials with a coercive force of not more than $8 \cdot 10^{3}$ A/m. For films grown at a temperature of 100 °C coercive force increased up to the $2.5 \cdot 10^{4}$ A/m. Saturation magnetization was dependent on the orientation of the magnetic field relative to the plane of the sample and is achieved at 0.1–0.5 T.

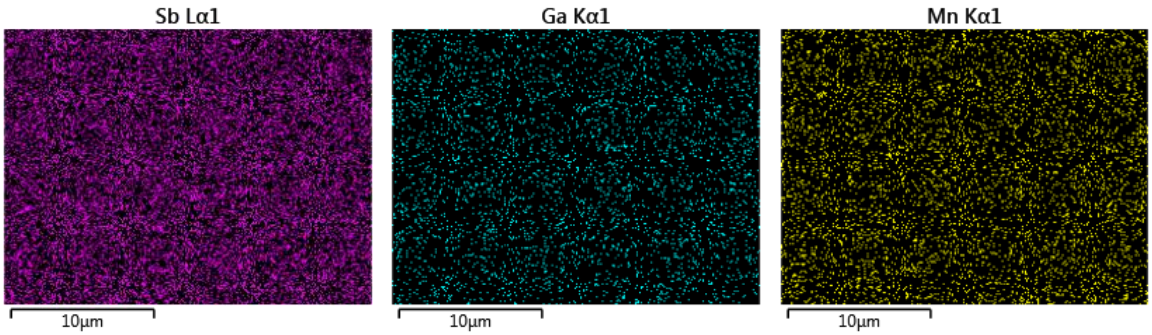

Figure 1. Distribution of elements Sb, Ga, Mn on the film surface.

[1] V. Kochura, B.A. Aronzon, K.G. Lisunov, A.V. Lashkul, A.A. Sidorenko, R. De Renzi, S.F. Marenkin, M. Alam, A.P. Kuzmenko, and E. Lahderanta, Structural and magnetic properties of In1-xMnxSb: Effect of Mn complexes and MnSb nanoprecipitates, J. Appl. Phys, Vol. 113, p.083905, (2013).
[2] V.Ya. Panchenko, O.A. Novodvorsky, V.S. Golubev, Technology of laser-plasma deposition of the films nano thickness, The Science and technologies in the industry, № 4 (1), pp. 39-51, (2006), (in russian).
[3] S.F. Marenkin, V.M. Trukhan, S.V. Trukhanov, I.V. Fedorchenko, V.M. Novotortsev, Phase equilibria and electrical and magnetic properties of a eutectic in the GaSb-MnSb system, Russian Journal of Inorganic Chemistry, Vol. 58, No. 11, pp. 1324–1329. (2013), (in russian).

The optical and magnetic properties of $Si_{1-x}Mn_x$ films produced by the PLD method

O.A.Novodvorsky[1], V.V.Rylkov[2], S.N. Nikolaev[2], K. Yu. Chernoglazov[2], V. V. Tugushev[2], E. T. Kulatov[3], A.V.Shorokhova[1], A.S.Semisalova[4], N.S.Perov[4], E.A.Gan'shina[4], A. B. Granovskii[4], N.M. Krejnes[5], V.Ja.Panchenko[1]

[1] *Institute on Laser and Information Technologies of RAS, 140700 Shatura, Moscow Region, Russia*
[2] *National Research Centre, Kurchatov Institute, 123182 Moscow, Russia*
[3] *Prokhorov General Physics Institute, Russian Academy of Sciences, ul. Vavilova 38, Moscow, 119991 Russia*
[4] *Faculty of physics, M.V. Lomonosov MSU, 119991 Moscow, Russia*
[5] *PL Kapitza Institute of Physical Problems RAS, 117334 Moscow, Russia*

e-mail: onov@mail.ru

Magnetic semiconductor systems based on Si attractive to create spintronic elements easily integrate into existing microelectronic technology. We have recently found that in films Si1-xMnx with a slight excess Mn (x = 0.52-0.55) Curie temperature ($T_C \geq 300$ K) increases by more than an order of magnitude compared to MnSi ($T_C = 30$K). In this case the concentration of charge carriers (holes) drops sharply, and their mobility at 100 K on the order increases compared with MnSi [1]. In this paper, film Si1-xMnx thickness 60-70 nm with Mn content x = 0.52 obtained by pulsed laser deposition on substrates of Al2O3 (0001). Details of the deposition of films and their structural features are described in [1]. The method [2] allows to avoid the hitting of the droplets on the growing film which presence is a primary factor of film quality loss in PLD. In Si1-xMnx films with a slight excess of Mn (x = 0.52) made a comparative study of the anomalous Hall effect (AHE) conductivity $\sigma_H^a(w=0,T)$ (w- frequency) and dynamic transverse conductivity $\sigma_H^a(w,T)$ defining equatorial Kerr effect (TKE). Found a good correlation in the behavior of dependency $\sigma_H^a(w=0,T)$ and $\sigma_H^a(w,T)$, indicating the absence of isolated ferromagnetic clusters , ie the global (uniform) magnetization of the samples [3]. In thus identified homogeneous samples were studied features of their magnetic anisotropy using magnetization measurements and ferromagnetic resonance (FMR).

Study of magneto-optical and transport properties have been performed on the same samples made in the form of a double cross. Measuring the conductivity and the Hall effect were carried out in the temperature range 5-200 K in magnetic fields of up to 2.5 T. The conductivity AHE was the standard way: $\sigma_H^a \cong \rho_H^a / \rho_{xx}^2$ where ρ_H^a and ρ_{xx} - Hall and longitudinal resistance. TKE was researched using p-polarized light (the angle of incidence of 68°) in the spectral range 0.5-4 eV at temperatures of 30-350 K in magnetic fields up to 3.5 kOe. FMR was measured in a magnetic field parallel and perpendicular the planes of a film up to 10 kOe at temperatures of 5-300 K and frequencies of exciting radiation of 17.43 and 9.42 GHz. Magnetic measurements were also executed in longitudinal and cross configurations on the magnetometer Quantum Design MPMS-XL-7 at temperatures of 10 – 100 K (data at more high temperatures are analyzed in [1]). Good correlation in behavior of AHE and TKE in the range of temperatures of 30 - 170 K for sample Si1-xMnx with x≈0.52, indicating global nature of ferromagnetic transition with $T_C \approx 310$K Curie's temperature is shown. Comparison of dependences of M(H) received for a field of focused in the plane and perpendicular to the plane of a sample, testifies to its plane magnetic anisotropy. The magnetization of saturation found from measurements of FMR in longitudinal geometry of Ms ≈ 930 emu/cm^3, in ≈2 of time exceeds the magnetization received from measurements of the magnetic moment. For FMR experiments in cross geometry the satisfactory consent (Ms ≈ 450 emu/cm3) is reached.

Work is performed with support of grants of the RFBR (13-07-12087, 13-07-00477, 14-07-00688a).

[1] V.V.Rylkov, S.N. Nikolaev, K. Yu. Chernoglazov et al. High-temperature ferromagnetics nestekhiometricheskikh of of Si1-xMnx (x ≈ 0.5) alloys Pisma JETF vol 96, pp.272-280, (2012).
[2] O.A. Novodvorsky, A.A. Lotin, E.V. Khaydukov, Utility model RF patent 89906, Published 20.12.2009, bulletin 35.
[3] V.V. Rylkov, E.A. Gan'shina, O.A. Novodvorskii, Defect-induced high-temperature ferromagnetism in Si1−xMnx (x ≈ 0.52–0.55) alloys. Europhys. Lett.vol. 103, pp. 57014 p1-p6,(2013).

Synthesis of thin films of CdS on amorphous substrates by the PLD method

I.A. Petukhov[1], D.A.Zuev [2], O.D. Khramova [2], O.A. Novodvorsky[2], A.A.Lotin [2], L.S.Parshina [2], B.K.Ivanov [3], M.H.Rumyantseva [1]

1 Lomonosov Moscow State University, Chemical faculty, 119991, Moscow.
2 Institute of laser and information technologies of the Russian Academy of Sciences, 140700, Moscow region, Shatura, Svyatoozerskaya St., 1.
3 Institute of the general and inorganic chemistry of a name of N. S. Kurnakov of the Russian Academy of Sciences, 119991, Moscow, Leninsky Avenue, 31.

onov@mail.ru

Thin films of A^2B^6 semiconductors serve as components of multilayered thin-film structures of micro-and nanophotonic devices, in particular, thin-film solar elements.
This work is devoted to research of influence of density of energy on targets and temperatures of a substrate (Ts) on phase structure, a microstructure and optical properties of CdS thin films deposited on glass substrates by the method of the pulse laser deposition (PLD) with use of nanosecond impulses of the second harmonica of YAG:Nd3+laser, energy density on a target varied in the range of 1.5 - 5.5 J/cm^2.CdS is the direct gap semiconductor of n-type and its band gap is 2.42 эВ in a cubic phase. The CdS thin films crystallize in two phases: cubic with structure of sphalerite and hexagonal with structure wurtzite [1-4]. By the X-ray phase analysis method it is established that the CdS films received by us represent mix of two phases (fig.1a): hexagonal phase with structure wurtzite (111 - 26,5^0) and a cubic phase with structure of sphalerite (220 - 43,4^0).

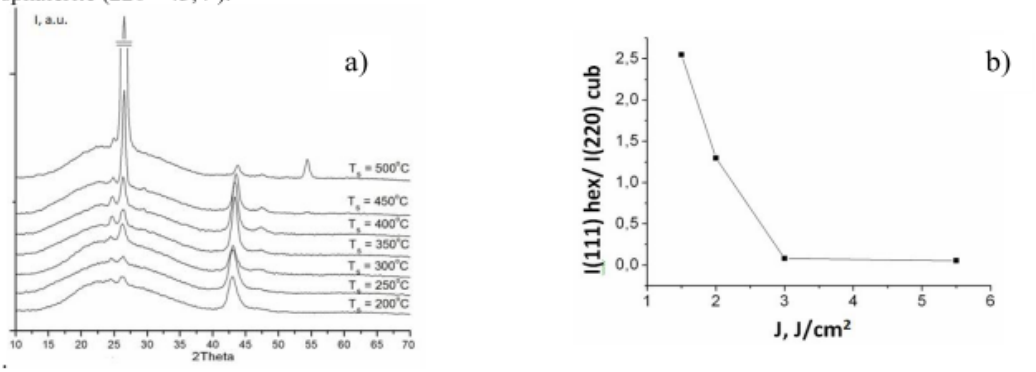

Fig. 1.a- Diffraction pattern of films of CdS received at various temperatures of a substrate (Ts = 200÷500 of °C) at J=3J/cm2. b). Ratio of intensity of peaks of the cubic and hexagonal phases CdS on the diffraction pattern of CdS films depending on density of energy of a laser impulse (J).

In this work it is shown that the variation of density of energy of the laser (J) on targets and temperatures of a substrate (Ts) result in changes of phase structure of CdS films. Thus, the relative maintenance of hexagonal and cubic phases in the composition of the CdS films deposited by the PLD method, it is possible to vary by selection of parameters of laser synthesis.

The absorption spectra of samples were received from which band gap was determined. In process of increase of temperature of a substrate from 200 °C to 500 °C the increase in band gap was observed from 2.16 till 2.33 eV that corresponds to increase a part of the hexagonal phase CdS in two-phase mix.
Thus, the mechanism of increase band gap and possibility of direction, by a ratio of the cubic and hexagonal phases CdS at growing on an amorphous substrate were found that expands the range of application of CdS nanometer films of for devices micro- and nanophotonics.
This work has been supported by grants RFBR № 14-07-00408-a, 12-02-33022-mol-a-ved.

[1] S.Chun, Y.Jung, J.Kim, D.Kim. The analysis of CdS thin film at the processes of manufacturing // Journal of Crystal Growth vol. 326, pp.152–156, (2011)
[2] D.W. Lane. A review of the optical band gap of thin film CdS_xTe_{1-x} // Solar Energy Materials & Solar Cells vol..90, pp.1169–1175, (2006).
[3] X.L. Tong, D.S. Jiang, L. Liu, Z.M. Liu, M.Z. Luo. Effect of the laser fluence on structural and optical characterization of thin CdS films synthesized by femtosecond pulsed laser deposition // Optics Communications vol . 270, pp.356–360 (2007).
[4] S.Mishra, A.Ingale, U.N. Roy, A. Gupta. Study of annealing-induced changes in CdS thin films using X-ray diffraction and Raman spectroscopy // Thin Solid Films vol. 516, pp. 91–98, (2007).

Influence of the plume energy on the SnO_2:Sb films characteristics by using the PLD droplet-free method

L.S. Parshina[1], O.A. Novodvorsky[1], O.D. Khramova[1], I.A. Petukhov[2], A.A. Lotin[1], V.A. Mikhalevskiy[1], A.V. Shorokhova[1]

1 - Institute on Laser and Information Technologies of RAS, 140700, Shatura, Russia
2 - M.V. Lomonosov Moscow State University, Faculty of chemistry, 119991 Moscow, Russia

ParshinaLiubov@mail.ru

Films of transparent conducting oxide (TCO) widely are used as transparent high-conductivity thin-films materials for application in different regions, such as solar cells, gas sensors, optoelectronic devices, high-temperature mirrors and flat-panel displays [1]. Indium tin oxide (ITO) films usually are used for these applications owing to their unique optical and electrical properties [2]. However, the important deficiency of the ITO films applications is their high cost and the high temperature of growth that makes difficult their deposition on the flexible polymer substrates [3]. Alternative for the ITO films is the SnO_2:Sb (ATO) films for which there is a perspective of the temperature deposition reduction [4]. The PLD method permits the SnO_2:Sb films to crystallize at the lower substrate temperatures relative to the other physical vapor deposition techniques due to the high kinetic energies (> 1 eV) of the ionized and ejected particles in the laser-produced plasma [5]. Therefore, the production and investigation of the high-conductivity transparent in the visible range SnO_2:Sb thin films remain the actual task.

High-conductivity transparent in the visible range SnO_2:Sb thin films (100 nm thickness) have been produced by the pulsed laser deposition (PLD) method on quartz substrates without a post-deposition annealing at various energy of the deposited particles. The SnO_2:Sb thin films has been grown by using the speed separator at the different levels of the antimony doping from 0 at. % to 8 at. %. The structural, electrical, and optical properties of these films have been investigated as a function of doping level, substrate temperature, oxygen partial pressure during deposition and deposited particles energy. XRD analysis indicated that the films grown at low temperatures (25-200 °C) were amorphous, while films grown at the higher temperatures (> 300 °C) showed a crystalline structure. The dependence of the SnO_2:Sb films lattice parameters on the target energy density has nonmonotonic character. The minimum resistivity of the SnO_2:Sb films has been $1{,}2 \cdot 10^{-3}$ Ohm·cm. The optical transmittance spectra of the SnO_2:Sb films produced at the established optimal PLD conditions and the antimony concentrations were informed that the films had a high transparent in the visible range from 400 nm to 700 nm. The average transmittance of the SnO_2:Sb film was observed to be 85 %. The surface morphology of the films received by using the speed separator of the deposited particles has been investigated. The surface roughness of such films didn't exceed 2 nm.

This work has been supported by grants RFBR № 14-07-00408, 14-07-00688, 12-02-33022, president grant MK-6798.2013.9

[1] A. Goetzberger and C. Hebling, Photovoltaic materials, past, present, future, Solar Energy Materials and Solar Cells, vol. 62, pp. 1-19, (2000).
[2] E. Terzini, P. Thilakan, C. Minarini, Properties of ITO thin films deposited by RF reactive magnetron sputtering at elevated substrate temperature, Materials Science and Engineering: B, vol. 77, pp. 110-114, (2000).
[3] D.A. Zuev, A.A. Lotin, O.A. Novodvorsky, F.V. Lebedev, O.D. Khramova, I.A. Petukhov, Ph.N. Putilin, A.N. Shatokhin, M.N. Rumyanzeva, A.M. Gaskov, Pulsed laser deposition of ITO thin films and their characteristic, Semiconductors, vol. 46, № 3, pp.410-413, (2012).
[4] H. Kima and A. Pique, Transparent conducting Sb-doped SnO_2 thin films grown by pulsed-laser deposition, Applied Physics Letters, vol. 84, №2, pp. 218-220, (2004).
[5] D.B. Chrisey and G.K. Hubler, Pulsed laser deposition of thin films (New York : John Wiley and Sons), Chapter 3, (1994).

Structural and morphological properties of Nb thin films grown by pulsed laser deposition

A. Lorusso[1], F. Gontad[1], A. Perrone[1], I. Koutselas[2], N. Vainos[2]

1-University of Salento, Department of Mathematics and Physics "E. De Giorgi", and National Institute of Nuclear Physics, 73100 Lecce, Italy

2-Department of Materials Science, University of Patras, 26500 Patras, Greece

Main author email address: antonella.lorusso@le.infn.it

Niobium (Nb) thin films were grown on Si(100) substrates by pulsed laser deposition (PLD) in high vacuum at room temperature under different laser fluences (4.8-30 J/cm^2). The influence of laser fluences on the structural and morphological properties of the films was studied by X-ray diffraction (XRD) and scanning electron microscopy (SEM). XRD investigations showed a polycrystalline structure of the deposited films. The droplet density on the film surface was extremely low and decreased with the laser fluences. Profilometric measurements of the deposited Nb films revealed a slight asymmetry related to the plume deflection effect. The measured electrical resistivity of the Nb film was higher than that of high purity Nb bulk. The ablation rate and deposition rate are also presented and discussed.

Fabrication and application of nanosecond laser-generated surface nanostructures on polyimide

L. Bayer[1, 2], P. Lorenz[1], M. Ehrhardt[1], K. Zimmer[1], L. Engisch[2]

1 Leibniz-Institut für Oberflächenmodifizierung e. V., Permoserstr. 15, 04315 Leipzig, Germany
2 Hochschule für Technik, Wirtschaft und Kultur Leipzig, P.O. Box 301166, 04251 Leipzig, Germany

pierre.lorenz@iom-leipzig.de

Nanostructures exhibit a growing commercial interest where a fast, cost-effective, and large-area production is attainable. Laser methods have a great potential for the easy fabrication of nanostructures. In this study, the laser-induced nanostructuring and their application fields on polyimide (PI) foils is presented where the formation of nano-sized cone structures on PI, produced by laser irradiation near the ablation threshold, is studied. The properties of the laser-induced 3-D conical surface structures on PI dependent on the laser parameters are analysed by optical, scanning electron (SEM) as well as atomic force microscopy (AFM). For example, the cone density dependency on the laser parameters (see Fig. 1 (a)) allows the fabrication of a microscopic QR-code (see Fig. 1 (b)) and the grey-tone images (see Fig. 1 (c) and (d)) with very low thermodynamic damage outside the irradiated area. Furthermore, these images can be used for high-security applications: it is possible to create pictures with very high resolution with special optical properties due to the 3D-cone structures on the PI (see Fig. 1 (d)).

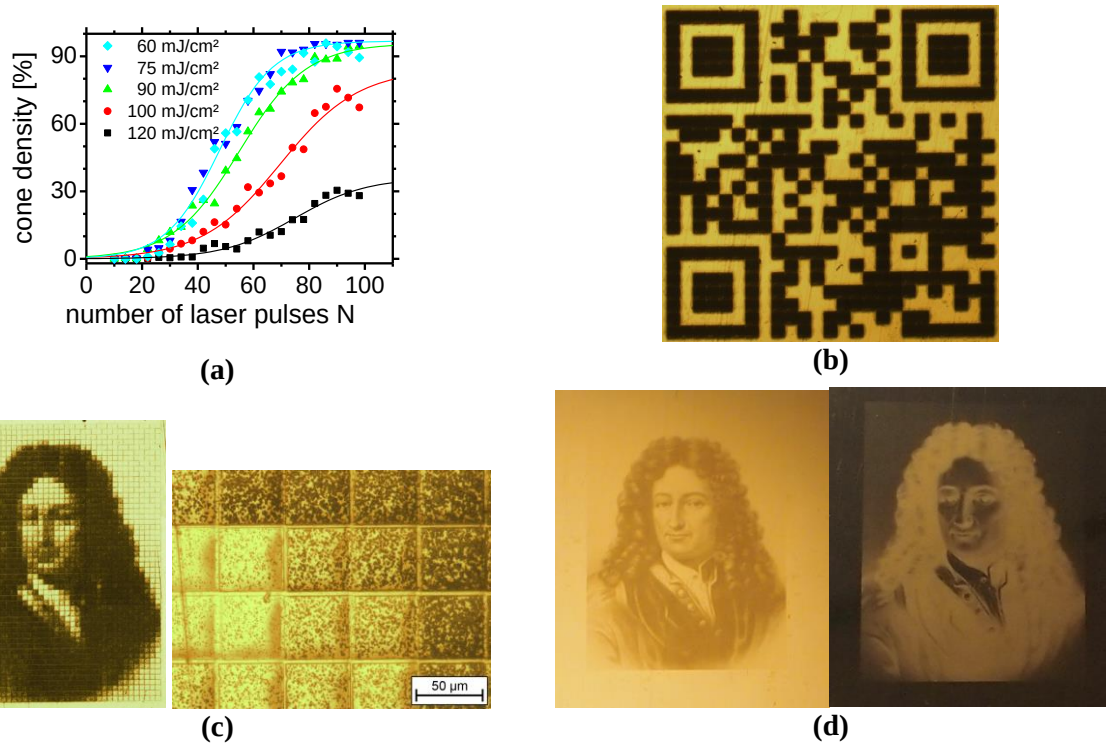

Figure 1 (a) Laser-induced cone density on polyimide dependent on the laser parameters (laser fluence Φ and number of laser pulses N) at a laser spot size of 50 x 50 µm²
(b) optical microscopic image of a laser-fabricated QR-Code on polyimide (laser spot size 50 x 50 µm², Φ = 35 mJ/cm², N = 75)
(c) (left) optical microscopic image of a low-resolution image of Gottfried Wilhelm Leibniz on polyimide (image size: 2 x 2.6 mm², resolution: 40 pixel x 52 pixel) produced with a laser spot size of 50 x 50 µm² and different laser parameters and cone density, respectively. (right) higher magnified optical view of the Leibniz image at the neck position
(d) optical image of a high-resolution image of Gottfried Wilhelm Leibniz (image size: 2 x 1.535 cm², resolution: 400 pixel x 307 pixel) at bright and dark background.

Formation of Aerosol Particles by Physical and Chemical Vapor Deposition in Field of Laser Radiation

V.V. Levdansky[1], J. Smolik[2], V. Zdimal[2]

1- Heat and Mass Transfer Institute NASB, 15 P. Brovka Str., 220072 Minsk, Belarus
2- Institute of Chemical Process Fundamentals AS CR, v.v.i., Rozvojova 135, 165 02 Prague, Czech Republic

Main author email address: vlev5@yahoo.com

Mechanisms of aerosol particle formation by vapor deposition are of interest for different kinds of atmospheric phenomena (e.g. formation of water drops and smog particles) and for nanotechnology processes (e.g. production of nanoparticles). It is known that the gas-to-particle conversion can be realized by physical and chemical vapor deposition. Resonance laser radiation can affect formation of aerosol particles due to heating of the gas-particle system as well as due to resonance effects related to a change in such parameters as sticking coefficients of vapor and foreign gas molecules at the particle surface, the energy of evaporation (desorption) of these molecules and the rate constants in the equations for chemical reactions (in the case of chemical vapor deposition). The paper deals with the theoretical study of the influence of resonance radiation on formation of aerosol particles by physical and chemical vapor deposition in the presence in the system of an adsorbable foreign gas.

It is shown that excitation of vapor and/or foreign gas molecules by resonance radiation can lead to a change in the equilibrium condition in the particle-vapor-foreign gas system and accordingly to a change in the critical size of the particles (clusters). Resonance radiation can increase the rate of evaporation of molecules from aerosol particles in several ways. The particle temperature increases under the influence of resonance radiation due to particle heating by radiation flux and deactivation of excited by resonance radiation gas molecules on the particle surface. It leads to both an increase in the rate of evaporation of molecules of the main component from the particle and the desorption rate of adsorbed molecules of a foreign gas from the particle surface. The last factor decreases the blocking effect of foreign gas molecules in relation to phase transitions on the particle surface that in turn increases the rate of phase transitions (condensation and evaporation of molecules of the main component). Moreover, excitation of vapor and foreign gas molecules in the field of resonance radiation can lead to a change in the sticking coefficient of these molecules. It is shown that above-mentioned processes can affect the rate of nucleation and the particle growth rate.

In the case of chemical vapor deposition resonance radiation can excite precursor molecules in a gas phase that leads to a decrease in the activation energy of decomposition of precursor molecules. This in turn can affect processes taking place on the particle surface and accordingly the particle growth rate. It should be noted that evaporation of molecules (atoms) from aerosol particles that are formed by chemical vapor deposition is often not taken into account. In the general case the particle growth rate depends on both the incorporation of molecules (atoms) into the particle and its evaporation. It is shown that in the general case the joint influence of resonance and thermal effects in chemical vapor deposition under the influence of resonance radiation can lead to the appearance of a maximum in the dependence of the particle growth rate on the radiation intensity.

It is shown that in the case of nanoscale aerosol particles the influence of size effects, related to the dependence of the parameters describing physicochemical processes in the gas-particle system on the particle size, can also affect particle formation by physical and chemical vapor deposition.

Atomic-force microscopy of silver iodide nanocrystals under laser stimulated surface optical sensitization

S. Vinogradov[1], M. Kononov, V. Kononov, V. Savransky

1- Prokhorov General Physics Institute of the Russian Academy of Sciences, Russia, 119991, Moscow, Vavilov Str., 38
sergeivinograd@gmail.com

Following our previous works [1, 2] we have investigated silver halide nanocrystals by atomic-force microscopy (AFM) in the process of laser stimulated surface optical sensitization by molecules of sensitizer. Silver iodide nanocrystals were used in the shape of thin polycrystalline film on glass substrate while molecules of arsenaso III sublimated from solid phase onto nanocrystals surfaces. For achieving surface optical sensitization of silver iodide nanocrystals the film surface was exposed by 540 nm laser radiation which is in arsenazo III absorption band. AFM was appled for investigation of silver iodide nanocrystals photochemical transitions in the surface optical sensitization process (Fig.1).

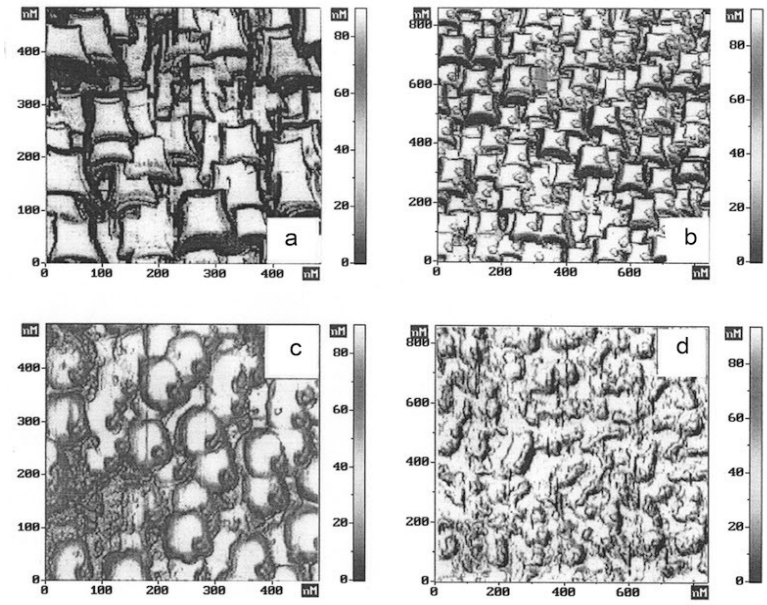

Figure 1. AFM-images of thin polycrystalline silver iodide film transformations under surface optical sensitization.

Figure 1a corresponds to clear silver iodide nanocrystals while images 1b-1d illustrate nanocrystals transformation up to semi-amorphous film. Fig.1b shows silver iodide nonocrystals with anomic silver nanoclusters resulting surface optical sensitization process. Thus AFM-images of different serial phases of thin polycrystalline silver iodide film exposed by laser radiation in the present of arsenaso III molecules and stimulating laser radiation were obtained. For the first time AFM-images of atomic silver clusters in silver halide nanocrystals as well as resulting destruction of nanocrystals were demonstrated.

[1] S.V. Vinogradov, M.A. Kononov, V.V. Savranskii, S.I. Valyanskii, M.F. Urbaitis, Effect of optical sensitisation on a surface plasmon resonance, Quantum Electronics, vol. 33, pp. 711–713, (2003).
[2] S.V. Vinogradov, M.A. Kononov, S.I. Valyanskii, A.G. Makarov, V.V. Savranskii, Surface optical sensitization of a thin polycrystalline silver iodide film by brilliant green molecules, Bulletin of the Lebedev Physics Institute, vol. 39, pp. 12-15, (2012).

Method of deposition nanoparticles from small colloidal drop

A. Antipov, S. Arakelian, S. Kutrovskaya, A. Kucherik, A. Osipov

Department of Physics and Applied Mathematics, Stoletovs' Vladimir State University,

Gorky st. 87, Vladimir, 600000 Russia

Phone: +7(4922) 477796

Fax: +7(4922) 333369

E-mail: osipov@vlsu.ru

The scheme of nanoparticle deposition from colloidal small droplets deposited on the surface of the solid substrate was used for the formation of planar structures. The main idea of the method is the obtaining of the planar structures using pinning effect. Pinning effect occurs when the droplet of colloidal solution is small enough for making an additional energy barrier which is made by precipitated particles near the perimeter of the drop. The energy barrier prevents the drop border movement. Because of this effect the droplet evaporates without diameter changing.
It is necessary to satisfy the condition $B_0 \ll 1$ for the pinning effect realization. In this case the surface tension forces (hold the spherical droplet shape) are stronger than the gravitational (flatten droplet).

$$B_0 = \frac{g(\rho_d - \rho_m)d^2}{\sigma}, \quad (1)$$

where B_0 – Bond number, g – the free fall acceleration, ρ_d – of the droplet liquid phase density, ρ_m – the density of the medium in which the droplet is.
The purpose of this work is the comparison of the nanoparticle deposition processes from colloidal droplet using various regimes. During the first regime the natural colloidal droplet evaporation was used, during the second one the volume of the droplet was heated by the laser radiation.

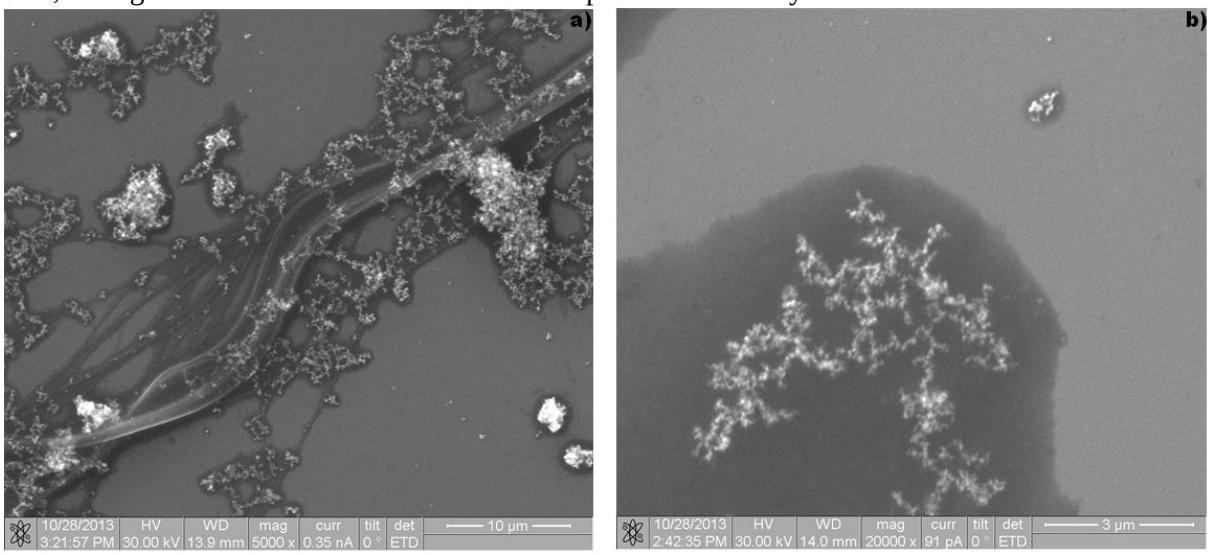

Figure 1 The deposition of metal clusters and the formation of fibers during the natural evaporation of a droplet (a), the cluster deposition and formation using laser radiation on the droplet volume (b). Figures have gotten on Raster Electron Microscope Quanta 200 3D.

Spectroscopic and Pulse Generation Investigation of Co^{2+}:MALO Saturable Absorber as Separate Sample and as Thermally Bonded with Active Media

J. Mlynczak[1], N. Belghachem[1], K. Kopczynski[1], J. Mierczyk[1]

1- Institute of Optoelectronics, Military University of Technology
Gen. S. Kaliskiego 2 Str. 00-908 Warsaw, Poland

jmlynczak@wat.edu.pl

Because of their simplicity, q-switching saturable absorbers are widely used in lasers to generate pulses at wide range of wavelengths [1, 2]. The output characteristics of such lasers strongly depend on the principal parameters of saturable absorbers such as the ground state absorption cross section, the excited state absorption cross section the dissipative losses [3, 4]. Thus to design a laser with desired temporal and power characteristics these parameters have to be known with high accuracy. These parameters can vary over wide ranges even for the absorbers characterized by the same small signal transmission and thickness so they should be known for each single sample before applying it to a laser.

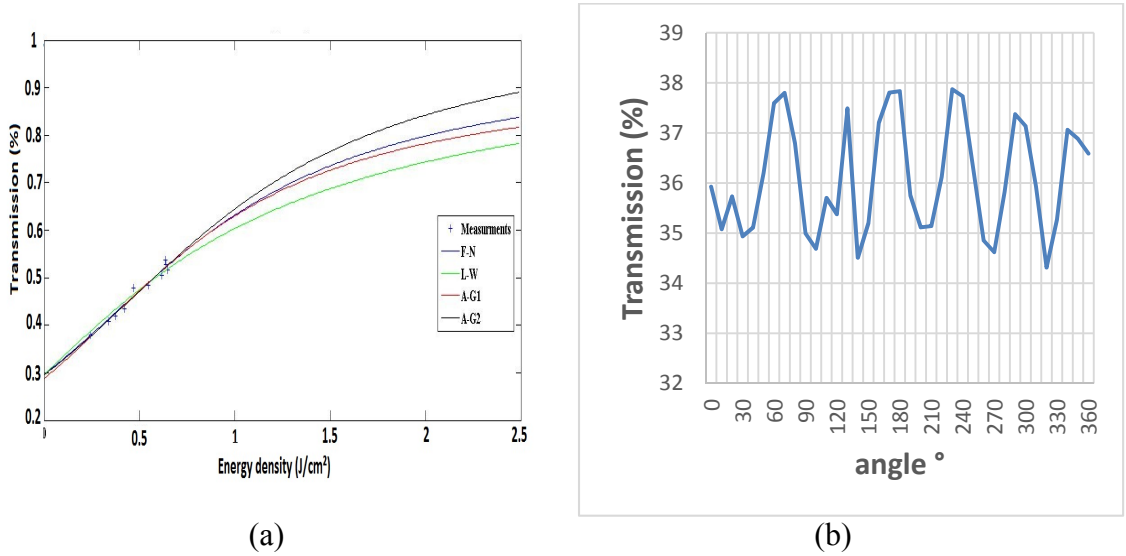

(a) (b)

Figure 1. (a) Non-linear abosption of a Co^{2+}:MALO sample and the curve fitting using three different models. (b) MALO:Co transmission anisotropy at 1535 nm

The non-linear absorption and the anisotropy of a set of Co^{2+}:MALO saturable absorbers were investigated at the wavelength of 1535 nm and 1332 nm, and their main parameters were calculated using three different models [5]. Figure 1 shows the experimental results and the approximation using these models. Those samples were thermally bonded to the glass samples doped with Er and Yb ions. Finally the pulse generation using Co^{2+}:MALO samples and the glass samples (separately and thermally bonded) were investigated and compared in both cases.

[1] Y. Kalisky, Cr4+-doped crystals: their use as lasers and passive Q-switches, Prog. Quantum. Electron. Vol. 28, pp. 249–303, (2004).
[2] J. Mlynczak, K. Kopczynski, Z. Mierczyk, M. Malinowska, P. Osiwianski, Pulse generation at 1.5 μm wavelength in new EAT14 glasses doped with Er3+ and Yb3+ ions, Optoelectronics Review, Vol. 20, No. 1, pp. 14-17, (2012).
[3] J.J. Degnan, Optimization of passively Q-switched lasers; IEEE J Quantum Electron. Vol. 31, pp. 1890-1901, (1995).
[4] J. Mlynczak, K. Kopczynski, Z. Mierczyk Optimization of Passively Repetitively Q-Switched Three-Level Lasers, Journal of Quantum Electronics, Vol. 44, No. 12, pp. 1152-1157, (2008).
[5] J. Mlynczak, K. Kopczynski, Comparison of parameters of q-switching saturable absorbers estimated by different models and the impact of accuracy of input data on the results of the estimation, Optical Materials, Vol. 36, pp. 867-872, (2014)

Variations in electrical response of thin-film multilayer structure based on PZT to the modulated laser irradiation

O.Sergeeva[1], A.Bogomolov[1], I.Pronin[2], V.Senkevich[2], E.Kaptelov[2]

[1]*Laboratory of Ferroelectrics and Piezoelectrics, Tver State University, 170002, Tver, Russia*
[2]*Laboratory of Ferroelectrics, Ioffe Institute, 194021, St.-Petersburg, Russia*

E-mail: o_n_sergeeva@mail.ru

In the work, an electrical response of the thin-film PZT-PbO composite capacitor structure was studied as a result of modulated laser irradiation. Thin-film PZT-PbO composite were prepared by RF magnetron sputtering of ceramic PZT+10% mol. PbO target onto «cold» silicon substrate preliminary covered by thin platinum layer surved as a bottom electrode of the structure and then annealed at elevated temperatures in the air atmosphere. The thickness of ferroelectric thin-film composite was as much as 300 nm. As a top electrode of ferroelectric capacitor platinum contact pads were used. Rectangular modulated pulses of laser beam (wavelength 630 nm) were used as a source of heat and light exposure. As a result of irradiation to the structure, an electric response whose signal direction and form having been changed varied with annealing temperatures. As a result of irradiation we observed electrical response whose configuration, the amplitude and direction varies with the annealing temperature, Fig. 1

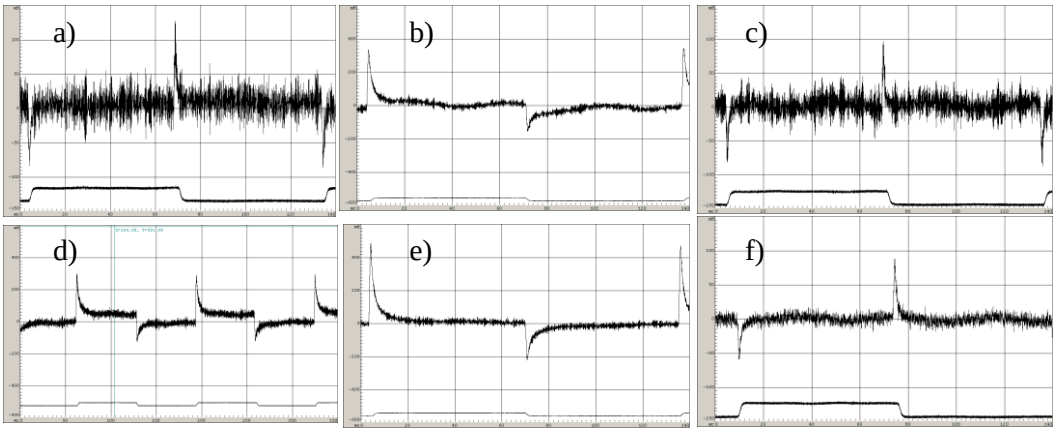

Figure.1. Oscillograms of electrical response of PZT-PbO composite films annealed at elevated temperatures: a – 535 °C; b– 545 °C; c – 555 °C; d – 560 °C; e – 565 °C; f – 570 °C

Changing of polarity and shape of the electric response to heat (and simultaneously optical) radiation was associated with a change of lead content (PbO) in the film as well as the behavior of the dielectric constant depending upon the annealing temperature. Apparently, we have observed responses were different in nature. The responses shown in Fig. 1 (a, c, f) correspond to real pyroelectric effect [1], reflecting the presence of macroscopic polarization vector oriented in the direction to bottom interface of the composite. The constant component of the response (Fig. 1, d) is associated with a photoelectric effect induced by asymmetric Schottky barrier on top and bottom interfaces due to effective layers of PbO characterized by semiconductor properties. Layers of PbO in the intergranular space of perovskite grains provide pass-through conductivity [2]. The disappearance of the constant component of the signal (Fig. 1, b, e) means a decrease in the content of PbO in the composite and abuse pass-through conductivity. Preservation of the impulse response of the same polarity indicates differentiation of photoresponse from the effective layers of PbO with a help of dielectric layers of PZT. The results obtained are discussed.

[1] Bogomolov A.A., Sergeeva O.N., Kiselev D.A., Pronin I.P., Afanasjev V.P. Pyroelectric and photoelectric responses of capacitors based on thin PZT films // Phys. Solid State. V. 48,. N.6. P.1194–1196 (2006)
[2] Gushchina E.V., Ankudinov A.V.; Delimova L.A.; Yuferev V.S., Grekhov I.V. Spreading resistance microscopy of polycrystalline and single-crystal ferroelectric films // Phys. Solid State. V. 54, N.5. P. 1005-1007 (2012).

Laser Forming of Micropeaks on Curved Surfaces of Glass-Carbon Plates

T. Sokolova[1], E. Surmenko[1], V. Shesterkin[2], A. Konyushin[1], Yu. Chebotarevsky[1], I. Popov[1]

1- Saratov State Technical University named after Yu.A. Gagarin, 77 Polytechnicheskaya st., 410054, Saratov, Russia
2- JSC "SPE "Almaz", 1 Panfilova st., 410033, Saratov, Russia
sokolova@pribor-t.ru

Graphite with its modifications, in particular glass-carbon, is a very promising substance for the manufacture of emitting electronic devices because of its unique properties. This material is treated well by laser radiation. It has excellent absorption capacity at 1064 nm wavelength, which is the most characteristic of the process equipment. Besides, glass-carbon has the valuable property of being able to self-organize nanostructures on its surface under laser action.
It was found out that the curved emission surface provides the higher density of electronic streams. In this case the micropeaks are formed on a curved surface so that the symmetry axis of each of them coincide with the radius of curvature of the surface. This design allows to maintain laminar electron trajectories.
The curved surface can be obtained by any appropriate way, in particular, by laser milling. Matrix of peaks is formed by laser micrograving. Peaks have a conical shape, the axis of symmetry of each is directed along the radius of curvature of the surface (Fig.1).

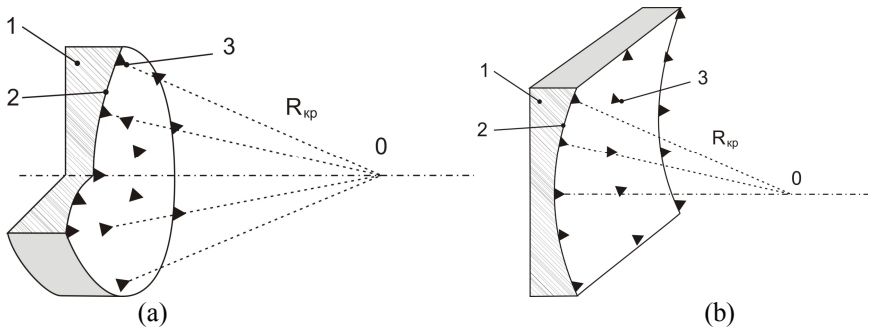

Figure 1 Structuring of the spherical (a) and cylindrical (b) glass-carbon surfaces: 1 – perform; 2 - concave spherical surface with a required radius of curvature $R_{кр}$,; 3 – conical micropeak.

Laser micrograving of surface is performed by 1.06 μm solid-state Nd:YAG-laser, power 10-20 W, pulse repetition rate 1-10 kHz. Wherein the preform performs a swing in an arc about the center of curvature O with a successive circular (for spherical preform) or linear (for cylindrical preform) shift. There is a self-organized nanorelief on the tops of the micropeaks.
The proposed solution results to increase the density of the electron beam current by more than 10 times compared to the previous model with a flat surface [1].
Acknowledgements: The work was partly supported by Russian Scientific Fund (appl. 14-12-00395); equipment of VCCU "Laser & Optical Technologies".

[1] T. N. Sokolova, E.L. Surmenko et al, Laser structuring of glass-carbon for improvement of its emitting properties, Bern Open Publishing / ALT Proceedings, vol.1, https://bop.unibe.ch/ALT-Proceedings/article/view/44, (2012).

Pore collapse dynamics in coatings under the laser annealing.

M.S. Grigoryeva[1,2], A.P. Kanavin[1,2] and I.N. Zavestovskaya[1,2]

1 – P.N.Lebedev Physical Institute of Russian Academy of Sciences,

Leninsky prosp. 53, 119991, Moscow, Russia

2 – National Research Nuclear University MEPhI (Moscow Engineering Physics Institute),

Kashirskoe shosse, 31, 115409, Moscow, Russia

e-mail: zolotykh@lebedev.ru

A self-consistent model of the pore collapse in the metal coatings under the laser annealing has been developed. In the approximation of melting front constant velocity the change of pore size and material porosity has been obtained depending on distance from the melting front. In the present work the dynamics of coatings porosity decrease due to the pore collapse in the melting material has been investigated.

The authors consider the case when the spherical pores isolated from each other are formed under the motion of melting front. The pore size is determined by the initial size of coatings defects. Under laser melting of the coating the melted material flows into the empty pores and they collapse. The dynamics of the pore collapse in a self-consistent way is determined by the process of heat conductivity and the melt hydrodynamics. In the present paper the authors take into account both the liquid “local” motion near the arbitrary chosen pore, which leads to the flow of liquid into the pore and results in the change of the pore size, and the “macroscopic” averaged motion of liquid from the surface to the melting front caused by the change in the volume occupied by the liquid.

On the one hand, the collapse velocity of a single empty pore in the melt is defined by the surface tension force, and, on the other hand, by the pressure in the melted material at a certain distance from the pore. The melt macroscopic motion from the surface to the sample depth is conditioned by the difference in the pressure at the coating surface and in the sample depth. So, the dynamics of liquid flow into the pores and the macroscopic translatory motion of the melt from the surface to the sample depth turn to be connected via the pressure at the melt given depth. The pressure value essentially depends on the velocity of the melting front motion, and is determined by the heat conductivity processes, which, in its turn, depend on the material porosity.

Modeling of Nanosecond Laser Vaporization of Metals. In Near Critical Region

V.I.Mazhukin[1], A.A.Samokhin[2], M.M.Demin[1], A.V.Shapranov[1]

[1]Keldysh Institute of Applied Mathematocs, Russian Academy of Sciences, Moscow, Russia
e-mail: vim@modhef.ru
[2]Prokhorov General Physics Institute, Russian Academy of Sciences, Moscow, Russia

Theoretical and experimental-investigations of laser vaporization of metals in near critical region which are continued for decades (see, e.g., [1,2] and references therein) remain incomplete in several aspects including unresolved problems of metal-dielectric transition and explosive boiling. In this paper nanosecond laser heating of liquid metal film (Al, thickness 417 nm, initial particles number $5\ 10^5$) from subcritical to supercritical states is investigated in the framework of molecular dynamic simulation combined with a continuum description of conduction band electrons system. As in the case of dielectric film considered before [3] it is possible to discriminate four different regimes of film behavior depending on the laser: intensity: quasi-stationary regime with surface evaporation, explosive (volume) boiling, spinodal decomposition and supercritical fluid expansion. It should be mentioned that occurrence of explosive boiling in metals is not so evident as in dielectrics because of high values of metal absorption and heat conduction coefficients In the considered and more thick films explosive boiling can repeat itself as it was predicted forty years ago [4] and recently confirmed numerically [5] Recoil pressure pulsation due to explosive boiling can be used as a marker of approaching critical parameters values in irradiated sample.

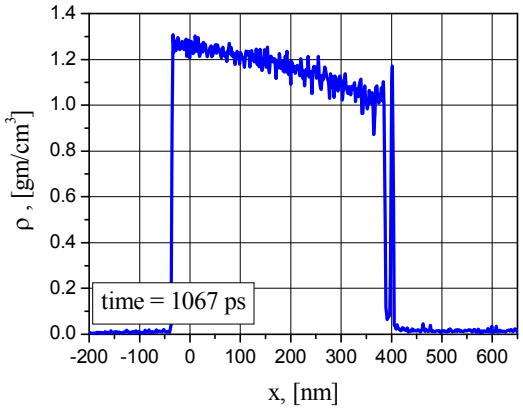

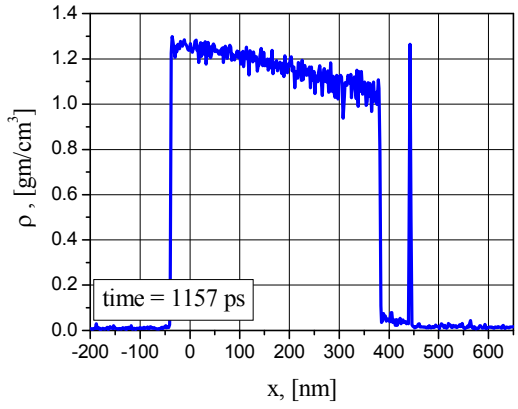

[1] A.A. Samokhin “First-order phase transitions induced by laser radiation in absorbing condensed matter” Proc. Institute of General Physics (USSR: Academy of Sciences) 13, p.1 (1990)
[2] C. Wu, L.V. Zhigilei “Microscopic mechanisms of laser spallation and ablation of metal targets from large-scale molecular dynamics simulations” . Appl. Phys A **114**, p.11 (2014).
[3] V.I.Mazhukin, A.V.Shapranov, A.A.Samokhin, A.Yu.Ivochkin “Mathematical modeling of non-equilibrium phase transition in rapidly heated thin liquid film” Mathematica Montisnigri 27, p.65 (2013)
[4] A.A. Samokhin “On some peculiarities of laser-induced intense vaporization of condensed matter” Quantum electronics 1. p.2056 (1974)(in Russian)
[5] V.I.Mazhukin, A.A. Samokhin, M.M.Demin, A.V.Shapranov “Explosive boiling of metals during nanosecond laser pulse action” Quantum electronics 44, p. 283 (2014)
[6] V.I.Mazhukin, A.A. Samokhin, M.M.Demin, A.V.Shapranov. "Modeling of nanosecond laser vaporization and explosive boiling of metals". Mathematica Montisnigri 29, p.68 (2014)

Numerical Simulation of Laser Welding Deformation of Auxiliary Heat Source Controlled Aluminum Alloy Sheet Plate

Bizhe.Dong [1], Rongshi. Xiao[2]

Beijing University of Technology ,No. 100, Pingleyuan, Chaoyang District Beijing 100124 ,China

Weiye4869@126.com

Abstract: AA 2524 is a new type aluminum alloy with the highest damage tolerance and considered to be the primary material of choice for the skin of aircraft. Since the aluminum alloy material has a large coefficient of thermal expansion, the welding deformation and residual stress produced during the welding process are significant factors impacting the precision and performance of welding structure members, and it is still a significant topic that shall be solved urgently in the industrial production. This paper proposes a new aluminum alloy welding deformation control craft with laser on the upper side and electric arc down, which takes the 2524-T3 aluminum alloy with 1.5mm thick as experimental materials and adopts fiber laser and TIG electric arc in the experiment. With finite element method (FEM), simulation of laser welding deformation of the sheet plate is conducted, and the influence rules of different heat source loading methods on the deformation, as well as the mutual relation between auxiliary heat source temperature and residual stress changes are analyze in the deformation control process, so as to confirm appropriate heat source matching mode. On that basis, three-dimensional entity finite element mode of the auxiliary heat source weld zone is restored with ABAQUS technology for local plastic strain process, and the macro-cell technology is successfully transformed to the whole unit model for predicting the overall deformation control. According to the comparative research results, the auxiliary heat source added at the bottom can effectively reduce the welding deformation, and the optimized heat source matching model can also reduce the welding deformation.

Keyword: AA2524; Laser welding; Deformation control; Auxiliary Heat Source

Measurement of Temperature and Temperature Profile of Gaseous Flames using Holo-Shear Lens

Varun Kumar, Shilpi Agarwal, Manoj Kuamr and Chandra Shakher*

Laser Applications and Holography Laboratory, Instrument Design Development Centre, Indian Institute of Technology Delhi, Hauz Khas, New Delhi -110016

**Main author email address: cshakher@iddc.iitd.ac.in*

A hologram of a point source is usually known as hololens can function, both as negative and positive spherical lens. If two such holographic lenses are displaced with respect to each other and recorded on the same high resolution recording material. It is called holo-shear lens. These lenses can be used as lateral shearing interferometer [1-3]. It has already been demonstrated that two slightly displaced off-axis zone plate (holo-shear lens) acts as a double frequency grating. This paper describes the holo-shear lens made on dichromatic gelatin for measurement of temperature and temperature profile of gaseous flames.

When a collimated beam of laser light incident on the holo-shear lens through the flame, it will generate two laterally shifted wave fronts. Shearing interferometric fringes appear in the common area of original and displaced wavefront. These fringes can be used to determine the gradient of wavefront generated due to temperature field.

In this paper the construction of holo-shear lens and measurement of temperature field in gaseous flame is presented. The sensitivity of measurement and the spatial resolution will also be presented.

[1] J. C. Wyant, Double frequency grating lateral shear interferometer, Applied Optics, 14, pp. 2057-2060, (1973)

[2] P. hariharan, W. H. Steel and J. C. Wyant, Double grating interferometer with variable lateral shear, Optics Communication, 11, pp. 317-320, (1974)

[3] C. Shakher, K. Matsuda, and K. Tenjimibayashi, Testing of off-axis parabola by holo-shear lens, Proc. SPIE Vol. 3739, pp. 341-345 (1999).

THz Hadamard Transform Imager

T. Vasile[1], V. Damian[1], Daniela Coltuc[2], M. Petrovici[2]

1 - Lasers, National Institute for Laser Plasma and Radiation Physiscs, P.O.Box MG-36, RO-077125 Bucharest-Magurele, Romania
2 - Electronica Aplicata si Ingineria Informatiei, Univ. Politehnica Bucuresti, Bucharest, Romania

E-mail: tiberius.vasile@inflpr.ro

Over the past few years a great struggled was made for developing methods and devices for THz imaging. The most common method to obtain THz images is by raster scanning the object relative to a focused THz beam plane. Although this method reaches its goal in the end, the acquisition is time consuming and it involves moving parts. An alternative to this method is by using, THz sensitive, focal plane detector arrays. The improvements brought by such detectors are incomparable regarding real time image acquisition and the lack of moving parts, but this to confronts a major limiting factor regarding low sensitivity in THz range and purchase price.
Taking into account the above mentioned, our approach in this matter is the development of a device for image reconstruction using only one detector, and a series of image encoding binary masks; no moving parts necessary. The encoding sequence is projected using a digital micro-mirror device DMD and for each mask a voltage is acquired with a pyroelectric detector. Fig. 1. (a), (b)

(a) (b)

Figure 1. (a) DMD projecting one of the encoding masks of 63/65 pixels in bundle of 12/12 micro-mirrors. (b) Phyroelectric detector 0.1-30 THz range

The method is used in conjunction with one pixel detection type of setup and relies on a mathematical apparatus known as Hadamard Transform, more specifically a class of Hadamard matrix called S-matrix. Fig.2.

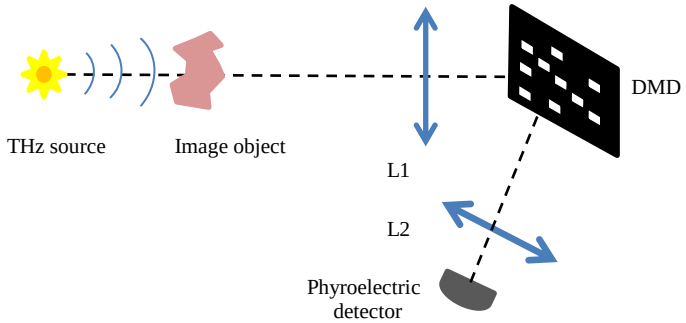

Figure 2. THz Hadamard Imager optical setup

[1] M. Harwit, N.J.A. Sloane, Hadamard Transform Optics (Academic Press), Chapter 3, (1979).

THz Generation by Combined One- and Two-photon Resonant Excitations in an Ensemble of Three Level Quantum Systems

E. Gaižauskas[1], O. Khasanov[2], V. Vaičaitis[1]

1- Vilnius university Laser Research Centre, Saulėtekio al.10, LT 10222 Vilnius, Lithuania
2- Scientific-Practical Material Research Centre, Belarus National Academy of Sciences, 19 Brovki str., Minsk 220072 Belarus

E-mail address: eugenijus.gaizauskas@ff.vu.lt

The theory of THz generation supported by amplification without inversion in the ensemble of three-level quantum system (TLQS) is developed. In the proposed scheme optically active vibration transitions from the ground state was driven by strong laser pulse and weak probe trough the forbidden in dipole approximation electronic state (se Figure 1a). An analytical expression for the gain of the law frequency wave is obtained from the set of modified Bloch and Maxwell equations in the case of undepleted pump approximation. An example of the dynamics of THz radiation generation under subluminal propagation of THz polarization source is shown in Figure 1b .

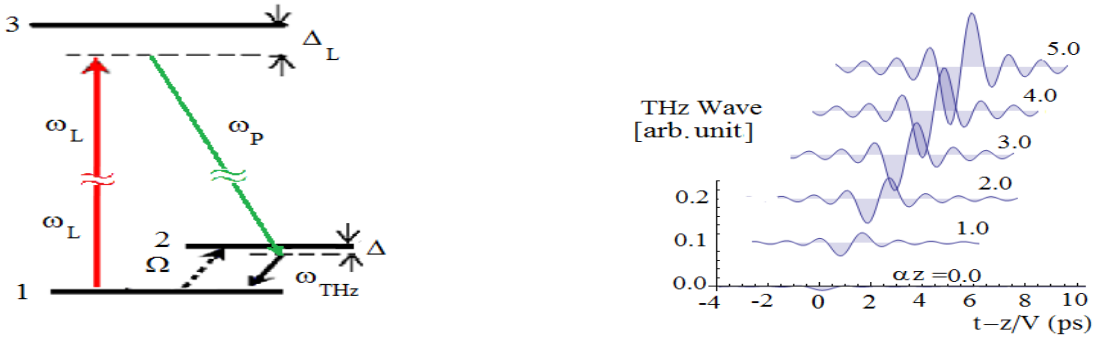

(a) (b)

Figure 1. (a) Two- and one-photon excitations in three-level configuration of TLQS. A relative strong laser pulse at frequency ω_L excites the two-photon transition $|1\rangle \rightarrow |3\rangle$ and a weak probe having frequency ω_P drives the transition $|2\rangle \rightarrow |3\rangle$. Coherent phonon-polariton excitation at the transition $|1\rangle \rightarrow |2\rangle$ radiates in THz range. (b) Dynamics of THz radiation generation under subluminal propagation of THz polarization source. Amplitudes of THz radiation are shown in vertically offsets at normalized (to the two-photon absorption length) propagation distances αz. In the vertical axis the arbitrary axis used to express relative grow of the THz amplitude as compared to the pump.

More comprehensive analysis for the precise evaluation of the conversion efficiency of the method was provided by the numerical analysis of the set of Maxwell-Bloch equations. Meanwhile, the results presented in this presentation substantiate the originally proposed scheme of the optical rectification method, offering strategy of design and making new materials for it. One of the possible directions comes from mature semiconductor manufacturing technologies, such as quantum dots in semiconductors nanoparticles. It is known, that resonant interaction with optical light fields is strongly enhanced here in comparison with atomic systems due to the quantum confinement effect [1, 2].

[1] P. Chen, C. Piermarocchi, and L. J. Sham. Phys. Rev. Lett. 87(6), 067401 (2001).
[2] E. Hanamura, Phys. Rev. B 37, 1273–1279 (1988).

Behavior of aqueous lysozyme solution when it's heated

M.I. Prudyvus, K.V. Fedorova, G.P. Petrova

Faculty of Physics
M.V.Lomonosov Moscow State University
Leninskie Gory, Moscow 119991 Russia

email address: fedorova@physics.msu.ru

Proteins tend to form inactive clusters at high temperatures. However, the protein clusters are one of the main reasons for the mass production of proteins with altered structure. Such proteins may serve as a cause of pathological conditions or lead to death [1].Lysozyme has many potential therapeutic applications to a wide range of human diseases. Lysozyme is part of the innate immune system and modify its level in the organism or its activity leading to various diseases (e.g., neonatal bronchopulmonary dysplasia, [2]). It's important to study the structure of lysozyme, and to find the influencing factors [3].

In this work, properties of macromolecules of lysozyme have been investigated with temperature change in the range from 20 to 40 °C by method of dynamic light scattering.

Experiments were performed in a pure solution, and using the stabilizing additives (NaCl, CaCl) having an ionic strength of 0,01. The concentration of lysozyme in all cases was 1 mg / ml.

Was found, the temperature range in which there is a change of the molecular structure of lysozyme (It this temperature range from 20 to 30 °C, according to theoretical sources). A restructuring of the active site of lysozyme, which apparently affects the size of the molecule. Calcium ions stabilize the active center when heated and do not prevent thermal aggregation of lysozyme.

Sodium ions have little effect on the restructuring of the active site of lysozyme. In this case, the process of cluster formation is stopping with increasing temperature in the studied range. Hysteresis phenomenon manifests itself actively in this experiment.

There are various structural changes in the enzyme, when the temperature of the aqueous solution of lysozyme changing from 20 ° to 40 ° C. They cause a change in the size and activity of the enzyme's molecule.

It can be concluded that the ions of sodium and calcium partially prevents changes in the structure of lysozyme.

The work was supported by RFBR grant № 12-02-00434.

[1] M. Bucciantini, E. Giannoni, F. Chiti, F. Baroni и L. Formigli, «Inherent toxicity of aggregates implies a common mechanism for protein misfolding diseases,» Nature, т. 416, pp. 507-511, 2002).
[2] M. Revenis и M. Kaliner, Lactoferrin and lysozyme deficiency in airway secretions: association with the development of bronchopulmonary dysplasia, т. 121, J. Pediatr, 1992, pp. 262-270
[3] Petrova G.P. "Physical Mechanisms of "Poisoning" the Living Organism by Heavy Metals" in the book ENVIRONMENTAL MONITORING, Ed.by E.O.Ekundayo, INTHECH open , 2011

The study of surface enhanced Raman scattering by steroids

O. P. Cherkasova[1,2], A.G. Milekhin[2,3]

1-Institute of Laser Physics of SB RAS, pr. Lavrentyeva, 13/3, Novosibirsk, 630090 Russia

2-Novosibirsk State University. Pirogov str. 2, Novosibirsk, 630090 Russia

3-A.V. Rzhanov Institute of Semiconductor Physics, pr. Lavrentieva, 13, Novosibirsk, 630090 Russia

e-mail: o.p.cherkasova@gmail.com

The steroid hormones influence on many physiological processes in humans is well known. The determination of the levels of steroid hormones is an important issue for the inspection of endocrinological disorders related to adrenal or gonadal function. Steroids have rather complex molecular structure, show significant reactivity with similar physical and chemical properties and are often located in low quantities in multicomponent matrices. The determination of steroids and their metabolites in biological samples can be done by chromatography, mass spectrometry, immunoassays and other methods of analysis with a high accuracy. However, these methods are time consuming and expensive. In this regard, the development of new operational methods of analysis is highly relevant.
The steroids differ only by the position of functional groups attached to the four-ring core and by the oxidation state of the rings. Spectral properties of steroids are well described in UV and IR spectral range. The lowest-lying vibrational signatures in corticosteroids are unique [1].
The effect of enhancement of Raman scattering by vibrational states of biologically active substances plays a principal role for the determination of small amounts of these substances [2]. Steroids have not been investigated by using this technique yet.
The paper discusses a film formation technique of steroid hormones on metal micro-and nanostructures fabricated on solid substrate by using nanolithography process, the approaches of controlling their properties as well as the mechanisms of enhancement of Raman scattering by steroid molecules.

This work has been supported by Russian Science Foundation (project №14-12-01037).

[1] I. N. Smirnova, D. A. Sapozhnikov, A. V. Kargovsky, V. A. Volodin, O. P. Cherkasova, R. Bocquet, A. P. Shkurinov, “Lowest-lying vibrational signatures in corticosteroids studied by terahertz time-domain and Raman spectroscopies Vibrational Spectroscopy”, vol. 62, pp 238–247 (2012).
[2] R. Stosch, F. Yaghobian, T. Weimann, R. J. C. Brown, M. J. T. Milton, B. Güttler, “Lithographical gap-size engineered nanoarrays for surface-enhanced Raman probing of biomarkers”, Nanotechnology, vol. 22, 105303 (6pp) (2011).

The interaction of cesium with globular proteins in model and native serum solutions of healthy and cancer patients by static light scattering (SLS)

I.A. Sergeeva, A.V. Komarova, V.V. Gibizova, A.V. Shlenskaya, A.D. Maslennikova, G.P. Petrova

Lomonosov Moscow State University, Faculty of Physics, GSP-1, Leninskie Gory, Moscow, 119991, Russian Federation

sergeeva@physics.msu.ru, vika2000-05@mail.ru, petrova@phys.msu.ru

Currently, the most rational medical developed many methods of treating diseases associated with changes in the properties and concentrations of the major serum proteins such as albumin and γ- globulin.

The relevance of this work is related to the extensive use of cesium chloride in various branches of medicine, in particular, using cesium chloride as an additional parameter in the diagnosis of cancer

This paper investigates the influence of cesium on globular proteins - albumin and γ-globulin - in model and native serum samples of healthy people and cancer patients.

Studies of serum model systems showed that for healthy patients dependence of the scattering parameter cH/R_{90} has a positive slope, for cancer patients scattering parameter slope becomes negative. With the addition of cesium chloride sign of the intermolecular interaction does not change (positive slope remains the same), and serum samples ill patients - is reversed (negative slope becomes positive). Thus, the coefficient of intermolecular interaction B - its sign and magnitude - is the most important diagnostic parameter.

The effective mass of the scattering particles in model solutions "cancer" blood containing ions CsCl, significantly greater than the mass of model solutions for a “healthy” blood, which is probably due to the interaction of the protein molecules γ-globulin and cesium ions in the first case.

Research on native serum samples confirmed the results obtained for model systems: for healthy patients positive slope of the concentration dependence of the scattering parameter is saved by adding cesium chloride; canser patients for the concentration dependence of the slope changes from negative to positive.

The highest value of the effective mass of the scattering is observed when the native serum solutions of human cancer patients with the addition of cesium chloride salt, indicating that the interaction with the cesium ions with the protein γ-globulin in this case.

On the basis of the experiments can be developed alternative methods of diagnosis and treatment of cancer in the early stages.

В настоящее время в медицине разрабатываются наиболее рациональные способы лечения многих заболеваний, связанных с изменением свойств и концентрации основных белков сыворотки крови, таких как альбумин и гамма-глобулин.

Актуальность данной работы связана с широким применением хлорида цезия в различных отраслях медицины, в частности, с использованием хлористого цезия в качестве дополнительного параметра при диагностике онкологических заболеваний [1, 2, 3].

Данная работа посвящена исследованию влияния ионов хлорида цезия на глобулярные белки – альбумин и γ-глобулин – в модельных и нативных образцах сыворотки крови здоровых и онкологически больных людей.

Исследования модельных систем сыворотки крови показали, что для здоровых пациентов зависимость параметра рассеяния имеет положительный наклон, для больных пациентов наклон параметра рассеяния становится отрицательным. С добавлением хлорида цезия знак коэффициента межмолекулярного взаимодействия не меняется (положительный наклон сохраняется), а в образцах сыворотки крови больных пациентов - меняется на противоположный (отрицательный наклон становится положительным). Таким образом, коэффициент межмолекулярного взаимодействия – его знак и величина – является наиболее значимым диагностическим параметром.

Значение эффективной массы рассеивающих частиц в модельных растворах «больной» крови, содержащих ионы CsCl, значительно больше значения массы для модельных растворов «здоровой» крови, что, вероятно, связано со взаимодействием молекул белка γ-глобулина и ионами цезия в первом случае.

Исследования на нативных образцах сыворотки крови подтвердили результаты, полученные для модельных систем: для здоровых пациентов положительный наклон концентрационной зависимости параметра рассеяния сохраняется при добавлении хлорида цезия; для больных пациентов наклон концентрационной зависимости меняется с отрицательного на положительный.

Наибольшее значение эффективной массы рассеивающих части наблюдается в случае нативных растворов сыворотки крови онкологически больных людей с добавлением соли хлорида цезия, что указывает на взаимодействие ионов с цезия с белком γ-глобулином в данном случае.

На основании проведенных экспериментов могут быть разработаны альтернативные методы диагностики и лечения онкологических заболеваний на ранних стадиях.

[1] Jose A. Centeno, Joseph P. Pestaner, Bennet I. Omalu, Norca L. Torres, Frances Field, Glenn Wagner and Florabel G. Mullick. Blood and Tissue Concentration of Cesium after Exposure to Cesium Chloride. Biological Trace Element Research. 2003.
[2] Sartori H.E. Cesium Therapy in Cancer Patients. Pharmacology Biochemistry & Behaviour. Vol. 21. 1984.
[3] Jin Zhong, Weiguo Yao, Weihua Lee. Cesium chloride protects cerebellar granule neurons from apoptosis induced by low potassium. International Journal of Development Neuroscience. 2007.

Photoluminescent silicon nanoparticles in water suspension stabilized by dextran coating

M.B. Gongalsky[1], Yu.I. Bezsudnova[1], V.Yu. Timoshenko[1]

1- Lomonosov Moscow State University. 1, Leninskie gory, Moscow, Russia.

E-mail: mgongalsky@gmail.com

Silicon nanoparticles (SiNPs) are very promising in biomedicine due to their high biocompatibility and biodegradibility. They can be used both for therapy and diagnotics of various diseases including cancer (e.g. photodynamic cancer therapy). Mainly, diagnostics is based on photoluminescent (PL) properties of SiNPs, which is quite efficient (quantum yield ~ 10%) in the near infrared range of spectrum (700-900 nm) [1]. This takes effect only if each SiNPs consists of agglomerated silicon nanocrystals with average size less than 5 nm. But the important challenge today is a creation of stable water suspensions of SiNPs, because this form is required for biomedical procedures. Relatively fast dissolution of SiNPs leads to both high biocompatibility and unstability. Dextran coating was successfully used for making biocompatible suspension, but its influence to the photoluminescent properties of SiNPs still hasn't been well-investigated [2].

In present work we used SiNPs made from so-called porous silicon. This material was formed via electrochemical procedure in HF-based solutions. Then porous silicon was grinded in a high energy planetary mill in liquid medium. There were two series of samples: uncoated and coated by dextran. Dextran coating was performed by ultrasonication for 30 minutes. Then suspentions were centrifuged in different regimes. Final average diameter of SiNPs was about 100 nm according to dynamic light scattering measurements. Dextran coating is a very simple procedure by comparison with another ones, e.g. PVA/PLGA coating, which demostrated enhancement of the PL of SiNPs [3].

We measured time-dependencies of the integrated PL of SiNPs in a days to weeks time scale. All the samples demonstrated significant degradation of the PL properties during the storage of the suspension, but dextran coating almost 2 times slowed down degradation process (10 days for coated SiNPs vs. 5 days for uncoated SiNPs). This was explained by decrease of the dissolution rate of dextran-coated SiNPs in water, which is vulnerable for the PL. Same effect was observed for suspensions with different concentration of SiNPs, but the diffence between coated and uncoated samples was maximal for lowest concentration of SiNPs in solution (~10 mg/l). Same conclusions could be made by analizing evolution of the maximum position of the PL spectra of SiNPs, which correlates with the average diameter of the nanocrystals. Blue shift of the spectra of uncoated SiNPs during the storage points to the significant size reduction generated by their dissolution, while the form of the spectra of dextran-coated nanoparticles was much more stable.

Also significant rising (up to 10 times) of the quantum yield after centrifugation was found. This could be explained by dominant sedimentation of huge low-porous SiNPs, which have much lower quantum yield of PL.

Thus biocompatible and biodegradible silicon nanoparticles were successfully coated by dextran, which prevented them from fast dissolution and significantly stabilized their PL. Such coating is very promising for biophotonic applications.

[1] A.G. Cullis, L.T. Canham, P.D.J. Calcott, The structrural and luminescent properties of porous silicon, J. Appl. Phys., vol. 82, p. 909, (1997).

[2] J.H. Park, L. Gu, G. Von Maltzahn, E. Ruoslahti, S.N. Bhatia, M.J. Sailor, Biodegradible luminescent porous silicon nanoparticles for in vivo applications, Nat. Mat., vol. 8, pp. 331-336, (2009).

[3] M.B. Gongalsky, A.Yu. Kharin, L.A. Osminkina, V.Yu. Timoshenko, J. Jeong, B.H. Chung, Enhanced photoluminescence of porous silicon nanoparticles coated by bioresorbable polymers, Nanoscale Res. Lett., vol. 7, p. 446, (2012).

Aluminum phthalocyanine crystal nanoparticles for fluorescence diagnosis and photodynamic therapy

Makarov V.I.[1], Ryabova A.V.[1], Pominova D.V.[1], Zharova T.A.[2], Ivannikov S.V.[2], Rudolf Steiner[3], Loschenov V.B.[1]

[1]*Prokhorov General Physics Institute, Russian Academy of Science, Moscow, Russia*
[2]*Sechenov First Moscow State Medical University, Moscow, Russia*
[3]*Institut für Lasertechnologien in der Medizin und Meßtechnik at the University of Ulm, Germany*

Fluorescence diagnosis and photodynamic therapy with photosensitizers in molecular or nanoform showed high efficiency of the treatment of various pathologies of cancer and non-cancer genesis. Aluminum phthalocyanine (AlPhc) crystal nanoparticles (NP) do not fluoresce, but it can be used as an "indicator" of inflammation, because under the influence of external factors NP begin to show the properties of free AlPhc molecules. Photoactivity occurs in the body after the application of NP-AlPhc only in diseased biological tissues whose microflora and immune system response differ from healthy biological tissue.

In the present study the possibility of NP-AlPhc application for fluorescent diagnostics and photodynamic therapy of the joints diseases was evaluated. The mechanism of the photoactivity in pathologically changed biological tissues of the joint has been proposed (changes in the fluorescence spectrum with the appearance of photodynamic potential). The method of in vivo fluorescent monitoring of joint arthrosis photodynamic therapy was developed.

AlPhc fluorescence intensity increase was obtained in diseased biological tissue of joint. Investigation of its growth dynamics was conducted, which can be used for the diagnosis of inflammatory diseases. Distinct photobleaching (decrease in fluorescence intensity) was observed after laser treatment of inflammation. In case of using of AlPhc in molecular form this effect is absent, so it’s impossible to explain the appearance of photoactivity with dissolving of NP-AlPhc in biological tissue. To explain this effect, a model of the transition of surface AlPhc molecules from para- to ortho-position in relation to the plane of the NP-AlPhc crystal was proposed.

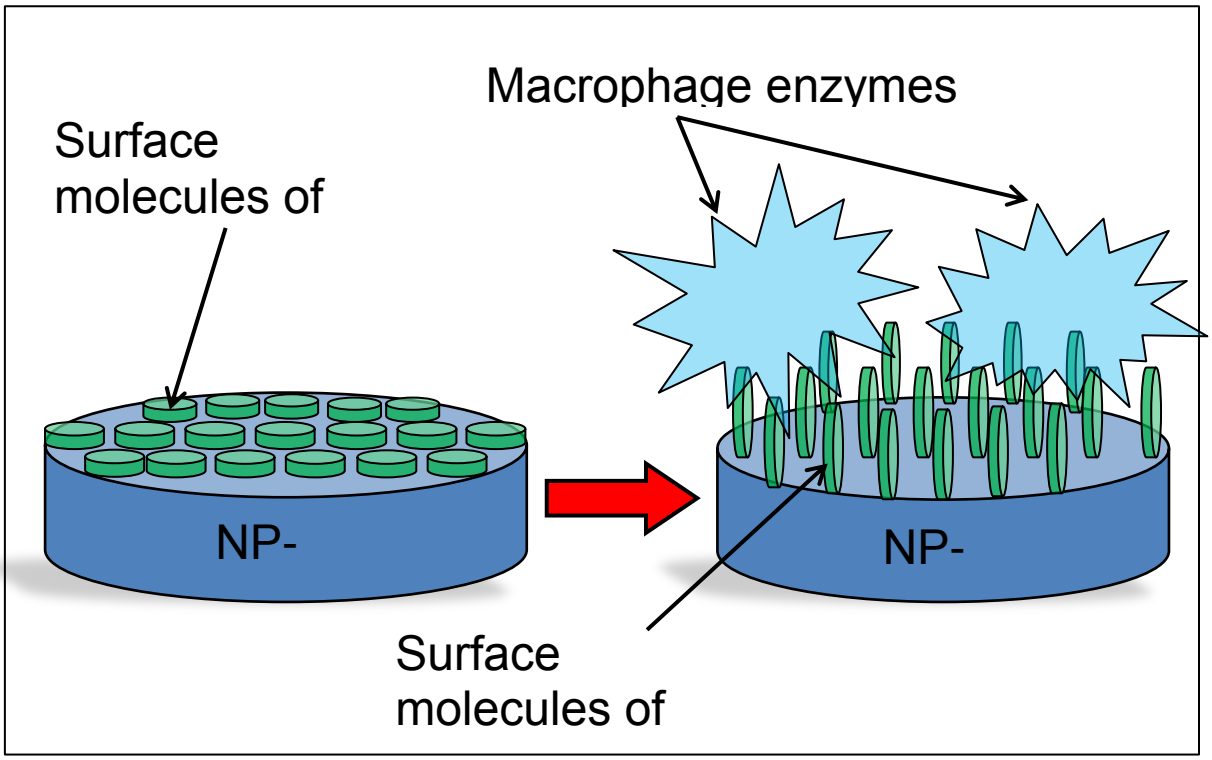
Macrophage enzymes
Surface
molecules of
NP-
NP-
Surface
molecules of

The investigation of nanoparticles application for teeth enamel microdamages diagnostics

[1]Sinyaeva M.L., [1]Admakin O.I., [2]Ryabova A., [2]Volkova A.I., [2]Loschenov V.B., [2]Konov V.I.

[1]-*Sechenov First Moscow State Medical University, Bol. Pirogovskaya 19, Russia, Moscow*
[2]-*General Physics Institute of RAS, Vavilova str., 38, Russia, Moscow*

E-mail address: siniaeva@mail.ru

Diagnostics of enamel microdamages has a great importance in dentistry to prevent caries. Microdamage of enamel is connected with local deficit of Ca in it, which is characterized by change of contence, shape, size and mutual orientation of hydroappatitus crystals (the basic structure of enamel).

Recently in dentistry the following diagnostic methods of early caries and tooth enamel damage have been used: visual review of oral cavity, zoned probe, vital painting of enamel by special drag. The main disadvantage of those methods is that they are not supposed to diagnose enamel microdamages. Also absence of quantitative evaluation of results and as a result subjectiveness of decision is a big obstacle for diagnostics.

The opportunity of fluorescence diagnostics of enamel structure changes detection with the use of aluminium phthalocyanine nanoparticles as an exogenous fluorophor, was studied. The aluminium phthalocyanine nanoparticles were obtained by means of ultrasonic dispergation of photosensitizer crystals. Influence of the nanoparticles size and stabilization methods on accuracy of the diagnostics was investigated.

The approbation of this method was carried out on extracted teeth (in-vitro). The distribution of aluminum phthalocyanine fluorescence in the enamel surface relief was investigated by means of laser scanning confocal microscopy with spectral resolution. The enhancement of fluorescence of aluminium phthalocyanine nanoparticles in tooth enamel microdamage was discovered.

The new quantitative method of express-diagnostic of teeth enamel microdamages detection will be introduced.

1. Sinyaeva M.L., Vasilchenko S.Yu., A.I. Volkova, Korovin S.B., Mamedov Ad.A., Kuzmin S.G., Luk'yanets E.A., Loschenov V.B., Konov V.I. The use of nanoparticles of aluminum phthalocyanine for detecting of teeth enamel microdamages. // J. Nanotecnology in Russia. 2007. V.2. № 11-12. Pp. 58-63. [Article in Russian].
2. S.Yu. Vasilchenko, A.I. Volkova, A.V. Ryabova, V.B. Loschenov, V.I. Konov, A.A. Mamedov, S.G. Kuzmin and E.A. Lukyanets. Application of aluminum phthalocyanine nanoparticles for fluorescent diagnostics in dentistry and skin autotransplantology. // Journal of Biophotonics. 2010. T. 3, No. 5–6. P. 336–346.

The device for simultaneous stereotactic surgery and spectroscopic control

Grachev P.V.[1], Zelenkov P.V.[2], Zhukov V.Y.[2]

[1] *A.M. Prokhorov General Physics Institute of Russian Academy of Sciences, Moscow, Russia*

[2] *N.N. Burdenko Institute of Neurosurgery, Moscow, Russia*

Mail to: p.v.grachev@gmail.com

Background and objective. Stereotactic biopsy brain tumors used in neurosurgery for tumor tissue sampling for histological and immunohistochemical analysis. Navigation to target tissue performed in three-dimensional space. The target coordinates determines by the MRI or CT images of brain.

A traditional biopsy method has a significant percentage of false negative results. Reason of this can be in various grade of malignancy of different parts of one tumor, mismatch between the true location of the tumor and the location calculated from the MRI or CT images. In addition, the stereotactic biopsy may be accompanied by life-threatening complications such as intracerebral hemorrhage vascular lesions on the path of biopsy cannula. Currently, there is no possibility of identifying the vessels during advancement the biopsy cannula. Objective of this study is the increasing of efficiency and safety stereotactic biopsy.

Materials and methods. In current clinical practice widely used spectroscopic control using protoporphyrin IX as tumor marker. Protoporphyrin IX accumulation in tumors induced by introduction into the organism of 5-aminolevulinic acid, which selectively accumulates in tumor tissues due to enzymatic disorders in rapidly proliferating tumor cells. Simultaneous applying stereotactic biopsy and spectroscopic control could help to increas of efficiency and safety stereotactic biopsy.

Results. We developed special stereotactic biopsy cannula with a laser spectroscopic control, which allows evaluating the type of tissue through which passes biopsy cannula, to identify the most informative area for biopsy, and to promptly change the trajectory of the cannula with the appearance of blood vessels. Thus, the developed system can increase diagnostic accuracy (sensitivity) of the method of stereotactic biopsy of brain tumors and reduce the risk of complications associated with this procedure.

The developed device was used in stereotactic biopsy procedure and helped to achieve a positive result. Application of the device allowed to obtain new information about brain tissue state and to correct data for further tumor resection.

PHOTOLUMINESCENCE, BIOIMAGING AND SONOSENSITISING PROPERTIES OF NANOPARTICLE SUSPENSIONS PREPARED FROM SILICON NANOWIRES

L.A. Osminkina[1], V. Sivakov[2], U.A. Natashina[1], E Tolstik[2], A.A. Kudryavtsev[3] and V.Yu. Timoshenko[1]

[1] *Lomonosov Moscow State University, Physics Department, 119991 Moscow, Russia*

[2] *Leibniz-Institute of Photonic Technology, Albert-Einstein Street 9, Jena 07745, Germany;*

[3] *Institute of Theoretical and Experimental Biophysics, Russian Academy of Science, Pushino, 142290 Moscow region, Russia*

osminkina@vega.phys.msu.ru

Recently, a lot of bio-applications of different silicon nanostructures are reported. The most popular material in this field of interest is silicon nanoparticles (SiNPs), prepared from porous silicon (PSi). PSi consists of a network of intersecting silicon nanocrystals (nc-Si) separated by nanometer-sized pores [1]. Usually PSi films are formed by a method of electrochemical etching of bulk crystalline silicon (c-Si) in hydrofluoric acid (HF). But it is known another cheap and efficient method of the formation of PSi-like structure, named silicon nanowires (SiNWs), based on metal-assisted chemical etching (MACE) of c-Si [2]. In this paper we propose method of the formation of SiNPs, based on ultrasound grinding of MACE-grown SiNWs. We have shown that prepared SiNPs can be used as a photoluminescent (PL) labels in bio-imaging and as sensitizers in sono-dynamic therapy (SDT) of cancer.

SiNWs were formed by metal (silver)-assisted wet chemical etching of heavily boron-doped (100)-oriented single crystalline silicon wafers (see inset in Fig. 1a). A TEM image of SiNPs is presented in Fig. 1(a). The prepared aqueous suspensions of SiNPs exhibit efficient room temperature photoluminescence (PL) in the spectral region of 600–1000 nm that is explained by the radiative recombination of excitons confined in small silicon nanocrystals, from which SiNWs and also SiNPs consist of (see inset Fig. 1b).

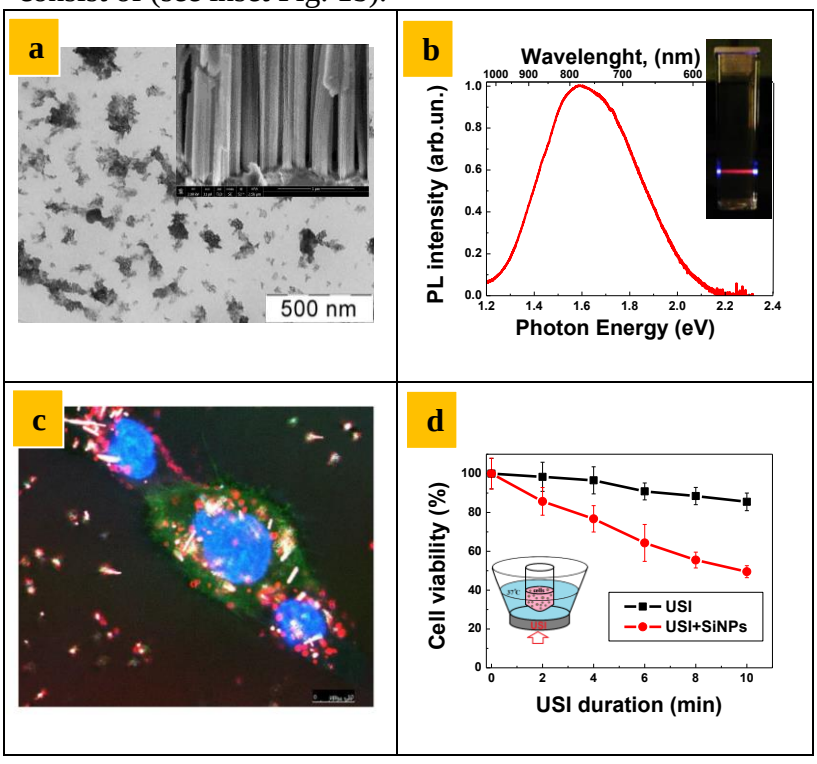

Fig.1 (a) TEM of SiNPs (SEM of SiNW arrays in inset), (b) PL spectra of aqueous suspensions of SINPs, (c) PL images of living CF2Th cells with SiNPs, (d) viability of Hep2 cells vs USI duration (set-up of in-vitro experiments in inset).

On the one hand the in vitro studies have demonstrated low cytotoxicity of SiNPs and possibilities of their bio-imaging applications (see Fig. 1c). On the other hand, it has been found that SiNPs can act as efficient sensitizers of ultrasound (USI) induced suppression of the viability of Hep2 cancer cells (see Fig. 1d).

The obtained results indicate possible applications of SiNPs prepared from SiNWs in both diagnostics and therapy (theranostics) of cancer.

References:

1. A.G. Cullis, L.T. Canham, P.D. Calcott, J Appl Phys **82**, 909 (1997).
2. K.A. Gonchar, L.A. Osminkina et al JNO **7**, 602 (2012).

Pointing stability challenges after 25-m beam propagation under vacuum on CETAL laser facility

S. Reyné[a,†], F. Giambruno[a], A. Pacholski[a], C. Grigoriu[b], Ioan Dancus[b], Liviu Neagu[b], Ion Morjan[b] and M. Le Pennec[a]

[a] *ARDoP, 4 Rue Angiboust, Parc de la Fontaine de Jouvence F-91462 Marcoussis, France*

[b] *INFLPR, Str. Atomistilor, Nr. 409 PO Box MG-36, 077125 Magurele, Bucharest, Romania*

[†]email: stephane.reyne@ardop.com

ABSTRACT

Over the past years, the ultra-intense laser field has continued to flourish as demonstrated by a growing number of scientific and technological projects. In particular, Europe's commitment towards ultra-high intensity physics is exemplified by the involment of several European countries pooling research, network resources and experience to succeed in the completion of different (multi) PetaWatt-class laser facilities. Some institutes such as INFLPR (National Institute for Laser, Plasma & Radiation Physics) in Romania has already paved the way and just fully funded the procurement of the 1.12 PW CETAL laser. The latter is typically dedicated to experiments involved in fields of high-intensity laser-matter interactions. This facility is at the state of the art in term of laser source and such laser is generally associated to beam transportation line (BTL) to achieve the beam to the target chamber. At this stage, scarce laser source manufacturers do not generally supply the beam transport. Beamline is either made by institutes themselves or public tenders can be an alternative solution. Precisely in this Romanian project, French company ARDoP was awarded for the delivery a turn-key system, including the design, material supply and installation on site. Basically, one of the main challenge of CETAL transportation line is to ensure the optical performances (before focusing) to be as close as possible to the laser source; namely after propagating over several meters from the compressor exit. The pointing stability requested must be fewer than μrad RMS over 500 shots, which is actually one of these challenging parameters to be fulfiled, and wavefront quality must be better than lambda. The 810 nm CETAL beam of 25J, with a pulse duration less than 25 fs, at a rep rate of 0.1 Hz has to be transported over 25 meters of propagation, including a periscope system with beam deviation at 30 degrees. Beam diameter is 160 mm at FWHM and has to be transported under vacuum at 10^{-5} mbar. These technical conditions imply appropriate vaccum, mechanical and optical design which has been simulated through a CAD software so as to minimize the risks. This resulted in a beam transport line including five 230 x 310 mm^2 mirrors and one $F/20$ aperture off-axis parabolic mirrors. All the optical parts are integrated into motorized mounts wich are controlled and remotely. CETAL beam transport line has now been finished to be installed. Final acceptance tests clearly show that overall optical performances are fulfiled in term of pointing stability and wavefront deformation after propagation.

Keywords: Ultra-short laser pulse, high-intensity laser, pointing stability, wavefront deformation, laser beam propagation

Test-bench for laser damage experiments with sub-15 fs ultrashort pulses

O. Utéza*[,1], Y. Azamoum[1], R. Clady[1], N. Sanner[1], M. Sentis[1], Yu Li[2], Shen Yan Long[2]

[1] Aix Marseille Université, CNRS, LP3 UMR 7341, 13288, Marseille, France
[2] State key laboratory of Laser Interaction with Matter, Northwest Institute of Nuclear Technology (NINT), Xian, China

[*] Corresponding author email address: uteza@lp3.univ-mrs.fr

Laser damage and ablation of optical materials and components is a key point for safe operation of high energy ultrashort laser facilities (PW laser systems and beyond) and enhanced development of micromachining processes. Indeed, laser damage of dielectric material in ultrashort regime (down to < 15 fs) has been shown to be highly deterministic [1] which is favorable to the definition of industrial processes requiring fine tuning of the laser ablation phenomenon. It was also shown that laser damage and ablation took place at rather low irradiation fluences compared to longer pulse durations [2,3] posing the problem of the fragility of optical materials and components used in high peak power laser systems. Moreover, the mechanisms of laser-matter interaction remain largely unclear and scarcely studied at such short pulse durations (<< 30 fs) and further experimental and theoretical developments are desirable to clarify all the electronic aspects of the interaction (characteristics of the free electron-hole plasma developing at the material surface in strongly nonequilibrium thermodynamic conditions) on the damage ablation phenomenon.

Additional complexity arises when considering pulses of extremely short pulse duration down to few optical cycles. Such pulses have extremely broad spectrum difficult to manipulate and are highly subject to beam distortions due to their high intensity rapidly yielding to deleterious phase modulations. The difficulty to manipulate them severely increases in dense media and can also take place in air [4]. In that context, specific studies need to be performed to characterize the propagation of the ultrashort laser beam in various regimes of laser fluences and intensities to infer precise data on damage and ablation of optical materials and components.

The purpose of this work is thus to measure reliably the laser-induced damage threshold (LIDT) at the surface of materials exposed to single pulses of pulse duration < 15 fs (using 1on1 protocol), providing feedback to builders and suppliers of intense laser infrastructures as well as to the scientific community involved in ultrashort laser damage. We also aim to determine laser-induced ablation threshold (LIAT) of materials and related characteristics (like morphology and affected zone) to help the development of micromachining processes based on ultrashort lasers. Our presentation will first be devoted to the description of a laser test-bench operated in air (later in vacuum) and able to study laser – matter interaction with femtosecond pulses down to pulse duration of a few optical cycles (< 15 fs). We then characterize the propagation of ultrashort pulses to estimate the onset of nonlinear effects in air (with measurement of the nonlinear index n_2) and to determine the exact conditions in which the LIDT and LIAT thresholds are measured. Finally, we illustrate the accuracy of our approach by measuring LIDT and LIAT fluences of materials extensively used in optics and photonics (like for instance fused silica).

[1] N. Sanner, O. Utéza, B. Chimier, M. Sentis, P. Lassonde, F. Légaré, J.-C. Kieffer, "Towards determinism in surface damaging of dielectrics using few-cycle laser pulses", Appl. Phys. Lett. **96**, 071111 (2010).
[2] B. C. Stuart, M. D. Feit, S. Herman, A. M. Rubenchik, B. W. Shore, and M. D. Perry, "Nanosecond-to-femtosecond laser-induced breakdown in dielectrics", Phys. Rev. B **53**, 1749 (1996).
[3] B. Chimier, O. Utéza, N. Sanner, M. Sentis, T. Itina, P. Lassonde, F. Légaré, F. Vidal, and J. C. Kieffer, "Damage and ablation thresholds of fused silica in femtosecond regime: relevant physical criteria and mechanisms", Phys. Rev. B **84**, 094104 (2011).
[4] D.E. Laban, W.C. Wallace, R.D. Glover, R.T. Sang, D. Kielpinski, "Self-focusing in air with phase-stabilized few-cycle light pulses", Opt. Lett. **35** (10), 1653 (2010).

Generation and characterization of a sub-picosecond laser-based hard X-ray K_α source with a high pulse repetition rate

Y. Azamoum*, V. Tcheremiskine, P. Blandin, R. Clady, L. Charmasson, N. Sanner, O. Uteza and M.Sentis

Laboratoire Lasers, Plasmas et Procédés Photoniques (LP3)
Aix-Marseille Université - UMR 7341 CNRS, Luminy, Marseille, France.
**Contact: azamoum@lp3.univ-mrs.fr*

We report our latest results on the development of a bright hard-x-ray quasi-monochromatic K_α source, generated by interaction of intense (~10TW) and energetic (>100 mJ) femtosecond laser pulses (25 fs) with a solid target at high pulse repetition rate (100Hz). The source exhibits an isotropic x-radiation with a dominant K_α line emission (at photon energy determined by target material) in addition to a weak bremsstrahlung continuum.

Femtosecond hard x-ray pulses have found widespread application in transient x-ray diffraction and their usefulness in bio-medical imaging is assessed. In fact, the short pulse duration allows high temporal resolution (fs scale) required to investigate and probe fast changes in local structures of condensed matter [1]. Furthermore, a brilliant x-ray source of 10 µm size (FWHM) offers high spatial resolution and high image contrast, when the phase-contrast technique is applied [2].

In this project we aim to reach a micrometric source size (comparable to the laser spot size) with a sub-picosecond duration. The challenge is to develop a stable and reliable highly energetic x-ray source at 17 keV Kα line emission (Mo target) with relatively high pulse repetition rate (100 Hz).

In recent years, bright and ultra-short x-ray sources with sub-picosecond pulse duration were developed worldwide. These sources are generated either by accelerated charged particles in synchrotrons, such as SLS using bunch "slicing" technique, or in free electron laser (FEL) systems (LCLS, FLASH…)[1]. Or by laser-plasma interaction such as betatron radiation (electrons accelerated by laser wakefield) and K_α x-ray sources. Despite the best source features in synchrotron beamlines and FEL, the huge, costly installations and limited access make the laser-based x-ray sources complementary and affordable at a laboratory scale for applications. Indeed, due to the recent progress in the ultra-intense fs laser technologies, such laser-based x-ray sources are now available at many scientific laboratories.

By focusing an intense fs laser pulse on a solid target, a solid density plasma is formed on target surface where electrons are accelerated in laser field by several nonlinear absorption processes. For non-relativistic regime of strong laser-matter interaction (10^{16}-10^{18} W/cm^2) and high-contrast p-polarized fs pulses, vacuum heating (Brunel effect) is the dominant absorption mechanism. Thus, a fraction of laser energy is transferred to electrons reaching hundreds keV energy (hot electrons). Coming in collisions with atoms of target material, hot electrons scatter producing spectrally continuous bremsstrahlung radiation and characteristic line emission. Owing to fast energetic relaxation of hot electrons in the target material, the produced x-ray pulse has sub-picosecond duration.

Photon fluxes of K_α emission of up to 10^{10} photons/s have been attained using laser systems delivering few mJ per pulse with 1-kHz repetition rate [3]. We expect to reach higher K_α photon fluxes (up to 10^{12}photons/s) using the laser system "ASUR" [4]. Note that "ASUR" is a unique high-contrast (10^9 @ns and 10^8@10ps) laser delivering 10TW/250mJ/25fs pulses with 100 Hz repetition rate and an average power of 25W (delivered to LP3 by Amplitude Technologies).

Measurements of the main source characteristics (source size, spectrum, conversion efficiency, etc) will be presented. Experimental setup includes a vacuum interaction chamber with a silver-coated off-axis parabolic mirror (metal-substrate, f/3.5, f=150 mm), which focuses an intense fs laser pulse into a small spot on the surface of a motorized rotating disk target in Mo (17keV). The interaction chamber is coupled to the final vacuum compressors through a separate vacuum chamber, where an adaptive deformable mirror is installed. Available diagnostics for controlling the x-ray source characteristics include X-PMTs, X-spectrometers and X-CCDs.

Preliminary results on x-ray generation by Molybden target show production of more than 10^9 x-photons under single laser pulse of 100mJ energy focalized into a spot diameter of 6 µm FWHM (without the use of the deformable mirror).

[1] T. Elsaesser and M. Woerner, *J, Chem. Phys*.140, 020901 (2014)

[2] R. Toth, J. C. Kieffer, S. Fourmaux, T. Ozaki and A. Krol, *Rev. Sci. Instrum*. 76, 083701 (2005).

[3] F. Zamponi, Z. Ansari, C.v. Korff Schmising *et al*., *Applied Physics A*, vol. 96, pp. 51-58, 2009.

[4] Utéza O, Blandin P., Charmasson L., Coustillier G *et al.* 'ASUR: Plateforme d'Applications des Sources laser Ultra-Rapides pour l'imagerie X et l'interaction laser-matière' – *UVX 2012, EDP Sciences* 01004 (2013).

Industrial sponsors

INDUSTRIAL LASER RANGE :

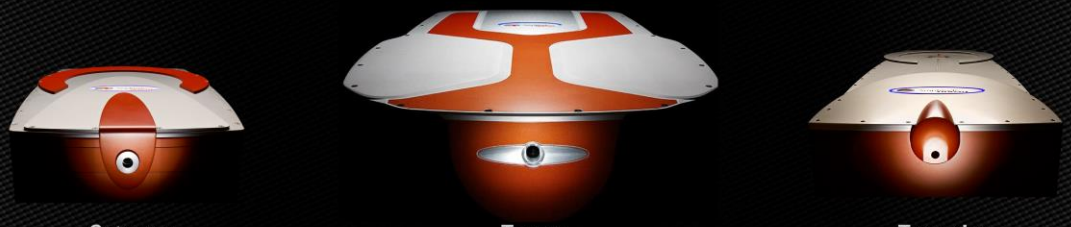

Satsuma Tangor Tangerine

Highest optical performance and reliable lasers in their class

- ultra compact
- 24/7 operation
- validated for the most demanding industrial applications

ULTRAFAST LASERS
designed for industry

Ultrafast Science MicroMachining Metrology Biology TeraHertz

Amplitude SYSTEMES

nothing but ultrafast

www.amplitude-systemes.com

Amplitude TECHNOLOGIES

The ultimate laser systems

PULSAR for particle acceleration

- High peak power up to 1 PW
- High temporal contrast down to 10^{-12}
- Dedicated CONTROL / COMMAND

AURORA for ultrafast science

- High power CEP stabilized laser (> 20 W at 1-10 kHz)
- Ultra-short pulse duration down to 15 fs
- CEP single-shot measurement and control

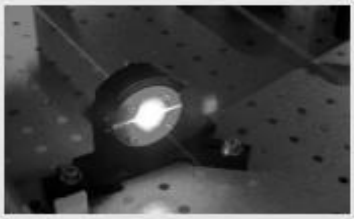

nothing but ultrafast

5/6/2014

AMPLITUDE TECHNOLOGIES
2-4, rue du Bois Chaland – CE 2926 Lisses
91029 EVRY Cedex – France
info@amplitude-technologies.com
www.amplitude-technologies.com

MOTION CONTROL

Our Solutions at Your Service

Over 40 years of proven performance, expertise and experience.

For Motion, Think Newport™

Newport®

Experience | Solutions

ROPER SCIENTIFIC™

Z.I. Petite Montagne Sud – Lisses – 8 rue du Forez – C.E. 1702 – 91017 EVRY CEDEX – FRANCE
Tel : 33 (0) 1 60 86 03 65 – Fax : 33 (0) 1 60 86 07 09 – E-mail : info@roperscientific.fr

ROPER SCIENTIFIC FRANCE offers a world of high performance imaging solutions for a broad range of industrial and scientific applications.

Life Science Imaging

- Fluorescence Microscopy
- Single Molecule Fluorescence
- Live Cell Imaging
- Low Light Applications
- Super-resolution Microscopy
- STORM, FRET, GFP
- OEM Applications

PHOTOMETRICS

Physical Science Imaging and Spectroscopy

- Astronomy, BEC, PIV
- Single Molecule
- Raman, LIBS, Fluorescence
- X-Ray Imaging
- Semiconductor
- Combustion
- Hi-res Industrial Imaging
- Optics-based Solutions
- OEM Solutions

Princeton Instruments

Digital Imaging Made Easy

- All Optical Lens Imaging Applications
- Publication and Documentation
- Plug & Play, easy Firewire connectivity
- Color, High Resolution Applications
- OEM Applications

QIMAGING

Princeton Instruments

Princeton Instruments - now combined with Acton Research, designer and manufacturer of world renown monochromators and spectrographs as well as high-performance optical coatings - is the world's leading designer and manufacturer of high-performance light detection systems for spectroscopy, imaging and X-ray applications. Princeton Instruments has shaped the "state of the art" in CCD, EMCCD, and ICCD camera technologies since the early 1980s.

Princeton Instruments' key innovations include a first-in-the-industry spectroscopy camera which included a photodiode array (and later, the first to use a CCD), as well as the first high-performance, gated, intensified CCD camera.

Imaging Group - Astronomy, BEC, Combustion, PIV, Single Molecule, Surface and Material Analysis, PSP, Nanotechnology, Semiconductor, Web Inspection, Document and Film Capture, Digital Radiography, Ophthalmology

Spectroscopy Group - Raman, LIBS, NIR, Absorption, Fluorescence, Luminescence

X-Ray Group - EUV, Lithography, XRS, Plasma, Diffraction, Microscopy, Tomography

Acton Optics & Coatings - Medical, Semiconductor, Material Processing, Analytical Instrumentation, Aerospace and Defense.

The MICRO-OPTICS Supplier

SILIOS Technologies is an SME, located in the Rousset industrial zone near Aix-en-Provence. **SILIOS Technologies** is specialized in design and manufacturing of micro-optics, diffractive optics, multispectral filters and optical instrumentation. **SILIOS Technologies** owns a 600 m² clean room and electronic lab for production of prototypes to small and medium size series.

SILIOS Technologies produces diffractive optical elements for UV, Visible, NIR and mid-IR spectral ranges (from 193 nm up to 10,6 µm) i.e. for Nd: YAG, CO2, Nd: Yag doubled and tripled, excimers , fiber and disc lasers, in CW or pulsed nano, pico seconds regimes and also for femto-seconds lasers.

The top products are:

- DOEs for homogenization of SHG pump lasers for Ti:Sa very intense lasers
- DOEs for Top-hat, line, multi-spots and Donut shapes generation for industrial applications
- DOEs for Multi-spots laser beamshaping for medical applications
- Phase screens for simulation of atmospheric turbulences
- Multi-wavelengths filters for multi-spectral imaging applications

The top applications are:

- Security of Ti:Sa crystal and improvement of femtosecond beam quality for multi-TW and PW lasers. (532nm high energy lasers)
- Cutting quality improvement of thick metallic material (1,06µm and 10,6µm lasers)
- Welding process improvement of plastic material (1,9µm laser)
- Improvement of micro-tooling process (Femtosecond laser)
- Back side Cmos imagers manufacturing process (Excimer laser)
- Silicon Wafer dicing process (355 nm laser)
- Skin treatment improvement (2,94µm laser)
- Eye surgery improvement (Lasik) (Excimer laser)
- …

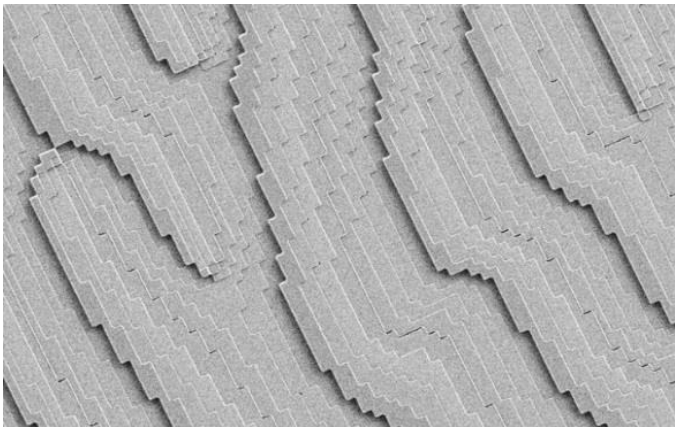

MEB image of a DOE

Focus on SHG Diffractive Homogenizers

One of the major bottlenecks still to be overcome in the pumping of large Ti:Sapphire crystals, in order to reach Petawatt–level laser amplification, is the careful control of the spatial intensity distribution of high energetic SHG pump lasers. Today, commercially available nanosecond Nd:Glass and Nd:YAG lasers, exhibit poor spatial profile quality which can lead to local hot spots, responsible for strong intensity modulations, and enhance parasitic transverse lasing. Another challenging aspect of these intense lasers is the performance of the large aperture Ti:sapphire crystal amplifiers, which must achieve Petawatt-level laser amplification without crystal damage.

For these reasons, in order to amplify femtosecond pulses to the Petawatt level, it is mandatory to keep the pump beam intensity profile as “clean” as possible and the homogenization of the typically poor spatial uniformity of the pump laser input, which can lead to dangerous local hot spots in the Ti:sapphire crystal, becomes a key element.

That is why, **SILIOS Technologies** has developed an efficient diffractive homogenizer, the SHGH 100 for such applications. The homogenizer is a diffractive optic pseudo-random phase plate made of silica, which has a high damage threshold (> 10J/cm2) and a high transfer efficiency coefficient (≥80%). In its production, an eight phase level DOE is engraved into a 1 mm thick fused silica substrates by means of a plasma etching process.

The use of these SHG Diffractive Homogenizers is key to the performance of the PW laser, they allow the intense laser to operate at higher energy by generating very uniform second harmonic pump beams at the Ti:sapphire crystals, which minimise the risk of damage due to hot-spots. The crystal can thus be pumped at an intensity closer to its damage threshold, allowing the amplifier to work more efficiently. The amplified near infra-red beam has a very smooth profile, also free from hot-spots that could damage the gratings in the pulse compressor.

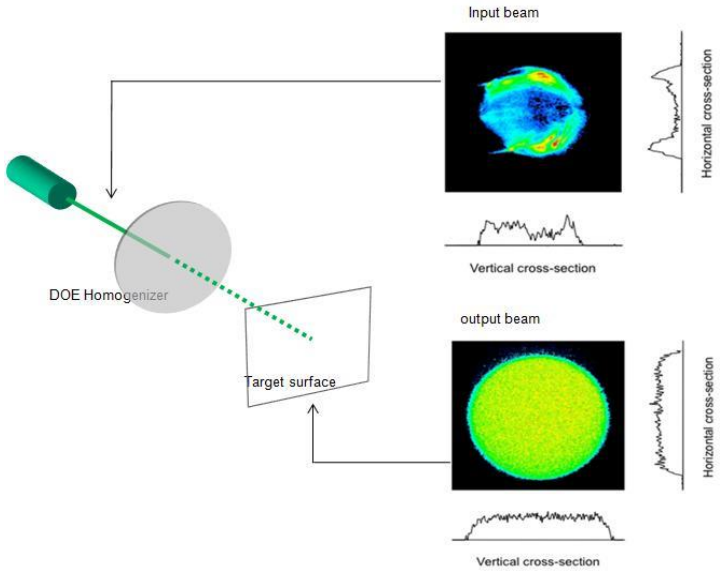

SHGH 100

Z.I Peynier-Rousset
Rue Gaston Imbert prolongée
13790 Peynier (France)

Tel : +33 442 53 89 60
Fax : +33 442 53 89 59

Email : contact@silios.fr
Web site : www.silios.com

List of Participants

Name	First name	Email	Country
Abramov	Dmitrii	awraam@mail.ru	Russia
Achim (Popa)	Cristina	cristina.achim@inflpr.ro	Romania
Agarwal	Shilpi	sipi.agarwal@gmail.com	India
Al Kattan	Ahmed	al-kattan@lp3.univ-mrs.fr	France
Alexander	Shkurinov	ashkurinov@gmail.com	Russia
ALLIO	Emmanuelle	allio@lp3.univ-mrs.fr	FRANCE
ALLONCLE	PATRICIA	alloncle@lp3.univ-mrs.fr	FRANCE
Andersen	Peter	peta@fotonik.dtu.dk	Denmark
Antipov	Aleksandr	aantipov@vlsu.ru	RUSSIA
Arakelian	Sergey	arak@vlsu.ru	Russia
Aristov	Andrei	aristov@lp3.univ-mrs.fr	France
azamoum	yasmina	azamoum@lp3.univ-mrs.fr	France
Bagratashvili	Victor	victor.bagratashvili@gmail.com	Russia
Batani	Dimitri	batani@celia.u-bordeaux1.fr	France
Belghachem	Nabil	nbelghachem@wat.edu.pl	Poland
Bellemain	Jean-Luc	bellemain@lp3.univ-mrs.fr	FRANCE
BELLOUARD	Yves	yves@bellouard.eu	The Netherlands
BORISOVA	EKATERINA	borisova@ie.bas.bg	Bulgaria
Bratu	Ana-Maria	ana.magureanu@inflpr.ro	Romania
BRENIER	Alain	alain.brenier@univ-lyon1.fr	France
Brunner	Daniel	dbrunner@ifisc.uib-csic.es	Spain
Bulushev	Evgeny	e.d.bulushev@gmail.com	Russia
CAMY	Patrice	patrice.camy@ensicaen.fr	France
Charmasson	Laurent	charmasson@lp3.univ-mrs.fr	France
Cherkasova	Olga	o.p.cherkasova@gmail.com	Russia
Choi	Kyung Sook	kscp530@naver.com	Korea
Clady	Raphael	clady@lp3.univ-mrs.fr	France
Courvoisier	Francois	francois.courvoisier@femto-st.fr	France
Coustillier	Gaelle	coustillier@lp3.univ-mrs.fr	France
COUTAZ	jean-louis	jean-louis.coutaz@scienceactions.asso.fr	France
COUTAZ	Jean-Louis	coutaz@univ-savoie.fr	France
Danilov	Artem	danilov@lp3.univ-mrs.fr	FRANCE
Darmo	Juraj	juraj.darmo@tuwien.ac.at	Austria
Delaporte	Philippe	delaporte@lp3.univ-mrs.fr	France
Denker	Boris	bid44@list.ru	Russia
DONG	BIZHE	weiye4869@163.com	China
Dorchies	Fabien	dorchies@celia.u-bordeaux1.fr	France
Dorofeeva	Liudmila	avp@bmp.ilc.edu.ru	Russia
Doroshenko	Maxim	dorosh@lst.gpi.ru	Russia
DOSKOLOVICH	LEONID	leonid@smr.ru	RUSSIA
Doskolovich	Olga	doskolovich@mail.ru	Russia
Dubrov	Alexander	avdaemon@mail.ru	Russia
Dubrova	Galina	dubrovav@gmail.com	Russia
Dumitras	Dan	dan.dumitras@inflpr.ro	Romania
Dzhun	Irina	irinkin123@mail.ru	Russia
Esaulkov	Mikhail	esaulkov_mich@mail.ru	RUSSIE
Esenaliev	Rinat	riesenal@utmb.edu	USA
Esenalieva	Rauza	rosaesenalieva@yahoo.com	USA
FATOME	Julien	julien.fatome@u-bourgogne.fr	France
Fedorov	Nikita	fedorov@celia.u-bordeaux1.fr	France
fedorova	ksenia	fedorova@physics.msu.ru	russia
Fedyanin	Andrey	fedyanin@nanolab.phys.msu.ru	Russia
Fokin	Vladimir	Vladimir.Fokin@phystech.edu	Russia
Frenz	Franziska	frenzm@ethz.ch	Switzerland
Frenz	Martin	frenz@iap.unibe.ch	Switzerland

Gaizauskas	Eugenijus	eugenijus.gaizauskas@ff.vu.lt	Lithuania
Gallais	laurent	laurent.gallais@fresnel.fr	France
Gamaly	Eugene	eugene.gamaly@anu.edu.au	Australia
Genina	Elina	eagenina@yandex.ru	Russia
Gerhard	Christoph	gerhard@hawk-hhg.de	Germany
GOGOI	ANKUR	ankurgogoi@gmail.com	India
Golovan	Leonid	golovan@physics.msu.ru	Russia
Grachev	Pavel	p.v.grachev@gmail.com	Russia
Graf	Thomas	graf@ifsw.uni-stuttgart.de	Germany
Grigoryev	Alexey	aleksgr@gmail.com	Russia
Grigoryeva	Maria	zolotikh.m@gmail.com	Russia
GROJO	DAVID	grojo@lp3.univ-mrs.fr	France
Grossenbacher Romano	Monika	romano@iap.unibe.ch	Switzerland
Guizard	Stephane	stephane.guizard@cea.fr	France
Hebling	Janos	loki@fizika.ttk.pte.hu	Hungary
Hermann	Jorg	hermann@lp3.univ-mrs.fr	FRANCE
Hervy	Adrien	adrien.hervy@sagem.com	France
Ionin	Andrey	aion@sci.lebedev.ru	Russia
Ionina	Nina	nion@sci.lebedev.ru	Russia
ITINA	Tatiana	tatiana.itina@univ-st-etienne.fr	France
Ivleva	Liudmila	ivleva@lst.gpi.ru	Russia
Jiang	Lan	jianglan@bit.edu.cn	China
Jepsen	Peter uhd	puje@fotonik.dtu.dk	Denmark
Kabashin	Andrei	kabashin@lp3.univ-mrs.fr	France
khakamova	Natalia	khakamova@gpi.nsc.ru	Russia
Khazanov	Efim	khazanov@appl.sci-nnov.ru	Russia
Khazanova	Sofia	efimkhazanov@gmail.com	Russia
KHRAMOVA	OLGA	Okhram48@mail.ru	RUSSIA
kieffer	jean claude	kieffer@emt.inrs.ca	Canada
KNAP	Wojciech	knap@univ-montp2.fr	France
KNYAZEV	BORIS	ba_knyazev@phys.nsu.ru	RUSSIA
Knyazeva	Tatyana	bknyazev@academ.org	Russia
Konov	Vitaly	vik@nsc.gpi.ru	Russia
Kosareva	Olga	kosareva@physics.msu.ru	Russian Federation
KOZLOVA	NINA	kozlova_nina@mail.ru	RUSSIA
Kucherik	Alexey	kucherik@vlsu.ru	Russia
Kulchin	Yuriy	kulchin@iacp.dvo.ru	Russia
Kumar	Varun	varunphy@gmail.com	India
Kutrovskaya	Stella	11stella@mail.ru	Russia
KUZMIN	ALEXEY	alexeyhsgap@yandex.ru	Russia
Kuzmina	Maryana	kmsnn@mail.ru	Russia
Laguta	Oleksii	oleksii.laguta@univ-lille1.fr	France
Lampin	Jean-Francois	jean-francois.lampin@isen.iemn.univ-lille1.fr	France
Larin	Kirill	klarin@uh.edu	USA
Larina	Irina	larina@bcm.edu	USA
Leahy	Martin	martin.leahy@nuigalway.ie	Ireland
letartre	xavier	xavier.letartre@ec-lyon.fr	france
Leyder	Stéphanie	leyder@lp3.univ-mrs.fr	FRANCE
Liebetrau	Hartmut	Hartmut.Liebetrau@uni-jena.de	Germany
LIN	Jingquan	linjingquan@cust.edu.cn	China
Lisenkova	Olga	olissenkova@mail.ru	Russia
Liu	Bin	swdhlb@stu.xjtu.edu.cn	China
Logunov	Lev	lev-logunov@yandex.ru	Russia
Lorenz	Pierre	pierre.lorenz@iom-leipzig.de	Germany

Loshchenov	Maxim	maxvl@mail.ru	Russia
Louchev	Oleg	oleglouchev@riken.jp	Japan
Lu	Yongfeng	ylu2@unl.edu	United States
Lugovtsov	Andrei	anlug1@gmail.com	Russia
Luhautsou	Andrei	anlug@bmp.ilc.edu.ru	Russia
Makarov	Vladimir	vi.makarov@physics.msu.ru	Russia
Marinina	Tatiana	zavest@sci.lebedev.ru	Russia
Maximova	ksenia	maximova@lp3.univ-mrs.fr	FRANCE
Mazhukin	Vladimir	vim@modhef.ru	Russia
McGloin	David	d.mcgloin@dundee.ac.uk	UK
Mikhailov	Viktor	mihailov@kapella.gpi.ru	RUSSIA
MIKHALEVSKIY	VLADIMIR	uhr@inbox.ru	RUSSIA
Mikhaylova	Irina	nice.irina14@mail.ru	Russian Federation
Mikheev	Leonid	mikheev@sci.lebedev.ru	Russia
Mikolutskiy	Sergey	mikolserg@mail.ru	Russia
Mishina	Elena	mishina_elena57@mail.ru	Russia
monot	pascal	pascal.monot@cea.fr	france
Morozov	Mikhail	mikmyus@rambler.ru	Russia
Morozov	Viacheslav	morozov@phys.msu.ru	Russia
Mouskeftaras	Alexandros	mouskeftaras@lp3.univ-mrs.fr	France
Nagy	Attila	nagy.attila@wigner.mta.hu	Hungary
NIKOLAICHIK	ANDREI	nikol@nsc.gpi.ru	Russia
Nolte	Stefan	stefan.nolte@uni-jena.de	Germany
NOVODVORSKY	OLEG	onov@mail.ru	RUSSIA
Nylk	Jonathan	jn78@st-andrews.ac.uk	UK
Obraztsova	Ekaterina	E.a.obraztsova@gmail.com	Russia
Obraztsova	Elena	elobr@kapella.gpi.ru	Russia
Ochkin	Vladimir	ochkin@sci.lebedev.ru	Russia
Ostrovska	Lidiia	ostrov_li@mail.ru	Russia
Padgett	Miles	Miles.Padgett@glasgow.ac.uk	UK
Park	Kyung Hyun	khp@etri.re.kr	Korea
Parshina	Liubov	ParshinaLiubov@mail.ru	Russia
Pasiskevicius	Valdas	vp@laserphysics.kth.se	Sweden
Pasquier	Corinne	pasquier@lp3.univ-mrs.fr	France
Perevedentseva	Elena	elena@mail.ndhu.edu.tw	Taiwan
Perezhogin	Igor	i.a.perezz@gmail.com	Russian Federation
Petrov	Valentin	petrov@mbi-berlin.de	Germany
Petrovets	Tatiana	surmenko@pribor-t.ru	Russia
Pini	Roberto	r.pini@ifac.cnr.it	Italy
Polynkin	Pavel	ppolynkin@optics.arizona.edu	USA
Popp	Juergen	Juergen.popp@ipht-jena.de	Germany
Priezzhev	Alexander	avpriezz@gmail.com	Russian Federation
Priezzhev	Alexander	avp2@mail.ru	Russia
Puerto Garcia	daniel	puerto@lp3.univ-mrs.fr	France
Pustovoy	Vladimir	pustovoy@nsc.gpi.ru	Russia
Ralchenko	Victor	ralchenko@nsc.gpi.ru	Russia
Rode	Andrei	avr111@rsphysse.anu.edu.au	Australia
Roger	Thomas	t.w.roger@hw.ac.uk	UK
Rogov	Andrii	andrii.rogov@unige.ch	Switzerland
ROLLAND	Max	rolland@lp3.univ-mrs.fr	france
Romano	Valerio	valerio.romano@bfh.ch	Switzerland
ROY	Pascale	missions@synchrotron-soleil.fr	FRANCE
Rozhin	Alex	a.rozhin@aston.ac.uk	UK
Ryabchikov	yuri	ryabchikov@lp3.univ-mrs.fr	France
Ryazanova	Bela	lmikheev@mail.ru	Russia
Samokhin	Aleksander	asam40@mail.ru	Russia

Sampson	David	david.sampson@uwa.edu.au	Australia
SANNER	NICOLAS	sanner@lp3.univ-mrs.fr	france
Sarnet	thierry	sarnet@lp3.univ-mrs.fr	France
Séverin-Fabiani	Tatiana	tatiana.severin-fabiani@synchrotron-soleil.fr	France
MONTANT	Sebastien	sebastien.montant@cea.fr	FRANCE
Seghilani	Mohamed	mohamed.seghilani@ies.univ-montp2.fr	France
Selimis	Alexandros	selimis@iesl.forth.gr	Greece
SENTIS	Marc	Sentis@LP3.univ-mrs.fr	France
Sergeeva	Irina	sergeeva@physics.msu.ru	Russia
Sergeeva	Olga	o_n_sergeeva@mail.ru	Russia
Shakher	Chandra	cshakher@iddc.iitd.ac.in	India
Shakova	Natalia	natalia.shakhova@gmail.com	Russia
Shandybina	Galina	shandyb@lastech.ifmo.ru	Russia
Siv	Julie	jmoser@amplitude-technologies.com	France
Smits	Edsger	edsger.smits@tno.nl	The Netherlands
Sobol	Emil	esobol@rambler.ru	Russia
Sobol	Tatiana	en.sobol@gmail.com	Russia
Sobolev	Nikolai	sobolev@ua.pt	Portugal
Soifer	Viktor	soifer@ssau.ru	Russia
Soifer	Viktoriya	karelina@smr.ru	Russia
Sokolova	Tatiana	sokolova@pribor-t.ru	Russia
Solis	Javier	j.solis@io.cfmac.csic.es	Spain
Solovieva	Anna	ann.solovieva@gmail.com	Russia
Stankevicius	Evaldas	estankevicius@ftmc.lt	Lithuania
Stepanov	Andrey	step@ufp.appl.sci-nnov.ru	Russia
STOIAN	Razvan	razvan.stoian@univ-st-etienne.fr	France
SURMENKO	ELENA	surmenko@yandex.ru	RUSSIA
Tcheremiskine	Vadim	tcheremiskine@lp3.univ-mrs.fr	France
Terakawa	Mitsuhiro	terakawa@elec.keio.ac.jp	Japan
Timashev	Serge	serget@mail.ru	Russia
Trusovas	Romualdas	romualdast@ar.fi.lt	Lithuania
Tsibidis	george	tsibidis@iesl.forth.gr	Greece
Tsui	Ying	ytsui@ualberta.ca	Canada
Tuchin	Valery	tuchinvv@mail.ru	Russia
Tuchina	Natalia	tuchinana@mail.ru	Russia
Tzortzakis	Stelios	stzortz@iesl.forth.gr	Greece
UTEZA	Olivier	uteza@lp3.univ-mrs.fr	france
Vadimova	Olga	musfex@mail.ru	Russia
Vasile	Tiberius	tiberius.vasile@inflpr.ro	Romania
Veiko	Vadim	vadim.veiko@mail.ru	Russia
Veisz	Laszlo	laszlo.veisz@mpq.mpg.de	Germany
Veres	Miklos	veres.miklos@wigner.mta.hu	Hungary
Volyak	Tatiana	voliak@gmail.com	Russia
Weber	Rudolf	weber@ifsw.uni-stuttgart.de	Germany
Wintner	Ernst	ernst.wintner@tuwien.ac.at	Austria
wu	shikai	wushikai@bjut.edu.cn	P.R.China
Wyatt	Adam	adam.wyatt@stfc.ac.uk	United Kingdom
XU	Jian	jxu@riken.jp	Japan
Yakovlev	Evgeny	yak@lastech.ifmo.ru	Russia
Yao	Jinping	jinpingyao@siom.ac.cn	China
Yoshiki	Nakata	nakata-y@ile.osaka-u.ac.jp	Japan
Zabotnov	Stanislav	zabotnov@physics.msu.ru	Russia
Zagaynova	Elena	ezagaynova@gmai.com	Russia
Zavestovskaya	Irina	INZavestovskaya@mephi.ru	Russia
ZERGIOTI	IOANNA	zergioti@central.ntua.gr	Greece

Zhang	Zuxing	z.zhang13@aston.ac.uk	UK
ZHU	LI-GUO	zhuliguo@tsinghua.org.cn	P.R. CHINA